Measuring fire-induced change in the understorey of an Australian dry sclerophyll forest using remote sensing

A thesis submitted in fulfilment of the requirements for the degree of Doctor of Philosophy

Vaibhav Gupta

Master of Environment & Sustainability

School of Mathematical and Geospatial Sciences

College of Science Engineering and Health

RMIT University

April 2016

Declaration

I certify that except where due acknowledgement has been made, the work is that of the author alone; the work has not been submitted previously, in whole or in part, to qualify for any other academic award; the content of the thesis is the result of work which has been carried out since the official commencement date of the approved research program; any editorial work, paid or unpaid, carried out by a third party is acknowledged; and, ethics procedures and guidelines have been followed.

Vaibhav Gupta

2 April, 2016

Acknowledgements

I am happy to take this opportunity to express my humble gratitude to those associated with the research presented in this thesis. First and foremost, I most happily thank my supervisors, Dr. Karin Reinke and Prof. Simon Jones. I am fortunate to be involved with such a great team of supervisors who have contributed uniquely during the implementation of this research project.

I am greatly indebted to Dr. Karin Reinke for her role as principal supervisor. I will never forget the support and guidance given by Karin right from driving me to the study area every single time till completion of thesis writing. I am thankful to both Simon and Karin for all their feedback and discussions which have greatly helped me enhance my research and analytical acumen. I would also like to thank Mr. Lucas Holden for helping with the point cloud data capture in the field.

I would like to thank my employers Green Home Green Planet and the City of Casey. Without them it would have been impossible for me to continue with my research.

I would also like to thank all my fellow researchers in the lab in RMIT; especially Will, Mariela, Phil, Lola, Luke and Bryan for providing such a supportive and fun-filled environment to share ideas and experiences. Phil, thank you for introducing me to Lastools. My special thanks to Luke for helping me in processing and analysing point clouds and introducing me to FugroViewer and Cloud Compare. Another special thanks to Mariela for proof-reading parts of my thesis.

I wish to thank all my friends for their support. My special thanks to Gunjan, Pranali, Pintu Bhai, Dhar, Niraj, Vinayak, Jimmy, Evelyn, Deep, Devanjali and Indra for all those moments of laughter. My earnest gratitude to Mohsen for helping me in point cloud pre-processing. I would also like to thank the 15+ housemates I've had over the last five years for being there and cheering me up.

I am thankful for the constant, unfailing inspiration and encouragement, unbounded affection and care given throughout the course of my PhD by my mother, father, brother and other family members and I dedicate this thesis to my parents. I am indebted to my in-laws for their continuous mental support.

I am greatly indebted to my wife, Shreya for her love, unswerving support and motivation for enabling me to pass one of the most difficult and challenging periods of my life.

Table of Contents

List of Figures

List of Tables

List of Publications

Published peer-reviewed journal articles

GUPTA, V., REINKE, K.J., JONES, S.D., WALLACE, L., HOLDEN, L. 2015. Assessing Metrics for Estimating Fire Induced Change in the Forest Understorey Structure Using Terrestrial Laser Scanning. *Remote Sensing*, 7, 8180-8201.

GUPTA, V., REINKE, K.J., JONES, S.D. 2013. Changes in the spectral features of fuel layers of an Australian dry sclerophyll forest in response to prescribed burning. *International Journal of Wildland Fire.* 2013, 22, 862-868.

Published peer-reviewed book sections

GUPTA, V., REINKE, K.J., JONES, S.D. 2013. Observing the structural and spectral effects of fire on vegetation using remote sensing. In: Arrowsmith, C., Bellman, C., Cartwright, W., Jones, S. & Shortis, M. (eds.) *Progress in Geospatial Science Research*. RMIT University, Melbourne.

Peer-reviewed conference proceedings

GUPTA, V., REINKE, K.J., JONES, S.D. Multi-scale, multi-temporal analysis of NDVI in burned landscapes. Proceedings of the International Geoscience and Remote Sensing Symposium, 21-26 July, 2013, Melbourne, Australia.

GUPTA, V., REINKE, K.J., JONES, S.D. Detecting changes in burnt landscapes using a terrestrial LiDAR system. Proceedings of GSR_2 Symposium, 10-12 December, 2012, RMIT University, Melbourne, Australia.

GUPTA, V., REINKE, K.J., JONES, S.D. A review of remote sensing technologies for observing fire effects on vegetation. Proceedings of GSR_1 Symposium, 12-14 December, 2011, RMIT University, Melbourne, Australia.

Non-peer reviewed conference proceedings

GUPTA, V., REINKE, K.J., JONES, S.D. *In situ* observation of vegetation response to fire, Proceedings of XXII International Society for Photogrammetry and Remote Sensing, 25 August – 1 September, 2012, Melbourne, Australia.

Abstract

This research investigates the use of remote sensing technologies for measuring and mapping the changes in the forest understorey in response to prescribed burning. Remote sensing has been used extensively to map the burn areas in fire-affected landscapes, but less work has been done focussing on beneath the canopy. Sub-canopy vegetation layers are important for habitat and for understanding the fuel hazards they may pose to the risk of wildfire. Accordingly, instruments and approaches must be able to perform in both pre- and post-burn environments, and be able to provide meaningful measures of change.

Wildfires are increasing in intensity and frequency, and in response prescribed burning is used to mitigate threats posed by them. Quantifying post-fire effects is important for burn severity, ecosystem recovery and post-fire hazard assessments. This information will allow land managers and scientists to understand fires in their environmental, economic and social contexts and help formulate responses and policies accordingly. However, measures of fire effects and fuel hazards which are done via visual assessments are known to be subjective and inconsistent between assessors and over time. What is needed is an improvement in the reporting procedures around quantification of fire effects which are both repeatable and quantifiable.

In this research two remote sensing technologies were used to measure, map and track changes in the understorey of an Australian dry sclerophyll forest. Terrestrial Laser Scanning (TLS) was used to derive vegetation structure variables and HSR (HyperSpectral Radiometry) was used to derive vegetation physiological variables. The study site was located in St. Andrews, Victoria, Australia within which a control plot and three fire treatment plots were set-up and monitored over a two year period, before and after a prescribed fire event conducted in autumn 2012. The datasets collected were used for statistical and spatial analysis of changes in understorey vegetation, and to assess those metrics best suited for describing different vegetation responses to fire effects.

The first part of this research examined the potential of TLS to detect fire-induced change in the forest understorey. From TLS point clouds a total of 18 metrics were extracted which were tested against accuracy and reliability criteria. Three metrics; *mean* AGH_{change} (Above Ground Height), *median* AGH_{change} and *point* $count_{change}$ were shortlisted. To report different post-fire changes in burnt understorey, *mean* AGH_{change} metric was used. This metric was able to report fire effects such

as total burn area, measures of patchiness, spatial distribution of burnt and unburnt areas, fuel accumulation and prescribed burn efficiency across various temporal scales.

The second part of this research analysed hyperspectral data of the near-surface (grass) and surface fuel layer (litter). Spectral changes in the near-surface fuel layer were observed in Visible (550nm), Near-Infrared (680-750nm) and Middle Infrared (970nm, 1220nm, 1550nm) domains of the electromagnetic spectrum. For the surface fuel layer (litter) changes were observed in the Middle Infrared domain (1140nm, 1225nm and 1700nm). The greatest difference from pre-burn levels for both the fuel layers occurred within the first two weeks post-burn. Spectral indices corresponding to the above determined broad spectral bands were tested to ascertain which were best at characterising burnt from unburnt targets whilst also tracking recovery. Indices such as NDVI, NBR and D720 were found to be the most suitable for near-surface fuel layer whilst D1230 for surface fuel layer.

A preliminary investigation into comparing the change detected by the two remote sensing technologies suggested that physiological change detected by HSR, recorded vegetation recovery as early as six weeks post-burn. Structural change detected by TLS even after two years post-burn was recorded as being close to two weeks post-burn levels. This finding matched well with visual assessments of structural measures (plant cover and height).

The findings of this study suggest that improvements in reporting procedures around quantification of fire effects can be achieved using TLS and HSR technology. TLS-derived structural metric, *mean* AGH_{change} can accurately detect quantified measures of fire-induced change in forest understorey that can be validated with field assessments. It can also report post-fire effects at various temporal scales including area burnt, burn patchiness, fuel load accumulation and prescribed burn efficiency. Spectral indices such as NDVI, NBR and D720 were able to accurately detect both vegetation loss and recovery. There is merit in further investigating TLS and HSR in conjunction for quantified and robust reporting of fire effects. The change detected by these technologies can be linked to inform both vegetation recovery and fuel accumulation.

Chapter 1. Introduction

1.1 Background and rationale

In Australia, fire plays an important role in ecosystem succession as a prominent disturbance factor. It is an agent of environmental change at various spatial and temporal scales determining land use, productivity, carrying capacity and biodiversity. On regional and global scales, fire impacts hydrological, biogeochemical and atmospheric processes (Roy et al., 2002). It directly affects species diversity, increases habitat fragmentation and alters landscape functioning (Lozano et al., 2007).

Over the past decade, a surge in the incidence and frequency of large, uncontrolled fires has occurred on all vegetated continents (Bowman et al., 2009). This increasing trend of natural uncontrolled fires has coincided with the observed and predicted climate-warming trend in mid to high latitudes (Li et al., 2003). Human sources such as arson have also contributed to wildfires worldwide (Morris et al., 2011). Other studies have reported that wildfire activity is increasing in frequency, intensity and duration in response to global warming (Davies et al., 2008). In recent years, large fire events in the US, Greece, Portugal, Spain, Australia and Indonesia have caused grave environmental damage, human suffering and economic loss (Davies et al., 2008, Lentile et al., 2006b).

The overall dryness of the Australian landmass gives rise to many fire-prone regions. The nature of the seasonal and synoptic weather conditions that prevail over most of the continent makes fire a frequent event in most Australian ecosystems (Milne, 1986). In response, Australian forests have adapted physiologically to recurring fire events, and in the process have come to rely on fire for growth, survival, diversity, persistence, and reproduction (Bradstock et al., 2002b, Milne, 1986, Morrison et al., 1996). The dry sclerophyll forests of south-east Australia are among the most fire-prone forest communities in the world (Penman et al., 2007).

In many regions of the world including Australia, prescribed burns are now being carried out to reduce hazardous fuel accumulation, and to create a forest structure resilient to disturbance by fire (Knapp et al., 2006, Penman et al., 2007). In this way, prescribed burning can be defined as the deliberate application of fire to forest fuels, under specified weather conditions, so that well-

defined management goals are achieved (Wade et al. 1989). Prescribed burns are believed to decrease the intensity of subsequent wildfires by reducing the accumulation of highly flammable understorey fuels (Collett and Neumann, 1995). In particular, the finer aerated elements in fuel layers governing fire spread are targeted, whilst the horizontal and vertical community of the fuel complex is disrupted (Fernandes and Botelho, 2003). Such burns are typically of low to moderate intensity (Penman et al., 2007, Wain et al., 2008) and aim to generate sufficient heat to spread through the litter, small woody debris and standing fuel (for example grasses, understorey shrubs and dry bark on trees) whilst limiting impacts on lower forest canopy (Penman et al., 2007). Current burning regimes consist of 'best guess' management practices, with efforts being made only recently to understand how fire should be managed in different vegetation communities (Skull and Adams, 1996). Researchers such as Knapp et al. (2006) state that it is often assumed by land managers and fire scientists that prescribed burns approximate the disturbance historically produced by wildfire. This is not necessarily the case, thus it becomes challenging and important to ascertain the extent and severity of prescribed burns and their long- and short-term impacts on vegetation life cycles and overall ecosystem health.

Researchers such as Vila and Barbosa (2006) highlighted the need for information on burn areas and post-fire vegetation regeneration in response to increased prescribed burn activities taking place worldwide. Such information may assist land managers to assess the impacts of fires on landscapes and allow a deeper understanding of fires in environmental, economic and social contexts. Responses and policies can then be formulated accordingly (Roy et al., 2002, Van Wagtendonk et al., 2004b).

Remote sensing technologies can provide an efficient and economical tool for acquiring fire and fire-related information over large areas at regional to global scales (Roy et al., 2005) on a routine basis. Satellite data has the potential of providing repetitive and non-destructive alternatives to expensive and labour-intensive field measurements (Verbesselt et al., 2006). Apart from being used to detect active fires (Giglio et al., 2009, Justice et al., 2002), remotely sensed data particularly from space- and air-borne sensors have been used successfully to assess environmental conditions before and during fires events and to detect changes in post-fire spectral response (Lentile et al., 2006b). Remote sensing has also proved a useful tool for mapping the extent of the burn, understanding the biological responses due to burn severity, and quantifying the frequency and pattern of burn areas (White et al., 1996).

Remote sensing techniques have been used to understand fire impacts on the landscape since the 1980s. Early investigations in the applicability of remote sensing in this field were achieved through understanding fire impacts. The techniques developed assessed how 'severe', in terms of ecological change, a fire was on both local and regional ecosystems (Lentile et al., 2006b). These early studies estimated the change in vegetation structure and extent caused by the fire using multi-spectral responses measured by satellite sensors (for example Hall et al., 1980, Jakubauskas et al., 1990, Milne, 1986). More recently, studies have sought to relate ecological measures to fire-induced physical changes on the land surface (for example Epting et al., 2005, Van Wagtendonk et al., 2004b, Veraverbeke et al., 2011b).

Another emerging remote sensing technology that is being applied to environmental studies is Light Detection And Ranging (LiDAR). Traditionally being used to create Digital Elevation Models (DEM) and retrieve atmospheric particle concentrations (Lim et al., 2003), LiDAR technology is increasingly being used for a wide variety of environmental applications including automatic tree detection and tree diameter and height estimation (for example Simonse et al., 2003, Thies and Spiecker, 2004, Watt and Donoghue, 2005). Like remote sensing sensors, LiDAR sensors can also be deployed on platforms in space, air and on the ground. Airborne LiDAR Scanning (ALS) in particular is being used in burnt landscapes to quantify biomass loss due to fire (Heo et al., 2008) and ascertain crown mortality and burn severity (White and Dietterick, 2012). Limited research exists on the utility of Terrestrial Laser Scanning (TLS) to detect and measure changes in fire-affected landscapes (for example Loudermilk et al., 2009, Rowell and Seielstad, 2012). Therefore, opportunities exist to explore the potential of this technology for measuring structural changes in burnt landscapes, and to extend the observations of fire impact to include ecosystem processes such as fuel accumulation and vegetation recovery.

Established techniques for describing or quantifying the effects of a fire include destructive sampling of the remaining fuel and, more commonly, *in situ* visual estimates of post-burn variables, such as percentage surface burnt, percentage understorey cover burnt (grass and litter), percentage canopy scorch and burnt and litter depth post-burn (Fernandes & Botelho 2003). Routinely used field measures of burn severity such as the Composite Burn Index (CBI) are based on visual assessment and judgement (Key & Benson 2005). In Australia, the techniques for reporting burn severity are also based on visual field assessments which are subjective, qualitative and inconsistent between assessors (Watson et al. 2012). Lentile et al. (2009) have pointed out that appropriate use of remote sensing tools and techniques for assessing post-fire effects (burn severity and ecosystem response) require investigation of the biophysical relationships between remotely

sensed metrics of post-fire surface conditions with field measures of ecosystem condition. Others (Escuin et al., 2008, Jakubauskas et al., 1990) have described specific changes as a result of fire consuming the vegetation including destruction of chlorophyll, leaving the soil bare, charring the roots and altering both aboveground and belowground moisture. The ability to draw accurate links between fire effects and operational fire models whilst overcoming cost, time and technical challenges posed when collecting field data has also been acknowledged by several researchers (Hudak et al. 2009; Jakubowski et al. 2013; Loudermilk et al. 2009). These challenges require accurate and repeatable data to be collected, allowing for links between related parameters to be explored in a statistically robust manner.

Burn landscapes, often after a prescribed burn, consist of a mosaic of burnt patches that differ in severity, arising from differences in terrain, fuel moisture, vegetation type or prevailing weather conditions during fire (Bradstock et al., 1995). A current issue is the ability to accurately map burn severity, particularly that of the forest understorey. The limitations in passive remote sensing technologies mean the fine spatial scale required to understand fuel load consumption at the understorey level is not achievable through satellite or aerial imagery alone. Canopy obscuration, and the inability to directly observe smaller areas (Roff et al., 2005, Arnett et al., 2015) adds to the complexity of achieving accurate, fine-scale measurements. Even active remote sensing technologies such as airborne LiDAR have been unsuited for this purpose (Loudermilk et al. 2009). A study by Goodwin (2006) demonstrated that although airborne LiDAR was capable of estimating the mean understorey height and cover for low to medium canopy cover forests, estimates of maximum understorey height could not be measured reliably. Modern TLS systems can overcome these limitations whilst also overcoming shadowing effects of overstorey trees. Studies have investigated the potential of TLS in characterising understorey forest structure using TLS with very promising results (Loudermilk et al. 2007; Rowell & Seielstad 2012).

Furthermore, it has been pointed out by Lentile et al. (2006b) that although various spectral indices have been employed and widely used to measure and map post-fire ecological effects and fire-induced vegetation loss, remotely sensed metrics and field assessments remain poorly integrated. Interestingly, in the same paper they also argue that Two Dimensional (2D) satellite imagery does not permit complete analysis of structural components of vegetation. Hence, they suggest a convergence of two independent remote sensing technologies in the form of 2D satellite imagery (ASTER, MODIS, QuickBird, IKONOS, airborne hyperspectral sensors) and Three Dimensional (3D) LiDAR datasets. This will enable understanding of both physiological and structural change in vegetation post-fire and assessment of pre-fire fuel conditions.

Accurate and meaningful information quantifying the effects of prescribed burns on vegetation can help protect and maintain ecological assets. Duffy et al. (2010) pointed out that burn severity estimates are important in understanding the effects of fire on post-fire vegetation succession; which are still poorly understood in many forest types. Vegetation response will in part be driven by burn severity; it is believed that areas which experience fire of a higher severity take longer to recover than areas of lower severity. Such findings will be of importance to fire ecologists and botanists who are trying to understand ecosystem recovery as a result of prescribed burns. Long-term monitoring can help enhance our understanding of how vegetation changes over time since fire by providing an insight into fuel accumulation and vegetation recovery. A few studies (Röder et al., 2008) have used remote sensing to monitor long-term post-fire dynamics in burnt landscapes.

Burn area estimates are also important to land managers for land management reporting and policy adherence requirements. Further, land managers require tools that can help predict where and when severe, stand replacing fires (a fire that kills most of the trees in a section of a forest) are likely to occur (McLoughlin, 1998). Burn area and severity maps may also identify areas in urgent need of rehabilitation; driven partly by burn severity. Determining the perimeter of a fire as well as the distribution of severity levels inside it will facilitate the process of making decisions aimed at restoring the affected areas (Escuin et al., 2008, Roy et al., 2006b). Furthermore, Brewer et al. (2005) proposed that the burn area information also provided a method for updating current vegetation maps which serve as baseline information for future monitoring and provided an analytical basis for evaluating management and policy outcomes.

In summary, a number of key challenges have been identified relating to quantifiable, accurate mapping and monitoring of fire effects in the forest understorey over time. The research presented in this thesis aims to explore terrestrial remote sensing techniques to quantify and map fire-induced change in the forest understorey for up to two years post-burn. TLS will be used to quantify and map structural change, whilst field spectrometry will be used to detect physiological change. A preliminary investigation into comparing the change detected by TLS and HyperSpectral Radiometry (HSR) will also be conducted.

1.2 Research questions

The overarching aim of this thesis is to develop methods to improve the reporting procedures around quantification of fire effects following prescribed burns that are both repeatable and quantifiable. This will be achieved by identifying suitable metrics derived from multi-temporal

remotely sensed data for reporting of fire effects in burnt forest understorey. Monitoring of change in the understorey will be investigated for up to two years post-burn. In order to propose these metrics and report post-fire changes from TLS and spectral datasets, four research questions are investigated. These are as follows:

RQ1. What are the best performing TLS-derived metrics for measuring changes in burnt forest understorey?

This research question tests different metrics that can be derived from TLS data to measure and map changes in burnt forest understorey. This will include a number of data captures for up to two years following a planned burn event. The best performing metric will be assessed against criteria of *sensitivity*, *stability* and *similarity*. Metrics tested will include height-based, point density and intensity metrics.

RQ2. What are the post-fire effects observed in the burnt forest understorey as measured by the best performing TLS metric?

This research questions looks at describing different post-fire effects in the understorey landscape that occur over a two year period using the 'best' performing TLS-derived metric as determined from the findings of RQ1. The different fire effects detected using TLS will also be linked with field measures of burn severity and fuel hazard. Data validation between TLS measures and field measures (such as fuel hazard and burn severity) and change in understorey cover will also be carried out.

RQ3. What are the spectral changes observed in the forest understorey at different times since fire?

This research question identifies the key spectral changes observed in burnt forest understorey layers and describes the critical timelines of when these changes are observed. It explains the greatest deviation of spectral response from the pre-burn levels. Based on the identification of broad domains of the electromagnetic spectrum showing spectral changes, this research question will provide inputs to appropriate spectral indices that will be used to answer RQ4.

RQ4. Which spectral indices best identify fire impacts and vegetation recovery in the forest understorey?

This research question investigates the potential of various spectral indices in ascertaining burnt and unburnt understorey fuel layers whilst also tracking recovery. Links will also be drawn between remotely sensed measures and field measures of change in fuel cover. Because spectral data is captured at different vertical strata of the understorey of a dry sclerophyll forest, this research question will also look at the spectral indices at these different vertical strata.

1.3 Scope of thesis

This research investigates the application of two emerging and independent remote sensing technologies to detect burnt areas and report post-fire effects in the understorey of a dry sclerophyll forest of south-eastern Australia. The remote sensing instruments used were the TLS and HSR whilst field based measures included fuel hazard, burn severity and change in fuel cover. Whilst the TLS can help quantify structural change in the landscape, HSR will enable monitoring physiological response after prescribed burns. Although these two technologies are being treated independently in this research, a preliminary comparison of the change detected by each is explored in Chapter 8.

This study is limited to a single forest located in Victoria, Australia. Other forest types have not been considered within the context of the current study due to restrictions and logistics surrounding access and monitoring of forest burn sites. In this research, detection of burnt landscapes and their subsequent recovery will be monitored over a two year period post-burn. Spectral changes will be monitored for up to one-year post-burn. Structural changes will be monitored pre- and post-burn (within two weeks) and then at the end of two years from the burn event. Although high spatial resolution satellite systems such as Quickbird, Ikonos, Rapid Eye and WorldView-2 could prove useful in understanding the fire effects of prescribed burns in this research, the aim of this thesis was not to up-scale. The attempt here is to understand and quantify fire effects on the ground. The results herein may inform future projects investigating up-scaling to air- and space-borne sensors.

This research is a ground-based study using terrestrial remote sensing instruments. As such the scale at which data capture occurred was very ‘fine’ as compared to airborne imaging and ALS. The advantage of such an approach especially from the hyperspectral remote sensing point of view is that it facilitates capture of pure spectra devoid of the ‘spectral mixing’ effects which are encountered with both air- and satellite-borne remote sensing. Another advantage is that it enables detailed data capture underneath a canopy, an area not clearly visible to space- and air-borne platforms. It has been acknowledged that it is extremely difficult to interpret and quantify changes

in the understorey using air-borne remote sensing technology, as prescribed burns are often low intensity burns and as such their effects may not be visible in the canopy. The trade-off to this approach is that only a small area of the landscape can be investigated.

1.4 Thesis structure and outline of chapters

The thesis is presented in eight chapters as shown in Figure 1.1.

Chapter 1: Introduction

The first chapter introduces the research and provides a background and rationale for the study. The chapter also explains the research aim and objectives. It puts forward the research questions and the thesis structure in the form of an outline of the different chapters.

Chapter 2: Literature Review

Chapter 2 is divided into three sections. The first section provides a general introduction to prescribed burns and their effects on the different fuel layers of the Australian dry sclerophyll forests. The second section discusses the role of remote sensing in analysing fire effects on vegetation with a detailed discussion on various spectral indices employed for this purpose. The last section delves into the applications of TLS in change detection and fire-related studies.

Chapter 3: Methods

The third chapter describes the study area followed by a discussion on the sampling design undertaken in this research. The different remote sensing instruments used are also described.

Chapter 4: Assessing metrics for estimating fire induced change in the forest understorey using Terrestrial Laser Scanning

This chapter investigates the utility of TLS in detecting change in a burnt forest understorey. A total of 18 TLS-derived metrics were tested. The metrics were tested for their potential to detect changes in burnt landscapes against set criteria. This chapter answers research question 1 and concludes with the identification of the appropriate metric for reporting post-fire changes in the forest understorey.

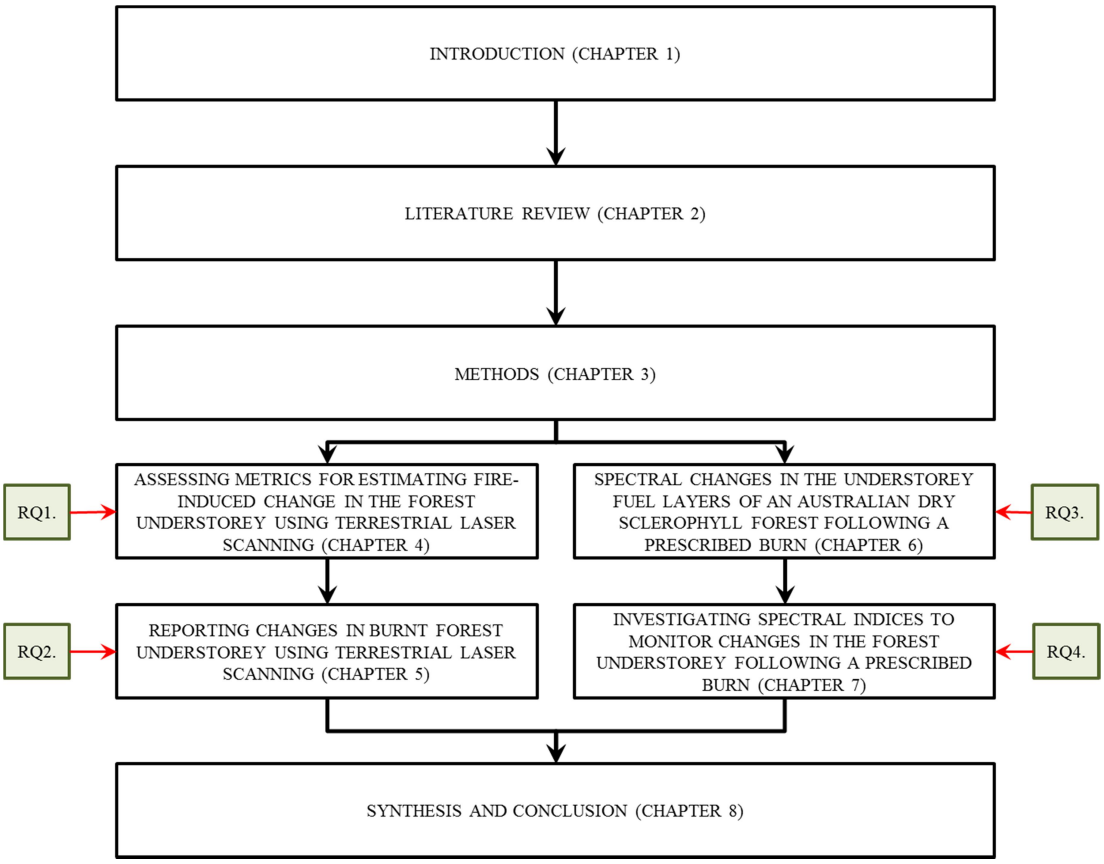

Figure 1.1 Thesis structure and chapters in this research.

Chapter 5: Reporting changes in burnt forest understorey metrics using Terrestrial Laser Scanning

This chapter applies the 'best performing' metric to report various post-fire effects in the burnt forest understorey at different epochs. Links are drawn with field measures of fuel hazard and burn severity. A validation is also carried out between measures derived from TLS metrics and field measures. This chapter answers research question 2.

Chapter 6: Spectral changes in the understorey fuel layers of an Australian dry sclerophyll forest in response to prescribed burning

Chapter 6 discusses the changes observed in the spectral features of fuel layers in response to fire using time-series spectral signatures and first-order spectral derivatives. This chapter answers

research question 3 and helps identify the broad domains of the electromagnetic spectrum so that appropriate spectral indices can be identified for further analyses.

Chapter 7: Investigating spectral indices to monitor changes in the forest understorey following a prescribed burn

This chapter applies spectral indices to discriminate between burnt and unburnt fuel targets whilst also tracking recovery following prescribed burns. Links are drawn between these remotely sensed derived metrics and field measures of change in fuel cover. The chapter concludes with the selection of optimum metrics which best detect burnt and unburnt understorey fuel targets whilst also tracking recovery. This chapter answers research question 4.

Chapter 8: Conclusion

Chapter 8 draws together the overall results and findings of this research, by providing answers to the four research questions posed. Thereafter an attempt is made at comparing the findings of change detected by TLS and HSR data in characterising change in burnt landscapes. The thesis concludes with a section on suggestions for future work.

1.5 Summary

This chapter introduced the research being presented in this thesis. It provided a brief overview of bushfires and prescribed burns and outlined the role of remote sensing in this domain. It identified the key challenges for the remote sensing of fire-affected landscapes and forest understorey and from this some key research questions were developed. These research questions are described and the overall thesis structure presented.

Chapter 2. A review of literature on measuring fire-induced change in sclerophyll forests

2.1 Introduction

This chapter examines the application of remote sensing technologies, in particular, how TLS and HSR can be used to advance our understanding regarding the impact of fire on vegetation and landscape. The first section examines wildfires in Australia and discusses the rationale for conducting prescribed burns. This section also highlights the effects of prescribed burns on Australian dry sclerophyll forests. A review of the utility of satellite remote sensing to map and measure burn severity and fire effects on vegetation and landscape is presented in the next section. A discussion of the different spectral indices to ascertain fire impact and severity is also presented. The last section discusses the potential of LiDAR, in particular, TLS for investigating the impact of fire on vegetation.

2.2 Fire effects on the Australian dry sclerophyll forests

2.2.1 Overview of wildfires in Australia

Australia is the most fire-prone continent and country on Earth (Gill, 1975). Fires impact the majority of the Australian continent and its forest types in a wide variety of regimes (Gill, 1999). Before the arrival of humans, lightning-ignited fires began to shape the Australian flora (Skull and Adams, 1996). Humans first arrived on the Australian mainland about 60,000 years ago and in Tasmania later (Golson, 1972). This marked the beginning of the use of an intensive fire management regime which eventually led to the widespread expansion of dry sclerophyll forests, and the contraction of wet non-sclerophyll forests (Nicholson, 1981).

Before European settlement, frequent and extensive natural fires and Aboriginal burning created a mosaic of frequently burned areas with light fuel loads that limited both the intensity and spread of

fire even under weather conditions favourable for catastrophic wildfires (Victorian Lands Alliance, 2010). The Aboriginal burning practices were permanently interrupted following European settlement which began over 200 years ago. This resulted in a loss of Aboriginal influence over land management leading to large tracts of land remaining unburnt (Florence, 1994). This has led to massive and continuing ecosystem change country-wide (Lewis, 1989).

Despite the hazard posed to communities, wildfire remains an important factor determining the growth, survival, diversity, persistence, floristics and structure of many plant species in the Australian forests (Bradstock et al., 2002a, Morrison et al., 1996). It has been demonstrated that heat stimulates seed germination in a wide range of species from some families including *Acacia* and *Senna*. Heating enables fracturing of the seed coat, thereby enhancing germination, particularly in hard-seeded species (Penman et al., 2008a).

The term bushfire is a uniquely Australian term that is used to describe an unplanned fire that occurs in the 'bushland', incorporating fires that happen in grass, forest, scrub and other vegetation categories (Bryant, 2008). In other words, bushfire refers to any fire that occurs outside of the urban environment. This is similar to the term wildfire or sometimes wildland fires used in the United States (Bryant, 2008). Such unplanned fires pose a threat to people, property and ecological values in a diversity of ecosystems and landscapes around the world (King et al., 2006). Bushfires are endemic to the Australian continent and are more prevalent during the southern hemisphere summer (December through February). Extensive bushfires have in the past caused substantial property losses (Chen and McAneney, 2004). Ever since the devastating 1929 fires and the subsequent Royal Commission Inquiry, the suppression of unplanned fires in Victoria has been given a high priority (Tolhurst et al., 1992).

Many factors determine the frequency of and areas burnt by unplanned fires. These include meteorological conditions at the time of burning, and the natural heterogeneity present in any landscape as a consequence of the landscape topography, the current vegetation mosaic and the historical fire regime (King et al., 2006). The 'regime' may include the intervals between fires; whether the fire burns peat or only the fuels above the soil surface; the intensities of the fires; and, the seasons during which fires occur (Gill, 1999). For example, two dendrochronological study sites in dry and wet eucalypt forests near Eden showed an increased frequency of fire scarring since European settlement. Similar research in the Snowy Mountains region showed the same pattern (Jurskis et al., 2003). This observed trend of intense fires was associated with a reduced occurrence of low-intensity fires.

2.2.2 Overview of prescribed burns in Australia

Fire management can be a controversial issue, based on factors such as what should be burnt, how often, when and why (Skull and Adams, 1996). Manipulation of fire is the primary landscape management tool in many environments and most conservation reserves (Gill, 1999). Fire management involves both the suppression of unwanted fires and the ignition of other fires under specified conditions for specified purposes (Gill, 1999). The most frequent fire management tool is prescribed burning (Jurskis et al., 2003), defined as the deliberate application of fire to forest fuels under specified conditions such that well-defined management goals are attained (Fernandes and Botelho, 2003).

The primary objectives of prescribed burning include the conservation of biodiversity, pasture management and property protection and hazard reduction (Leigh and Noble, 1981). Other purposes include assisting forests regenerate after timber harvesting, controlling weeds, insects and diseases (Fernandes and Botelho, 2003). The primary motivation behind prescribed burning in an Australian context is the reduction of wildfire hazard (Fernandes and Botelho, 2003, Penman et al., 2007, Wain et al., 2008), protecting forests and wildland resources and infrastructure at the urban interface, which ultimately affects human safety (Fernandes and Botelho, 2003, Gill, 1999). With major Australian cities experiencing rapid growth of peri-urban communities at the interface with agricultural lands and native vegetation, there is an increasing risk to peri-urban communities from wildfires and hence prescribed fire becomes an important fire management programme (Victorian Lands Alliance, 2010, Wain et al., 2008).

Prescribed burns implemented for the above purpose are typically of low to moderate intensity (Penman et al., 2007, Wain et al., 2008). This ensures that such fires do not burn the lower forest canopy, but are hot enough to maintain a spread through the litter, small wood debris and standing fuel (for example grasses, understorey shrubs and dry bark on trees) (Penman et al., 2007).

The rationale for fuel hazard reduction burning is clear-cut. Once a fire is ignited, its behaviour is determined by weather, topography and fuels (Fernandes and Botelho, 2003). It is conducted under dry and stable atmospheric conditions at the end of the summer to maximise consumption of large woody debris (Wain et al., 2008, Penman et al., 2007). Prescribed burns are undertaken in a mosaic pattern at a rotation of 5-12 years depending on the forest type, rate of fuel recovery, silviculture objectives and other considerations. The majority of burns in south-western Australia are undertaken in the spring months around October. Burns are also carried out in autumn even though

these tend to be hotter owing to lower fuel moisture and soil moisture content that is present at the end of summer droughts (Grigg et al., 2010). In southern Australia, fires in late summer or autumn are typically more intense than fires in spring. This is generally due to lower fuel moisture contents following the long summer drought (Smith et al., 2004b).

Prescribed burning activities limit the accumulation of highly flammable understorey fuels; humus, leaves, bark, desiccated ground vegetation and twigs of less than 6mm diameter (Collett and Neumann, 1995). They also prevent accumulation of the finer elements in those fuel layers that govern fire spread. Prescribed burns disrupt the horizontal and vertical continuity of the fuel complex (Fernandes and Botelho, 2003). This way, the practice of prescribed burns decrease the intensity of subsequent unplanned catastrophic wildfires (Fernandes and Botelho, 2003, Penman et al., 2007, Wain et al., 2008) whilst making it easier to suppress such fires (Wain et al., 2008).

Prescribed burns can be carried out at various spatial scales. Low intensity prescribed burns can be used to reduce fuel loads around high value built assets and urban interface zones. They can also be used at the landscape scale for strategic burning programmes (Wain et al., 2008). Prescribed burning conducted for fuel and habitat management is season dependent. Hence, it varies considerably from year to year. Typically, 150,000-200,000ha per annum are burnt in south-west Western Australia, predominantly during the spring months (Wain et al., 2008). In the south-eastern states, prescribed burning tends to be undertaken during autumn with an aggregated area of 100,000-150,000 ha per annum across New South Wales, Victoria and Tasmania (Wain et al., 2008). In Victoria, prescribed fire operations commenced during the 1950s, and an average of just under 130,000 ha of state forest, national parks and other protected land have been burnt annually since 1983 (Collett and Neumann, 1995). Tolhurst (1994) around the same time reported a slightly higher figure of approximately 150,000ha of native vegetation on public land being burnt annually.

While prescribed burning reduces the severity and impact of wildfires, the practice is controversial, with claims that it is ecologically damaging and leads to a decline in forest health (Burrows et al., 2010). Periodically, burning off ‘high risk’ vegetation such as *Eucalyptus* every 5-10 years does not provide enough time for the trees to flower and produce enough seed-bank reserve. Thus, in one fire season with an inappropriate fire frequency, the natural inhabitants of the area may be lost. This is especially important in Australia since trees such as eucalypts require 20-30 years or more before the fire can perpetuate the tree’s life cycle, by stimulating regeneration or seed release (Tran and Wild, 2000). If a fire goes through a stand before trees start to produce seeds, say in the first twenty years, the species will have no mechanism of regeneration and may be eliminated from the

area (Tran and Wild, 2000). Gill and William (1996), like Kellman (1986), showed that regular prescribed burning reduced biodiversity, however, they also stated that the absence of fire could reduce species richness.

Bradstock and Auld (1995) discussed that low-intensity, prescribed fires (used for fuel reduction) may be detrimental to the conservation of flora because the heat derived is insufficient to stimulate the germination of buried, dormant seeds. This was confirmed by other researchers including Catling (1994) and McLoughlin (1998) who further added that hard-seeded plants belonging to families such as *Myrtaceae*, *Casuarinaceae*, *Proteaceae* and *Leguminosae* fail to germinate in low-intensity fires because the heat was insufficient to fracture the seedcoat (Penman et al., 2008a). Luke and McArthur (1978) also expressed their views on this suggesting that the risk of losing nitrogen from the ecosystem was higher during low-intensity fuel-reduction burning. Inappropriately implemented fire regimes may also lead to a decline in plant populations (Bradstock et al., 1995).

Zammit (1988) states that frequent fires with short inter-fire intervals could result in the exhaustion of buds or carbohydrates stored in the lignotubers, thus resulting in the mortality of resprouters. However, Jurskis (2005) claims that in some situations, frequent burning is essential for forest and tree health. Watson (1998) provides a comprehensive review of the adaptations and responses of plants to different fire regimes, and he concludes that fire was a natural and necessary event in the regeneration of endemic species of Australia. In the aftermath of Victoria's 2009 'Black Saturday' bushfires, the Victorian Lands Alliance (2010) prepared a report citing evidence that low-intensity prescribed burning played a significant role in mitigating the severe ecosystem damage of the high-intensity summer bushfires.

As discussed above, fire is an essential component of the Australian ecosystem; a natural agent required for maintaining biodiversity and ecological health and in some cases a required ingredient that allows many species to survive. However, not all fires are natural or beneficial (Bryant, 2008). The above discussion also highlights that low-intensity prescribed burns carried out with the goal of reducing fuel in a habitat can be detrimental to the survival of that habitat since the change in fire regime can alter the natural vegetation occupying the area. Inappropriate fire regimes can lead to significant changes in community structure, including a substantial risk of extinction (Fisher et al., 2009).

2.2.3 Australian dry sclerophyll forests and fire

Table 2.1 below shows the general effects of a high-intensity fire on the different vertical strata of Australia's sclerophyll forests (Catling, 1994). The recovery processes, as listed in the table, varies according to geographic location. It should also be noted that in comparison to the dry sclerophyll forests, the wet-sclerophyll forests would have very different recovery processes (Tran and Wild, 2000).

Table 2.1 General effects of a high-intensity fire on Australia's sclerophyll forests (Catling, 1994, p 38).

Time after fire	The year post-fire	Years 2 – 4	Years 5 – 15	Years > 15
Canopy cover	Canopy removed or scorched	Canopy open	Canopy closing	Canopy near maximum
Understorey cover	Shrubs removed	Good shrub cover but not height	Shrubs taller	Shrubs at maximum but decreasing
Ground cover	Litter and ground vegetation removed	Ground vegetation thick	Ground vegetation dense but thinning	Litter increasing; ground cover decreasing

Based on previous literature it is likely that Australian environments that have not experienced a fire in over 15 years are likely to present a considerable fire risk, and possibly create an environment that is detrimental to species diversity.

According to Catling (1994), intense fires (more than 3500 kW/m^2) usually defoliate trees, destroy understorey shrubs and totally remove the forest floor cover. Such fires result in the rapid proliferation of shrub and coppice forest, seed germination, vegetative regeneration, and perpetuations of nitrogen-fixing plants such as native legumes.

Cary and Morrison (1995) also investigated the effects of different fire-free intervals in dry sclerophyll forest surrounding the Sydney region, and it general, three effects were identified:

i) Shorter fire-intervals (1-3 and 4-6 years) were linked to a decrease in the number of species, unequal abundance in the community (especially dominant *Proteaceae* shrubs);

ii) Fire interval of 1-6 years was associated with an additional reversible reduction in the number of fire-sensitive species; and

iii) Repetitions of 1-5 year fire intervals were associated with an increase in abundance of herbaceous fire-tolerant species.

Fire regimes can precipitate changes in floristic composition and structure resulting in local extinctions (William, 1991). A High-frequency of low-intensity fires, in particular, may result in one, or a combination of impacts including low species diversity, low ground cover, domination by bracken, tussock grass or sedge, erosion, reduction in terrestrial invertebrate diversity, loss of obligate seed regenerators and loss of soil-stored seed (Gill et al., 1999, Neyland and Askey-Doran, 1996).

2.2.3.1 Dry sclerophyll forests

Dry sclerophyll forests are the dominant vegetation type in south-eastern Australia. They are characterised by relatively open canopies and a dense, low layer of small-leaved, sclerophyllous undershrubs that cover much of the area (Cochrane, 1963). The openness promotes low levels of fuel moisture for extended periods (Bridges, 2004). These forests usually have an upper foliage density of 30-5% and tree height ranging from 5 to 30m (less than 10m = low open-forest, 10-30m = open-forest). The dominants are usually eucalypt species (Buchanan, 1989).

A dry sclerophyll forest has a shrubby understorey (Buchanan, 1989). Apart from the shrubs, the understorey also comprises grasses, sedges and heath species, most of them with fire adaptive traits (Tolhurst et al., 1992). Two factors control the distribution of dry sclerophyll forest. One is well-drained soils. These forests often develop on sandy soils which have little water-retaining capacity (Buchanan, 1989). Eucalypts have developed extensive, deep roots which is advantageous in the dry Australian climates (Tran and Wild, 2000). The other factor is nutrient-poor soils. Phosphorus levels in such soils are unusually low (Buchanan, 1989). Hence, to improve access to nutrient reservoirs, particularly phosphorus, eucalypts have evolved alliances with soil microbes and mycorrhizae. These evidently improve phosphorus intake and ensures eucalypts can grow where other trees starve (Tran and Wild, 2000).

Since the dry sclerophyll forests are extremely fire-prone and have adapted themselves to fire regimes, the intervals at which prescribed burns should be conducted assumes significance. According to Kenny et al. (2003), the accepted fire intervals for the Australian dry sclerophyll

forests has been estimated at between seven and 30 years. Table 2.2 indicates the fire regimes of some ecologically sensitive ecosystems (Tran and Wild, 2000). This suggests that dry sclerophyll forests require frequent fires to flourish, rejuvenate and survive.

Table 2.2 Ecologically sensitive fire regimes worldwide (After Tran and Wild, 2000). Reference to dry sclerophyll forests in the table has been shaded.

Priority for burns/fire regimes	Broad vegetation community type	Fire frequency recommendations		Geographic distribution
		Main	Other	
High	Wet Sclerophyll Forests	5; 20-50 years	More than 200 years	Western, Eastern and Southern Australia
High	Dry Eucalypt Open Forest with Grassy understorey	(minimum of) 4-5 years, 8 years	More than 10 years	Western, Eastern and Southern Australia
High	Dry Eucalypt Open Forest with Shrubby understorey	7-12 years		Western, Eastern and Southern Australia
High	Melaleuca Forest	More than 15 years		Northern Australia (Queensland and Northern Territory) and North-western Tasmania
High	Coastal Woodland Open Forest	(Minimum of) 8-10 years	More than 10 years, including high-intensity fire	Southern Australia
Medium	Subtropical Rainforests	Total exclusion, wildfire events may occur at more than 200-year intervals		Southern Queensland and Northern New South Wales
Medium	Dry Rainforest	Total exclusion		Northern Australia and Eastern Queensland
Medium	Mountain Heath	More than 15 years		Eastern Australia

Medium	Estuarine Complexes	More than 10 years	No fire	Coastal Australia
Medium	Wet Lowland Heath	(Minimum of) 8-10 years, but unsure		Northern and South-eastern Queensland
Medium	Dry Lowland Heath	(Minimum of) 8-10 years, but unsure		South-east Queensland and North Coast New South Wales
Low	Naturally Bare Areas	None states. Most likely fire is unimportant		Most of interior Australia
Low	Cleared Areas	None states. Most likely fire is unimportant		Peri-urban areas

2.2.3.2 Adaptation traits

Since fire and vegetation have had a long association with the Australian continent, native plants have evolved traits that enable them to survive and reproduce in fire-prone environments (Thomson and Leishman, 2005). The tolerance of different plant species to fire varies considerably, reflecting the evolutionary response of plants to fire regimes (Nambiar, 1985). Species possessing fire survival and regeneration adaptations can persist successfully within fire-prone communities. For species lacking adaptive traits, fire-induced mortality acts as an essential factor in regulating population growth and community composition (Bond and Van-Wilgen, 1996).

Plants in fire-adapted vegetation types have two primary ways of keeping their place in the community. Gill (1981) classified plants as non-sprouters or sprouters on the basis of whether mature plants subjected to 100% leaf scorch died or survived the fire.

Most adults of sprouting species also called resprouters or fire tolerant plants regrow from shoots after a fire. These shoots may come from root suckers or rhizomes, lignotubers, epicormic buds or active pre-fire buds (Gill, 1981). Lignotubers are large woody belowground nutrient storage organs which contain buds that can resprout after a fire or other stressful events such as breakage, drought, disease or insect attacks (Attiwill, 1994).

Similarly, epicormic shoots are branches derived from buds along the stem. These allow the plant to continue photosynthesis and growth when the fire has burnt the tree canopy (Skull and Adams, 1996). These features are common in species occurring within fire-prone woodlands, shrublands and savannas, most notably in Eucalyptus species (Gill, 1975).

The adults of non-sprouting species, also sometimes called obligate seeders or fire sensitive plants, die when their leaves are all scorched in a fire. These species rely on seed germination to maintain their presence in their community (Watson, 2001).

Trees in fire-prone areas tend to have thick non-combustible bark which protects perennial buds in the main stems and branches (Lacey et al., 1982). Plants with long, bare trunks and canopies held high above the ground can escape defoliation by fire (Bond and Van-Wilgen, 1996). Some plants, including gumtrees (Eucalyptus spp.) store seeds in woody, fire resistant fruit on the parent plant for release following fire (Auld, 1994).

Survival rates in the field for both non-sprouters and sprouters vary according to fire intensity (Morrison and Renwick, 2000). Some non-sprouters may survive a low-intensity fire if 100% leaf scorch does not occur (Bond and Van-Wilgen, 1996). On the other hand, a very high-intensity fire may result in the death of a high number of individuals within a population that usually resprouts following fire (Knox and Clarke, 2006).

2.2.4 Fire effects on vegetation

Even though fire has been a common agent of temporal and spatial change in the plant species composition of the dry sclerophyll forests of Australia since the mid-quaternary, the long-term effects of fire on Australian plant communities is poorly understood (Raison, 1980). Fire regimes are determined by how often fire occurs (frequency), when it occurs (season) and how intensely it burns (intensity) (Cary and Morrison, 1995). Lang (1999) suggests including fire extent in addition to the three interrelated components mentioned above. There are different fire types: ground fires that burn underground and affect the organic layers in the soil while barely consuming elevated fuels; surface fires that burn just above the ground surface; and crown fires which burn in the canopies of trees (Bond and Van-Wilgen, 1996). Both catastrophic bushfires and the lack of fires have been responsible for species extinction in Australia (Gill, 1994).

The vertical strata into which the dry sclerophyll forests are categorised comprise canopy (trees), elevated (shrubs), near-surface (grass) and surface fuel layer (litter). Fire impacts the different strata of the dry sclerophyll forest differently. The dry sclerophyll forest has been discussed at various strata levels in this research. This is because the vegetation species investigated in this study belong to different vertical layers.

In general, both heat and smoke as a result of the burns are considered the primary fire cues for triggering germination (Penman et al., 2008a). Native species in fire-adapted systems respond positively to fire while exotic species are suppressed (Thomson and Leishman, 2005). No sclerophyllous plant has ever been reported as having been made extinct as a direct result of burning. However, some species have been eliminated from local areas as a result of frequent fires. For example, Mountain Ash and Alpine Ash were lost in some parts of the Central Highlands of Victoria when burnt in 1926 and again in 1939 (Tolhurst et al., 1992).

The time it takes plants, animals and soils to recover after a fire is related to the fire's behaviour (Tolhurst et al., 1992). Fire intensity and rate of fire spread are in turn directly affected by the weight of fine fuel (Bridges, 2004). The vertical distribution of fuel in sclerophyll forests is important as crown fires develop where there is a continuous fuel profile. Where there is only low understorey vegetation, it takes a fire of greater intensity to develop into a crown fire (Smith et al., 2004b).

In the years after a fire, plant communities change in structure, dominance and above-ground composition. Immediately after a fire, the ground is predominantly bare. Sprouts of resprouting species are the first signs of life to reappear. Then with adequate soil moisture, seedlings can be found (Watson, 2001). In many systems, species richness peaks in the early years post-fire, while both short-lived herbs and more persistent species are present (Posamentier et al., 1981). At this stage, the vegetation structure is relatively simple and open (Coops and Catling, 2000). Grass and herb species grow and flower, however, some shrub species will not yet have reached reproductive maturity (Harrold, 1979). Over the years, litter builds up, and structure becomes more complex with canopy cover being restored (Coops and Catling, 2000).

2.2.4.1 Canopy: Trees

Fire impacts on forest stands may include direct effects such as loss of trees and changes in stand structure due to mortality and injury to tree crowns, boles and fine roots near the soil surface. Possible indirect effects of fire include changes in growth due to tree damage, reduced competition or changes in soil moisture and nutrient availability. If prescribed burning reduces competition from understorey vegetation or improves soil fertility, tree growth may be stimulated. On the other hand, if prescribed burning reduces soil fertility substantially, or damages or kills trees, forest stand productivity could decline (Guinto et al., 1999).

Guinto et al. (1999), working in the dry sclerophyll forests in Queensland, Australia, found that while growth responses to long-term fire treatments were variable, repeated low-intensity burning had no adverse effects on stem diameter growth of dominant trees. They also noted that fire and tree growth responses were probably forest type and site specific.

Since fire has been a part of the Australian ecosystem for thousands of years, all vegetation species have regeneration strategies to cope with periodic fire disturbance (Tolhurst et al., 1992). Eucalypt stands are highly resilient to fire disturbance, which has a short and efficient recovery period following a fire, and may experience different structural changes under high fire frequencies compared to other forests owing to their capacity to resprout rather than regenerate from seed. However, the survival of individual eucalypt trees is dependent on their size and physiognomic attributes. Resprouting ability or vigour can decrease when fires occur too frequently due to depletion of carbohydrate reserves (Pekin et al., 2009). Small trees seemed to be slow growing and significantly reduced in size or killed by burning. The main effect of burning on trees was reduced cover. Tree density was seen to remain about the same after burning (Tolhurst et al., 1992).

Eucalypts exhibit a range of features to cope with fire. These features can vary across species and populations subject to fires of various intensities and frequencies (Wardell-Johnson, 2000). They have the ability to resprout through budding from below ground (lignotuber- in young and old trees) or above ground (epicormic buds) (Buchanan, 1989, Burrows et al., 2003). Epicormic buds are hidden and protected by bark. After the removal of leaves by fire, the plant uses energy in the stem and roots to produce clusters of shoots. Strange fuzzy looking trees clothe the landscape; but in a short-time, the natural shape of the tree develops (Buchanan, 1989).

In a study conducted by Burrows et al. (2010) in the jarrah forests of south-west Australia, they concluded that stem growth was consistently lower in the long unburnt treatment compared with burnt treatments. The growth rate of the dominant trees was least affected by competition from other trees. Over the 20 year interval between growth measurements, the large and dominant trees in the long unburnt (25 years) treatment grew slower than the same group of trees in the burn treatments. Hence, they concluded that a long period of fire exclusion could slow tree stem growth. Also, 25 years of fire exclusion in the low rainfall jarrah forest resulted in higher top-soil nutrient levels, but lower tree-stem growth rates, especially of dominated trees, compared with forests that had been burnt, frequently or infrequently.

Abbott and Loneragan (1983) reported an increased stem growth of jarrah for up to four years following a single high-intensity fire that killed (scorched or defoliated) the canopy foliage of most trees. This was attributed to the flush of healthy new foliage that resprouted following the fire, to interrupted flowering and seed production and a post-fire nutrient pulse (Grove et al., 1986).

2.2.4.2 Elevated Fuel Layer: Shrubs

A decline in standing understorey plant species richness with increasing time since fire was demonstrated by Penman et al. (2009). This study conducted in the south-west dry sclerophyll forest of Australia spanned a 33 year post-fire period. They reported an initial increase in species richness during the first four years post-fire. They attributed the changes in species richness to species depletion from the standing flora as well as significant changes in species composition.

Tolhurst (1992) concluded from their study that elevated fuels such as shrubs took much longer to return to pre-burn cover and height. Based on the initial recovery rates for elevated fuels measured by them in their study, they found that shrub height could take at least ten years to return to pre-burning conditions. They also reported that cover could be expected to return to pre-burn levels much faster than height, but overall the structure of elevated fuels could be expected to remain significantly altered for at least ten years. This expectation was found to be consistent with Fox et al. (1979), who found that the height of understorey shrubs increased at a consistent rate for at least ten years after burning. A similar finding was obtained by Will Van Loon (1977), who found that shrub height increased for at least 25 years. Autumn burning changed the structure of the shrub layer more dramatically, increasing the number of new plants, but decreasing the height and cover of existing plants (Tolhurst et al., 1992).

Forests on French Island, Victoria, Australia demonstrate the importance of fires for maintaining a healthy understorey. Around 1980, most of the forest sites had a healthy understorey dominated by tea-tree species and Silver Banksia. It also contained many other shrubs found in the adjacent heathlands. However, in the absence of fire, by around 1995, the dense, healthy understorey had begun to die away. This led to a more open understorey dominated by grasses. This process has continued to the present time. In recent years, a few patches have been burnt which has led to a temporary dense proliferation of some wattle and pea species. However, in general, the understorey has continued to lose its density (Lacey, 2009). This gives an interesting picture of the dynamics of these forests. Prolonged disturbance led to the formation of a dense, healthy understorey while the

absence of burning or other disturbance led to the formation of an open understorey. This goes against the common belief that fire is needed to keep an understorey (Lacey, 2009).

2.2.4.3 Near-surface fuel: Grass

The tussock-grass is well adapted to survive a fire. In the absence of fire, tussock grows and forms a continuous ground cover of both living and dead material. It has also been noted that long unburnt sites are poorer in the number of non-grass species (Gott, 2005).

In their study, Tolhurst et al. (1992) reported that a single autumn burn dramatically increased the tiller density of tussock-grass, but cover and height were reduced. The stimulation of tillers by burning seemed to be greater under autumn conditions than spring conditions, but the regenerative energy was less in autumn, possibility as a result of moisture and temperature stress during the preceding summer and early autumn period.

Sprouts were observed only after the existing plants had been burnt. Sprouts appeared within about four weeks of burning (Tolhurst et al., 1992). The burn extended the period of shoot growth during the first two years after burning. Sprouts and seedlings grew within two months post-fire and burning had a negligible effect on the timing of flowering and seed-set (Tolhurst et al., 1992).

2.2.4.4 Surface fuel: Litter

A fire of moderate to high intensity can completely clear the plant litter from an area, thus resulting in the exposure of bare soil (Tran and Wild, 2000). This leads to increased risk of erosion, especially if sufficient amounts of rainfall occur after the fire. Therefore, apart from reducing the acidity of the soil, fire can accelerate soil erosion and increased runoff (Tran and Wild, 2000). Leaf and twig litter accumulate quickly after burning, and based on a study by Tolhurst et al. (1992), the levels were not significantly different from those in the unburnt areas within a 2-4 year period of the fires.

Litter accumulation after a fire in an open eucalypt forest was investigated by Fox et al. (1979). They concluded that litter accumulation showed an exponential increase with time since fire over a period from one to nine years. They also investigated the litter composition dynamics over this epoch. The bark was found to be the most important component for the first year followed by leaves that formed the bulk of the litter up to nine years after the fire. After that, it was found that wood was the major component of litter.

2.2.5 Fire effects in the landscape

Fire impacts vegetation and its effects on the surrounding environment can be observed in a number of ways. To understand the complex interaction between fires and ecosystems, two different orders of fire effects were proposed by Key (2005). He defined first order effects as consequences of ecological components or conditions that existed before a fire. They are also called immediate or direct effects because of the direct consequences of the fire combustion which may include injury and death of animals and plants, fuel consumption, heating up of the soil and production of smoke and ash (Chen et al., 2008). The interval for sampling first order effects is relatively short following fire since many fire effects fade and tend to get altered by biophysical processes.

Second order effects can be defined as the indirect results of fire and include processes that were not significantly present before the fire but developed indirectly after the fire. Some of these effects include soil erosion, vegetation succession, habitat changes and local climate change (Chen et al., 2008). The second order effects may be observed for many years and are a long term result, in comparison to first order effects which last for only a short time after the fire event.

As a result of vegetation combustion in response to fire, two different post-fire materials are produced. When complete vegetation combustion occurs in the presence of unrestricted oxygen supply, it leads to the formation of ash. Ash is often white or light coloured, and it often linked to high fire intensity. This material does not persist for very long and tends to be almost completely erased by wind and rainfall within a few days after the fire (Pereira et al., 1997b).

On the other hand, when incomplete vegetation combustion occurs under the conditions of restricted oxygen supply, black ash or char is produced which indicates less severe fire behaviour (Pereira et al., 1997b). Char tends to persist for longer in comparison to ash. Hence, fire affected landscapes tend to retain their black appearance even after several months following the fire event.

Fires can alter natural ecosystems in many ways. This includes changing the soil structure (Thomson and Leishman, 2005), nutrient composition and availability (including nitrogen and phosphorus) and soil moisture (Gott, 2005, Guinto et al., 1999), remove shading (Gott, 2005) and litter layer (Thomson and Leishman, 2005) and increasing the light intensity at ground level (Thomson and Leishman, 2005).

Fires can also create appropriate conditions that can stimulate seed germination (Gott, 2005, Thomson and Leishman, 2005) and regeneration of plants from underground organs (Gott, 2005) whilst also removes competitors (Guinto et al., 1999, Thomson and Leishman, 2005). The appropriate conditions for seeds to germinate post-fire include an abundant supply of nutrients from the litter that has been burnt (Raison, 1980) thus establishing direct contact with soil rather than litter, increased available sunlight and greater penetration of rainfall (Buchanan, 1989). Following a fire, there is a temporary increase in the availability of exchangeable calcium, organic carbon, extractable phosphorus, nitrogen and other nutrients (Tomkins et al., 1991). These nutrients are added at the surface from ash deposition due to combustion of organic matter and increased mineralisation from soil pH changes and a reduction in carbon-nitrogen ratios (Waring and Schlesinger, 1985).

Although nutrient availability is higher in the 'ash-bed', nutrient losses are often significant during and following fire, causing long-term nutrient depletions (Grove et al., 1986). Nutrient losses during fire result from volatilisation and removal of nutrients in smoke particles, air currents and updrafts (Raison, 1980).

Furthermore, the post-fire increase in denitrification and leaching acts to reduce soil nutrient concentrations (Flinn, 1985). Whilst the long-term effects of burning regimes on soil fertility and nutrient cycling are difficult to predict, they are dependent on complex interactions between the soil, climate and vegetation (Raison, 1980). Soil nutrient losses due to fire may potentially exceed the benefits of increased nutrient availability, especially in ecosystems with closed nutrient cycles such as rainforests (Waring and Schlesinger, 1985). Hence these ecosystems require long-term stability of efficient nutrient accumulation, retention and recycling.

2.3 Passive remote sensing of burn mapping

Several researchers have demonstrated the utility of remote sensing for mapping fires, burned areas and fire effects on vegetation in a wide range of landscapes across various continents. These include Australian Tropical savannah (Bowman et al., 2003), dry sclerophyll forests (Boer et al., 2008b, Milne, 1986, Penman et al., 2007), African savannah (Hudak and Brockett, 2004, Smith et al., 2005), European Mediterranean environments (Malak and Pausas, 2006, Veraverbeke et al., 2011b), shrublands in Spain (Martín et al., 2002, Roldán-Zamarrón et al., 2006), American Boreal forests (Barrett et al., 2010, French et al., 2008, Murphy et al., 2008) and Boreal forests of Canada (Fraser et al., 2003, Remmel and Perera, 2001). This increasing trend of using remote sensing to map fires coincides with a growing interest in understanding the impacts of fire on vegetation communities (for example Chafer et al., 2004, Chen et al., 2011, Chen et al., 2015, Díaz-Delgado et al., 2003, Edwards et al., 2013, Epting et al., 2005, Hammill and Bradstock, 2006, Lentile et al., 2009, Rogan and Franklin, 2001, White et al., 1996).

2.3.1 Remote sensing platforms and sensors

The analysis of post-fire effects from satellite imagery has been around since the 1980s. Scientists have used air- and space-borne remote sensing for the direct monitoring of active fires, mapping burned areas and assessing the impacts of biomass burning. Measuring fire effects within burned areas continues to remain an active area of research (Roy et al., 2006a). Advancement in computer technology and training in the use of information generated from remotely sensed data has led to an increase in the use of such products by land managers and scientists for forest fire management and research. This has led to a greater demand for the additional fire information products that are currently being developed (Kasischke et al., 2007).

Many satellite remote sensing systems have passive sensors measuring the reflection or emission of electromagnetic radiation from earth's surfaces. Multispectral satellite sensors use radiometers that are sensitive to narrow bandwidths (bands) of the electromagnetic spectrum (Lentile et al., 2006a). Several studies have shown the potential of different remote sensing satellite systems for fire and burn severity mapping and post-fire vegetation recovery. These range from medium to coarse spatial resolution imagery from Landsat (Brewer et al., 2005, Cocke et al., 2005, Hall et al., 1980, Milne, 1986), SPOT (Chafer et al., 2004, Hammill and Bradstock, 2006, Silva et al., 2005), AVHRR (Martin and Chuvieco, 1995a, Remmel and

Perera, 2001) and more recently MODIS (Martín et al., 2002, Roldán-Zamarrón et al., 2006, Walz et al., 2007). Applications of new sensors such as SPOT-Vegetation, and MODIS in the study of fire effects on vegetation is being seen as an attempt to either overcome the limitations found using Landsat or NOAA images or complement their advantages (Martín et al., 2002).

Data from the AVHRR sensor is restricted by a relatively large pixel size (that is 1.1 km). Global satellite data has been obtained at no cost from a series of different satellites for over two decades (Lentile et al., 2006a). The MODIS, in particular, generates the MODIS burned area product (MCD45) (Roy et al., 2006c) which can enable long-term fire information in resource management and environmental assessment (Justice et al., 2002). This is helpful when monitoring fires across a large spatial scale but not so much for small localised fires, such as prescribed burns. Indeed, Boyd et al. (2005) suggest that although fine resolution sensors (between 20 m and 80 m) are sufficient to capture the spatial pattern of burn scars, at coarser resolutions, the burn scars are unlikely to be detected with a high degree of certainty.

Landsat has been the most sought after satellite sensor for mapping burned areas and severity because of the sensitivity of bandwidths to green vegetation and its moderate spatial resolution. This enables the degree of heterogeneity within large remote fires to be assessed (Lentile et al., 2006b). The utility of some satellite sensors with a high spatial resolution and frequent revisit time such as RapidEye and WorldView-2 has not been demonstrated as widely so far. Both these satellite sensors possess a red edge band and, at least, one in the NIR region (Worldview-2 has two that is 770-895nm; 860-1040nm) which suggests that the post-burn landscape devoid of green vegetation could show very low reflectance in the red edge domain and thus help quantify fire effects on vegetation.

Hyperspectral remote sensing sensors are being increasingly used to detect and map burned areas and severity of fires. Hyperspectral remote sensing collects spectral data in many narrow contiguous spectral bands (less than 10nm bandwidth) throughout the visible and solar-reflected infrared portions of the spectrum (Goetz et al., 1985). Such sensors provide detailed spectral information associated with biochemical and physiological properties of vegetation (Gamon et al., 1992). They can also improve the characterisation of burned forests (Numata et al., 2011) and post-fire maps by providing fine-scale quantitative information about post-fire ground cover and conditions (Robichaud et al., 2007).

Since each pixel of a hyperspectral image retains the characteristic features of the individual spectra from each of the components of reflective materials, spectral unmixing of individual

pixels can be achieved by identifying endmember spectra. This can help estimate the fractional component spectra and thus the physical fraction component of the materials within the pixels (Roberts et al., 1993). The applicability of hyperspectral remote sensing to map fractional cover of ash, soil, green and non-photosynthetic vegetation in post-fire areas has also been demonstrated by several researchers (Kokaly et al., 2007, Robichaud et al., 2007). Most hyperspectral sensors are mounted on aircraft and capture data at high spatial resolutions although space-borne sensors (for example Hyperion) also operate. However, as most hyperspectral observations are from aircraft, opportunities for multi-temporal analysis are limited (Lucas et al., 2008).

2.3.2 Remote sensing of vegetation

The spectral range 400 to 2700nm is the most sought after by researchers studying leaf reflectance. This is because incident solar radiation occurs predominantly at these wavelengths and because spectrophotometric instrumentation measures reflectance in this region. In other words, a major portion of leaf reflectance can be detected and measured by remote sensing systems in this wavelength range. The leaf reflectance is low (generally less than 5%) in the ultraviolet and in the far infrared wavelengths (Knipling, 1970). Strong correlations exist between remotely sensed data and the concentration of many biochemical substances and processes within vegetation canopies (Curran et al., 1997).

Remote sensing of vegetation in this range, encompassing the VIS and NIR domains of the electromagnetic spectrum is used to detect the distribution, health, productivity, biomass and physiological status of plants (Buschmann and Nagel, 1993). Such assessments are also of great value for applications such as determining the extent to which vegetation is stressed or at risk from fire (Peñuelas and Filella, 1998). In these broad wavelengths, plant reflectance is governed by leaf pigment properties (mainly chlorophyll), internal structure and the water content (Clevers et al., 2002, Peñuelas and Filella, 1998). For this purpose reflectance signals are usually measured in the green, red and far red region of the spectrum (Buschmann and Nagel, 1993, Peñuelas and Filella, 1998). A typical spectral reflectance curve for green vegetation is shown in Figure 2.1.

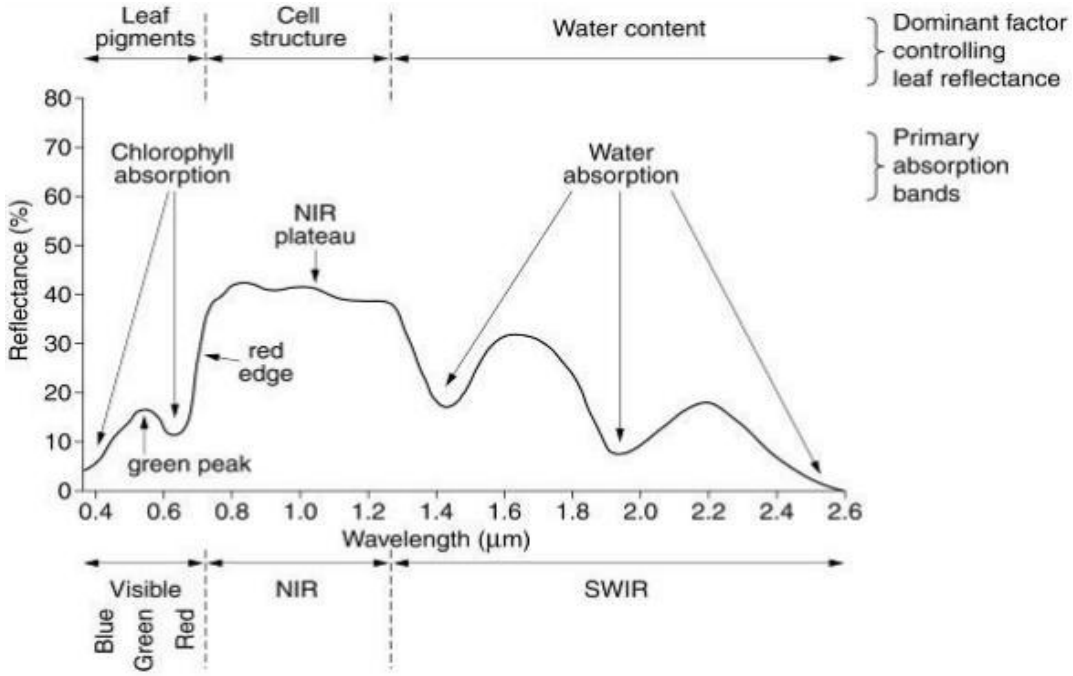

Figure 2.1 Typical spectral reflectance curve for vegetation (From Keyworth et al., 2009, p 20).

In the visible part of the spectrum, 400 to 700nm, the leaf reflectance is quite low, about 10%, with a peak at about 550nm, in the green region. The reflectance in this domain is determined by the pigmentation of the plant, primarily leaf pigments, although the carotenoids, xanthophylls and anthocyanins also have an effect (Gates et al., 1965). For example, chlorophyll absorbs strongly in the blue (450nm) and red (670nm), also known as the chlorophyll absorption bands (Govender et al., 2009). The peak at 550nm accounts for the green colour of plants perceived by the human eye, due to strong absorption of the red and blue wavelengths and the reflection of green wavelengths (Govender et al., 2009, Knipling, 1970). When the plant is subjected to stress that hinders normal growth and chlorophyll production, there is less absorption in the red and blue regions and the amount of reflection in the red wavelength increases (Govender et al., 2009).

The reflectance increases to about 50% in the infrared over the range 700-1300nm but decreases gradually to a low value at about 2500nm (Gausman, 1974). Absorption is high in the visible and the infrared beyond 1300nm, but is minimal across the infrared from 700 to 1300nm.

The strong absorption by a leaf in the infrared beyond 1300nm is mainly due to water absorption (Knipling, 1970). The high infrared reflectivity (between 40–60%) of leaves appears to be caused by their internal cellular structure and discontinuities (Sinclair, 1968) and the

mechanism of internal reflection (Knipling, 1970). The cuticular wax on a leaf is nearly transparent to visible and infrared radiation, and very little of the solar energy incident on a leaf is reflected directly from its outer surface. The radiation is diffused and scattered through the cuticle and epidermis to the mesophyll cells and air cavities in the interior of the leaf. Here the radiation is further scattered as it undergoes multiple reflections and refractions where refractive index difference between aid and hydrated cellulose walls occur (Sinclair, 1968).

Beyond 1300nm, the incident energy upon the vegetation is largely absorbed or reflected with very little transmittance of energy. Three strong water absorption bands are noted at 1400nm, 1900nm and 2700nm (Sims and Gamon, 2003) and other compounds such as lignin, starch and cellulose (Peñuelas and Filella, 1998). A strong correlation exists between reflectance in the MIR region (1300-2500nm) and vegetation water status, and this has been demonstrated by various researchers (Curtis, 1978, Woolley, 1971).

Hyperspectral remote sensing data can provide a significant enhancement of spectral measurement capabilities over conventional remote sensing systems that can be useful for the identification and subsequent modelling of terrestrial ecosystem characteristics (Shafri et al., 2006). Hyperspectral data can also provide improvements in spectral information content when compared with broad bands. Some areas of application include detecting plant stress (Carter, 1993), measuring plant chlorophyll content (Blackburn and Steele, 1999), identifying small differences in percentage green vegetation cover (McGwire et al., 2000), extracting nitrogen and lignin (Curran, 1994) and leaf pigment concentrations (Blackburn and Steele, 1999).

2.3.3 Spectral changes in the landscape and vegetation after fire

Since fire alters the landscape significantly, it must lead to spectral changes in the post-fire landscape. Based on this idea, Chuvieco and Congalton (1988) were the first to consider spectral characteristics of post-burn signals as the starting point for research on remote sensing of burned areas. The spectral signature of burned landscapes immediately following a fire is composed of the reflectance properties of soil, char, ash, moisture and living and dead vegetation (Rogan and Franklin, 2001).

Even though reflectance properties of burned landscapes immediately post-burn are a mixture of different elements, Robinson (1991) pointed out two entirely different post-fire signals. These two distinct spectral signals were chiefly due to the deposition of charcoal (char) and the alteration of vegetation structure and abundance, commonly designated by the fire scar. The

first type of signal results from the complete combustion of vegetation in an unrestricted supply of oxygen. It produces ash which persists for a relatively short duration, as it is almost completely erased by wind and rainfall within a few days or weeks after the fire. The second signal is more stable and results from the incomplete combustion of vegetation under more restricted oxygen supply conditions. This is called char and it can persist for several years. It causes the burnt landscape to appear black (Pereira et al., 1997a).

Since the first signal which results from the deposition of ash persists only for a short time after the fire, research into the spectral characteristics of vegetation structure and abundance as a result of fire gained momentum. Iverson et al. (1989) stated that manifestations of fire damage could be morphological and/or physiological. Morphological damage is commonly seen in post-fire landscapes. It is evident through change in plant shape, defoliation and chlorophyll destruction, charring of roots and stems, loss of branches and alteration of aboveground and belowground moisture (Escuin et al., 2008).

In addition, to morphological damage, Murtha (1978) described physiological damage to vegetation as also being a product of burn severity. It is expressed through decreased plant photosynthates, deterioration of chloroplasts, and interruption of translocation agents such as water.

To be able to remotely assess physiological changes in vegetation in response to a burn event through remote sensing, it is important to understand those domains of the electromagnetic spectrum which are most sensitive to these changes. It is a well-documented fact that blue (400–500 nm), green (500–600 nm), red (600–700 nm) and MIR (1300–1800 nm and 2050–2400 nm) wavelengths are sensitive to the physiological components of vegetation (Nelson, 1983). The NIR (700–1000 nm) region is also known to be sensitive to plant cellular structure and has been routinely used to monitor forest mortality due to fire and other agents (Iverson et al., 1989).

Hence, burn severity mapping is typically conducted using a combination of information from the visible (particularly red), NIR and MIR portions of the electromagnetic spectrum (Barrett et al., 2010). The changes that are exploited by these broad domains of the electromagnetic spectrum are directly related to fire effects on the vegetation and landscape. These are the bands most sensitive to variations in soil colour (VIS and MIR), soil composition (MIR), and moisture and chlorophyll (NIR) which are significantly affected by a burn event (Barrett et al., 2010). Burned surfaces are partially or totally devoid of green vegetation and characterised by dry soil surfaces. The addition of black (that is decrease in reflectance) and grey (that is increase in

reflectance) char to the soil surface, and exposure of soil due to vegetation removal can also alter the reflectance in a post-fire scene (Tanaka et al., 1983).

Fire reduces the absorption of visible wavelengths by leaf chlorophyll as a result of their destruction. This leads to an increase in the reflectance in the visible and a reduction in the NIR region of the electromagnetic spectrum (Escuin et al., 2008, Rogan and Yool, 2001). Leaf tissue damage leading to a decrease in total NIR reflectance is also diagnostic of leaf water stress (Jensen, 2009). In contrast, MIR reflectance typically increases following a fire due to a reduction in crown shadow, tree canopy and a decrease in canopy moisture (Van Wagtendonk et al., 2004b, White et al., 1996). Therefore, from a remote sensing perspective, fire altered surfaces are brighter than unburned surfaces in the VIS and MIR wavelengths (Rogan and Yool, 2001).

2.3.4 Spectral vegetation indices for fire-related applications

This section of the chapter covers a comprehensive list of Vegetation Indices (VIs) that have been used to map and study the impact of fire on vegetation. Most of these indices were established to assess different characteristics of vegetation cover mainly foliage pigment content (for example chlorophyll, carotenoid) and canopy water content.

Traditional remote sensing approaches used for monitoring vegetation make use of VIs. A VI is made up of a combination of various spectral bands. The aim is to enhance the spectral contribution of green vegetation while minimising contributions from soil background, sun angle and atmosphere (De Jong and Epema, 2001). They are dimensionless, radiometric measures usually involving a ratio and/or linear combination of two or more satellite image bands (Huete, 1988). Because of their simplicity, VIs have been used extensively to map biophysical parameters such as LAI, above ground biomass and more recently mapping burn area and severity. Numerous VIs have been developed to make quantitative estimates of different vegetation metrics such as percentage ground cover, leaf area index, plant height, biomass and plant population (Perry Jr and Lautenschlager, 1984). They show better sensitivity than individual spectral bands for the detection of biomass (Bannari et al., 1995).

VIs are useful in the interpretation of remote sensing images for a wide range of applications including detecting land use changes, and evaluating vegetative cover density. A VI is formed from a combination of spectral bands whose values are divided, multiplied, added together or formed as a linear equation or ratio. This produces a single value that indicates the amount of characteristics of vegetation cover (De Jong and Epema, 2001, Jackson and Huete, 1991,

Wiegand et al., 1991). The different vegetation covers sometimes can be distinguished according to their unique spectral behaviour in relation to overall ground elements (Tucker, 1979).

The VIs presented in this thesis are categorised into six groups according to the information obtained from them. These groups are as follows: 1) greenness 2) chlorophyll 3) leaf pigment content, 4) light use efficiency 5) water content, 6) dry plant matter and 7) fire related.

2.3.4.1 Greenness

Indices responsive to vegetation 'greenness' belong to the group of greenness vegetation indices. Such indices are combinations of reflectance measurements that are sensitive to the combined effects of foliage chlorophyll concentration, foliage clumping, canopy leaf area and canopy architecture.

a. Normalised Difference Vegetation Index (NDVI)

One of the oldest, most well known and most frequently used VI in various environmental applications is the NDVI. It was proposed by Rouse et al. in 1973. It is one of the two most popular satellite derived VIs identified in literature dealing with burn severity measures (Chafer, 2008).

When vegetation is healthy and green, there is high reflectance in the NIR (due to scattering within leaf cells) and low reflectance in the red spectral region (due to absorption by chlorophyll) which results in high NDVI values (Tucker, 1979). This combination of its normalised difference formulation and use of the highest absorption and reflectance regions of chlorophyll make it robust over a wide range of conditions.

Equation 2.1 shows how NDVI is derived.

$$\frac{NIR - RED}{NIR + RED} \quad \textbf{(2.1)}$$

Narrowband versions of NDVI have also been used when field hyperspectral radiometers and airborne hyperspectral scanners have been used to capture spectral data (for example Peñuelas et al., 1997, Serrano et al., 2000, Sims and Gamon, 2003). This is shown in equation 2.2.

$$\frac{R800 - R680}{R800 + R680} \quad \textbf{(2.2)}$$

Peñuelas et al. (1997) have reported that this narrowband version of NDVI was found to be highly correlated with the NDVI values calculated from the same data following the spectral NOAA-AVHRR bands. Whilst NDVI has been related to canopy cover, leaf area and the fraction of Photosynthetically Active Radiation (fPAR) (Numata et al., 2011) it is increasingly being used for fire-related vegetation mapping. This includes the utility of NDVI in mapping burn areas (Chuvieco et al., 2002, Pereira et al., 1997a) and monitoring and assessing post-fire vegetation recovery (Díaz-Delgado et al., 2003, Jakubauskas et al., 1990). This is possible because of its strongly established relationship with aboveground biomass in various ecosystems (Henry and Hope, 1998).

Spectral reflectance curves for healthy vegetation show a dramatic increase in reflectance in the NIR portion, while the adjacent red portion of the spectrum absorbs the light. This dramatic difference in spectral response is accentuated with NDVI, for which burned areas respond with an increase in red reflectance and a decrease in NIR reflectance. The value of this index ranges from -1 to +1; however the common range for green vegetation is 0.2 to 0.8. One known caveat of NDVI is its propensity to saturate in dense vegetation conditions when Leaf Area Index (LAI) becomes high (Potter et al., 2012).

b. Global Environment Monitoring Index (GEMI)

This index was developed by Pinty and Verstaete (1992) to give a measure of the general status of vegetation using satellite remote sensing as shown in equation 2.3.

$$\gamma(1 - 0.25 \times \gamma) - \left(\frac{RED - 0.125}{1 - RED}\right) \quad \textbf{(2.3)}$$

$$Where\ \gamma = \frac{2(NIR^2 - RED^2) + 1.5NIR + 0.5 \times RED}{NIR + RED + 0.5}$$

In comparison to NDVI, GEMI is less affected by soil and atmospheric variations (Katagis et al., 2011). It has also proven to be more sensitive in burned land discrimination (Chuvieco et al., 2002). Since GEMI is sensitive to the general status of vegetation, it should be sensitive to fire effects on vegetation. Through their research, Katagis et al. (2011) concluded that GEMI performed slightly better than the other indices (that is NDVI, SAVI and BAI) to map burned areas and monitor post-fire vegetation recovery. Trombetti et al. (2006) reported similar findings wherein GEMI was the most important variable useful in discriminating burnt areas when only post-fire data was considered. However, when change between pre- and post-fire seasons was considered, vegetation indices such as NDVI and GNDVI highlighted more important changes.

2.3.4.2 Chlorophyll

The concentration of chlorophyll pigments relate strongly to the photosynthetic potential of a plant and therefore are indicative of its overall physiological status (Blackburn and Steele, 1999, Peñuelas and Filella, 1998). Spectral bands in the VIS and NIR regions of the spectrum have been used to develop a number of indices for monitoring, analysing and mapping temporal and spatial variation in vegetation structure and certain biophysical parameters (Gitelson et al., 2002a) because of the sharp contrast between soil and leaf reflectance in these spectral bands (Peñuelas and Filella, 1998).

a. Transformed Chlorophyll Absorption in Reflectance Index (TCARI)

This index is a variant of the Modified Chlorophyll Absorption in Reflectance Index (MCARI) proposed by Daughtry et al. (2000) which in turn was a variant of the Chlorophyll Absorption in Reflectance Index (CARI) developed by Kim et al.(1994). CARI was designed to reduce the variability of the photosynthetically active radiation due to the presence of diverse non-photosynthetic materials. It uses bands corresponding to the minimum absorption of the photosynthetic pigments, centred at 550nm and 700nm in conjunction with the chlorophyll *a* maximum absorption band, around 670nm (Haboudane et al., 2002).

MCARI measures the depth of chlorophyll absorption at 670nm relative to the reflectance at 550nm and 700nm. Kim et al. (1994) showed that change of background reflectance affected the reflectance slope between 550nm and 700nm and to compensate for these effects, the TCARI was conceived by Haboudane et al. (2002). It is defined by equation 2.4 as shown below:

$$3[(R760 - R670) - 0.2(R700 - R550) \times \left(\frac{R700}{R670}\right)] \quad \textbf{(2.4)}$$

This intrinsic index is still sensitive to the underlying soil reflectance properties, particularly for low LAIs (Rondeaux et al., 1996). In order to address that, TCARI is divided by the Optimised Soil-Adjusted Vegetation Index (OSAVI) which was proposed by Rondeaus et al. (1996). It is defined by equation 2.5.

$$\frac{(1 + 0.16) \times (\frac{R800}{R670})}{R800 + R670 + 0.16} \quad \textbf{(2.5)}$$

The application of the ratio TCARI/OSAVI has been demonstrated by several researchers to make accurate predictions of crop chlorophyll content from hyperspectral remote sensing imagery (Haboudane et al., 2002, Wu et al., 2008). This index has however not been used to estimate changes in chlorophyll content of vegetation in response to wildfires or prescribed burns. It is calculated as shown in equation 2.6

$$3[(R760 - R670) - 0.2(R700 - R550) \times \left(\frac{R700}{R670}\right)] \times \frac{R800 + R670 + 0.16}{(1 + 0.16) \times (\frac{R800}{R670})} \quad \textbf{(2.6)}$$

2.3.4.3 Leaf pigments content

The leaf pigment VIs is designed to provide a measure of stress-related pigments present in vegetation. Stress-related pigments in leaves include carotenoids and anthocyanins, which are present in higher concentrations in stressed vegetation. These VIs are not designed to measure chlorophyll.

a. Carotenoid Reflectance Index 1 and 2 (CRI1 & CRI2)

Both these indices measure reflectance that is sensitive to carotenoid pigments in plant foliage. Higher CRI1 values mean greater carotenoid concentration relative to chlorophyll. CRI2 which

is a modification of CRI1 provides better results in areas of high carotenoid concentration. These are indicative of plant stress (Gitelson et al., 2002b). Higher CRI1 and CRI2 values mean greater carotenoid concentration relative to chlorophyll. These two indices are defined by equations 2.7 and 2.8 as shown below:

$$\frac{1}{R510} - \frac{1}{R500} \quad \textbf{(2.7)}$$

$$\frac{1}{R510} - \frac{1}{R700} \quad \textbf{(2.8)}$$

The value of both these indices range from 0 to more than 15, however, the common range for green vegetation lies between 1 to 12 for CRI1 and 1 to 11 for CRI2. CRI1 was used in a study of burn severity using hyperspectral data obtained from Hyperion (Numata et al., 2011). Results of this research suggested that although both NDVI and CRI are related to the amounts of chlorophyll in leaves, NDVI becomes saturated or insensitive to changes in vegetation with high leaf area index values while CRI could distinguish burnt forests from unburnt ones, even as forest recovery occurred.

2.3.4.4 Light use efficiency

These indices are designed to provide a measure of the efficiency with which vegetation can use the incident sunlight for photosynthesis. Such indices use reflectance measurements in the visible spectrum to take advantage of relationships between different pigment types to assess the overall light use efficiency of vegetation.

a. Photochemical Reflectance Index (PRI)

This index is sensitive to changes in carotenoid pigments (particularly xanthophyll pigments) in live foliage. Carotenoid pigments are indicative of photosynthetic light use efficiency and are found in higher concentrations in plant leaves that are either stressed or senescing/dead (Gamon et al., 1992). It is also a fundamental determinant of Net Primary Productivity (NPP) (Numata et al., 2011) This index is defined by equation 2.9.

$$\frac{R531 - R570}{R531 + R570} \quad \textbf{(2.9)}$$

The value of this index ranges from -1 to +1. The common range for green vegetation is -0.2 to +0.2 (ENVI, 2009). Although this narrowband index is applied to study vegetation productivity and stress, it has also been applied to map burn severity using hyperspectral datasets (Numata et al., 2011).

b. Structure Insensitive Pigment Index (SIPI)

This index is related to the ratio between carotenoids and chlorophyll and may be useful in assessing changes in these pigments (Peñuelas et al., 1995). It is defined by equation 2.10.

$$\frac{R800 - R445}{R800 - R680} \quad \textbf{(2.10)}$$

SIPI is estimated using blue, NIR and red bands that are sensitive to both carotenoid and chlorophyll pigment changes. Increases in SIPI are thought to indicate canopy stress which is related to carotenoids. It can be used to monitor vegetation health, physiological stress, crop production and yield analysis. The value of this index ranges from 0 to 2. The common range for green vegetation is 0.8 to 1.8 (ENVI, 2009).

c. Normalised Phaeophytinisation Index (NPQI)

NPQI has been proven to be a good measure of chlorophyll degradation (Barnes et al., 1992) and an early detector of vegetation stress in some studies (Jurskis et al., 2003). It is defined according to equation 2.11.

$$\frac{R415 - R435}{R415 + R435} \quad \textbf{(2.11)}$$

d. Normalised Chlorophyll Pigment Index (NCPI)

This index is primarily used for the assessment of chlorophyll content of crop canopies (Merzlyak et al., 1999). It uses a combination of blue and red bands. An increase in NPCI indicates vegetation senescence during which there is a loss of chlorophyll. It is defined by equation 2.12

$$\frac{R680 - R430}{R680 + R430} \quad \textbf{(2.12)}$$

2.3.5.5 Water content

These VIs provide a measure of the water content in the foliage canopy. Water content is a key attribute of vegetation because higher water content indicates healthier vegetation. Most of these vegetation indices use bands in the Infrared and Short-Wave Infrared (SWIR) to take advantage of known absorption features of water by the leaves.

a. Water Index (WI)

The WI is a reflectance measurement that is sensitive to changes in canopy water status. With an increase in water content of vegetation canopy, the strength of absorption around 970nm increases relative to 900nm (Peñuelas et al., 1997). This index has been found to be highly correlated with plant water content in several species of trees, shrubs, crops and grasses. This index is very useful for monitoring canopy stress and fire hazard condition analysis (ENVI, 2009). It is defined as shown in equation 2.13 below.

$$\frac{R900}{R970} \quad \textbf{(2.13)}$$

The common range for green vegetation is between 0.8 to 1.2 (ENVI, 2009). Some of its fire related applications include its ability to detect regeneration from burned landscapes. Trombetti and Lasaponara (2005) used this index in along with others derived from MODIS data to detect fire effects on forests. They suggested that when plants dried, the value of this index decreased, however, it was not very sensitive until the drying process was well in advance. Another study by Rahman and Gamon (2004) concluded that WI performed better than NDVI at detecting fresh and dry biomass, water content and plant area index of burned and unburned grasslands.

b. Moisture Stress Index (MSI)

This vegetation index is sensitive to increasing leaf water content. As the water content of leaves in vegetation canopies increases, the strength of the absorption around 1650nm increases. Because absorption at 820nm is nearly unaffected by changing water content, it is used as the reference wavelength (Ceccato et al., 2001). This MSI is inverted relative to the other water VIs;

higher values indicate greater water stress and less water content. MSI is defined as shown in equation 2.14 below.

$$\frac{R1650}{R820} \tag{2.14}$$

The value of this index ranges from 0 to more than three. The common range for green vegetation is between 0.4 and 2 (ENVI, 2009). Applications of this index include canopy stress analysis, fire hazard condition analysis and studies of ecosystem physiology. Hunt and Rock (1989) have shown that the MSI computed at the leaf and landscape scale using Daedalus Thematic Mapper Airborne Simulator data performed better when used for the estimation of equivalent water thickness than for the estimation of vegetation status indicators.

c. Normalised Difference Water Index (NDWI)

This index is sensitive to changes in vegetation canopy water content because the 860nm and 1240nm wavelengths are located in the high reflectance plateau where the contribution of vegetation scattering to reflectance is similar (Roberto et al., 2011). This index is defined in equation 2.15.

$$\frac{R860 - R1240}{R860 + R1240} \tag{2.15}$$

The value of this index ranges from -1 to +1. The common range for green vegetation is -0.1 to +0.4 (ENVI, 2009). A study conducted by Serrano et al. (2000) revealed that both NDWI and WI were reliable indicators of relative water content at the leaf, canopy and landscape scale. This index has been used to map burn area (Trombetti et al., 2006), fire effects (Trombetti and Lasaponara, 2005) and burn severity mapping using Hyperion hyperspectral datasets (Numata et al., 2011).

d. WI/NDVI

This ratio was tested by Peñuelas and Inoue (1999) while intending to improve WI as a leaf Relative Water Content (RWC) indicator by dividing by NDVI. The rationale behind this approach was that while WI changed with structural leaf characteristics such as cell wall elasticity, NDVI followed both structural and colour changes (due to loss of pigments) in drying

leaves. As a result, this ratio is more successful for estimating RWC than the WI itself. This ratio is defined in equation 2.16 below.

$$\frac{R900}{R970} \times \frac{(R800 + R680)}{(R800 - R680)} \quad \textbf{(2.16)}$$

The applicability of this index to detect burnt areas and fire effects has been demonstrated by Trombetti et al. (2006) and Trombetti and Lasaponara (2005) respectively. Results indicated that the ratio worked well across different fire-affected areas. It was also shown that post-fire characterisation was more evident when this ratio was used as opposed to using water indices such as WI and NDWI.

2.3.4.6 Dry plant matter

Dry plant material is often classed as Non-Photosynthetic Vegetation (NPV). This comprises non-green plant parts such as dry leaves, bark and wood. Spectrally, NPV is highly variable. Both soil and litter are not easily discriminated in the VIS and NIR wavelengths.

a. Cellulose Absorption Index (CAI)

A lignocellulose absorption trough at 2100nm in the reflectance spectra of dried shrubs has been observed (Nagler et al., 2000). This is likely due to the presence of cellulose, hemicellulose and lignin (Kumar and Skidmore, 2006). Using this spectral feature, the spectral index CAI was developed by Nagler et al. (2003) and is defined by equation 2.17.

$$0.5 \times (R2020 + R2200) - R2100 \quad \textbf{(2.17)}$$

This index has been used for discriminating plant litter from soil (Nagler et al., 2003).

2.3.4.7 Fire related

These indices have been developed over the last two decades due to the growing interest in mapping burned areas and burn severity by remote sensing scientists.

a. Normalised Burn Ratio (NBR)

Lopez Garcia and Caselles (1991) developed the Normalised Difference (ND) index to enhance the biophysical relationships with burned vegetation. This ND was subsequently modified slightly by Key et al. (2002) and named the NBR. Since then, the Landsat sensor-based NBR is the most widely used burn index on large wildfires (more than 200 ha) for burn area, perimeter and severity detection (Cocke et al., 2005).

NBR is defined as shown in equation 2.18 below.

$$\frac{NIR - MIR}{NIR + MIR} \quad \textbf{(2.18)}$$

NBR is similar to the NDVI and is often employed in remote sensing of burned landscapes and to determine burn severity. It uses the reflectance from the NIR and MIR bands because these bands are most sensitive to vegetation change due to fire (Norton et al., 2009). Healthy green vegetation reflects NIR energy. Conversely, NIR response decreases where ever the vegetation is sparse. Rock and bare soil reflect maximally in MIR bands. Imagery captured over a forest pre-burn will have high NIR band values and very low MIR band values. Post-burn imagery will have low NIR and high MIR values (Clark and Bobbe, 2006). NBR is directly controlled by surface conditions, such as canopy and soil surface charring, and not subsurface conditions, such as depth of duff composition (Epting and Verbyla, 2005).

The difference in the reflectance between these two wavelengths can be attributed to fire-induced changes in soil moisture, canopy cover, biomass, charring and exposed soil (Malone et al., 2011). In the northern hemisphere, NBR has been shown to be superior to NDVI in terms of measuring burn severity (Epting et al., 2005, Lopez Garcia and Caselles, 1991). However this has been questioned by Roy et al. (2006b). A major limitation in using NBR for forest fire related studies in Australia is that Landsat data is not always available over south-eastern Australia where cloud cover is regular (Chafer et al., 2004, Hammill and Bradstock, 2006).

Since fire effects on vegetation produce a reflectance increase in the red and MIR spectral regions and a drop in the NIR reflectance (Pereira et al., 1999), bi-temporal image differencing is frequently applied on pre- and post-fire NDVI or NBR images (Veraverbeke et al., 2011b). The advantage of these pre/post-fire differenced indices is that they permit a clear discrimination between unburned sparsely vegetated areas and burnt areas, which has been identified as a key obstacle in mono-temporal imagery (Key and Benson, 2005).

b. Difference Normalised Burn Ratio (dNBR)

The temporal difference between the pre- and post-burn NBR values is called Normalised Difference Burn Ratio (dNBR). It is believed that this difference between the two burn epochs presents sufficient distinction between burnt and unburnt areas whilst providing a scaled measure of the magnitude of change caused by fire, hence the burn severity (Van Wagtendonk et al., 2004b). As shown below in equation 2.19, dNBR is composed of the post-fire NBR subtracted from the pre-fire NBR (Norton et al., 2009).

$$NBR(prefire) - NBR\ (postfire) \tag{2.19}$$

The multi-temporal dNBR index has been assumed to be directly proportional to burn severity. This has been demonstrated by several researchers (for example Cocke et al., 2005, Epting et al., 2005, Kokaly et al., 2007, Van Wagtendonk et al., 2004b). It is for this reason that dNBR is widely used by land managers in the US to assess landscape-level burn severity (Clark and Bobbe, 2006, Lutes et al., 2006).

c. Burn Area Index (BAI)

This index was defined by Martin (1998) and is used to discriminate fire affected areas. It is the only index specifically designed for post-fire effects applications which focus on the red-NIR feature space (Harris et al., 2011). This index is computed from the spectral distance from each pixel to a reference spectral point, where recently burned areas tend to converge and aims to increase the charcoal signal this way (Chuvieco et al., 2002). It is defined in equation 2.20 below.

$$\frac{1}{[(0.1 + RED)^2 + (0.06 + NIR)^2]} \tag{2.20}$$

BAI has been applied to map burned areas (Boschetti et al., 2010, Katagis et al., 2011) and assess burn severity (Harris et al., 2011). Although Chuvieco et al. (2002) have demonstrated BAI's higher sensitivity than NDVI, GEMI and SAVI to detect burnt areas, they do emphasise that since BAI was designed to enhance the charcoal signal in post-fire images, it presents potential confusion with low-reflectance targets such as water bodies and cloud shadows.

d. Char Soil Index (CSI)

This index is defined as the simple ratio between the NIR and SWIR reflectance as shown in equation 2.1217 below.

$$\frac{NIR}{SWIR} \tag{2.21}$$

Its applicability to estimating burn severity was first demonstrated by Smith et al. (2005). It is also suitable for mapping burnt areas (Boschetti et al., 2010, Veraverbeke et al., 2011a) given that it makes use of the characteristic post-fire reflectance increase in the SWIR spectral domain (1300-2500nm) in combination with the NIR reflectance drop due to vegetation removal.

e. Mid-InfraRed Burn Index (MIRBI)

This index which was conceived by Trigg and Flasse (2001) has been used to discriminate burned landscapes from unburned ones. It is defined in equation 2.22.

$$10lSWIR - 9.8sSWIR + 2 \tag{2.22}$$

As shown above, this index uses only SWIR wavelengths. It makes use of the increase seen in this region of the electromagnetic spectrum following a fire. This index has been used to map burned areas (Boschetti et al., 2010, Smith et al., 2007) and measure burn severity (Harris et al., 2011).

2.3.5 Derivative spectroscopy

Derivative analyses of spectra have been shown to be superior to broadband ratio indices in plant stress detection (Estep and Carter, 2005). Derivative analysis of spectral data is considered useful in removing the effects of illumination variations (Demetriades-Shah et al., 1990, Tsai and Philpot, 1998). This is particularly important in research where spectral data is captured across various temporal scales, spanning across different seasons. Derivative analysis has also been shown to be effective in reducing background effects when the spectral pattern of background materials have a lower frequency of variation (Pu and Gong, 2011).

Various studies have successfully employed derivative analysis for extracting parameters from vegetation (Estep and Carter, 2005, Kumar and Skidmore, 1998, Smith et al., 2004a). However, higher-order spectral derivative processing is susceptible to noise while lower-order derivative

(first-order derivative) is less sensitive and hence more efficient in operational remote sensing (Pu, 2012).

2.3.6 A review of studies involving remote sensing of fire effects

The assessment of fire-effects, both short- and long-term, at various temporal and spatial scales has been conducted using a broad range of *in situ* and remote methods. Some selected examples from the literature are presented in a table in Appendix 10.1. This table provides examples of studies that have employed remote sensing to quantify and map fire effects in the landscape for a wide variety of forest types. This table also highlights the evolving nature of both field data capture and remote sensing methods employed to quantify fire effects. The fire effects most commonly studied using remote sensing includes burn area mapping, severity and post-fire vegetation recovery.

Since the mid-1980s, numerous remote sensing techniques have been developed to assess how 'severe', in terms of ecological change, a fire is on both local and regional ecosystems (Lentile et al., 2006a). Early studies inferred that fire caused changes in vegetation condition which were measured by analysing spectral changes. However, the more recent studies have sought to relate ecological measures to fire-induced physical changes on the land surface.

Hall et al. (1980) classified multi-temporal Landsat Multi-Spectral Sensor (MSS) data of tundra fires in north-western Alaska into light, moderate and severe fires as defined by the abundance of live post-fire vegetation. Their findings reported that the most severely burned portion showed minimal recovery based on the Landsat-derived spectral data.

Milne (1986), used both the supervised and unsupervised classification of Landsat data to examine its usefulness in mapping and monitoring burn severity and vegetation regeneration patterns in south-east Australia. It was concluded from this research that the large-area repetitive type coverage of Landsat imagery in digital form provide a useful dimension to environmental studies concerned with the mapping and monitoring of Earth resources, especially those subject to rapid and dramatic change. Another study based its assumptions on the fact that pattern of post-fire vegetation regeneration of a burnt area could be monitored using sequential Landsat images and that the apparent recovery sequence is usually associated with an initial increase in reflectance in both the visible and infrared parts of the spectrum followed by a gradual decrease in the reflectance values. The first change was attributed to the exposure of underlying rock and

soil surface due to removal of dead vegetation and ash while the latter follows the reappearance of photosynthetically active vegetation colonising the bare surface (Milne, 1986).

Similarly, Jakubaukas et al. (1990) concluded from their research that patterns of post-fire vegetation recovery and change were evident in the classified Landsat data. The researchers also concluded that their results agreed with vegetation regrowth trends observed in ground-based studies of fire damaged areas. White et al. (1996) used field data, post-fire aerial photographs and Landsat data from a variety of vegetation types (Steppe, shrublands, grasslands, conifer forests) in Montana to compare remotely sensed measures of severity and achieved a classification accuracy of 63%.

More recent burn severity studies have investigated the use of various spectral indices. The Normalised Differenced Vegetation Index (NDVI) has been widely used to assess post-fire vegetation regrowth. This is appropriate as long as a direct change in green vegetation cover is the main ecological process being measured. Several studies have applied NDVI to assess post-fire effects (Chafer et al., 2004, Hammill and Bradstock, 2006, Remmel and Perera, 2001, Solans Vila and Barbosa, 2009). Chafer et al. (2004), for example, used NDVI from SPOT data to deduce burn severity in the Australian woodlands. They achieved a classification accuracy of 88%. Remmel and Perera (2001) derived NDVI from AVHRR data to map fire extents. They reported that ground-truthed fire sizes and shapes correlated with the AVHRR/NDVI-mapped areas.

Apart from NDVI, other spectral indices that have been employed include the Normalised Burn Ratio (NBR). The NBR has been most commonly used for burn severity assessment of forested regions because it incorporates information about the spectral changes at the surface to infer post-fire effects. This index incorporates the observed decrease in spectral reflectance in the visible-mid-infrared region with a corresponding increase in mid-infrared reflectance. The modification of the NBR, differenced Normalised Burn Ratio (dNBR) is also used in conjunction with NBR for mapping burn severity (Brewer et al., 2005, Cocke et al., 2005), and infer the degree of post-fire ecological change (Epting and Verbyla, 2005, Lentile et al., 2007). In comparison to the use of NDVI, NBR has provided a higher classification accuracy of burnt areas and burn severity.

A common approach that demonstrates the utility of NBR and dNBR is through correlation with a field measure of fire/burn severity such as the Composite Burn Index (CBI). CBI is derived by making visual estimates of the impacts of fire in five different strata (substrates, herbs/low

shrubs, tall shrubs/saplings, intermediate trees and big trees), and averaging the values for each stratum for a single measure (Key and Benson, 2006). For example, Miller and Yool (2002) conducted a study on post-fire canopy mapping using dNBR severity maps and supervised classifications generated from Landsat TM in the Conifer forests and woodlands of the Western United States.

Cocke et al. (2005) derived dNBR from Landsat ETM+ data and supplemented it with CBI field measures both pre- and post-fire in the pine forests of Western United States. They reported that this methodology accurately identified severely burned areas. Brewer et al. (2005) followed a similar approach and derived dNBR from Landsat TM data in a variety of land cover types (for example grassland, shrubland, forests) in the western United States. They reported a 96% burn severity mapping accuracy when the land cover was considered.

Other studies have reported mixed correlation results between dNBR and CBI. For example, post-fire vegetation interaction was investigated by Epting and Verbyla (2005) using dNBR and other indices derived from Landsat TM imagery. They reported an R2 value of 0.52 between dNBR and Composite Burn Index (CBI) for different fire events. Miller and Thode (2007) reported an R^2 value of 0.49 between CBI and dNBR maps to quantify burn severity in conifer forests and shrublands of Sierra Nevada. However, a modified version of dNBR, the relative differenced normalised burn ratio (RdNBR) showed a higher correlation with CBI with an R2 value of 0.61. Murphy et al. (2008) have also reported a low R2 value 0.36 between dNBR and CBI. But despite these results, the general consensus across the United States is that NBR or dNBR can be used to generate maps of burn severity across different vegetation and ecosystem types based on Landsat TM/ETM+ or SPOT data (Kasischke et al., 2007, Key, 2005).

The use of differenced satellite images captured before and after a wildfire has become the most accepted methodology used in analysing post-burn severity (Chafer et al., 2004, Cocke et al., 2005, Díaz-Delgado et al., 2003, Malak and Pausas, 2006). The method is based on differencing pre- and post-fire satellite images using specific electromagnetic wavelengths that are sensitive to the effects of fire (that is changes in green vegetation, moisture or bare ground). This method has been used to examine variations in burn severity (Chafer et al., 2004, Díaz-Delgado et al., 2003). Although numerous remote sensing investigations on burn severity mapping have been undertaken, reliable accuracy (that is approximately 85%) is yet to be gained using standard methods over different vegetation types (Michalek et al., 2000, Pereira, 1999).

The use of remote sensing for burn severity and vegetation mapping and monitoring in response to fire has been long researched since the 1980s. However, what has changed since this time is the way in which remote sensing is used. Researchers have moved from applying image differencing based on supervised and unsupervised classification to spectral indices based analysis or hybrid approaches using indices and vegetation classification algorithms. Some of the spectral indices most useful for monitoring fire effects in the landscape are NDVI and dNBR. Landsat TM is found to be the most popular platform for observing these effects. However, hyperspectral satellite sensors such as Hyperion on board Earth Observing-1 Mission satellite are increasingly being used in the last few years. This is because studies have indicated that discrete narrowband data from the electromagnetic spectrum is more sensitive in obtaining qualitative and quantitative information on vegetation condition as compared to broad wavebands (Carter, 1998, Thenkabail et al., 2002).

2.4 LiDAR and its applications in burn mapping

Light Detection and Ranging or LiDAR is an active remote sensing technology that enables the acquisition of highly accurate measurements of an object's dimensions, spatial positioning, texture and colour in both two and three dimension (Keane, 2007). LiDAR is similar to radar in that it exploits electromagnetism for the detection and ranging of spatial objects, and it is similar to optical forms of remote sensing in the sense that it uses optics for the refraction of these electromagnetic waves (Van Leeuwen and Nieuwenhuis, 2010). These systems enable the non-destructive, rapid and precise digitisation of physical scenes into three-dimensional (3D) point clouds (Dassot et al., 2011).

The basic measurement made by a LiDAR sensor is the distance between itself and a target surface. This is obtained by determining the time interval between an emitted laser pulse and its return after being reflected off a target. Multiplying this time interval with the speed of light yields a measurement of the round-trip distance travelled. Dividing this value by two gives a measure of the distance between the sensor and the target (Lefsky et al., 2002).

The frequency of the pulse emission is such that a large number of points are recorded per survey, thus the resulting dataset is called a 'point cloud' which can contain about 40 million reflection points (Keane, 2007). The intensity of the return is also recorded and can be quantised to either 8 or 16 bits (Watt and Donoghue, 2005). Intensity is defined as the ratio of the strength of reflected light to that of emitted light. It is influenced by the reflective ability of the target (Song et al., 2002).

A laser scanner sensor can be operated on different platforms (that is spaceborne, airborne or ground-based). When in the air, it is usually referred to as Airborne Laser Scanner (ALS) whereas on the ground it is either a Terrestrial Laser Scanner (TLS) or terrestrial LiDAR. Deployment of these sensors on different platforms enable acquisition of a variety of information at various spatial scales that can be used for a variety of applications (Lim et al., 2003).

TLS technology has evolved rapidly in recent years. Key improvements in the area of speed of data acquisition and ease of deployment have made laser scanning more feasible as a data collection method for a wide area of applications (Keane, 2007). It has also enabled successful measurement of complex structures in the field with both high accuracy and precision (Hopkinson et al., 2004). The most common TLS sensors are manufactured by the same companies that build airborne LiDAR sensors such as Leica, Optech and Riegl; although there are other systems as well (for example Trimble, Topcon and research systems like Echidna).

Given improvements in this technology over recent years, the use of such sensors has resulted in the proliferation of a large number of applications as opposed to traditional surveying and engineering applications. The various applications involve digitising external surfaces of buildings and archaeological sites (Dassot et al., 2011), monitoring of building, bridges and open mines (Popescu, 2011), and recording geological structures and vegetation analysis (for example Danson et al., 2007, Jupp et al., 2009, Simonse et al., 2003).

2.4.1 Environmental applications of LiDAR

The most common platforms on which LiDAR sensors are deployed for environmental applications are airborne and ground-based systems (Moskal and Zheng, 2011), referred to as ALS and TLS respectively. LiDAR data provides the needed resolution and detail of forests, rangelands, watersheds, roads and other valued resources to inform and improve management decisions in the field of environmental science. Unlike two-dimensional imagery (for example satellite and aerial), the vertical component of 3D LiDAR data allows the user to separate ground from other information. This information, in particular, is being utilised by foresters and land managers with a vision of automating forest inventories.

Traditionally, the primary product of a LiDAR survey for resource management was obtaining Digital Elevation Models (DEM) for the purpose of hydrological, geomorphological and other applications, ignoring the vegetation information contained in them (Hudak et al., 2009). It is only recently that this component of LiDAR data has been put to use by land managers and ecologists. Developments in LiDAR remote sensing applications for environmental studies are occurring rapidly, and they are driven by intensive research and increasing availability of LiDAR data from commercial and governmental sources. Two general application trends can be observed: (1) characterising the topographic features and (2) assessing the 3D structure of vegetation canopies (Popescu, 2011). Table 2.3 gives a brief overview of some selected examples of case studies demonstrating the utility of TLS in environmental applications.

Most of these studies have utilised TLS technology to quantify forest bio-metrics for the purpose of forest inventories. Most methods deployed for estimating and quantifying canopy structure are limited in their capacity to make detailed and spatially explicit measurements. They are also very laborious, time-consuming and costly (Henning and Radtke, 2006). Some of the common forest metrics that have been extracted and quantified from TLS include DBH, tree height and crown width. These have shown good agreement with TLS derived parameters (for example Huang et al., 2009, Jupp et al., 2009, Moskal and Zheng, 2011).

Table 2.3 Environmental applications of Terrestrial Laser Scanning (TLS) in extracting forestry parameters.

Study Area	Objective	TLS Instrument	Field data for direct comparisons with TLS	Results	Reference
Tussock-Tundra Arctic shrubs, Alaska, USA	Aboveground biomass and leaf area	Reigl VZ-400	Leaf and stem dry mass	Biomass and leaf area can be accurately estimated using TLS from scans taken at multiple distances.	Greaves et al. (2015)
Pine forest, East Texas, USA	Modelling biomass change	Leica ScanStation2	Tree height, DBH, crown width, distance and azimuth from plot centre	High degree of correlation between field measures and TLS parameters.	Srinivasan et al. (2014)
Pine forest, Finland	Automatic stem mapping	Leica HDS 6000	Plot density, DBH and tree height	Overall stem detection accuracy of 73% achieved.	Liang et al. (2012)
Pine forest, Colorado, USA	Understorey fuel characterisation	Optech ILRIS^{TM} 3_6D-HD	Mean height, ground cover classification as shrub, grass, forb or litter	TLS offers opportunities to quantify biomass loss due to fuels consumption.	Rowell and Seielstad (2012)
Pine forest, England	Forest canopy fuel	Riegl LMS-Z390i	DBH, crown diameter, height and crown base height within eight 10m radius plots. Four perpendicular transects (N, S, E, W) from the centre of the plot to characterise understorey vegetation.	This study represents the first attempt to assess the potential of a TLS to derive important canopy fuel characteristics at a plot level.	García et al. (2011)
Four diverse forest types, Washington, USA	Basic forest inventory parameters	Leica HDS 3000^{TM}	DBH, basal area and tree height	TLS based metrics explained 91.17% of the variation in DBH at individual tree level.	Moskal and Zheng (2011)

Study Area	Objective	TLS Instrument	Field data for direct comparisons with TLS	Results	Reference
Spruce forest, Germany	Leaf areas of individual trees	Riegl LMS-Z360	Tree height, DBH	Estimate of Laser Leaf Area (LLA) was linearly related and on an average 10% lower than the Allometric Leaf Area (ALA).	Huang and Pretzsch (2010)
Pine forests, Tumbarumba, Australia	Forest LAI profiles and structural parameters	Echidna®	Destructive sampling of four trees to determine height, crown radius, crown thickness and DBH	Good agreement between estimated and modelled tree parameters.	Jupp et al. (2009)
Pine forests, Ichauway, USA	Fuel volume and loading	Optech ILRIS 3_6D	Maximum fuel-bed, litter depth and presence/absence of fuels and vegetation types recorded in 26 geo-referenced 4mx4m plots	Ground-LiDAR volume estimates were correlated with biomass and leaf area for individual shrubs. It was more sensitive to capturing the height variation than traditional point intercept sampling.	Loudermilk et al. (2009)
Conifer forest, China	Forest structural parameters	Riegl LMS-360i	Tree height, DBH	High correlation with field measured tree height and DBH.	Huang et al. (2009)
Conifer forest, Austria	Forest structural parameters	Riegl LMS-Z420i Faro LS 800 HE80	Tree height, DBH	More than 97% of the trees detected automatically. RMS error of 1.8cm and 2.7m for DBH and tree height respectively.	Maas et al. (2008)

Study Area	Objective	TLS Instrument	Field data for direct comparisons with TLS	Results	Reference
Conifer and deciduous forest, Austria	Tree detection and diameter estimation	FARO LS 800 HE80	Tree height, DBH	Robust tree detection of 97.4% obtained.	Bienert et al. (2007)
Pine forest, Switzerland	Forest canopy gap fraction	Riegl LMZ210i	Hemispherical photos	The information content of the laser scans appeared to be similar to that of the hemispherical photos.	Danson et al. (2007)
Pine forests, Ichauway, USA	Fine-scale fuel bed structure	Optech ILRIS 3_6D mounted on a mobile platform	Maximum fuel-bed, litter depth and presence/absence of fuels and vegetation types recorded in 30 geo-referenced 4mx4m plots	Demonstrated the applicability of ground-based LiDAR for modelling forest fuel.	Loudermilk et al. (2007)
Deciduous forest, Italy	Structural tree modelling	Z&F GmbH Laser Measurement System LARA 53500	DBH, destructive sampling	n/a	Teobaldelli et al. (2007)
Deciduous forest, USA	Multidimensional characterisation of forest canopy structure	Riegl MLS-Z210	Tree heights, positions, DBH	Ground based laser scanning provides high-resolution, spatially explicit measures of plot-level forest canopy structure.	Henning and Radtke (2006)

Study Area	Objective	TLS Instrument	Field data for direct comparisons with TLS	Results	Reference
Upland conifer forests, England	Tree diameter	Riegl LPM-300VHS high-speed laser scanner	DBH and tree height	Accurate measurements of tree diameter can be derived directly from the laser scan in instances where the sensor's view of the tree is not obstructed.	Watt and Donoghue (2005)
Southern Black Forest foothill range, Germany	Forest inventory	Z&F Imager 5003	DBH, height of crown base, tree height	Inventory parameters which are derived from models based on a high amount of directly-measured 3D coordinates show smaller errors	Thies and Spiecker (2004)
Southern Black Forest foothill range, Germany	Forest structural parameters	Z&F Imager 5003	DBH, tree position	26 out of 28 trees detected correctly with differences of less than 20cm in DBH.	Simonse et al. (2003)
Upland conifer forests, England	Forest parameters	Riegl LPM-300VHS high-speed laser scanner	DBH, total tree height	TLS can be used accurately to measure forest parameters – tree diameter, total tree height, taper and density at plot level.	Watt et al. (2003)

Another widely reported forestry application involving TLS is the automatic detection and delineation of trees in the forested landscape. The end goal is to estimate timber volume for forest inventorying, which is of particular importance in production forests.

An emerging application of TLS is around detecting change in forested landscapes. This typically involve multi-temporal scans conducted either in single- or multi-scan modes. Changes in forested landscapes typically look for changes in tree biomass, forest structure and understorey. Such change detection applications can help reduce uncertainties in the forest carbon budget (Srinivasan et al., 2014). They can also help quantify biomass loss due to events such as fires and floods. Change detection in burnt landscapes using laser scanning is relevant to this research; however, limited research exists in the domain of TLS. The next section gives an overview of both ALS and TLS applications in burnt landscapes.

2.4.2 Applications of LiDAR in characterising forest understorey

Detecting and quantifying the properties of the understorey using LiDAR technology has been less widely studied. Reported attempts (Loudermilk et al., 2009, Riano et al., 2003) quantifying various properties of the understorey have utilised a variety of metrics derived from both airborne and TLS data for fire-behaviour monitoring purposes as outlined in Table 2.4. These metrics, which are primarily point density or height-based, have been used successfully to predict and estimate various understorey vegetation properties including volume, density, cover, height and biomass to varying degrees (Goodwin, 2006, Rowell and Seielstad, 2012).

2.4.3 Applications of LiDAR in burnt landscapes

Recent work (for example Heo et al., 2008, Roff et al., 2005, Wulder et al., 2009) demonstrates the increased uptake and utility of LiDAR datasets to quantify fuel load and changes in burnt landscapes. ALS has been used to estimate fuel loads which are critical parameters for understanding fire behaviour. In their report, Roff et al. (2005) concluded that ALS could play a critical role in assessing fuel load attributes relating to overstorey and understorey canopy and topography. They also stated that ALS technology has proven to be better than aerial photography, airborne hyperspectral sensors (for example AVIRIS) and airborne profiling radar at estimating these critical fire attribute parameters.

Table 2.4 LiDAR derived understorey metrics used by researchers to map understorey vegetation.

Metric	Property	Metric Type	Scale	LiDAR Platform	Application	Study
Variety of Height-based Metrics	Cover Height	Height	Plot	Airborne	Understorey plant invasion	
Variety of Height-based Metrics	Cover Height	Height	Plot	Airborne	Wildfire behaviour modelling	Jakubowski et al. (2013)
Variety of Height-based Metrics Ratio of Points Above and Below the Inflection Point	Cover	Both Point Density and Height	Plot	Terrestrial	Fire behaviour modelling	Rowel and Seielstad (2012)
Proportion of number of understorey laser hits after applying intensity filter Number of LiDAR points per square metre under 1.5m	Cover	Point Density	Plot	Airborne	Ecological management	Wing et al. (2012)
Presence or absence of laser points within each cm^3 space	Volume	Point density	Plot	Terrestrial	Fire behaviour modelling	Loudermilk et al. (2009)
% of ground returns % of returns between 1 and 2.5m	Cover Distribution	Point Density	Plot	Airborne	Ecological management	Martinuzzi et al. (2009)
Difference between pre- and post-fire LiDAR elevation	Cover Biomass	Height	Landscape	Airborne	burn severity	Wang and Glen (2009)
Proportion of corrected number of understorey laser hits	Cover	Point Density	Plot	Airborne	Ecological and forestry	Goodwin (2006)
Proportion of corrected number of understorey laser hits	Cover	Point Density	Landscape	Airborne	Fire behaviour modelling	Riano et al. (2003)

Indeed others such as Lentile et al. (2006b) have pointed out that 2D satellite imagery limits inferences about structural parameters of crowns which are known to influence burn severity (that is height, base height and bulk density). They also recommend incorporating information from both two (satellite) and three-dimensional (LiDAR) datasets to improve estimates of post-fire effects and pre-fire fuel conditions.

Heo et al. (2008) used an integrated method for estimating forest-fire loss using a variety of geospatial datasets. They used infrared aerial images to delineate fire damaged regions within the forests. Tree heights were derived from airborne LiDAR (Optech ALTM 30/70) and verified by TLS datasets (CYRAX 2500). Other information about the trees within the fire-damaged forests was obtained from the GIS layers of the Korean national forest inventory. Once tree heights were computed, stand volumes of forests were estimated using Tree Volume Equations (TVE). Results of this research indicate that estimates of fire loss derived from LiDAR-derived tree heights were more accurate than those obtained from conventional methods (for example those that are mostly based on field surveys of either direct observations taken with surveying equipment or indirect observations with rough sketches on top of topography and cadastral maps).

A study carried out in 2009 by Wulder et al. (2009) evaluated the utility of LiDAR to detect fire-induced changes in the vertical forest structure. They conducted two ALS transects both pre- and post-burn. Their findings suggest that in the pre-burn LiDAR transect, there were no significant differences for any of the structural attributes (that is average canopy height, volume) between forests located within and outside the fire perimeter; whilst significant differences were observed in the post-fire transect. They also concluded that measures of vegetation fill post-fire and absolute change in crown closure and relative change in average canopy height were useful for characterising post-fire effects.

Another study tried to link change in average vegetation height pre- and post-fire to burn severity (Wang and Glenn, 2009). ALS data was captured using an Optech 50-KHz instrument. They achieved a fire-severity classification map with 84% overall accuracy. However, a more important finding of this research was that the researchers found that ALS was sensitive at discriminating between moderate and high fire-severity classes. This has been reported by researchers in the remote sensing community as a big challenge.

Angelo et al. (2010) in their study used vertical profiles obtained from LiDAR in conjunction with advanced classification techniques to predict the time since fire status of the vegetation in an oak

scrub ecosystem in Florida. This is based on the hypothesis that vegetation patches that have experienced more recent disturbance will be distinct in their vertical structure from those that have not been disturbed and are in later successional stages. The findings of this study suggest that LiDAR derived vertical profiles can be used by natural resource managers to predict the successional status of vegetation with a high degree of accuracy.

Another study carried out by Wing et al. (2010) applied LiDAR to measure trees in burned landscapes. Although this study did not aim to quantify the amount of vegetation lost or detected structural changes occurring after the fire, the researchers made use of LiDAR intensities to see if any differences existed between live and dead trees. LiDAR data for this research was captured using an Optech ALTM 30/70 Airborne Laser Terrain Mapper. The results indicated that the mean and maximum LiDAR intensities were significantly different between live and fire-killed trees in two of the tree sites. Other results from this research indicate that no significant differences were detected between field-based and LiDAR-derived horizontal positions of trees in burned landscapes.

ALS and multispectral imagery were used to determine conifer mortality and burn severity in the 2009 Lockheed fire (Redwood forests, California) (White and Dietterick, 2012). They used a total of four airborne LiDAR datasets over the burned forest since 2008. Two preliminary results were discussed. Canopy cover as calculated with LiDAR following the fire drastically decreased in 2010. Digital Surface Models (DSM) were also generated from three LiDAR datasets to identify trees removed because of the fire. Magnussen and Wulder (2012) used ALS to study post-fire canopy height recovery in Boreal forests.

Rowel and Seielstad (2012) demonstrated the potential of a TLS system to characterise grass, litter and shrub fuels in burned longleaf pine forests. A variety of height-based metrics were extracted from each grid cell including inflection point, maximum frequency value and ratio of points above and below the inflection point. In was concluded from this research that the variability in height distributions post-fire was negligible for litter and grass fuel types while the shrub fuels were the exception. They attributed this to the hardwood retention by them which accounted for 19% of the laser points residing above the inflection point as compared to 0.3-2.0% for other fuel classes.

It is evident that advances in LiDAR technology have enabled their utility in a wide area of applications within the domain of environmental management. This is a very promising prospect as well-resourced government agencies can conduct periodic high-resolution LiDAR surveys for a

wide variety of applications. ALS is increasingly beginning to be used in burnt landscapes to detect structural changes in vegetation, assessing forest fire loss and determine canopy mortality and burn severity. As suggested by White and Dietterick (2012), utilising high-resolution remote sensing products such as LiDAR both before and after a disturbance can further enhance our understanding of how forest attributes respond to disturbance. Together in conjunction with 2D satellite imagery, remote sensing has the potential to improve estimates of post-fire effects on the landscape.

Although most of the above discussed studies have utilised only ALS to ascertain fire effects on the canopy and modelling forest-fire loss, the utility of TLS remains relatively unexplored. Research into the utility of TLS for change detection in burnt landscapes particularly the understorey whilst linking them with field-based assessments of fire effects will help broaden our understanding of fire effects on the landscape. Quantifiable measures of understorey fuel consumption in response to prescribed burns assume significance in a country like Australia where government agencies routinely carry them out to reduce accumulation of catastrophic fuel loads.

2.4.4 Advantages and disadvantages of TLS

TLS possesses several advantages which have led to its increased utility in environmental management. TLS provides non-destructive and quantifiable measures of forest structure that is hard or impossible to obtain using traditional methods. Their non-destructive measures make it possible to record information at any given moment that can be made available to a user at a later date, if necessary. As such, it is possible to assess the growth parameters of trees and the evolution of stands over time. From an ecological point of view, using TLS should be a more convenient way to sample vegetation given their non-destructive nature (Dassot et al., 2011).

Although ALS has been typically used in forestry for large-scale remote sensing of forest structural parameters, they have been unsuitable for measuring understorey vegetation. This is because the obstruction from the forest canopy limits the horizontal resolution to a few decimetre scale (Loudermilk et al., 2009). On the other hand, TLS is capable of capturing detailed information, far beyond what air- and space-borne laser scanning are capable of (Van Leeuwen and Nieuwenhuis, 2010).

Although this technology would be of great benefit for forest planning and monitoring, tree physiology and conservation studies; the technology also has limitations. Compared to other sensor technologies, TLS is restricted by its short and limited working range. Whereas this technology, in

principle, allows for the ranging of objects beyond 50m, the capacity to map trees is much reduced due to occlusion caused by lower branches, surrounding trees and understorey. This phenomenon leads to lower point density and therefore to poor descriptions in the upper part of crowns and partially or wholly hidden trees (Van der Zande et al., 2006). Nevertheless, this can be avoided by operating the TLS in a multi-scan mode even though this can make data processing computationally expensive and complex.

The other disadvantage of this technology are the associated high costs per area of acquisition and data processing (Van Leeuwen and Nieuwenhuis, 2010). Whilst TLS are tools that provide comprehensive information about forest structure, especially if using several scans and high-resolution scans; using TLS in a multi-scan mode increases measurement times. In addition, reference points need to be placed in the field to merge scans, which adds to the processing steps. Using high resolution scans also increases data loading and processing times (Dassot et al., 2011).

Another factor that must be considered to obtain high-quality point clouds is weather conditions. The wind constitutes the most troublesome factor since it depreciates vegetation description, especially in the upper part of the canopy. The displacement of vegetation elements during a progressive scan means that they are scanned at different positions, leading to a poor description of tree axes and foliage distribution and the increase of noise points. Rain also reduces point cloud quality by intercepting numerous laser beams, resulting in an increase in noise points (Dassot et al., 2011).

As with any technology, there is always a trade-off involved. In the case of TLS, it can be summarised as a trade-off between the scale and resolution of data capture. Whilst TLS provides high-resolution 3D point cloud data; it is often restricted by the range over which it can operate. For the desired application, TLS can be the most suitable tool with which to acquire very rapid and detailed high-resolution scans of the landscape. However, it is important to acknowledge the limitations of the TLS so that better judgements about its data can be made.

2.5 Summary

This chapter provided a review of literature required to identify gaps in current research and knowledge. As such, the importance of bushfires in an Australian context was discussed. A detailed discussion on the fire effects on vegetation and the rationale for conducting prescribed burns was also presented. Thereafter, the role and utility of remote sensing technology to study the impact of

fire across the landscape was presented. A detailed review of the most popular vegetation and burn indices derived from remote sensing data were identified and described. The role of LiDAR in measuring fire effects was discussed in the last section. In addition, the uptake of TLS technology in a variety of environmental applications was also highlighted.

Chapter 3. Methods

3.1 Introduction

This chapter explains the method used in this study. The study area and the survey design are described. The survey design includes plot selection and individual target selection within them for remote sensing data capture. The next section describes the hyperspectral instrument used and the protocol followed for capturing spectral data. The last section describes the TLS set up for data capture in the study area.

3.2 Study area

The study area is located in School Road Reserve, St Andrews, Victoria approximately 45km north-east of metropolitan Melbourne ($37^0$36'7"S, $145^0$15'57"E) as shown in Figure 3.1. It is situated at an altitude of 120m with a slope of 15^0 and a north-easterly aspect. St Andrews has had a history of fires. The first recorded fire in this area dates back to 1898. The 1939 bushfires also affected St Andrews (South et al., 2012). The devastating bushfires of 1962 also impacted St Andrews (Bryant, 2008). The last time prescribed burns were conducted here was back in 1997 (Hill and Broughton, 2009).

The geology of the study area is dominated by sedimentary rocks. It also had a high erosion hazard due to hard-settling soil surfaces (South et al., 2012). The forest type is typical of a dry sclerophyll forest with a grassy understory growing on rocky soils (Keith, 2004) (Figure 3.2). In general dry sclerophyll forests vary considerably both in the composition of canopy species and in structure and composition of the understorey (Goodwin, 2006). The canopy in St Andrews was dominated by eucalypt tree species comprising *Eucalyptus goniocalyx* (Long-leaf box), *Eucalyptus macrorhyncha* (Red Stringybark), *Eucalyptus polyanthemos* (Red Box) and *Eucalyptus mellidora* (Yellow Box). The forest was very open with the absence of shrubs. The average height of the canopy was between 10-12m. The grasses mainly comprised *Poa sieberiana* (Grey tussock-grass).

3.2.1 Study plots

Four circular plots of 10m radius were identified. One plot acted as the control and was left unburnt, whilst the remaining three plots received a fire treatment and referred to as fire-altered plot 1, fire-altered plot 2 and fire-altered plot 3. All the plots were easily accessible via the fire management tracks. Plots were homogenous and contained plant species which were representative of the grassy dry sclerophyll forest in south-eastern Australia.

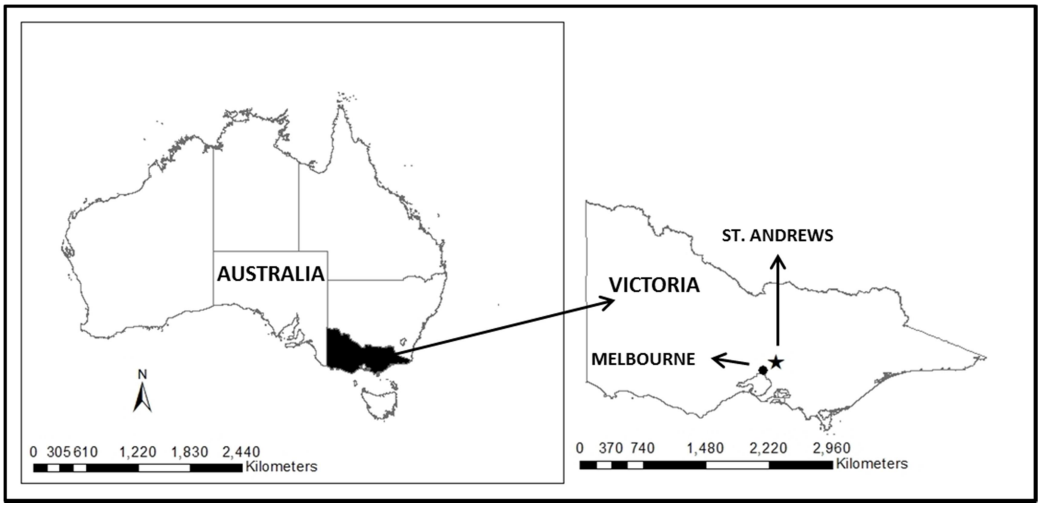

Figure 3.1 Location of the study area (St. Andrews) in Victoria, Australia.

Figure 3.2 Forest type in the study area typical of an Australian dry sclerophyll forest with a grassy understorey.

3.2.2 Plots and targets selection

Fuels in Victorian forests can be divided into four vertical strata, each based on its position in the vegetation profile as shown in Figure 3.3 (Hines et al., 2010). Within each plot, targets representative of the vertical strata were selected. Targets were chosen to represent the common land covers across the prescribed burn area and at different strata levels of the fuel layers (that is near-surface fuel and surface fuel). Since the elevated fuel layer was virtually absent, no targets representative of this fuel layer were investigated in this research. The absence of elevated fuel in such forests could be a result of closing canopy which restricts the amount of light reaching the ground (Hines et al, 2010).

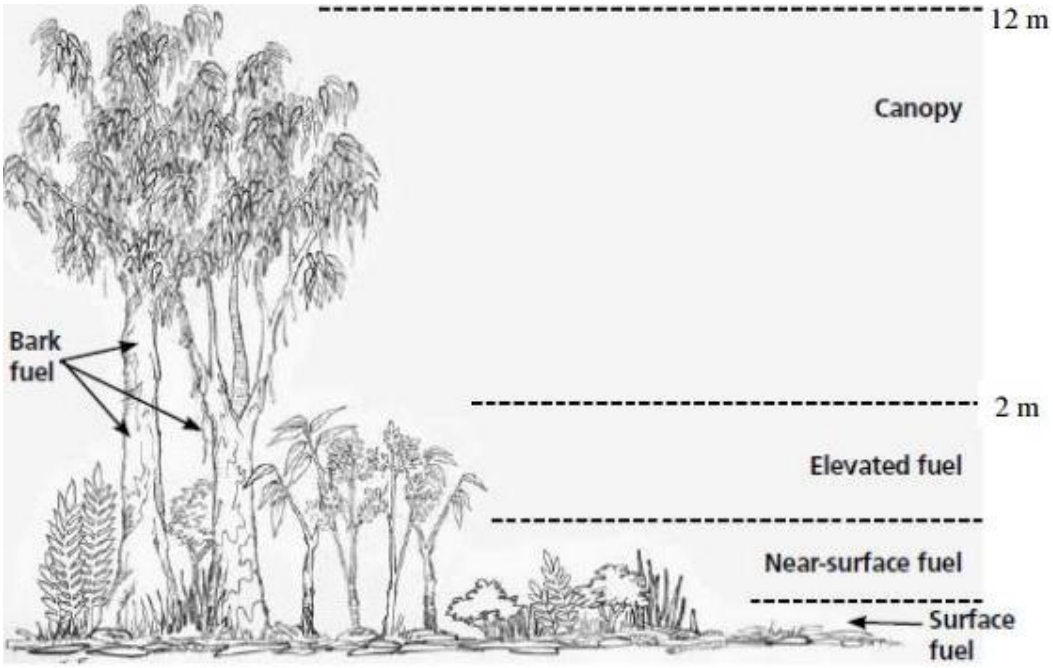

Figure 3.3 Vertical stratification of fuels in Victorian dry sclerophyll forests (Hines et al., 2010)

Within each study plot, one vegetation target representative of the near-surface (grasses) and surface fuel layer (litter) were selected. Spectral measurements were obtained from each of these targets. Table 3.1 lists these different targets with their corresponding position in the vertical strata and the scale at which spectral data capture occurred.

Land cover representing near-surface fuel layer comprised Grey tussock-grass (*Poa sieberiana*) while the surface fuel layer was represented by litter. The sample specimen chosen corresponding to live vegetation were both healthy and mature.

Table 3.1 Different targets selected in the plot from which spectral measurements were recorded.

Target name	Position in the vertical strata	Scale of spectral data capture
Litter	Surface fuel layer	0.5×0.5m
Grass	Near-surface fuel layer	0.5×0.5m

3.3 The burn event

The planned burn was carried out by Parks Victoria and the Department of Sustainability and Environment (DSE), Victoria state government. The area burnt was approximately 19ha. It was conducted on 15 April 2012 (autumn) to develop fuel reduced areas of sufficient width and continuity to reduce the spread of wildfire and exclude fire from the surrounding suburbs and riparian zones. The objective was to obtain burn coverage between 70-89% and to reduce the overall fuel hazard to below 'High' in 90% of the target area. Fuel breaks were developed around the control plot. Each of the other three plots received different fire treatments to simulate different fire intensities and severities.

3.4 *In situ* spectra measurement

3.4.1 Hyperspectral radiometer

Reflectance spectra of the fuel layers were measured in the plots using the Analytical Spectral Device (ASD) Fieldspec®3 (ASD, 1999). The FieldSpec®3 is an optical instrument and measures light in a near continuous spectrum between wavelength range 350-2500 nm. Light being measured passes through a fibre optic cable to three detectors covering separate spectral ranges. Separate fibre bundles within the optical cable supply light to the individual detector arrays. Different fore optics may be fitted to the end of the fibre optic cable to accommodate different measurement requirements and the fibre may also be used in the 'bare fibre optic' mode that is without a fore optic.

The VNIR (Visible/Near-Infrared) detector uses a single 512-element Si photodiode array to cover the 350-1000nm region, whilst two TE cooled, graded index LnGaAs photodiode arrays cover the SWIR (Short-Wave Infrared) regions of approximately 1000-1800nm (referred to as the NIR-1 region) and 1800-2500nm (NIR-2). The spectral sampling interval is 1.4nm for the VNIR detector

and 2.0nm for the NIR detectors, and spectra are resampled internally by the ASD into 2151 bands at 1.0nm interval.

The spectral resolution expressed as the Full-Width Half Maximum (FWHM), is 3nm (measured at 700nm) for the VNIR detector and 10nm (measured at 1400nm and 2100nm) for the NIR detectors. In practice, this means that each sample signal is a composite of the energy registered over 3 and 10nm respectively, following a bell-shaped or Gaussian curve. Published Noise Equivalent Delta Radiance Figures (NeDL) for the ASD®3 show the VNIR detector has a higher signal-to-noise ratio than the NIR detectors (VNIR $1.1x10^{-9}$, NIR-2.2.$1x10^{-9}$ and NIR-2 $4.0x10^{-9}$ $W/cm^2/nm/sr$ respectively).

3.4.2 Criteria for target selection for appropriate spectral reflectance data capture

Certain environmental conditions are assumed to exist when conducting field spectroscopy. These factors influence spectral measurements *in situ*. To enable consistency in hyperspectral data capture and to aid in inter-comparison especially in a multi-temporal study some environmental factors need to be considered (McCoy, 2005). The criteria for a target to be considered suitable for spectral data collection for this research have been described in Table 3.2.

Table 3.2 Criteria used for target selection for spectral data collection in this research.

Criteria	Description
Homogeneity	The target should be 100% homogenous over the desired Ground Field of View (GFOV) where possible. This is important from a data capture point of view to enable pure endmember spectra of the target to be collected.
Clear Sky View	The target for which spectral data is to be captured should receive direct solar illumination during the time of data capture (that is minimal obscuration caused by the canopy). All the targets chosen in this research for spectral measurements met this criterion. Spectral data was captured at or around solar zenith i.e sample ±2 hours of solar noon. View angle was at or around $\pm5^0$ nadir.

3.4.3 Considerations while measuring reflectance spectra

The accuracy and consistency with which spectral data measurements are recorded using a hyperspectral radiometer are based on a few factors. These factors are discussed below.

3.4.3.1 Appropriate Ground Field of View (GFOV)

The spectrometer's Field Of View (FOV) in combination with the distance to the target determines the area that is being sensed. Figure 3.4 shows the FOV geometry by which one can determine the optimum distance from instrument to target. GFOV is calculated using Equation 3.1

$$2 \times (h \times Tan\frac{\theta}{2}) \quad \textbf{(3.1)}$$

For the targets (grass and litter), h was equal to 1m. The sensing fibre optic cable of the ASD which was held directly over the target to capture spectral reflectance measurements was used without a fore optic that is in bare fibre optic mode. This bare fibre optic has a FOV of 25^0.

Hence, substituting these values in Equation 3.1 a GFOV of approximately 0.5m was simulated. This is directly related to the homogeneity of the targets (grass and litter) being 100% across a 0.5×0.5 m area to enable recording of a pure endmember spectra.

3.4.3.2 The reference panel fills the FOV

This criterion must be met to ensure that the spectral curve is representative of the reference panel. To avoid spectral radiance from adjacent materials from influencing the spectral data capture, the GFOV should not be greater than fill no more than one-half of the reference panel. The reference panel used for calibrating the ASD for the field campaigns had the dimensions of 0.3×0.3m. Thus, the height at which the bare fibre optic was held 0.5m above the reference panel.

3.4.3.3 The target fills the FOV

The area from which spectral data is captured should be at least twice the diameter of the FOV. For the purpose of this research, to capture pure endmember spectra, 100% of each of our targets (Grey Tussock grass and litter) had to be homogenous across a 0.5×0.5m.

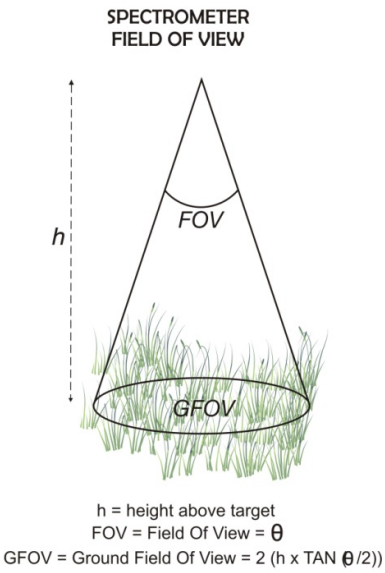

Figure 3.4 Geometry of the Field Of View (FOV). The diameter of the base of the cone at the distance h, must be computed (From McCoy, 2005).

3.4.3.4 Irradiance is constant while measuring both the reference panel and the target

Even if the sun is shining in a clear sky, it is possible to have small differences in solar irradiance due to thin cirrus clouds not visible to the naked eye. These minor effects cannot be controlled. However, the effects of the differences in illumination conditions can be controlled by re-optimising the ASD by taking measurements from the reference panel before spectral data capture from the targets at regular intervals.

3.4.4 Hyperspectral data capture

All hyperspectral measurements were captured between 10.00 and 14.00 hours to coincide with solar NADIR using the FieldSpec 3 (Analytical Spectral Devices, Boulder, CO, USA). This instrument covers the electromagnetic wavelength range of 350–2500nm. The bare fibre optic with a FOV of 25^0 was used for spectral data capture in the field. The height at which the bare fibre optic was held was 1m to simulate a GFOV of approximately 0.5m.

Each target measurement was preceded by a reference measurement viewing a horizontally placed standardised white Spectralon panel (Warsash Scientific, Redfern, NSW, Australia) to normalise for both the incoming irradiance illuminating the target and for instrument condition (change in spectroradiometer sensitivity due to temperature and electronic effects). This also enabled

monitoring for changing light conditions and conversion of the measured target radiance to apparent reflectance. A total of 15-20 spectra were recorded for each target. Each spectra captured was an average of 30 spectral measurements. They were recorded at point locations at the centre of the target to ensure spectral data capture from a homogenous target.

3.4.5 Spectral data processing

The reflectance was converted from reflectance factor into percentage, averaged, smoothed and plotted to show any changes in reflectance over the one year time period. Hyperspectral bands corresponding to atmospheric water vapour absorption were removed as shown in Appendix 10.3. The raw spectra were smoothed using a weighted mean moving average filter (Naesset, 1997) as shown in equation 3.2 below. A five-point weighted average gave sufficient smoothing without loss of fine spectral detail.

$$\frac{\rho m-2\ +\ 2\rho m-1\ +\ 4\rho m+1\ +\ 2\rho m+1\ +\ \rho m+2}{10} \qquad \textbf{(3.2)}$$

In equation 3.2, ρ_m is the weighted mean calculated for the *m*th spectral value.

Derivative spectroscopy concerns the rate of change of reflectance with wavelength. This technique was used to identify peaks, troughs and other spectral features that may indicate stress in the canopy and near-surface fuel targets in response to prescribed burns. It is a well-documented fact that first-order derivative analysis whilst enhancing spectral regions of change also removes some unwanted effects such as Bidirectional Reflection Distribution Function (BRDF) (Tsai and Philpot, 1998) and soil background signals (Demetriades-Shah et al., 1990). It also reduces the effects of scattering. In comparison to higher order spectral derivatives, first-order derivative is less sensitive to noise and hence more effective in operational remote sensing (Pu, 2012). The first derivative was calculated by dividing the difference between successive spectral values by the wavelength interval separating them. In this case a 9nm interval was used. Calculation of first-order derivatives was performed on the spectra before removing noisy water vapour regions.

3.5 Terrestrial Laser Scanning (TLS)

3.5.1 Instrumentation

The TLS used in this research was the Trimble CX. The Trimble CX system specifications are summarised in Table 3.3. This laser scanning system uses a 660nm wavelength (red) laser with a scanning rate of up to 54,000 points per second. The maximum field of view supported by this instrument is 300^0 in the vertical and 360^0 in the horizontal plane. It can register laser returns between 0.5m and 80m (at 90% target reflectivity).

The Trimble CX collects for each sampled point return the following attributes:

(1) x,y,z coordinate values with respect to the position of the laser sensor; (2) intensity values; and (3) true colour (RGB-red, green, blue) obtained from an integrated and calibrated digital camera within the instrument.

Table 3.3 Manufacturer specifications of the Terrestrial Laser Scanning (TLS) instrument (Trimble CX) used in this study.

Specification Type	Specification Value
Calibrated range	80m to 90% reflective surface, 50m to 18% reflective surface
Scan rate	54,000 points per second
Output angle accuracy	0.002^0=35μrad (horizontal and vertical)
Vertical scanning angle	300^0
Horizontal scanning angle	360^0
Spot size	8mm @ 25m; 13mm @ 50m
Laser wavelength	660nm (red)
Weight	11.8kg
Dimensions (L×W×H)	12×52×35.5cm

3.5.2 Data acquisition

TLS data coincident to field measures was acquired pre-burn on 8 March, two weeks post-burn on 30 April 2012 and then two years on 19 June 2014 (Figure 3.6). The scanner was mounted on a

tripod and was placed at the centre of each plot. Scans were obtained in a single-scan mode. The height of the scanner above the ground was set at 1.5m. Trimble Access software loaded on the Tablet PC was used to change the laser scan settings. The scanning resolution was set to 1cm at 10m distance. The scans were performed covering 360^0 horizontally and 300^0 vertically. Each hemispherical scan took approximately 45 minutes to complete.

To ensure inter-comparison between scans from the same plot pre- and post-burn, the scan station was set over a known point using a video-based azimuth. Registration was achieved by using permanent reference targets in the plot. The Trimble CX scanner also enabled capturing photographs which it automatically stitched onto the 3D point cloud. The photographs were used as a visual reference only. The scanner setup in the field is shown in Figure 3.5.

Figure 3.5 TLS setup in the field.

3.6 Field data assessments

3.6.1 Fuel hazard assessment

A pre-burn fuel hazard assessment was carried out in all the four study plots pre-burn and the control and fire-altered plot 3 two years post-burn. The main purpose of the fuel hazard assessment was to make a rapid, visual assessment of the fuel arrangement and potentially correlate it with burn severity and also to assess fuel consumption by the prescribed burn event. The fuel hazard assessment was based on the Overall Fuel Hazard Assessment Guide (Hines et al., 2010). The

process of assessing fuel hazard using this guide relies on visual assessment. Variables assessed include: near-surface percentage cover, near-surface average height, surface litter percentage cover, average litter depth and were evaluated against standard photos and illustrations.

3.6.2 Burn severity assessment

Burn severity of prescribed burns was carried out based on a number of variables used in Australia and worldwide. Within Victoria, it is based on the Burn Severity Assessments Field Guide (DSE, 2010). It involves recording variables such as percentage area burnt, percentage canopy burnt, percentage canopy scorched and percentage near-surface fuel burnt within six weeks post-burn.

3.6.3 Land cover proportions

A 3 × 3m mixed land cover grid was set-out in the control and fire-altered plot 3. The grid comprised nine 1 × 1m cells. Within each cell a visual assessment of the land cover proportion was noted concurrent to TLS surveys pre-burn and two weeks post-burn. The different land cover elements recorded as a percentage were near surface live vegetation, litter, bare earth, and area burnt. The results are presented in Appendix 10.2.

3.6 Summary

This chapter described the study area and survey design employed in this research. The *in situ* remote sensing instruments (ASD and TLS) used in this research were also described including their set-up and data capture. Field data captured including fuel hazard, burn severity and land cover proportions was also discussed.

Chapter 4. Assessing metrics for estimating fire induced change in the forest understorey using Terrestrial Laser Scanning

[This chapter has been published as the following peer reviewed publication:
GUPTA, V., REINKE, K.J., JONES, S.D., WALLACE, L., HOLDEN, L. 2015. Assessing Metrics for Estimating Fire Induced Change in the Forest Understorey Structure Using Terrestrial Laser Scanning. *Remote Sensing*, 7, 8180-8201.]

4.1 Introduction

This chapter describes the methodology employed to obtain metrics for detecting fire induced change in the forest understorey using TLS. Bi-temporal TLS data which was captured pre- and post-burn has been used in this chapter. To begin with, this chapter introduces the method undertaken in detail which includes point cloud pre-processing and metrics derivation. The results of change detection by various metrics are described in detail which includes both descriptive statistics and field data. The following section discusses the utility of metrics based on set criteria. A discussion on links between the changes observed using TLS-derived metrics and changes observed on the ground is also made. The chapter concludes with a section on the recommendations of metrics to be used that can assist in ascertaining burnt and unburnt areas in understorey forest following prescribed burns.

4.2 Method

4.2.1 Study area and field data

The study area was located in St Andrews, approximately 45km northeast of metropolitan Melbourne, Victoria, Australia. The study was conducted in a dry sclerophyll forest with a grassy

understorey. The site can be described as open Eucalypt woodland with an average canopy height between 10 and 12 m. The midstorey vegetation layer was notably absent. The understorey was dominated by a variety of Tussock grass species with heights ranging from 30 to 50 cm. Two circular plots of 9 m radius were identified which were similar in topography (i.e., flat), vegetation species composition and arrangement. The extents of the plots were chosen to be close to the guidelines set out for the visual field assessment of burn severity developed by the Department of Environment, Land, Water and Planning (DELWP).

A planned burn was carried out by Parks Victoria and the DELWP on 15 April 2012. One plot received a fire treatment (fire-altered plot) which acted as the change agent while the other plot was left unburnt and acted as the control. A burn severity assessment was conducted approximately two weeks after the planned burn on 27 April 2012. This visual assessment followed the methods described for use by local land managers. The variables recorded in the understorey layer were percentage of the plot burnt, pre- and post-fire % cover (grass and litter), pre- and post-fire litter depth, post-fire leaf fall cover and char depth.

4.2.2 Terrestrial laser scanner surveys

The TLS instrument used in this research was a Trimble CX which utilises a combination of time-of-flight and phase-based measurement principles. Bi-temporal TLS data was acquired pre-burn on 8 March 2012 and post-burn on 30 April 2012 for each plot. All scans were obtained in a single-scan mode with the scanner located at the centre of the plot at an above ground height of 1.5 m. The angular point spacing was set to 1cm at 10m distance. The scans were performed to capture the scanner's full range of view (360° horizontally and 300° vertically). Each hemispherical scan took approximately 45 minutes to complete. Co-registration between the bi-temporal scans was achieved by using permanent reference targets (stainless steel tags) fixed to the stems of trees within the plot.

4.2.3 Point cloud pre-processing

The raw point clouds were processed following the steps depicted in Figure 4.1. Initially, the raw point clouds were exported to ASCII format using Trimble's proprietary software (Trimble Realworks software version 6.5, 2009). Ground points were then identified in the fire-altered point clouds using the lasground tool of lastools (Isenburg and Schewchuck, 2007).

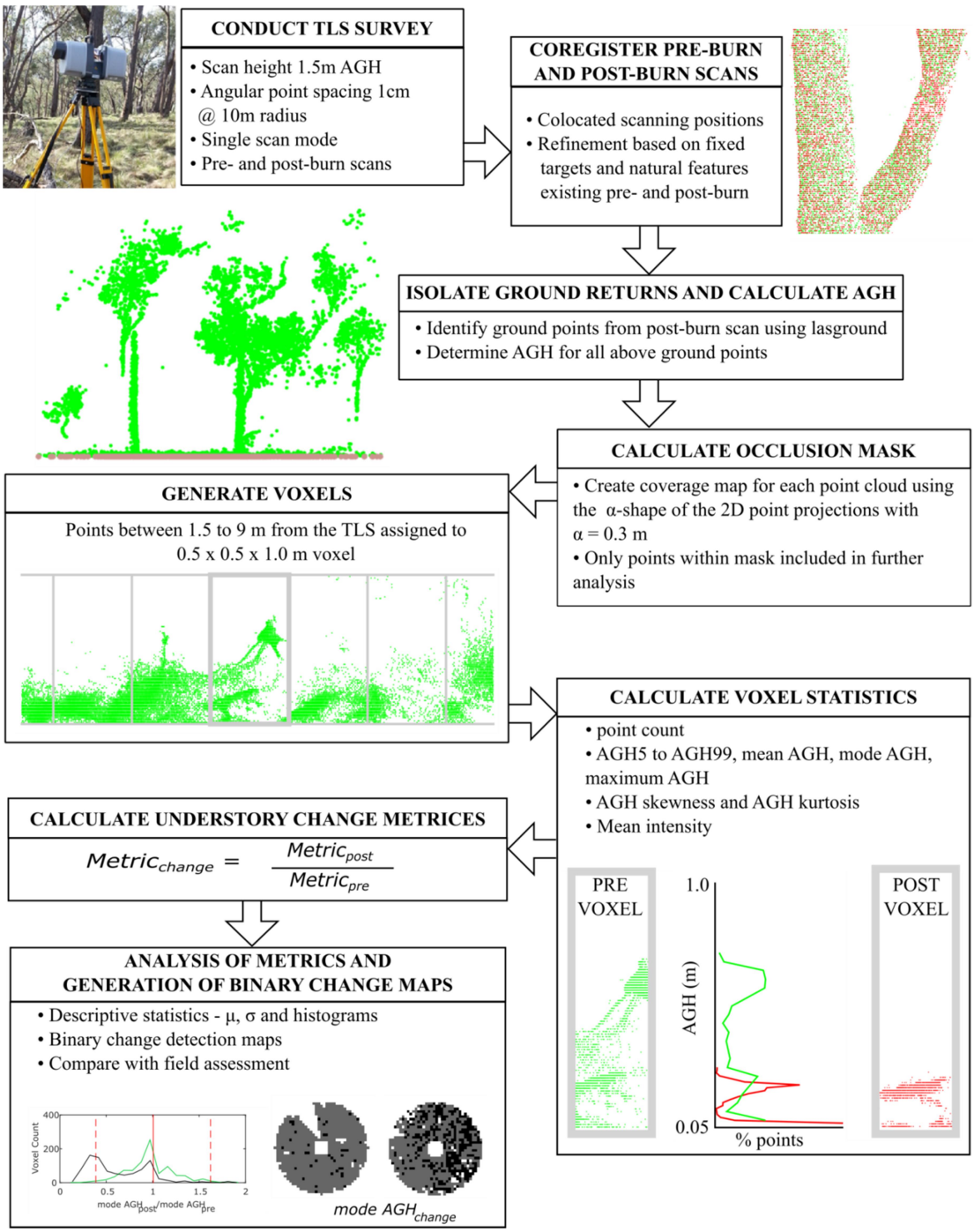

Figure 4.1 The workflow of TLS data processing for deriving understorey change detection metrics.

We trialled several of the verbose options of lasground and visually assessed the results to determine the optimum combination for this landscape type. The '-not_airborne' option which is recommended for extracting ground points from TLS data produced the best result and was therefore used to extract ground points. This allowed for a TIN representation of the ground surface to be generated. The final ground density after filtering was 2996.70 points/m^2. The Above Ground Height (AGH) of all points within the pre- and post-burn point clouds were then determined based on this ground surface representation.

The ground points from the post-burn scans were used in the normalisation process of both pre- and post-burn point clouds to avoid introducing discrepancies in further analysis due to differing representations of the ground.

Points within the understorey were then selected as those with AGH between 5 and 100cm. A minimum threshold was used due to uncertainty in ground detection results. This ensured any remaining ground points were excluded from the change detection analysis. The maximum threshold was selected based on the properties of the understorey vegetation in the study area. To avoid differences in occlusion between data capture events, caused by small variations in instrument set up for instance, points within areas deemed as occluded in one or both of the point clouds were removed from further analyses. This was achieved by creating a coverage map for each point cloud using the α-shape of the 2D point projections with $\alpha = 0.3$m. The coverage map was then used to clip the alternate point cloud.

This resulted in two sets of point clouds of pre and post-burn with equal areas of occlusion across the plot area. Understorey points were then assigned to 0.5×0.5×1.0m voxels. Any voxels containing fewer than 10 points in either post- or pre-burn point clouds were considered still as being affected by occlusion. This approach also helped eliminate spurious points which were present in all point clouds. These corresponding voxels in both point clouds were removed from further analyses. The point count per voxel was more than 2000 in this research.

4.2.4 Metrics extraction

Change in the understorey is likely to be represented within each voxel's point cloud as a change in the number of points or change in the AGH distribution. As such, for each point cloud metrics describing these properties were derived for each voxel. These are listed in Table 4.1.

In all, a total of 18 metrics were extracted and tested. In order to map and comparatively assess the likelihood of change indicated by each of these metrics, the proportion of post- and pre-burn measures was computed following equation 4.1.

$$Metric_{post-burn} \Big/ Metric_{pre-burn} \quad \textbf{(4.1)}$$

The use of proportion to assess change allowed for a unitless comparison between metrics and also accounted for variations in some of the laser properties which are affected by the radial distance from the scanner (that is, point count decreases towards the edge of the plot).

A value for $Metric_{change}$ close to 1 indicates that no change has occurred in the metric between scans. Voxels with $Metric_{change}$ value of less than 1 indicate a decrease in that metric and a value of greater than 1 indicates that the metric has increased. It is expected that a loss of understorey biomass due to burn will create a decrease in most metrics including the point count and AGH percentiles. For each change metric, Mean (μ) and Standard Deviation (σ) for the population of voxels in each plot pre and post-burn was computed. A voxel was determined to have been altered by the burn where the change detected by the metric was greater than $\mu_{control} \pm 1.64 \times \sigma_{control}$ (90% confidence interval). This allowed a burn map to be generated. Finally, in order to provide a quantified estimated of change the understory, height differences were computed based on differences in AGH95 and AGH99. The $\mu_{control}$ and $\sigma_{control}$ are being used because the control plot represents the 'natural-change' environment. In a no-change environment, the ratio-based metrics should show a value of 1 between the post- and pre-burn measures in the control plot indicative of no change. Nonetheless, some change is expected to occur in the control plot. These are expected to be subtle and may include phenological change, wildlife movement and wildlife foraging activity. This approach also allows any small errors in co-registration of the point clouds to be excluded from being mapped as change.

4.2.5 Occlusion impact assessment

TLS surveys were performed in single-scan mode to allow for the most rapid data collection. Nevertheless, occlusion has been identified as a major issue for measuring forest properties with TLS technology (Dassot et al., 2011). In order to assess the impact of

occlusion on the ability of the metrics to remain robust and detect change in the vegetated understorey, bootstrapping analysis was applied.

Table 4.1 TLS-derived metrics used in this research to characterise change in forest understorey. These metrics were computed for each voxel in both pre- and post-burn point clouds.

Metric Name	Metric Description
AGH10, AGH20…AGH90, AGH95	Above Ground Height Percentiles (AGH50 is median height)
AGH mean	Mean Above Ground Height
AGH mode	Mode Above Ground Height
AGH maximum	Maximum Above Ground Height
AGH skewness	Skewness of Above Ground Height
AGH kurtosis	Kurtosis of Above Ground Height
Mean intensity	Mean intensity of TLS returns
Point count	Point count of TLS returns

Stems (modelled as cylinders of random diameter between 0.1 and 0.5 m) were created and placed in the plot. All points which would have been occluded by the stem were then removed. Modelled stems were randomly located within the plot to simulate visible plot areas at 5% increments from 5% to 70%. Figure 4.2 shows some randomly generated stem maps. Bootstrapping analysis was then applied on the voxels of the two plots with n = 50. The μ and σ was then calculated for all the TLS-derived metrics.

4.2.6 Metric assessment

The criteria for metric's ability to detect change induced by prescribed burn were based on three factors: *sensitivity*, *stability* and *similarity*. *Sensitivity* relates to the ability of the metric to detect change (in the fire-altered plot). *Stability* relates to the metric showing the least change in the control plot which was assessed based on the μ, σ of $Metric_{change}$ in the control plot along with the percentage of voxels recording change. *Similarity* relates to the ability of the metric to identify spatial patterns of change which are similar to visual assessments. To summarise, to be used in measuring fire effects in the understorey, TLS derived metrics should detect very little change in the control plot whilst detecting a change in the fire-altered plot that matches well with true change on the ground.

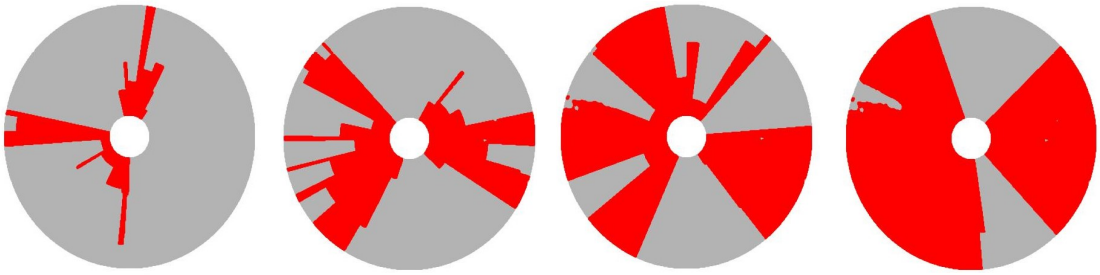

Figure 4.2 Randomly generated stem maps simulating plot coverage at 10%, 30%, 50% and 70% respectively. Red areas correspond to visible plot area.

4.3 Results

4.3.1 Field assessment

As expected, the control plot which received no fire treatment showed no discernible change due to the burn. However, defoliation of a fallen tree in the south-east region of the plot represented a loss of biomass within the height range of the voxels between surveys resulting in a small, localised change. The qualitative field assessment suggested that the prescribed burn resulted in a mosaic burn pattern with 60%–70% of the plot estimated to be affected by fire. Figure 4.3A demonstrates the patchy nature of prescribed burn. The understorey forest on the eastern side of the plot showed a larger and uniform burnt area as compared to the west (Figure 4.3B) and a large unburnt area in the south-western edge of the plot slightly away from the plot centre (Figure 4.3C). Apart from that, there were unburnt patches interspersed with burnt patches all around the plot. The severity class identified based on the field assessments suggested a variable intensity of fire ranging from a warm ground burn to an intense understorey fire.

4.3.2 TLS change detection

4.3.2.1 Descriptive statistics

In 16 of the 18 TLS-derived metrics, the mean of the change metrics in the control plot varied between 0.95-1.01 (σ = 0.14–0.45) as listed in Table 4.2. The mean for both *AGH skewness*$_{change}$ and *AGH kurtosis*$_{change}$ were exceptions to this trend and showed a much higher value of 1.36 (σ = 10.91) and 1.53 (σ = 2.84), respectively. Percentage of voxels in the control plot which were classified as having undergone change varied between 1% and 9% for all 18 metrics.

(A) (B) (C)

Figure 4.3 (A) Patchiness of low intensity prescribed burns that result in a mosaic landscape of burnt and unburnt patches, (B) A large burnt area on the eastern side of the fire-altered plot, (C) Part of the unburnt patch in the south-western side of the fire-altered plot.

In the fire-altered plot, the metrics showed a much more diverse mean change which was recorded in the range of 0.48–1.19 (σ = 0.32−1.67) in contrast to the control plot. The percentage change recorded by these metrics was in the range of 18%–52%. The percentage of voxels affected by change because of the fire varied between 22% and 71%. $AGH\ skewness_{change}$ showed a mean value of 1.39 (σ = 17.06) which was quite similar to that from the control (μ = 1.36, σ = 10.91). $AGH\ skewness_{change}$ showed a lower mean value of 1.29 (σ = 2.09) in the fire-altered plot as compared to the control (μ = 1.53, σ = 2.84). The percentage of voxels identified as having undergone a change in the fire-altered plot was 3% and 2% for $AGH\ skewness_{change}$ and $AGH\ kurtosis_{change}$, respectively. The change in understorey vegetation height as computed by AGH95 and AGH99 metrics in the two plots is listed in Table 4.3. The mean change in the control plot was 1cm and 3cm (σ = 7−11 cm) for the AGH95 and AGH99 metrics, respectively, as compared to 5cm and 9cm (σ = 16−20 cm) in the fire-altered plot. This is a very small change at the plot level.

Table 4.2 Descriptive statistics of the change detected by various TLS-derived metrics and number of change voxels examined for the control and fire-altered plot. Statistics presented are aggregates of all voxels in each plot. Voxels recording a change have been computed as those having values greater than 1.64 × σ of μ for that particular metric.

Metric	Control Plot				Fire-Altered Plot			
	Statistic		Change		Statistic		Change	
	Mean (μ)	Standard Deviation (σ)	Number of Voxels	% of Voxels (n = 872)	Mean (μ)	Standard Deviation (σ)	Number of Voxels	% of Voxels (n = 925)
$AGH10_{change}$	0.99	0.14	60	7	0.76	0.38	587	63
$AGH20_{change}$	0.98	0.16	41	5	0.72	0.37	571	62
$AGH30_{change}$	0.98	0.15	57	7	0.72	0.38	604	65

$AGH40_{change}$	0.98	0.14	78	9	0.71	0.37	623	67
$AGH50_{change}$	0.98	0.14	64	7	0.72	0.36	598	65
$AGH60_{change}$	0.97	0.19	32	4	0.74	0.37	491	53
$AGH70_{change}$	0.97	0.21	31	4	0.76	0.38	449	49
$AGH80_{change}$	0.96	0.18	44	5	0.79	0.39	475	51
$AGH90_{change}$	0.95	0.18	56	6	0.82	0.42	451	49
$AGH95_{change}$	0.95	0.21	54	6	0.85	0.44	400	43
$AGH99_{change}$	0.95	0.26	69	8	0.82	0.44	344	37
mean AGH_{change}	0.96	0.13	70	8	0.76	0.32	563	61
mode AGH_{change}	1.01	0.38	39	4	0.70	0.54	320	35
maximum AGH_{change}	0.98	0.40	70	8	0.70	0.38	199	22
AGH skewness$_{change}$	1.36	10.91	6	1	1.39	17.06	26	3
AGH kurtosis$_{change}$	1.53	2.84	29	3	1.29	2.09	19	2
point count$_{change}$	1.00	0.45	37	4	0.48	1.67	653	71
mean intensity$_{change}$	0.99	0.15	64	7	1.19	0.41	506	55

Table 4.3 Summary statistics of the absolute change in height detected by AGH95 and AGH99. Statistics presented are aggregates of all voxels in each plot.

Metric	Control Plot		Fire-Altered Plot	
	Mean (μ)	Standard Deviation (σ)	Mean (μ)	Standard Deviation (σ)
AGH95	1 cm	7 cm	5 cm	16 cm
AGH99	3 cm	11 cm	9 cm	20 cm

Histogram distributions between the control and fire-altered plot for all the TLS metrics were plotted to ascertain if fire induced change was discernible. It is evident from Figure 4.4 that there were clear differences between the two plots across all but two metrics (*AGH skewness*$_{change}$ and *AGH kurtosis*$_{change}$). General trends suggest that histogram distributions were approximately normal in the control plot for most metrics. In the fire-altered plot most of the metrics exhibited either multi- or bi-modal distributions.

Histogram distribution of voxels in the control plot was approximately normal when computed using metrics such as $AGH50_{change}$ to $AGH99_{change}$, *mean* AGH_{change}, *point* $count_{change}$ and *mean* $intensity_{change}$. For these metrics the mode was centred between 0.9 and 1.0 with the mean and mode being coincidental. The histogram distribution of *point* $count_{change}$ metric (Figure 4.4l) was slightly

flatter in comparison to the metrics which were normally distributed ($AGH50_{change}$ to $AGH99_{change}$, *mean* AGH_{change}, and *mean intensity*$_{change}$). This is demonstrated by the large σ value recorded by *point count*$_{change}$ at 0.45 in comparison to the abovementioned metrics (σ = 0.14 − 0.26).

Histogram distributions for other metrics such as $AGH10_{change}$ to $AGH40_{change}$, (Figure 4.4a–d) and *mode* AGH_{change} (Figure 4.4n) showed multiple peaks in the control plot. The common factor between the histograms of these metrics is that the mode was centred between 0.9 and 1.0. The peak in the histograms for these metrics was seen to occur at 1.1–1.2. AGH metrics such as $AGH10_{change}$ and $AGH20_{change}$ exhibited a minor peak centred at 0.7–0.8 (Figure 4.4a, b). Histogram distribution of $AGH95_{change}$, $AGH99_{change}$ and *maximum* AGH_{change} (Figure 4.4i, m, o) exhibited a slight negative skew with the mode centred at 1.0–1.1. *AGH skewness*$_{change}$ and *AGH kurtosis*$_{change}$ (Figure 4.4p, q) histogram distribution was very flattish in comparison to the distribution of other metrics from the control plot. Both these metrics showed a very large variance.

The histogram distributions of the TLS-derived metrics were very different in the fire-altered plot. None of the distributions except *point count*$_{change}$ (Figure 4.4l) were unimodal. Histogram distribution of *point count*$_{change}$ was extremely positively skewed with the mode centred between 0 and 0.10. $AGH10_{change}$ (Figure 4.4a) distribution was multimodal with peaks at 0.4–0.5, 0.6–0.7, 0.8–0.9 and 0.9–1.0. Distributions of $AGH20_{change}$ to $AGH95_{change}$ and *mode* AGH_{change} were nearly bimodal with 0.4–0.5 and 0.8–0.9. For the remaining metrics ($AGH99_{change}$, *mean* AGH_{change}, *maximum* AGH_{change}, *AGH skewness*$_{change}$, *AGH kurtosis*$_{change}$, *AGH intensity*$_{change}$), the distribution was comparatively flat. The distribution of both *AGH skewness*$_{change}$ and *AGH kurtosis*$_{change}$ from the fire-altered plot in particular were similar to those from the control plot (Figure 4.4p, q).

Histogram distribution of *mean intensity*$_{change}$ (Figure 4.4r) was flatter in the fire-altered plot with a large variance. Barring the histogram distribution of *AGH kurtosis*$_{change}$ and *AGH kurtosis*$_{change}$ all others exhibited a much higher variation in the fire-altered plot in contrast to the control plot whilst also showing a change in the distribution.

4.3.2.2 Spatial distribution of change

The spatial distribution of change detected by the 18 TLS-derived metrics in the two plots is presented in Figure 4.5 as binary maps of ‘change’ and ‘no change’ categories. This Figure shows that no metrics reported a change (greater than $\mu \pm 1.64 \times \sigma$) in the majority of the control plot.

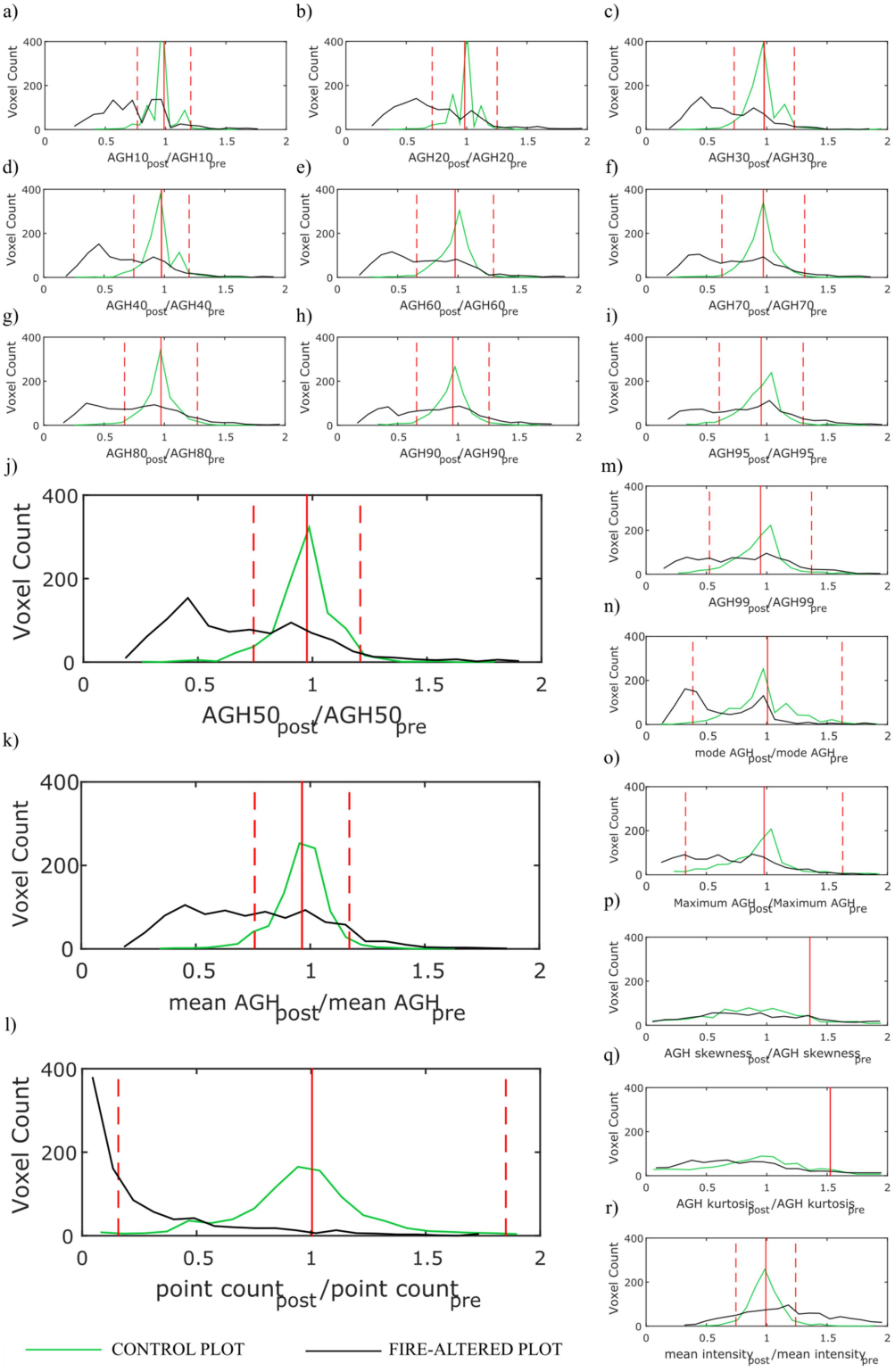

Figure 4.4 Histograms of voxels for the TLS-derived metrics in the control and fire-altered plot. The solid red line indicates μ change for that metric in the control plot. Voxels with values outside of the range defined by the dashed red lines (μ ± 1.64 × σ) are considered as fire-altered.

The percentage of plot area that showed a change in the control plot corresponded to 1%–9% of the voxels. In contrast, in the fire altered plot change was detected in 22%–71% of the voxels using 16 of the 18 TLS-derived metrics (except *AGH skewness*$_{change}$ and *AGH kurtosis*$_{change}$). *AGH skewness*$_{change}$ and *AGH kurtosis*$_{change}$ showed no difference between the control and fire-altered plot.

The spatial pattern and distribution of change in the control plot did not vary as much between the various metrics. There was some systematic change observed towards the south eastern part of the control plot using the *AGH*$_{change}$ percentiles (except *AGH99*$_{change}$), *mean AGH*$_{change}$, *point count*$_{change}$ and *mean intensity*$_{change}$. This region of change found in the control plot was at the location of the defoliated fallen tree. Apart from this the little change detected by all the metrics in the control plot appeared to be random with little evidence of clustering as is evident from Figure 4.5. In the fire-altered plot, the spatial pattern of change was markedly different as compared to the control plot. % of voxels affected by the fire ranged between 62% and 67% for *AGH10*$_{change}$ to *AGH50*$_{change}$ metrics. Most of the change detected by these five metrics was in the eastern and northern part of the plot with small unburnt patches interspersed. Most of the unburnt area was around the west and south western edge of the plot. The change detected by the remaining *AGH*$_{change}$ percentiles decreased from 53% (*AGH60*$_{change}$) to 37% (*AGH99*$_{change}$).

These upper *AGH*$_{change}$ percentiles detected more unburnt areas in north and north-west edge of the plot. *AGH95*$_{change}$ and *AGH99*$_{change}$ in particular detected patchy burnt areas within large contiguous unburnt areas which were quite opposite to the pattern of change detected by other *AGH*$_{change}$ percentiles and field assessments of plot areas burnt. These two metrics also detected a large burnt area only in a small section of the south-eastern edge of the plot. Spatial pattern of change detected by *maximum AGH*$_{change}$ and *mode AGH*$_{change}$ was similar to *AGH99*$_{change}$.

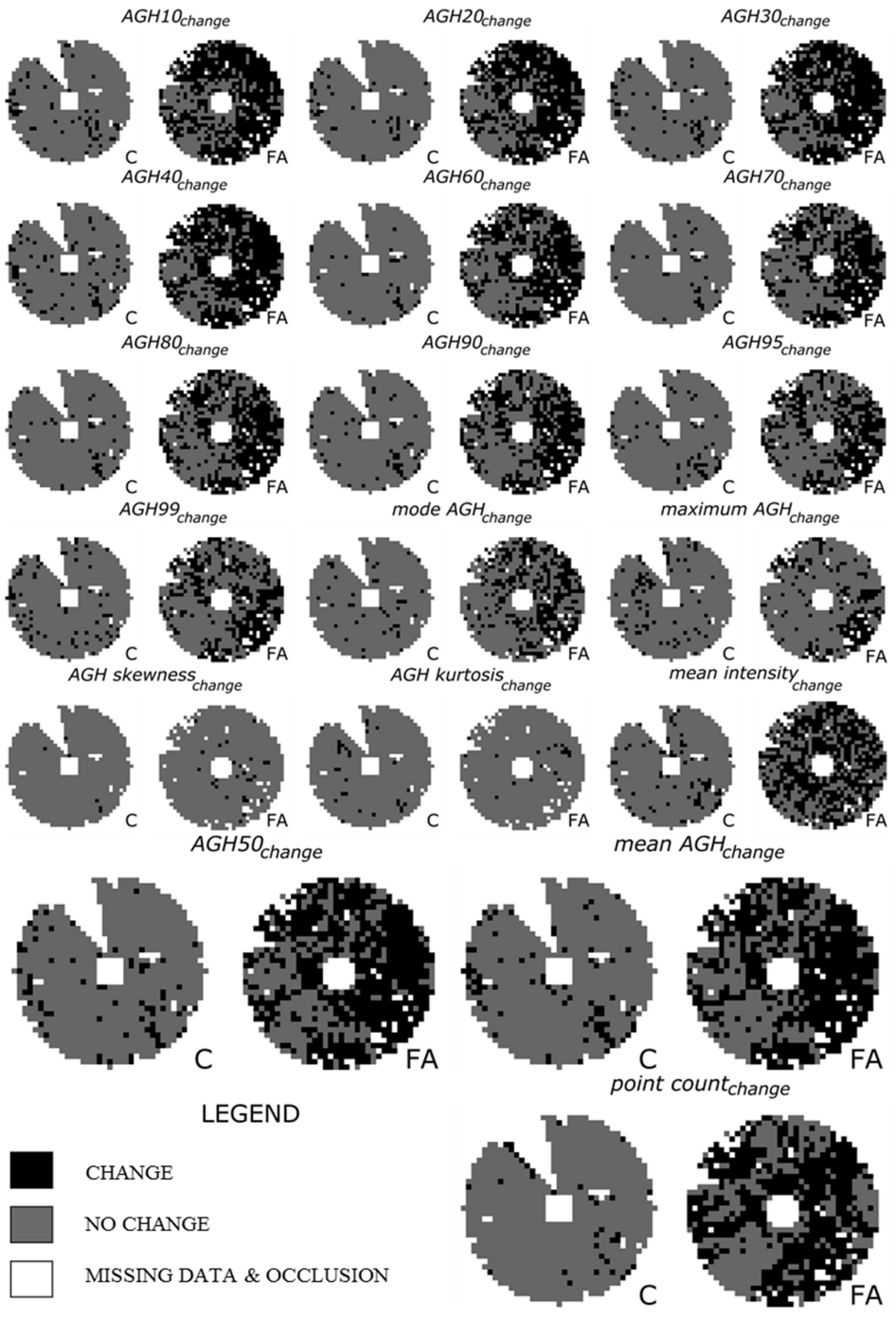

Figure 4.5 Spatial distribution of change detected by the various TLS-derived metrics in the control (C) and fire-altered (FA) plot. Blank areas correspond to occluded voxels or missing data. Areas of no change (grey) were calculated as having values within 1.64 ×σ of the μ from the control plot.

Maximum AGH_{change} detected even lesser burnt patches (22%) as compared to *mode* AGH_{change} (35%). *Mean* AGH_{change} detected change similar to $AGH10_{change}$ to $AGH50_{change}$ (61%). *Point* $count_{change}$ metric detected change in 71% of the voxels of the fire-altered plot.

Patches of no change were limited to the south-west part of the plot and smaller patches elsewhere interspersed with large patches of burnt areas especially in the western side. The pattern of change detected by *Point* $count_{change}$ was somewhat comparable to $AGH10_{change}$ to $AGH50_{change}$ and *mean* AGH_{change}. The *mean* $intensity_{change}$ metric showed an extremely patchy pattern with random burnt and unburnt areas throughout the fire-treated plot distinct from the change detected by the other metrics

4.3.2.3 Effects of occlusion

The mean value of the various AGH metrics showed very little change for the different visible plot area coverage in the control plot. As examples, the plots of AGH50, AGH90, mean AGH, point count and mean intensity are shown in Figure 4.6. The mean change decreased slightly from 0.008 cm at 5% plot coverage to 0.007 at 70% plot coverage using the mean AGH metric. The trend for AGH50 was similar to that of mean AGH. AGH90 showed an opposite trend of an increasing mean value from 0.012 cm at 5% plot coverage to 0.014 cm at 70% plot coverage. The point count decreased from 152 at 5% plot coverage to 88 at 70% plot coverage in the control plot (Figure 4.6). Mean intensity metric in contrast increased slightly from −0.10 to 0.20.

In the fire-altered plot, the change detected was relatively large compared to the control plot. The mean AGH metric increased from 0.03 cm at 5% plot coverage to 0.05 cm at 70% plot coverage. A similar trend was observed in AGH50 and AGH90 metric. The point count decreased sharply as compared to the control plot from 2570 at 5% plot coverage to 2100 at 70% plot coverage. Mean intensity metric showed an increase just like in the control plot.

A common trend observed in both the plots was that although the mean change in value by the various metrics was very small, the associated standard deviation values decreased with increasing plot area coverage. For example, the mean standard deviation values calculated using mean AGH decreased from 0.005cm (5% plot coverage) to 0.001cm (70% plot coverage) in the control plot and from 0.018cm (5% plot coverage) to 0.006cm (70% plot coverage) in the fire-altered plot. This was consistently observed across different metrics with larger standard deviation values at 5% plot coverage as compared to 70% plot coverage irrespective of the plots.

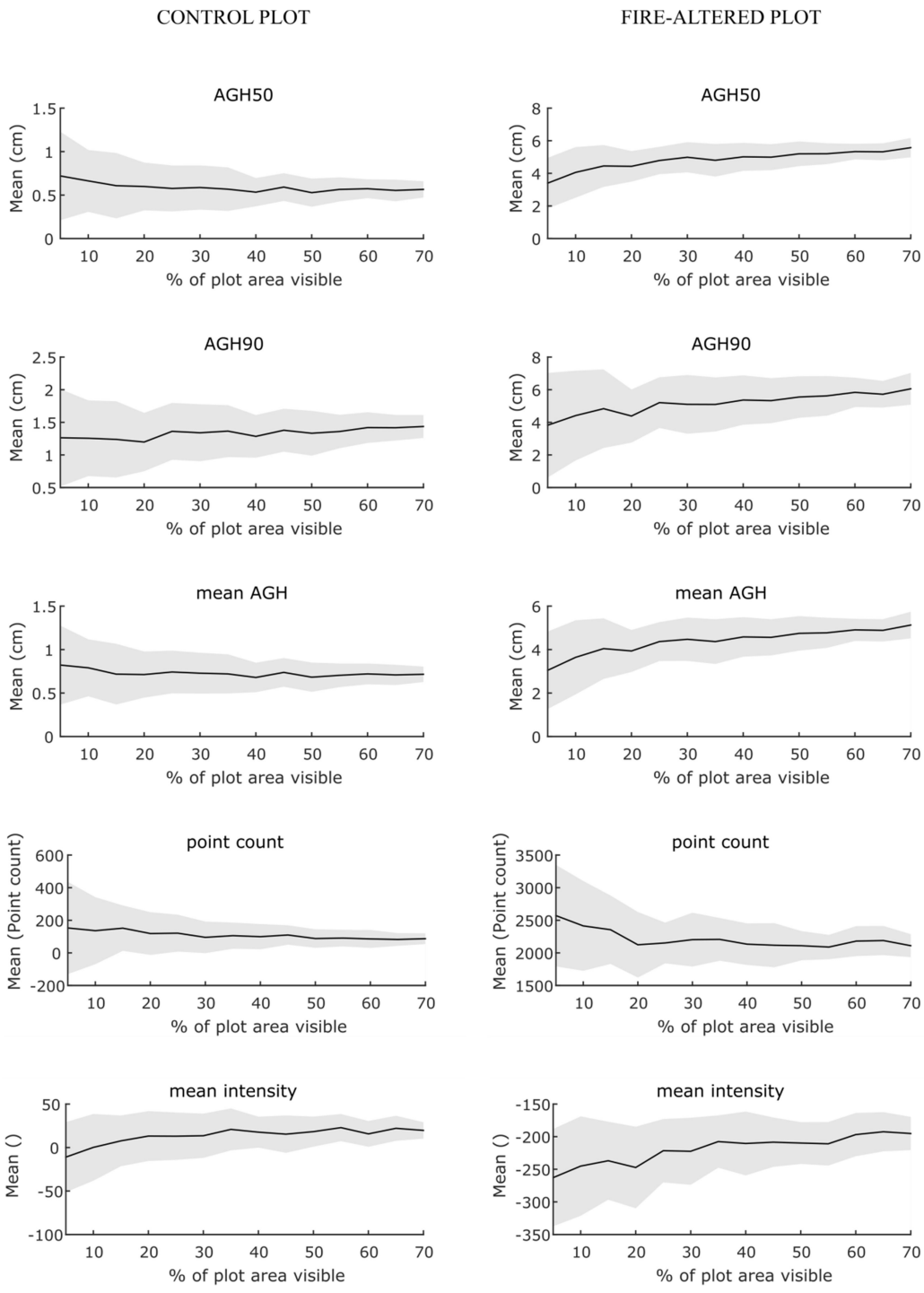

Figure 4.6 Mean and Standard Deviation (grey polygon) at different plot coverage for five sample metrics from the control and fire-altered plot.

4.4 Discussion

TLS technology is increasingly being used to produce accurate measurements of forest understorey conditions (Loudermilk et al., 2009, Olsoy et al., 2014, Vierling et al., 2013). However, the ability to monitor understorey forest dynamics (biomass loss or growth) using TLS has not been widely reported. Results obtained in this study indicate that fire-induced change, as an example of a disturbance in a forest understorey, is clearly discernible between multi-temporal TLS scans. The spatial distribution of change detected by most of the metrics in the fire-altered plot was found to be in agreement with visual field assessments demonstrating the concept of *similarity*. TLS derived metrics were assessed for correctly reporting minimal or no change in unaltered natural landscapes. In this study, this concept of *stability* was assessed using the control plot. All metrics showed only small changes between 1% and 5% in the control plot. The concept of *sensitivity* was explored by the ability of the metrics to detect fire-induced change in the forest understorey.

In the fire-altered plot, all metrics (except $AGH\ skewness_{change}$, $AGH\ kurtosis_{change}$ and $mean\ intensity_{change}$) showed a change between 30% and 52% whilst 10 of these exhibited bimodal distribution highlighting the subplot sensitivity of TLS metrics to detecting fire-induced change.

The methodology employed in this research is unique in that it applies bi-temporal TLS scans captured in single-scan mode to detect and quantify change in forest understorey. Scans were captured in single-scan mode and with a minimal fixed reference system which allowed for faster data acquisition and processing whilst also avoiding the need for co-registration (Liang et al., 2012, Litkey et al., 2008). It has been demonstrated that whilst TLS data acquired in single-scan mode suffers from some limitations such as occlusion (Dassot et al., 2011), such datasets still have utility in change detection studies as has been demonstrated in this chapter. However, in change detection studies in a forested environment, occlusion due to high tree densities needs to be carefully considered. The results of modelling the effects of occlusion in this chapter show that high levels of occlusion are likely to bias the results towards changes occurring closer to the scanner's location (the plot centre). Hence, for the change detection methods described in this chapter using TLS to be successful, it is recommended that at least 50% plot visibility needs to be achieved.

Given that the control plot received no burn it was reasonable to expect that there would be little or no change detected between the two TLS data capture. TLS-derived metrics recorded no change in metric values more than 90% voxels across the plot. The upper AGH_{change} percentiles ($AGH90_{change}$,

$AGH95_{change}$ and $AGH99_{change}$) were relatively less stable as compared to some of the lower AGH percentiles ($AGH10_{change}$ to $AGH50_{change}$) (for example $AGH95_{change}$.σ = 0.21 and $AGH50_{change}$ σ = 0.14) in the control plot. It could be that in the event of a low intensity change event such as prescribed burns, environmental factors such as wind can potentially affect the stability of these metrics because of movement of features in the landscape. It must be noted that during the second set of TLS data capture the conditions in the study area were extremely windy with faint drizzle which may have also contributed to noise in the point clouds. Another reason is that these upper AGH_{change} percentiles are also most likely to contain change in response to phenological growth and senescence in the control plot. However, the histogram distribution for some lower AGH_{change} percentiles ($AGH10_{change}$ to $AGH40_{change}$) was multimodal while for the other metrics it was normal. These lower AGH_{change} percentile metrics are likely to be affected by interaction with ground elements and thus may not be appropriate for describing unaltered understorey landscapes.

In the fire-altered plot, 16 TLS-derived metrics were reported as being sensitive at detecting fire-induced change in the forest understorey. This is supported by the σ values being much larger in the fire-altered plot (0.32–1.67) in comparison to the control plot (0.14–0.45) as listed in Table 4.2. A larger σ value is representative of unburnt patches interspersed with burnt areas in the fire-altered plot when examining the histograms. Histograms of AGH_{change} percentiles such as $AGH30_{change}$ to $AGH95_{change}$ exhibit bimodal distributions with peaks in the range of 0.3–0.5 and 0.8–1.1 in the fire-altered plot. The local maximum peak between 0.3 and 0.5 corresponds to voxels that have undergone fire-induced change. These voxels are also found to lie outside the dashed red line in Figure 4.4 which is indicative of a fire-induced change. Similarly, voxels around the local maximum peak centred at 0.8–1.1 are those belonging to unburnt patches in the forest understorey in the fire-altered plot. As stated earlier, values closer to 1 in ratio-based metrics is indicative of little or no change. Thus, the bimodal distribution exhibited by some TLS-derived metrics is able to account for populations belonging to two disparate groups. In this research these two groups would be burnt and unburnt forest understorey. The upper AGH_{change} percentiles ($AGH70_{change}$ to $AGH99_{change}$) and *maximum* AGH_{change} are shown to record a lower fire-induced change (37%–53% voxels) as compared to lower AGH_{change} percentiles (62%–67% voxels). The field based assessments recorded burn in 60%–70% of the plot area. This could be attributed to the environmental conditions (for example wind) and patchy nature of prescribed burns. If a voxel with dimensions 0.5 × 0.5 ×1.0 m was affected by fire, a few remaining stalks of grass may classify this voxel as being unburnt. These findings suggest that the upper AGH_{change} percentiles may not actually be appropriate for reporting fire-induced change following low intensity prescribed burns. The *mean intensity*$_{change}$ metric which was stable in the control plot showed a change in the fire-

altered plot. The change recorded was only 19% which suggests that the change detected by *mean intensity*$_{change}$ in the fire-altered plot could be due to a number of factors other than fire.

Although it has been established in this chapter that TLS technology and its derived metrics are sensitive at detecting fire-induced change in forested understorey, it is equally important to attempt to map where these changes have occurred on the ground. The patchy nature of prescribed burns is a well acknowledged fact (Penman et al., 2007). As shown in Figure 4.5, vast areas of the control plot recorded no change which was to be expected. However, the majority of the change detected in the control plot for most metrics was found to occur in a small localised area of the plot. This corresponded and could be explained due to the defoliation of a fallen tree. However, this change was not detected by *AGH99*$_{change}$, *mode AGH*$_{change}$ and *maximum AGH*$_{change}$ metrics as the large woody component of the tree was still present. This defoliation appears to present a similar pattern to fire induced change within the fire-altered plot where large woody debris was still present following prescribed burns. Whilst it was ascertained that the ideal metric should remain stable and detect little or no-change in the control plot, it would be inaccurate if the metric did not detect a real and a substantial non fire-induced change in the forest understorey even in the undisturbed plot.

In the fire-altered plot, unburnt patches interspersed with burnt patches are reported by the majority of the metrics (except *AGH skewness*$_{change}$ and *AGH kurtosis*$_{change}$). Figure 4.3A shows an image from the fire-altered plot highlighting the mosaic landscape as a result of the prescribed burn. Although the degree of patchiness and plot area burnt is extremely variable amongst the metrics (22%–71%), the ability of TLS technology to map this 'patchiness' is an extremely promising finding. The level of patchiness within burnt areas can determine the proportion of vegetation population exposed to heat. This can inform vegetation mortality rates and seed germination (Price et al., 2003, Turner et al., 1994). Patchiness can also help predict fire intensity. Low intensity fires are shown to be significantly patchier than higher intensity fires (Ooi et al., 2006). The pattern of the burn represented by the binary maps (Figure 4.5) for many metrics (*AGH10*$_{change}$ to *AGH50*$_{change}$, *mean AGH*$_{change}$ and *point count*$_{change}$) is similar and closer to the field assessments of burnt areas. This includes both the percentage area burnt and spatial distribution of burnt areas in the fire-altered plot. These metrics consistently detected a much larger burnt area on the eastern side of the plot (Figure 4.3B) in comparison to the west with a large unburnt patch in the south-west region of the plot.

From the above analysis $AGH50_{change}$, *mean* AGH_{change} and *point* $count_{change}$ seem to be the most suitable individual metrics for attributing change in an altered understorey forest whilst remaining stable in an undisturbed one. It is important to ensure that the metrics being used in change detection studies remain stable in an undisturbed landscape whilst remaining sensitive at attributing change in an altered landscape. It is also important to consider that the metrics being used report spatial distribution of change similar to change occurring on the ground. These findings suggest that TLS technology and TLS-derived metrics can be used to supplement the routine qualitative field assessments of change which are often based on visual estimates thereby providing a method to allow for a more quantified and accurate reporting approach. The burn maps showing the spatial distribution of change can be used by land managers to identify areas in need of urgent rehabilitation.

Future work could involve exploring the utility of the method presented in this research to quantify biomass change. This research could be further developed by exploring the binary change detection maps for mapping different burn severity levels. This could also help identify unburnt patches which can help in understanding ecological impacts on fire-sensitive plants, watershed hydrology and soil stability amongst others. This may involve using a combination of the metrics used in this chapter given their demonstrated differences in each metric shown here. Given that post-burn TLS scans were carried out within two weeks of the burn event, they helped ascertain change in the landscape in response to the burn. A longitudinal study involving multi-temporal scans over longer time scales can help monitor fuel accumulation, post-fire regeneration dynamics and vegetation senescence.

4.5 Summary

The objective of this chapter was to assess a set of TLS -derived metrics for detecting, analysing and visualising fire-induced change in a forest understorey following low intensity prescribed burns. The key findings of this chapter demonstrate that TLS technology can be effectively used in a single-scan mode to make repeated measurements in both an unaltered and altered forest understorey with a minimal fixed reference system. The method described in this chapter facilitates rapid data capture, easy post-processing of data and is fit-for-purpose in terms of the required accuracies to detect fire-induced changes in forest understorey. This chapter successfully demonstrated that three TLS-derived metrics $AGH50_{change}$, *mean* AGH_{change} and *point* $count_{change}$ are capable of attributing fire-induced change in forest understorey that can be qualitatively validated with field assessments. These metrics whilst detecting fire-induced change (*sensitive*) are also

capable of capturing the patchy nature of prescribed burns and produce burn maps comparable to visual field assessments of area burnt (*similarity*). At the same time, these three metrics report little or no change in an undisturbed (control plot) forest understorey (*stability*).

Chapter 5. Reporting changes in burnt forest understorey metrics using Terrestrial Laser Scanning

5.1 Introduction

Chapter 4 demonstrated the utility of TLS metrics derived from 3D point clouds for mapping fire-induced change in the forest understorey following prescribed burns. This chapter builds on those findings by applying TLS-derived metrics to quantify changes in a forest understorey at multiple times following prescribed burns. These fire effects include area burnt, patchiness, post-burn understorey fuel accumulation and prescribed burn efficiency. The TLS metric used to ascertain these fire effects is *mean* AGH_{change}. Validation between field observations and TLS data is presented. A discussion on the accuracy of TLS-derived measures of change compared to that of field assessments is also made in this section. The chapter concludes with a brief section on the potential of TLS in the field of mapping and measuring fire-effects on the landscape.

5.2 Methods

This section describes the change metrics calculated using TLS and field data. Validation of TLS data with the field data is also discussed followed by a description of the 'standard' visual assessments conducted post-burn.

5.2.1 Study area

Four understorey plots were used in this study. Three of these received a fire treatment and are referred to as fire-altered plot 1, fire-altered plot 2 and fire-altered plot 3 respectively whilst one remained unburnt (control).

5.2.2 Calculating change

This section discusses the change calculated in the field at different time epochs using *mean* AGH_{change}. Details on the derivation of this metric have been discussed in Section 4.2.3. *Mean* AGH_{change} was selected as the metric used to quantify changes in the understorey. *Mean* AGH_{change} was shown to be sensitive at detecting fire-induced changes in the burnt forest understorey, accurate at reporting change when compared to visual field assessments and stable when repeated observations were taken in an undisturbed forest understorey. Height-based measure of change in the understorey fuel height at each epoch was calculated using AGH95. This metric is preferred to other height-based metrics such as AGH99 and maximum height because they are prone to be affected by wind and can add noise to the point clouds.

5.2.2.1 Change in mean AGH metric

TLS data was captured in single-scan mode at different time epochs, pre-burn and two weeks post-burn in all the four plots. For the control and fire-altered plot 3, TLS data was also captured two years post-burn. TLS data could not be captured in the other two fire-altered plots at this epoch because of the (accidental) removal of reference target at the plot centre. Co-registration and metrics derivation was performed using the methods described in Chapter 4, Section 4.2. To map and comparatively assess the likelihood of change in understorey forest strata, *mean* AGH_{change} was employed to characterise change over the three different time epochs. Three equations were derived, each corresponding to a different time epoch. These will be referred to as *T1*, *T2* and *T3* respectively and are described in Table 5.1.

Table 5.1 Epochs for which change was calculated where A refers to the metric being reported. In this chapter, the metric is *mean* AGH_{change}.

Epoch	Formula	Application	Equation
T1	$Metric\ A_{post-burn\ 2\ weeks} / Metric\ A_{pre-burn}$	Burn area, patchiness	**5.1**
T2	$Metric\ A_{post-burn\ 2\ years} / Metric\ A_{post-burn\ 2\ weeks}$	Fuel accumulation	**5.2**
T3	$Metric\ A_{post-burn\ 2\ years} / Metric\ A_{pre-burn}$	Efficacy of the prescribed burn	**5.3**

The range of values derived from the equations 5.1-5.3 is between 0 and 2. The *mean* AGH_{change} metric detects a change in understorey cover if the mean height of vegetation within a voxel has changed relative to pre-burn levels. Values closer to 0 indicate a decrease in understorey fuel while those closer to 2 indicate an increase. No change corresponds to values near 1 and is indicative of an understorey fuel layer with little or no measurable change.

Epoch *T1* compares the understorey landscape two weeks post-burn to pre-burn measures. This temporal comparison measures immediate post-burn effects such as the extent and number of burnt area patches. These effects can also be described as first-order effects (Key, 2005) and are consequences to ecological components that existed before a fire. These may include loss of understorey vegetation biomass, woody fuel and litter. These effects on the biophysical components are generated from fire intensity (Key and Benson, 2005).Epochs *T2* and *T3* which measure long-term fire effects may help ascertain fuel load accumulation and the efficacy of prescribed burns respectively. This is an important aspect of fire ecology and management.

Temporal aspects of fire effects such as time-since fire and inter-fire interval can be ascertained from epochs *T2* and *T3*. Time-since-fire, which is defined as the number of years between the most recent fire, is a key indicator used in fire management for fuel hazard reduction due to often rapid rates of fuel accumulation following fire (Fernandes and Botelho, 2003). Inter-fire-interval, on the other hand, refers to the number of years between the two most recent fires and has been reported to be the more powerful factor of the two in discerning effects on forest understorey (Watson and Wardell-Johnson, 2004).

5.2.2.2 Spatial statistics

To report on the patchiness of the change in the understorey landscape, spatial statistics were computed. These statistics were calculated for both increases and decreases in understorey fuel load relative to pre-burn measures. Voxels were deemed to be connected and part of the same patch when any of their corners and sides touched. The patch statistics computed were the number of patches, mean patch size (sq. m) and standard deviation of patch size (sq. m).

5.2.3 Validation of TLS-derived change metrics

This section discusses the different field assessments recorded based on visual estimates of change in the plots at various epochs pre- and post-burn. It also discusses the accuracy assessment

undertaken which enables direct comparison between TLS-derived measures of change and visual estimates.

5.2.3.1 Field data assessments

a. Fuel hazard

A pre-burn fuel hazard assessment was carried out in all the four study plots pre-burn and the control and fire-altered plot 3 two years post-burn. The main purpose of the fuel hazard assessment was to make a rapid, visual assessment of the fuel arrangement and potentially correlate it with burn severity and also to assess fuel consumption by the prescribed burn event. The fuel hazard assessment was based on the Overall Fuel Hazard Assessment Guide (Hines et al., 2010). The process of assessing fuel hazard using this guide relies on visual assessment. Variables assessed include: near-surface percentage cover, near-surface average height, surface litter percentage cover, average litter depth and were evaluated against standard photos and illustrations.

b. Burn severity

Burn severity of prescribed burns was carried out based on a number of variables used in Australia and worldwide. Within Victoria, it is based on the Burn Severity Assessments Field Guide (DSE, 2010). It involves recording variables such as percentage area burnt, percentage canopy burnt, percentage canopy scorched and percentage near-surface fuel burnt within six weeks post-burn.

c. Land cover proportions

A 3 × 3m mixed land cover grid was set-out in the control and fire-altered plot 3. The grid comprised nine 1 × 1m cells. Within each cell a visual assessment of the land cover proportion was noted concurrent to TLS surveys pre-burn and two weeks post-burn. The different land cover elements recorded as a percentage were near surface live vegetation, litter, bare earth, and area burnt. The results are presented in Appendix 10.2.

5.2.3.2 Accuracy assessment

The metric *mean* AGH_{change} and field metrics were transformed to facilitate inter-comparison between TLS data and field-based visual assessments. Field metrics used were those for which proportions were recorded within the 3 × 3m grid was used. Data was transformed using equation 5.4.

$$(Metric_{Post-burn} - Metric_{Pre-burn}) / Metric_{Pre-burn} \quad \textbf{(5.4)}$$

The data is normalised on to a scale of -1 to +1. A negative value indicates a decrease in understorey fuel load whilst a positive value indicates an increase. Values close to zero correspond to no change.

The different field variables compared against the TLS-derived *mean* AGH_{change} were '*Near-Surface Live Vegetation'*, '*Litter',* '*Bare Earth'*, '*Near-Surface Live Vegetation and Litter'*, '*Near-Surface Live Vegetation and Bare Earth,*' '*Litter and Bare Earth'* and '*Near-Surface Live Vegetation, Litter and Bare Earth'*. Correlations between field measures and TLS-derived measures were conducted using Pearson product-moment correlation coefficient. This validation was performed only at epoch *T1* for the control plot and fire-altered plot 3.

5.3 Results

This section reports the changes in the forest understorey detected by the TLS metric *mean* AGH_{change} and field data for the different epochs.

5.3.1 TLS change detection and mapping

The change detected by *mean* AGH_{change} here is reported across three epochs: *T1, T2* and *T3*. Each epoch reports different post-fire effects such as burn area and extent, fuel accumulation and prescribed burn efficiency.

5.3.1.1 Epoch *T1*: Immediate post-fire effects

Epoch *T1* compares the changes in understorey fuel between two weeks post-burn to pre-burn. In this way, *T1* can help inform immediate post-burn effects such as the extent of burnt area patches. The *mean* AGH_{change} metric recorded lower mean values (decrease in understorey fuel) and higher standard deviation values for all fire-altered plots as compared to the control plot (Table 5.2).

Table 5.2 Summary statistics of the change detected by *mean* AGH_{change} for all the plots across the three epochs. Statistics presented are aggregates of all voxels in each plot. ND means no data was captured. (0 = Decrease in understorey fuel load, 1 = No change in understorey fuel load and 2 = Increase in understorey fuel load.)

Epoch	Control Plot		Fire-Altered Plot 1		Fire-Altered Plot 2		Fire-Altered Plot 3	
	μ	σ	μ	σ	μ	σ	μ	σ
T1	0.97	0.12	0.75	0.40	0.71	0.35	0.83	0.36
T2	0.90	0.23	ND	ND	ND	ND	0.77	0.42
T3	0.86	0.24	ND	ND	ND	ND	0.58	0.31

The percentage of change voxels (decrease and increase in understorey fuel load) was the lowest in the control plot (2.73–4.44%) as can be seen in Table 5.3. This indicates the least change in the forest understorey two weeks post-burn.

The normal distribution for the control plot for epoch *T1* is presented in Figure 5.1a and shows the mean and mode coincident and centred between 0.9 and 1.0. This indicates little change in the understorey vegetation between pre- burn and two weeks post-burn measures.

As shown in Figure 5.2a the spatial distribution of the change voxels in the control plot appeared to be random except some clustering observed in the south-eastern part of the plot. Large areas of the plot showed no spatial change. In the fire-altered plots, the percentage of voxels recording a decrease in understorey fuel load was between 47–67% while those recording an increase were approximately 7–15%.

The histogram distributions whilst being drastically different from the control plot also varied slightly from one another. Fire-altered plot 1 exhibited a near unimodal distribution with the mode centred between 0.4 and 0.5 (Figure 5.1a). Fire-altered plot 2 exhibited a nearly bimodal distribution with modal peaks at 0.4 – 0.5 and 0.9 – 1.0. In Fire-altered plot 3, the distribution was near-flat.

Table 5.3 Percentage of voxels affected by change. Total voxels per plot indicated by n. Change has been computed as those voxels having values less than (D), or greater than (I), 1.64 × σ of μ for *mean* AGH_{change} from the control plot. No data (ND) captured for fire-altered plots 1 and 2 at epoch *T2* and *T3*.

Epoch	Control (n = 878)		Fire-altered Plot 1 (n = 813)		Fire-altered Plot 2 (n = 815)		Fire-altered Plot 3 (n = 866)	
	D	I	D	I	D	I	D	I
T1	4.44%	2.73%	66.54%	8.49%	63.44%	7.12%	46.54%	14.78%
T2	0.58%	4.97%	ND	ND	ND	ND	24.35%	7.01%
T3	1.84%	3.33%	ND	ND	ND	ND	40.34%	2.40%

Pre-burn understorey fuel height in the control plot changed from 28cm pre-burn, to 27cm post-burn two weeks using AGH95 (μ = 1cm, σ = 7cm). The change in understorey fuel height was much greater in the fire-altered plots. It decreased from 28cm pre-burn to 21cm post-burn two weeks in fire-altered plot 2 (μ = 7cm, σ = 16cm). The change was similar in the other two fire-altered plots. In Fire-altered plot 3, it decreased from 35cm pre-burn to 30cm post-burn (μ = 5cm, σ = 16cm) whilst in fire-altered plot 1, from 26cm to 20cm (μ = 6cm, σ = 14cm).

The spatial distribution of change in fire-altered plots (Figure 5.2) appeared extremely patchy. These patches comprised large areas of decreased understorey fuel load and were interspersed with small patches of 'no change'. Fire treatment in fire-altered plot 1 resulted in an extremely patchy area of decreased understorey fuel load (Figure 5.2b). Fire-altered plots 2 and 3 produced areas of reduced understorey fuel which were relatively more contiguous in comparison to fire-altered plot 1. The *mean* AGH_{change} metric in fire-altered plot 2 detected a large patch of reduced understorey fuel load in the north-west area of the plot and smaller unburnt patches in the south-western area of the plot. The metric also detected a large unburnt area in the south-western edge of fire-altered plot 3 and smaller unburnt patches in the western area of the plot. Small areas of increase in understorey fuel from pre-burn levels were also detected in the fire-altered plots.

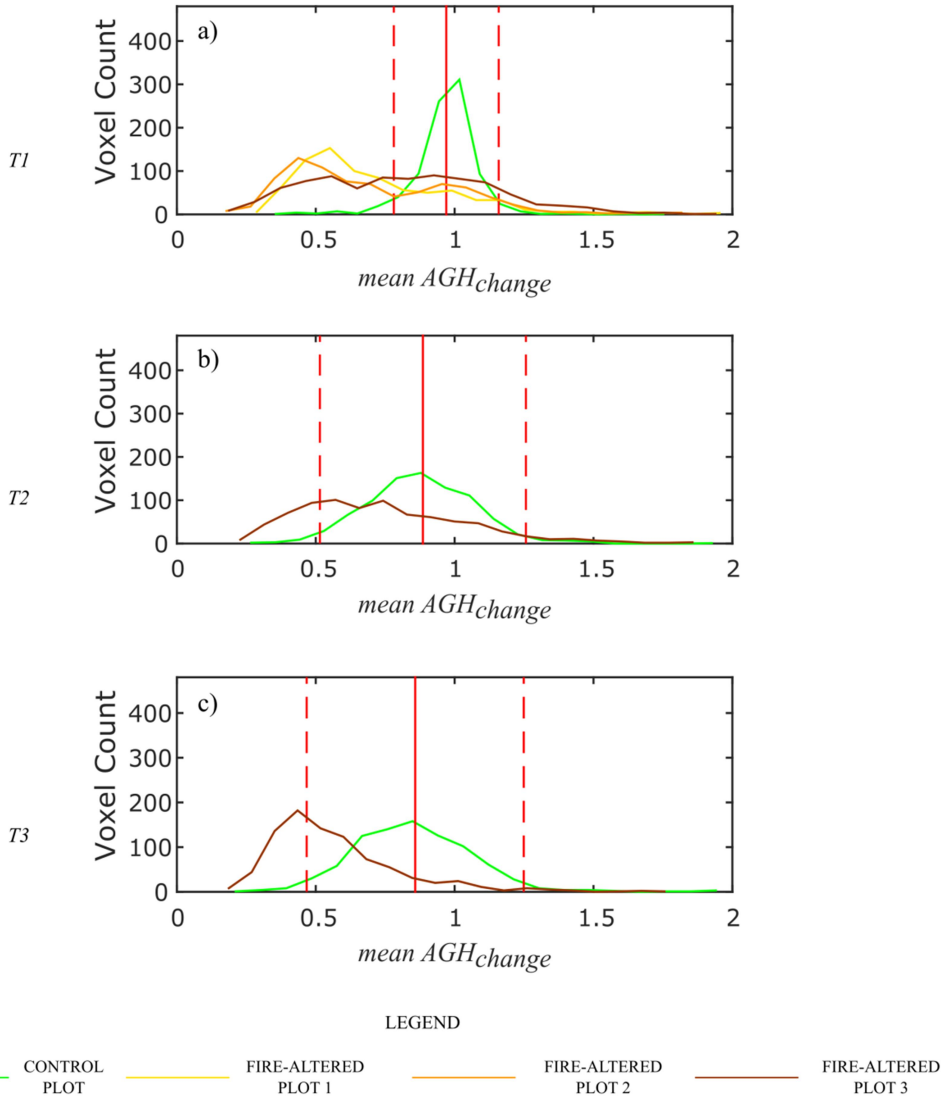

Figure 5.1 Histograms of voxels for *mean AGH_{change}* in the control and the three fire-altered plots across all the epochs. The solid red line indicates μ change for that metric in the control plot. Voxels with values outside of the range defined by the dashed red lines (μ ± 1.64 × σ) are considered as likely fire-altered. Values to the left of the dashed line indicate a decrease in biomass whereas values to the right of the dashed line increase an increase in biomass.

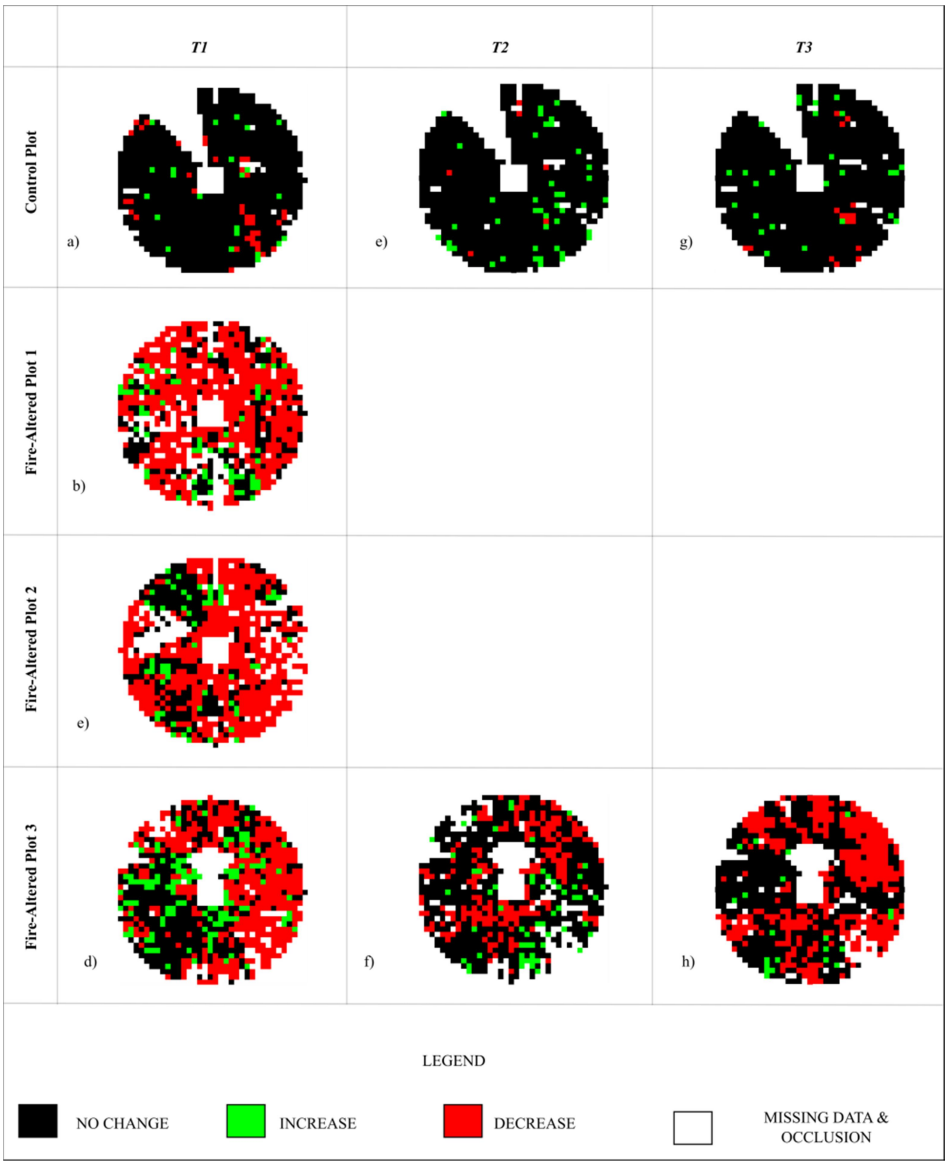

Figure 5.2 Spatial distribution of change detected by *mean* AGH_{change} in the four plots across all the epochs. Blank areas correspond to occluded voxels or missing data. Areas recording a decrease in understorey fuel (red) were calculated as having values less than -1.64 ×σ of the μ from the control plot whilst areas of increase in understorey fuel (green) as those having values greater than +1.64 ×σ.

The spatial statistics presented in Figure 5.3, show that mean patch size of change in understorey fuel load was the least for the control plot at *T1* (μ = 0.51 sq. m σ = 0.47 sq. m). Fire-altered plots 1 and 2 reported a similar number of patches with a reduction in understorey fuel (10 and 13 respectively). These two plots also recorded a similar mean patch size where a decrease in understorey fuel was observed (μ = 13.53 sq. m σ = 41.02 sq. m; μ = 9.94 sq. m σ = 30.05 sq. m

respectively). Fire-altered plot 3 showed the highest number of patches with a decrease in understorey fuel (n = 29) and recorded a low mean patch size (μ = 3.47 sq. m σ = 10.75 sq. m).

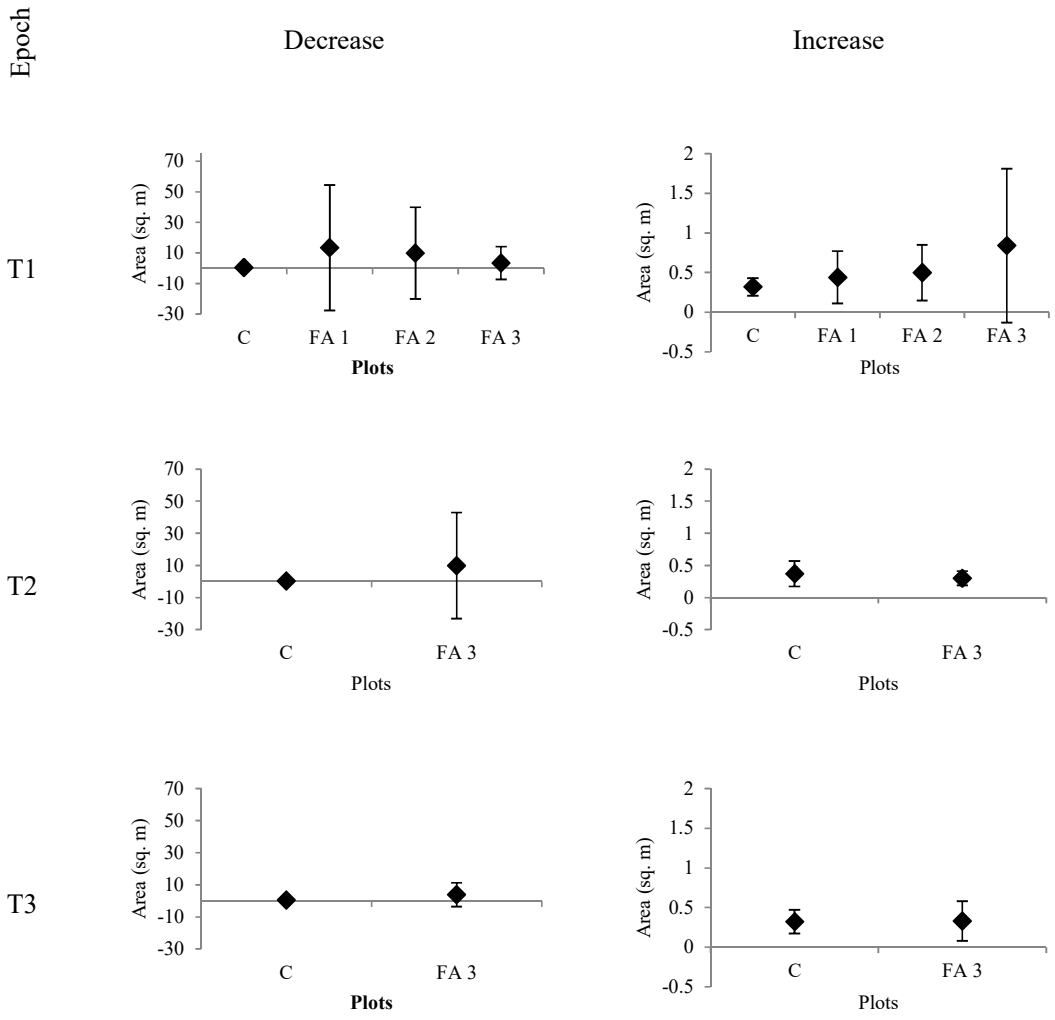

Figure 5.3 Spatial statistics computed for both the change scenarios (decrease and increase in understorey fuel load) in all the plots across all the epochs. (σ is plotted as error bars around μ)

5.3.1.2 Epoch *T2*: Fuel accumulation

Epoch *T2* compares the changes in biomass between two weeks post-burn to two years post-burn. Analysis of this epoch can help ascertain fuel accumulation since the burn event. The control plot indicated minimal fuel accumulation (μ = 0.90 σ = 0.23). This was not evident in fire-altered plot 3 where the mean change at *T2* (μ = 0.77, σ = 0.42) was lower as compared to *T1* (μ = 0.83, σ =

0.36). The histogram distribution of voxels as shown in Figure 5.1b indicate that it was normally distributed in both the control and fire-altered plot 3 when computed using *mean* AGH_{change}. The modal peak was centred between 0.9–1.0 in the control plot and 0.7–0.8 in fire-altered plot 3.

The percentage of voxels with a decrease in understorey biomass was lower in the control plot (less than 1%) as compared to fire-altered plot 3 (Table 5.2). For fire-altered plot 3, nearly 60% of the voxels recorded no change relative to post-burn two weeks levels, with almost 25% of voxels measuring a decrease and approximately 15% recorded an increase in fuel. The remaining 15% of voxels were obscured and removed from the dataset.

The understorey fuel height in the control plot decreased to 24cm two years post-burn from 27cm two weeks post-burn (μ = 3cm, σ = 10cm). The decrease was much larger in fire-altered plot 3. It reduced from 30cm two weeks post-burn to 20cm two years post-burn (μ = 10cm, σ = 17cm).

The spatial distribution of change supports the results reported in Table 5.2 showing that large areas of fire-altered plot 3 experienced no change in understorey fuel load (Figure 5.2f) at *T2*. The control plot too remained relatively unchanged (Figure 5.2e). The large unburnt area in the south-west edge of fire-altered plot 3 still showed no change in *T2*. Most of the patches recording a decrease in understorey fuel load were confined to the areas which either recorded no change or an increase in fire-altered plot 3 at *T1* (southern edge from the plot centre).Fire-altered plot 3 had 13 patches showing a decrease in understorey fuel, with the mean patch size being 9.83 sq. m (σ = 33.11 sq. m). In contrast, the control plot had only five patches with an average patch size of 0.25 sq. m (σ = 0 sq. m).

5.3.1.3 Epoch *T3*: Prescribed burn efficacy

Epoch *T3* compares changes in understorey fuel between pre-burn and two years post-burn. Analysis of this epoch can help indicate the burn efficiency of prescribed burns. The *mean* AGH_{change} metric detected a decrease in understorey fuel load for approximately 40% of the voxels in fire-altered plot 3 in comparison to less than 4% in the control plot (Table 5.2).

The histogram distribution of voxels at *T3* for the control plot was normal when plotted using *mean* AGH_{change} as shown in Figure 5.1c. In fire-altered plot 3 the distribution was normal however the mode was centred between 0.4 – 0.5 as compared to 0.8 – 0.9 for the control plot.

The understorey fuel height in the control plot calculated using AGH95 changed by 4cm (σ = 11cm). A much larger change in understorey fuel height was recorded in fire-altered plot 3 two years post-burn relative to pre-burn with a decrease by 15cm (σ = 14cm).

The spatial distribution of change as shown in Figure 5.2g indicates that the metric detected no change in large areas of the control plot. The *mean* AGH_{change} metric detected large patches in the eastern area of fire-altered plot 3 which continued to exhibit a decrease in understorey fuel load even after two years post-burn (Figure 5.2h). The unburnt patch along the south-west edge continued to show no change from pre-burn levels.

For this epoch, the fire-altered plot 3 had 23 individual patches showing a decrease in understorey fuel, with the average patch size being 3.84 sq. m (σ = 7.45 sq. m). By comparison, the control plot had only eight patches with an average patch size of 0.50 sq. m (σ = 0.42 sq. m).

5.3.1.4 Comparison between epochs *T1, T2* and *T3*

These results compared the measures observed for the different temporal combinations. *T1* measures the change between pre- and two weeks post-burn. *T2* measures the change between two years post-burn and two weeks post-burn. *T3* measures the change between two years post-burn and pre-burn. For all the three temporal epochs, the least change in understorey fuel was consistently observed in the control plot, with values ranging from 0.86 – 0.97 (see Table 5.2), remembering that values close to one are indicative of no change. An increase in standard deviation was observed in the control plot in *T2* (σ = 0.23) and *T3* (σ = 0.24) as compared to *T1* (σ = 0.12). However, the histogram distribution of voxels in the control plot was normal across all the epochs with the mean and mode being coincidental between 0.9 – 1.0. In fire-altered plot 3, the histogram distribution changed from being near flat at *T1* to flattish normal at *T2*. At *T3*, the histogram distribution of voxels was normal as shown in Figure 5.1.

The spatial distribution of change was similar across the three epochs in the control plot with more than 90% of the voxels measuring no change in understorey fuel load. In fire-altered plot 3, the percentage of voxels recording a decrease in understorey fuel load was highest for epoch *T1* (approximately 47%), followed by epoch *T3* (approximately 40%). For *T2* approximately 70% of the voxels showed no change in understorey fuel load. The spatial distribution of areas where a decrease in understorey fuel was recorded in fire-altered plot 3 could be discerned both at *T1* and

T3. As an example, the large area along the western edge of fire-altered plot 3 as shown in Figure 5.3 shows the persistent nature of these burn scars.

5.3.2 Field data assessment

5.3.2.1 Visual assessments

Visual assessment using photographic records showed that at two weeks post-burn, there was no observable difference in the control plot resulting from the surrounding prescribed burn. However, visual assessment of the fire-altered plots resulted in areas that were clearly burnt. Figure 5.4 illustrates the condition of each of the plots following the prescribed burn. Figure 5.5 shows the change in the condition of fire-altered plot 3 before the burn, two weeks post-burn and two years after the burn. These images show the vegetation structure, cover and density at the surface layer and how these were modified or removed due to fire over time. Whilst two years post-burn showed some regrowth in the understorey fuel it was not yet back to pre-burn levels in terms of both height and cover (Figure 5.5(C)).

(A) **(B)** **(C)** **(D)**

Figure 5.4 Post-burn images (taken two weeks post-burn) from the four plots ((A) control; (B) fire-altered plot 1; (C) fire-altered plot 2 & (D) fire-altered plot 3).

5.3.2.2 Fuel hazard visual assessment

a. Pre-burn

The near-surface (grass) and surface fuel (litter) layer showed similar cover and characteristics across the four plots pre-burn. Table 5.4 shows the percentage cover of the near-surface fuel varied between 30–40% for the fire-altered plots 1 and 2 while it was slightly higher in the control and fire-altered plot 3 at 50–60%. The average height for the near-surface fuel layer was 20–30cm for

all the plots with the exception of fire-altered plot 3 where it was slightly higher (30–40cm). The near-surface fuel hazard calculated was found to be *high* for all the plots.

(A) **(B)** **(C)**

Figure 5.5 Reference photos from fire-altered plot 3 (A) pre-burn, (B) post-burn two weeks & (C) post-burn two years.

The surface fuel layer showed greater variability in percentage cover than compared to the near-surface fuel. For the control and fire-altered plot 2, the surface fuel percentage cover was between 40–50% and for fire-altered plot 1; it was between 50–60%. It was lowest for fire-altered plot 3 at 15–20% (Table 5.4). The average depth of the surface fuel layer was 5-10mm in fire-altered plots 1 and 3 while it was slightly higher at 10-20mm in the other two plots. The fuel hazard computed for the surface fuel layer was moderate for all the plots except for fire-altered plot 3 which received a *low* fuel hazard rating. The combined near-surface and surface fuel hazard varied between *high* and *very high* across the four plots.

b. Two weeks post-burn

No fuel hazard assessment was taken two weeks post-burn.

c. Two years post-burn

Fuel hazard assessments suggested no discernible change in the near-surface and surface fuel attributes in the control plot (see Table 5.4). In fire-altered plot 3, the near-surface fuel cover had decreased from 50–60% to 30-40% whilst the average height remained below pre-burn levels at 10-15cm. However, the surface fuel characteristics, cover and depth were greater two years post-burn

compared to pre-burn levels. The combined fuel hazard for plot 3 was *low* two years after the burn in contrast to the control plot which received a fuel hazard rating of *high*.

Table 5.4 Fuel hazard assessment for the near-surface and surface fuel layers in the study plots before the prescribed burn and two years post-burn. (ND indicates no data captured.)

Fuel Layer	Plot	Key Attribute	Epoch		Fuel Layer	Key Attribute	Epoch		Combined near-surface and surface fuel hazard	Epoch	
			Pre-burn	Post-2years			Pre-burn	Post-2years		Pre-burn	Post-2years
Near-surface fuel layer (grass)	Control Plot	Cover (%)	50 – 60	50 – 60	Surface fuel layer (litter)	Cover (%)	40 – 50	40 – 50	Combined near-surface and surface fuel hazard	High	High
		Dead (%)	5 – 10	<5							
		Average Height (cm)	20 – 30	20 – 30		Average Depth (mm)	10 – 20	10 – 20			
		Fuel Hazard	High	High		Fuel Hazard	Moderate	Moderate			
	Fire-Altered Plot 1	Cover (%)	30 – 40	ND		Cover (%)	50 – 60	ND		High	ND
		Dead (%)	<5	ND							
		Average Height (cm)	20 – 30	ND		Average Depth (mm)	5 – 10	ND			
		Fuel Hazard	High	ND		Fuel Hazard	Moderate	ND			
	Fire-Altered Plot 2	Cover (%)	30 – 40	ND		Cover (%)	40 – 50	ND		High	ND
		Dead (%)	10 – 20	ND							
		Average Height (cm)	20 – 30	ND		Average Depth (mm)	10 – 20	ND			
		Fuel Hazard	High	ND		Fuel Hazard	Moderate	ND			
	Fire-Altered Plot 3	Cover (%)	50 – 60	30 – 40		Cover (%)	15 – 20	30 – 40		High	Low
		Dead (%)	10 – 20	5 – 10							
		Average Height (cm)	30 – 40	10 – 15		Average Depth (mm)	5 – 10	10 – 20			
		Fuel Hazard	High	Low-Moderate		Fuel Hazard	Low	Low			

5.3.2.3 Burn severity assessment

Two weeks following the burn, the post-burn near-surface percentage cover was recorded at 5–10% across the three fire-altered plots (Table 5.5). The near-surface percentage cover was 10-20% for both fire-altered plots 2 and 3, and 20–30% for fire-altered plot 1. The average surface fuel layer depth increased from pre-burn levels. It was 10–20mm in fire-altered plot 1 and 3 while 20–30mm in fire-altered plot 2. The percentage plot area burnt was recorded at 60–70% for all the fire-altered plots. The control plot showed no change in the understorey fuel two weeks post-burn.

5.3.3 Validation of TLS derived measure of change

Based on visual estimates, the forest understorey components (consisting of near-surface live vegetation, litter and bare earth) within the 3 × 3m grid of the control plot did not change within two weeks following the burn. Any observed changes were confined to the litter layer (Appendix 10.1) which decreased by a maximum of 20% within a 1 × 1m cell. '*Near-Surface Live Vegetation'* cover percentages were found to be identical pre- and two weeks post-burn. Very little change was observed in *'Bare Earth'* land cover element. These results were in agreement with the change estimated by the TLS metric *mean* AGH_{change} which recorded change between 5–20% across the 3×3m grid.

Table 5.5 Burn severity assessment for the near-surface and surface fuel layers in the study plots two weeks post-burn. These measures correspond to two weeks post-burn.

Fuel Layer	Key Attribute	Control Plot	Fire-altered Plot 1	Fire-altered Plot 2	Fire-altered Plot 3
Near-surface fuel layer (grass)	Cover (%)	50-60	5-10	5-10	5-10
	Re-growth (%)	0	<5	<5	<5
Surface fuel layer (litter)	Cover (%)	40-50	20-30	10-20	10-20
	Average Depth (mm)	10-20	10-20	20-30	10-20
	Area Burnt (%)	0	60-70	60-70	60-70

In fire-altered plot 3, there was a much bigger change in the forest understorey. Most of this fire-induced change was recorded in the near-surface live vegetation and litter cover. All the cells recorded a decrease in *'Near-Surface Live Vegetation'* corresponding to a 50–100% reduction in the near-surface live vegetation cover. Change in the *'Litter'* cover decreased by 83%. '

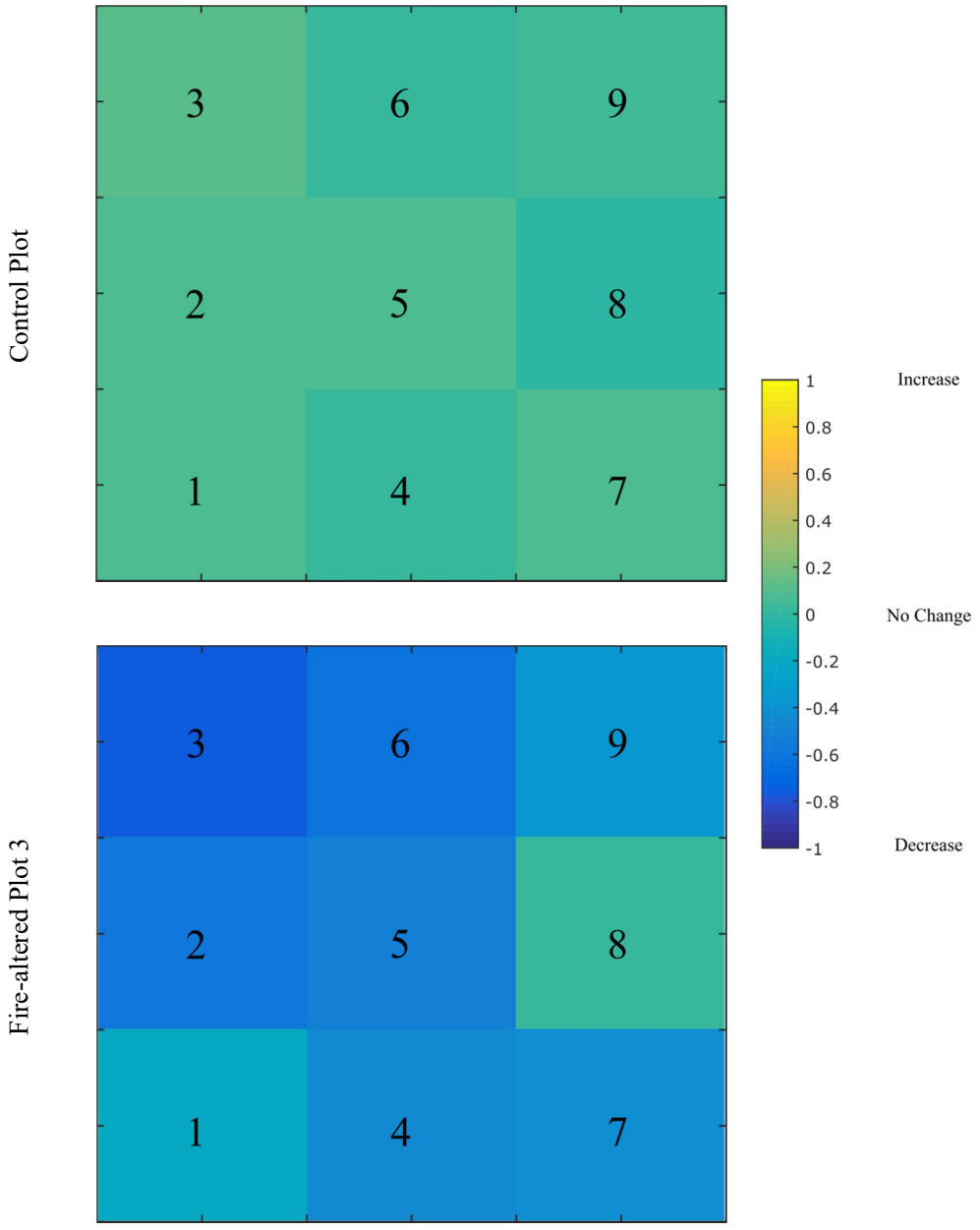

Figure 5.6 Spatial distribution of change detected by *mean* AGH_{change} metric in the 3 × 3m grid in the control and fire-altered plot 3. These measures are for *T1* epoch only.

Bare Earth' cover increased between 17–100%. Thus, across the three land covers recorded, *'Bare Earth'* cover increased whilst *'Near-Surface Live Vegetation'* decreased the most in fire-altered plot 3. The *mean* AGH_{change} metric also detected this large decrease in understorey fuel layer in response to the prescribed burn (see Appendix 10.2).

The spatial distribution of change in each of the nine 1 × 1m cells detected by *mean* AGH_{change} is shown in Figure 5.6. It indicates that the TLS-derived *mean* AGH_{change} metric did not detect a large change between the two data captures in the control plot. In contrast, the fire-altered plot 3 showed vast changes relative to pre-burn measures. Pearson product moment correlation between field metrics and TLS metrics is presented in Table 5.6. *Mean* AGH_{change} metric was highly correlated with *'Near-Surface Live Vegetation and Bare Earth'* (r = 0.71, p<0.05), *'Near-Surface Live Vegetation'* (r = 0.69, p<0.05) and *'Near-Surface Live Vegetation and Litter'* (r = 0.68, p<0.05).

Table 5.6 Pearson product moment correlation coefficient of field metrics against *mean* AGH_{change}. These measures are for epoch *T1*. (* significant at p<0.05)

Field Metric	*mean* AGH_{change}
Near-Surface Live Vegetation	0.69*
Litter	0.50
Bare Earth	-0.46
Near-Surface Live Vegetation and Litter	0.68*
Near-Surface Live Vegetation and Bare Earth	0.71*
Litter and Bare Earth	-0.25
Near-Surface Live Vegetation and Litter and Bare Earth	0.66*

TLS-derived height estimates using AGH95 pre-burn and two years post-burn were found to be comparable to field estimates of change in understorey fuel height. In the control plot, field based measures of understorey height were recorded at 20–30cm pre-burn and two years post-burn. TLS-based estimates recorded the average pre-burn height at 28cm and 24cm post-burn in the control plot. In fire-altered plot 3, TLS recorded 35cm pre-burn in comparison to 30–40cm as estimated based on visual assessments (see Table 5.4). Two years post-burn, whilst TLS recorded the understorey height at 20cm, it was estimated at 10–15cm based on field assessments.

5.4 Discussion

Multi-temporal TLS surveys can successfully help monitor understorey forest condition and enhance our understanding of various forest dynamics, both short- and long-term in the forest understorey. In addition to deriving typical height and volume estimates of vegetation structure, multi-temporal TLS surveys can map areas burnt and unburnt, detect vegetation regrowth and fuel accumulation. The spatial distribution of change detected across different burnt plots was found to be in good agreement with visual field assessments. The visual field assessment of change conducted in the control and fire-altered plot 3 also showed good agreement with TLS-derived measures of change.

5.4.1 Epoch T1: Immediate post-fire effects

Immediate post-fire effects encompass mapping the extent of burnt and unburnt areas. Epoch *T1* is a comparison between pre- and two weeks post-burn measurements. TLS was clearly able to discern burnt landscapes (fire-altered plots) from unburnt ones (control plot). This observation was supported by the absolute change in height (calculated using AGH95), histograms, change maps, spatial statistics. A change of 1cm in understorey fuel height was observed in the control plot with a much lower standard deviation of 7cm. In the fire-altered plots the reduction in understorey fuel height was in the range of 5–7cm which standard deviation values between 14–16cm. The histogram distribution of voxel for the control plot was normal with the mean and mode being coincident between 0.9–1.0. This finding, along with the change maps detecting no change in more than 95% of the voxels indicate that there was little or no change in the understorey fuel load. In fire-altered plots, the histogram distribution of voxels was bimodal or flattened, pointing to a loss of fuel from the forest understorey. The modal peak in comparison to the control plot was found to lie between 0.4–0.5 for all the fire-altered plots. This value lies outside the 90% probability range that such voxels are fire affected and have experienced loss in understorey fuel. The change maps too support this finding of detecting fire-induced change in the forest understorey using TLS point clouds.

Other immediate post-fire effects that could be successfully ascertained using TLS technology included the detection and mapping of the spatial distribution of burnt and unburnt areas. This could be subtly observed from the histogram distribution (especially for fire-altered plot 2) due to the presence of a small modal peak between 0.9–1.0. In a burnt landscape this is indicative of unburnt patches as it corresponds to little or no change in understorey fuel load. The area burnt was

found to be comparable to visual estimates of change in the forest understorey. An interesting observation was made with respect to the change map for Fire-altered plot 3 in *T1* epoch (Figure 5.2d). Whilst visual field estimates indicated that 60–70% plot area was burnt, *mean* AGH_{change} detected a decrease in understorey fuel in approximately 47% of the voxels. At the same time, an increase in understorey biomass was observed in approximately 15% of the voxels. There was no evidence of regrowth in the understorey vegetation within two weeks of the burn in fire-altered plot 3. This increase in understorey fuel could be attributed to two factors. Firstly, field assessments of burn severity conducted concurrently with the TLS scans indicate that the litter depth had increased in all the fire-altered plots relative to pre-burn levels due to localised leaf fall from the scorched canopy in response to the burn. Secondly, it is also possible that an increase in understorey fuel load immediately post-burn may be the result of fallen branches and limbs from the scorched canopy.

TLS was also able to detect different fire treatments based on changes observed in the fire-altered plots. Post-fire effects are driven by a variety of factors including pre-burn fuel load, fuel connectivity, vertical fuel arrangement, fuel moisture and fire intensity. The histogram distribution of voxels from fire-altered plots 1 and 2 was similar and indicates that they may have received a similar fire treatment. Histogram of voxels for fire-altered plot 3 indicates that the plot experienced a greater impact by the burn. This finding is also supported by the spatial statistics of the number of patches and mean patch size. Both Fire-altered plots 1 and 2 whilst recording the highest mean patch area also had the higher associated σ values. Fire-altered plot 3 whilst recording lower mean patch size also recorded a much lower σ in comparison to the other two fire-altered plots. However, patch size will also be affected by the degree of occlusion in the plots. Since TLS scans in this research were conducted in single-scan modes occlusion was present in all the plots. Both fire-altered plots 1 and 2 had approximately 18% voxels as occluded compared to fire-altered plot 3 which had 12%. Fire-altered plot 1, in particular, has numerous small areas of occlusion in comparison to the other two fire-altered plots.

5.4.2 Epoch T2: Fuel load accumulation

The epoch *T2* looks at comparing the change produced in the understorey landscape two years post-burn relative to two weeks post-burn. Analysis of this temporal factor can help in analysing fuel load accumulation. This is confirmed by the change in understorey fuel height, histogram distribution, change maps and spatial statistics. A reduction in understorey fuel height by 3cm is observed in the control plot (σ = 10cm). This could also explain the flattening of the normal

distribution of voxels in the control plot at *T2* relative to *T1*. This suggests an increase in within-plot variability which could be attributed to natural changes in the landscape including growth, senescence and wildlife grazing. However, these changes cancel each other out and hence appear negligible at the plot scale.

Results from fire-altered plot 3 have indicated that understorey fuel load accumulation was very low. There is an overall reduction in understorey fuel height by 10cm (σ = 17cm) at two years from the burn relative to two weeks post-burn measures. The histogram distribution is similar to *T1* which means that the understorey fuel has not changed significantly between two weeks post-burn and two years post-burn. The change maps also indicate that nearly 60% of the voxels show no change relative to two weeks post-burn levels. However, an increase in understorey cover, especially litter cover and depth has been observed based on visual field estimates. The litter cover has increased to 30–40% from 15–20% pre-burn and depth to 10–20mm from 5–10mm pre-burn. This difference observed between TLS and visual estimates can be due to a few factors. Firstly, the increase in litter depth is in the order of a few millimetres. This is a very small change at the plot scale and the TLS is perhaps not sensitive enough to detect it. Secondly, the ground filtering algorithm used for calculating understorey fuel height may have included elements from the litter and thus excluded them from the analysis. Thirdly, this observation could also be due to difficulties in differentiating ground elements from the post-burn growth of grass. However, an increase in the connectivity of the burnt patches is detected by TLS, demonstrated by the decrease in the number of such patches with an increase in mean patch area relative to *T1* levels. In comparison, the control plot showed no change in more than 95% of the voxels.

Apart from monitoring fuel accumulation, the mosaic pattern of burnt and unburnt patches can still be visualised in fire-altered plot 3. The large unburnt patches in fire-altered plot 3 such as the one in the south-west edge of the plot are consistently detected as no change. Although data was available from only one fire-altered plot, the ability of TLS to map the persistence of such unburnt patches two years from the burn event nonetheless is a very promising research finding. Such unburnt patches are known to act as sites that would continue to provide seeds to the overall seed bank in the forest (Penman et al., 2008b). Thus, mapping of such unburnt patches within the burn perimeter can inform land managers to protect them from further environmental damage.

5.4.3 Epoch T3: Prescribed burn effectiveness

Based on the TLS data captured in one fire-altered plot, findings of this study indicated that the prescribed burn was effective in reducing the understorey fuel load relative to pre-burn levels both in terms of cover and height. This means that fuel accumulation did not return to pre-burn levels within the two years duration of the study. It was shown that at *T3*, approximately 40% of the voxels in fire-altered plot 3 had understorey fuel load below pre-burn levels as compared to approximately 47% at *T1*. The understorey fuel height was also lower than pre-burn levels with a reduction by 15cm (σ = 14cm). In other words, the longer-term effects of the prescribed burn could be detected and mapped two years post-burn using TLS data. The histogram distribution of voxels from fire-altered plot 3 also confirms this. It also reveals an interesting trend (Figure 5.1c). The curve is unimodal with the mode between 0.4 – 0.5 whilst being between 0.9 – 1.0 for the control plot. This suggests that most of the understorey fuel load in fire-altered plot 3 was still fire-affected in comparison to control at *T3*. It was also below pre-burn fuel level in terms of both cover and height based on visual field assessments.

The spatial distribution of patches with a decrease in understorey fuel load in fire-altered plot 3 is similar to *T1*. The large patch on the western side of the plot which was burnt is still being mapped as fire-affected even though there is evidence of vegetation regrowth. This can be linked to the finding that near-surface fuel height is way below pre-burn levels (20–30cm) at 10–15cm in this plot. This measure of fuel height is close to TLS estimates of average understorey fuel height, recorded at 20cm, two years post-burn.

A noticeable difference in comparison to *T1* is that there are not as many voxels recording accumulation of understorey fuel. It could be that the branches and timber that fell off scorched canopy may have got displaced or removed from the landscape. Some unburnt patches from *T1* and *T2* have persisted in *T3* as well, especially in the western edge of the plot. A possible explanation for this observation could be that increased leaf drop has compensated for understorey fuel loss.

Not much difference was observed in the control plot between epochs *T3* and *T2*. The understorey fuel height at *T3* was similar to *T2* (μ = 4cm, σ = 17cm). The histogram was flattish-normal as was observed in *T2*. This similarly in the histogram distribution in these two epochs is because of increased within-plot variation recorded by the TLS two years post-burn. The spatial distribution of change as depicted by the change maps re-emphasise the ability of TLS to detect no change in an unburnt forest understorey.

5.4.4 Validation of TLS-derived measure of change

The positive correlation between TLS-derived *mean* AGH_{change} metric and field data suggests that TLS data can detect change in various understorey land covers such as near-surface live vegetation, litter and bare earth cover with a high degree of certainty. Strong positive and statistically significant correlations were found between '*Near-Surface Live Vegetation'*, '*Near-Surface Live Vegetation and Litter'*, *'Near-Surface Live Vegetation and Bare Earth'*.

In contrast, '*Near-Surface Live Vegetation, Litter and Bare Earth*', '*Bare Earth*' and *'Litter and Bare Earth'* metrics exhibited low non-statistically significant negative correlation. This can be explained by the fact that an increase in the bare earth cover in response to the fire would indicate a greater decrease in understorey cover detected by TLS. This is also the reason *'Litter and Bare Earth'* exhibited the lowest non-significant correlation with TLS metric. Across all the other field metrics a decrease in their cover corresponded to a decrease in the value of change detected by TLS metrics.

A strong correlation that is statistically significant is observed between '*Near-Surface Live Vegetation'* and *mean* AGH_{change} (r = 0.69) as compared to *'Litter'* could be attributed to near-surface fuel height and litter depth. The pre-burn mean near-surface fuel height was recorded at 20–30cm which decreased to less than 5cm two weeks post-burn. Whilst the litter depth had increased slightly to 10–20mm post-burn from 5–10mm pre-burn it was a very marginal change in comparison to near-surface fuel height. This also indicates that a change in near-surface fuel layer is the dominant change and is likely to be detected by TLS technology. The composite metrics involving near-surface live vegetation also outperformed those comprising litter and bare earth.

In addition to detecting change in understorey land cover, TLS-derived height estimates were also found to be comparable to field estimates of height. This agreement was much stronger in the control plot where TLS-derived estimates recorded understorey height as 28cm and 24 cm pre- and two years post-burn respectively in comparison to field estimates of 20–30cm at both these time periods. In fire-altered plot 3, TLS-derived understorey height estimate was recorded at 20cm in comparison to 10–15cm in the field.

5.5 Summary

This chapter demonstrated how TLS can be used to monitor forest understorey condition over a two year period and quantify post-fire effects. TLS-derived metrics such as *mean* AGH_{change} was used successfully to detect understorey change with a high degree of certainty when measured against field data. The spatial distribution of this change in the understorey landscape could also be detected and mapped that can also help identify burnt and unburnt patches. This is new information, not previously available using field data alone or passive satellite and aerial imagery. The patchy nature of prescribed burns was also readily mapped using TLS data. The utility of TLS technology in burnt landscapes as demonstrated in this chapter varies from immediate post-fire effects (burn area extent, patchiness) to fuel accumulation and prescribed burn efficiency.

Chapter 6. Spectral changes in the understorey fuel layers of an Australian dry sclerophyll forest in response to prescribed burning

[This chapter is based on the peer-reviewed publication:

GUPTA, V., REINKE, K.J., JONES, S.D. 2013. Changes in the spectral features of fuel layers of an Australian dry sclerophyll forest in response to prescribed burning. *International Journal of Wildland Fire.* 2013, 22, 862-868.]

6.1 Introduction

This chapter describes the changes in the spectral features that can be observed in the different understorey vertical strata of the Australian dry sclerophyll forest in response to prescribed burning. Spectral data captured in the wavelength range of 350-2500nm is used. This chapter introduces the method and describes the analyses of raw time-series and first-order derivative of spectral reflectance data for each of the vertical strata. The broad wavelength regions and narrow bandwidths of the electromagnetic spectrum where changes can be observed in response to fire are identified. A discussion on links between the spectral changes observed to physiological parameters is also made in this section. The chapter concludes with a section on the recommendations of broad wavelength domains and narrow spectral bands that can assist in ascertaining vegetation response and recovery in response to prescribed burns. This section also recommends suitable time-frames for acquisition of aerial and satellite imagery to study vegetation response to fire.

6.2 Methods

This section is discussed under two parts. The first part describes the field methods employed in the capture of spectral data. The second part discusses the steps undertaken to process hyperspectral data to produce both the spectral reflectance and first-order derivative curves.

6.2.1 Hyperspectral data capture

All hyperspectral measurements were captured between 10.00 and 14.00 hours to coincide with solar NADIR using the FieldSpec 3 (Analytical Spectral Devices, Boulder, CO, USA). This instrument covers the electromagnetic wavelength range of 350–2500nm. The bare fibre optic with a FOV of 25^0 was used for spectral data capture in the field. The height at which the bare fibre optic was held was 1m to simulate a GFOV of approximately 0.5m.

Each target measurement was preceded by a reference measurement viewing a horizontally placed standardised white Spectralon panel (Warsash Scientific, Redfern, NSW, Australia) to normalise for both the incoming irradiance illuminating the target and for instrument condition (change in spectroradiometer sensitivity due to temperature and electronic effects). This also enabled monitoring for changing light conditions and conversion of the measured target radiance to apparent reflectance. A total of 15-20 spectra were recorded for each target. Each spectra captured was an average of 30 spectral measurements. They were recorded at point locations at the centre of the target to ensure spectral data capture from a homogenous target.

6.2.2 Spectral data processing

The reflectance was converted from reflectance factor into percentage, averaged, smoothed and plotted to show any changes in reflectance over the one year time period. Hyperspectral bands corresponding to atmospheric water vapour absorption were removed as shown in Appendix 10.3. The raw spectra were smoothed using a weighted mean moving average filter (Naesset, 1997) as shown in equation 6.1 below. A five-point weighted average gave sufficient smoothing without loss of fine spectral detail.

$$\frac{\rho m - 2 \; + \; 2\rho m - 1 \; + \; 4\rho m + 1 \; + \; 2\rho m + 1 \; + \; \rho m + 2}{10} \qquad \textbf{(6.1)}$$

In equation 6.1, ρ_m is the weighted mean calculated for the *m*th spectral value.

Derivative spectroscopy concerns the rate of change of reflectance with wavelength. This technique was used to identify peaks, troughs and other spectral features that may indicate stress in the canopy and near-surface fuel targets in response to prescribed burns. It is a well-documented fact that first-order derivative analysis whilst enhancing spectral regions of change also removes some unwanted effects such as Bidirectional Reflection Distribution Function (BRDF) (Tsai and Philpot, 1998) and soil background signals (Demetriades-Shah et al., 1990). It also reduces the effects of scattering. In comparison to higher order spectral derivatives, first-order derivative is less sensitive to noise and hence more effective in operational remote sensing (Pu, 2012). The first derivative was calculated by dividing the difference between successive spectral values by the wavelength interval separating them. In this case a 9nm interval was used. Calculation of first-order derivatives was performed on the spectra before removing noisy water vapour regions.

6.3 Results

Results are discussed under four sections. The first two sections report the trends and spectral features observed in the near-surface fuel layer from the spectral signatures and first-order derivative curves. The last two look describe the changes observed with respect to surface fuel layer.

6.3.1 Time-series spectral signatures of the near-surface fuel layer

The time-series spectral signatures for the near-surface fuel layers over the one-year period including pre-burn from the four plots is shown in Figure 6.1 (a-d). Table 6.1 summarises the changes in three remotely sensed characteristics indicative of live vegetation including the green reflectance peak (550nm), red edge (680-750nm) and water absorption feature (970nm).

Pre-burn spectral measurements indicated these features as being present in the near-surface fuel layers. In the control plot (Figure 6.2 (a)); although there was some variability in the intensity of reflectance in week 2, the shape of the spectral signatures remained consistent throughout the data

capture campaign. The trends observed for the targets from the fire-altered plots were vastly different.

Spectral data captured in week two for the grass targets from the fire-altered plots exhibited very different spectral signatures as compared to the pre-burn signature (Figure 6.3). Both the shape of the spectral signature and intensity of reflectance changed. There was complete loss of spectral features indicative of live vegetation in all the fire-altered plots two weeks from the burn.

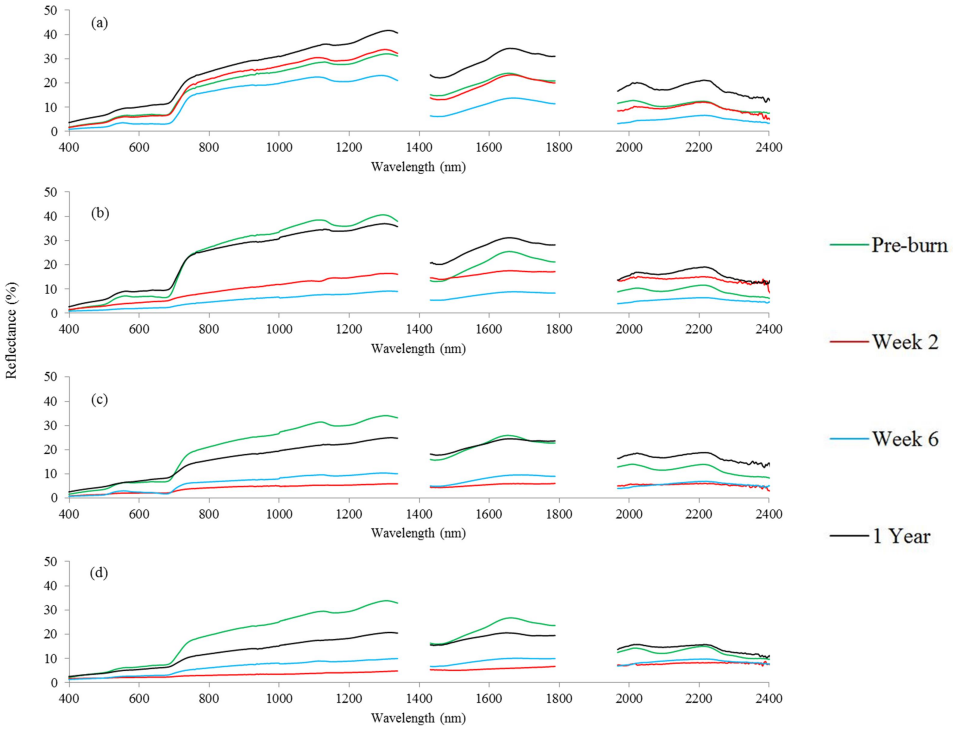

Figure 6.1 Time-series spectral signatures of the near-surface fuel layer from the (a) control plot, (b) fire-altered plot 1, (c) fire-altered plot 2 and (d) fire-altered plot 3.

In week six, the red edge feature was starting to reappear in the grass targets fire-altered plots 2 and 3. However, the red edge feature was still leaning towards the longer wavelengths in the electromagnetic spectrum. The reappearance of the green reflectance peak was only noticeable in the grass targets in fire-altered plots 2 and 3 but its reflectance intensity was still much lower than pre-burn levels. For the grass target from fire-altered plot 1, there was no difference in the shape of the spectral signatures obtained in week two and six from the burn event. Instead the intensity of the reflectance curve was seen to decrease further in week six. Also, the green reflectance peak did not seem to reappear in week six. The water absorption feature at 970nm was still absent.

At the end of one year the spectral signature was similar in both shape and intensity for the grass target from fire-altered plot 1. The spectral features, green reflectance peak, red edge and water absorption feature at 970nm were also identifiable in this spectral signature. For the grass targets from fire-altered plots 2 and 3, although the intensity of spectral reflectance was not close to the pre-burn levels, the three spectral features indicative of live vegetation were present.

Photographic evidence suggests there was complete burning of the near-surface fuel layer in the three fire-altered plots. This can be visualised in Figure 6.2 (b, c and d). The control plot showed no change from pre-burn levels in both height and cover. At one year from the burn event, the near-surface fuel target from the control plot remained unchanged. The near-surface fuel target from fire-altered plot 1 showed the greatest recovery as can be seen in Figure 6.3b. However, the targets from fire-altered plots 2 and 3 showed very little recovery in comparison.

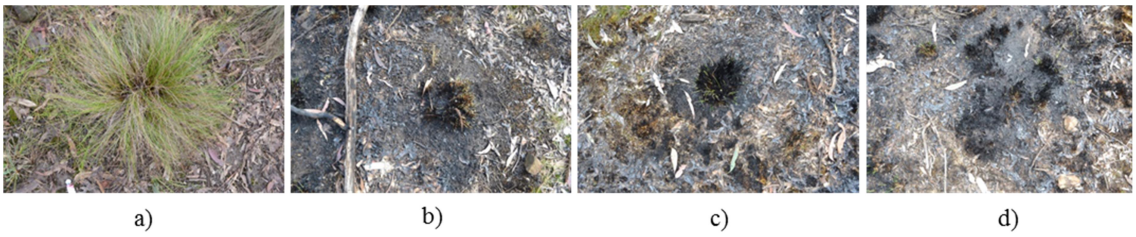

Figure 6.2 Evidence of complete burning of the near-surface fuel layer two weeks post-burn in b) fire-altered plot 1, c) fire-altered plot 2 and d) fire-altered plot 3. a) Is the near-surface fuel target from the control plot.

Figure 6.3 Near-surface fuel layer cover at the end of one year from the burn for the a) control plot, b) fire-altered plot 1, c) fire-altered plot 2 and d) fire-altered plot 3.

6.3.2 Time-series first derivative of reflectance curves for the near-surface fuel layer

The time-series first derivative of reflectance curves for the near-surface fuel layers over the one year period including pre-burn from the four plots is shown in Figure 6.4 (a-d). The first derivative

curve contained three distinct peaks in the control plot for all the periods for which data capture occurred.

The first, centred at 530nm, corresponded to the point of maximum slope as the reflectance increased in the green portion of the visible spectrum. The second, centred at 730nm, corresponded to the point of maximum slope at the red edge where the low red reflectance increased to the high NIR reflectance. The third peak centred at 1220nm. There were two distinct troughs identified at 1150nm and 1550nm.

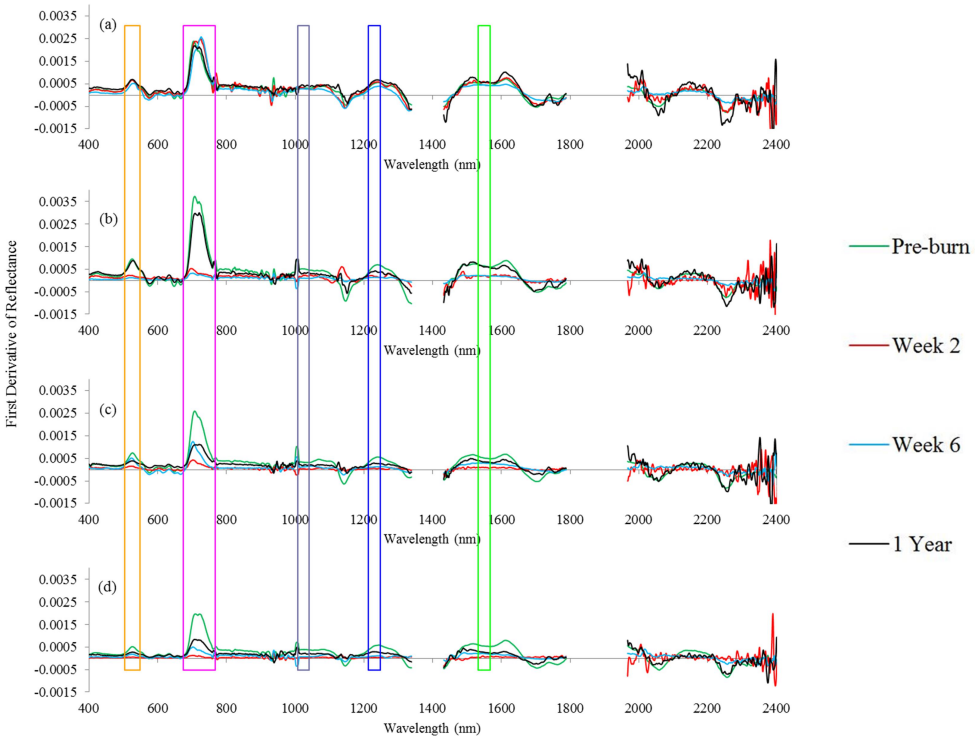

Figure 6.4 Time-series of first derivative of reflectance of the near-surface layer from the (a) control plot, (b) fire-altered plot 1, (c) fire-altered plot 2 and (d) fire-altered plot 3.

The trends observed in the burnt plots post-burn were vastly different from the control plot. Five narrow domains within the electromagnetic spectrum were identified where changes in the near-surface fuel layer was most noticeable between the burnt (fire-altered) and unburnt (control) plots. This has been highlighted in Figure 6.4. These narrow domains correspond to the following wavelength ranges; 500-550nm, 680-750nm, 1010-1030nm, 1200-1250 and 1530-1570nm. Table

6.2 summarises the changes in these five narrow domains of the Electromagnetic spectrum. The changes in these domains are discussed briefly in the subsequent paragraphs.

6.3.2.1 500-550nm spectral region

Figure 6.5 shows the first derivative spectral feature between 500-550nm for the near-surface fuel layer from the four plots. All the near-surface targets from the three fire-altered plots show complete absence of the peak at least till week two post-burn (Figure 6.5 (b), (c) and (d)).In fire-altered plot 2, the near-surface target exhibited reappearance of the peak as early as week 6.

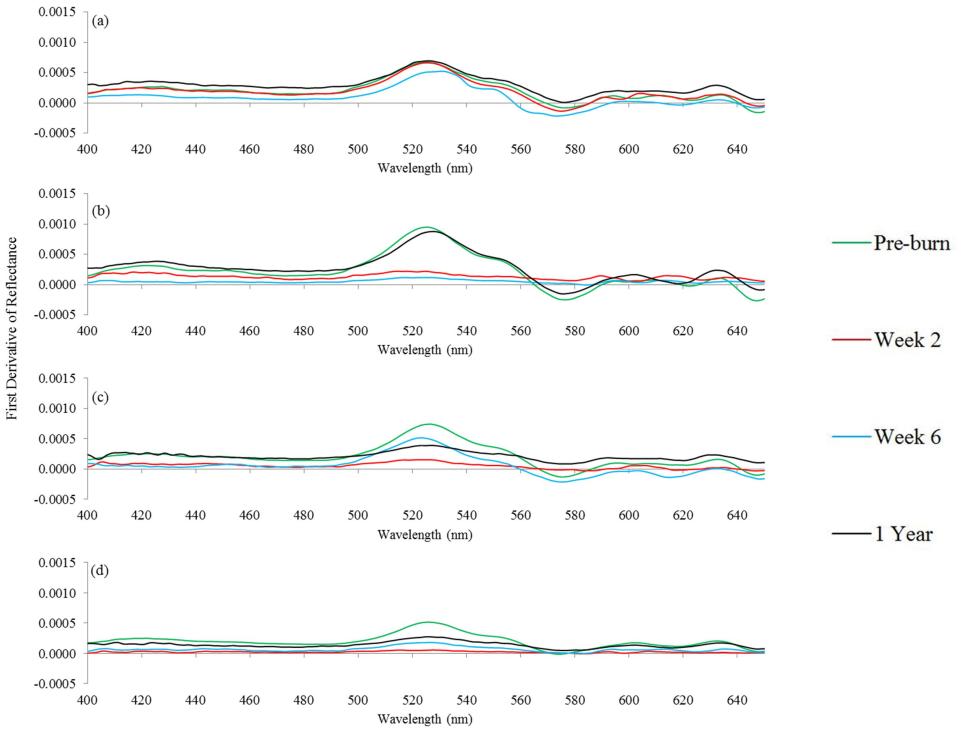

Figure 6.5 Time-series first derivative reflectance of the near-surface fuel layer from the (a) control plot, (b) fire-altered plot 1, (c) fire-altered plot 2 and (d) fire-altered plot 3 between the wavelength ranges of 400-650nm.

This trend was not noticeable in fire-altered plots 1 and 3. At one year from the burn event, the peak of the grass target from fire-altered plot 1 was identical to pre-burn levels in both shape and intensity. In the other two fire-altered plots, while the peak was evident it was still lower than pre-burn levels one year post-burn.

6.3.2.2 680-750nm spectral region

Figure 6.6 shows the first derivative spectral feature between 650-750nm for the near-surface fuel layers from the four plots. The peak centred at 730nm was present in all the four epochs for the near-surface fuel targets in the control plot (Figure 6.6 (a)). It was also present pre-burn in the three fire-altered plots.

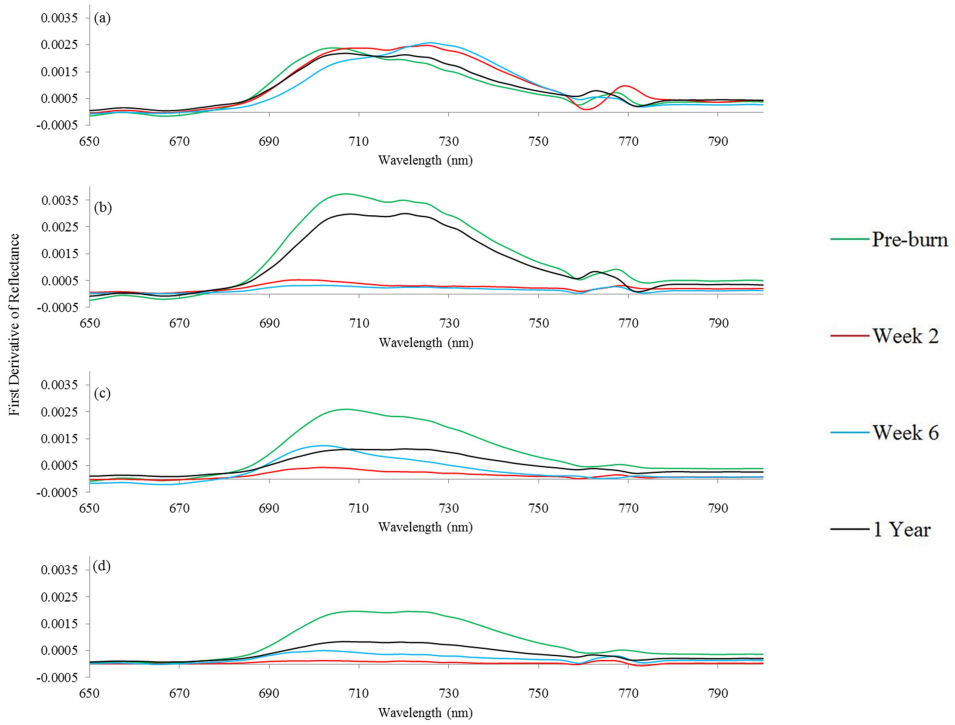

Figure 6.6 Time-series first derivative reflectance of the near-surface fuel layer from the (a) control plot, (b) fire-altered plot 1, (c) fire-altered plot 2 and (d) fire-altered plot 3 between the wavelength ranges of 650-800nm.

For the near-surface fuel targets the peak was flattened until week two in the three fire-altered plots (Figure 6.6 (b), (c) and (d)). Whilst it continued to be absent in the target from fire-altered plot 1 and 3, there was some evidence of the peak returning in the near-surface fuel target from fire-altered plot 2. At the end of one year from the burn, the peak of the near-surface fuel target from fire-altered plot 1 was closest to pre-burn levels both in terms of shape and intensity. In the other two fire-altered plots it was still much lower in intensity as compared to pre-burn levels.

6.3.2.3 1010-1030nm and 1210-1240nm spectral region

In comparison to the positive peaks centred at 530nm and 730nm, the spectral features between the wavelength ranges of 1010-1030nm and 1210-1240nm were much less noticeable. The intensity of reflectance between these wavelength ranges for the near-surface fuel targets in the control plot showed very little deviation from the pre-burn levels in terms of intensity throughout the data capture campaign (Figures 6.7 (a) and 6.8 (a)).

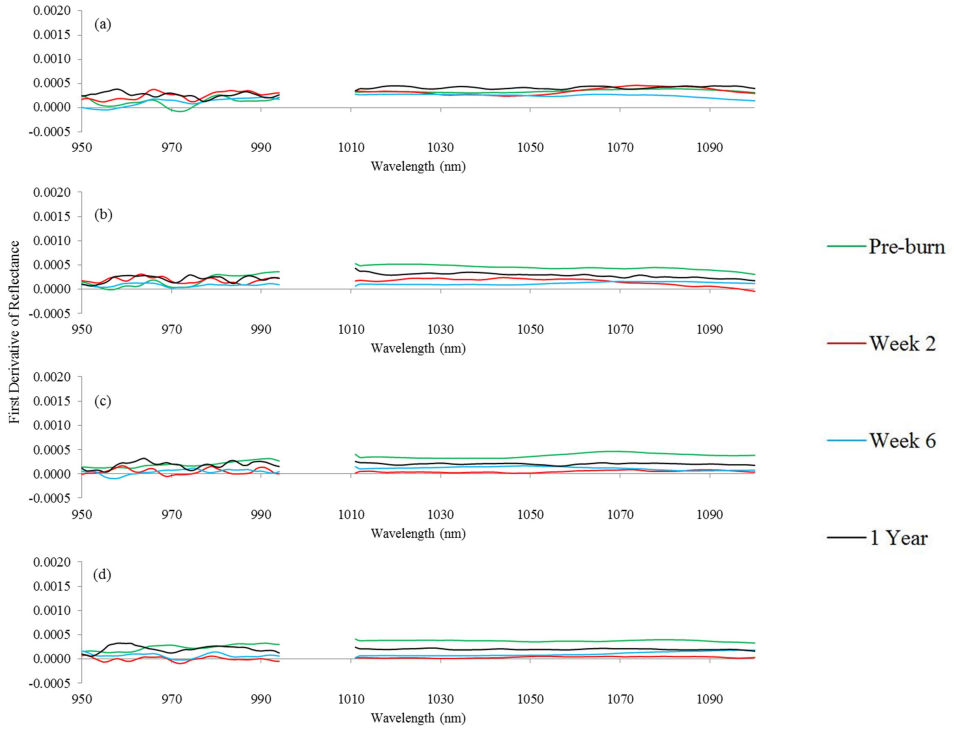

Figure 6.7 Time-series first derivative reflectance of the near-surface fuel layer from the (a) control plot, (b) fire-altered plot 1, (c) fire-altered plot 2 and (d) fire-altered plot 3 between the wavelength ranges of 950-1100nm.

Trends from the burnt plots post-burn indicate that both the spectral features were absent at least until two weeks post-burn. Trend of return to pre-burn levels was noticeable from six weeks post-burn onwards. However, at one year from the burn event both the spectral features were below pre-burn levels especially for the near-surface fuel targets from fire-altered plots 2 and 3.

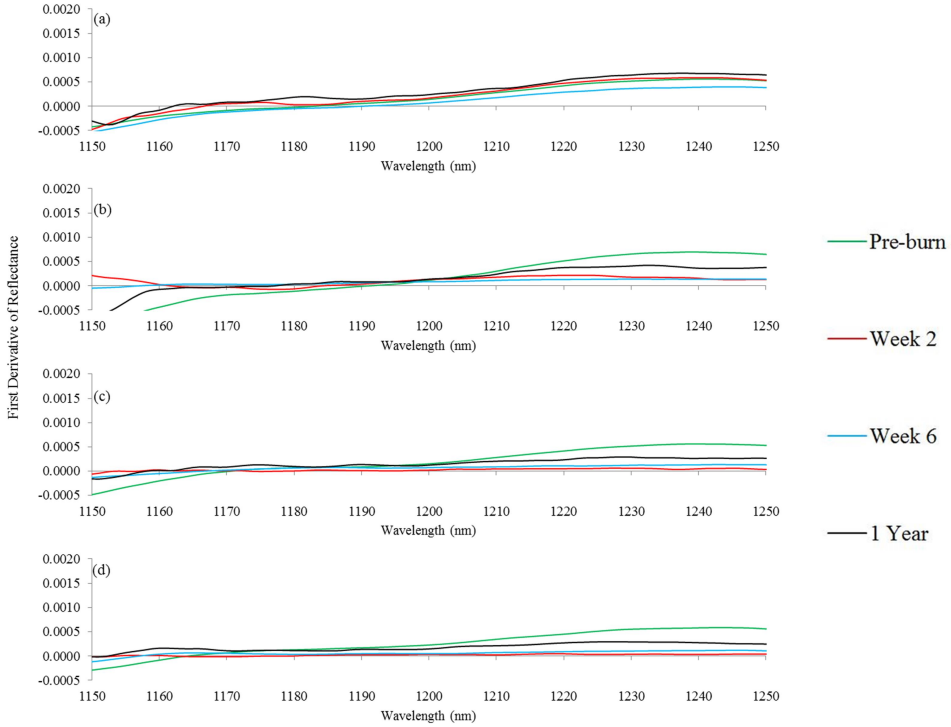

Figure 6.8 Time-series first derivative reflectance of the near-surface fuel layer from the (a) control plot, (b) fire-altered plot 1, (c) fire-altered plot 2 and (d) fire-altered plot 3 between the wavelength ranges of 1150-1250nm.

6.3.2.4 1530-1570nm spectral region

This domain of the electromagnetic spectrum corresponds to the trough centred at 1550nm. Figure 6.9 shows this spectral feature from each of the four plots across all the epochs of data capture. Whilst the difference in intensity at the 1550nm spectral feature was minimal in the control plot during the one year of spectral data capture, there were clear differences in the fuel targets from the other three plots. The intensity was lowest in week two in all the fire-altered plots. For targets in fire-altered plots 2 and 3, there was an increase in the intensity in week six. For the target from fire-altered plot 1, it remained at the week two levels. At one year from the burn event the intensity and shape of the spectral feature was back to pre-burn levels for the near-surface fuel target from fire-altered plot 1. For the other two fire-altered plots the intensity was still below pre-burn levels and slightly greater than week six levels.

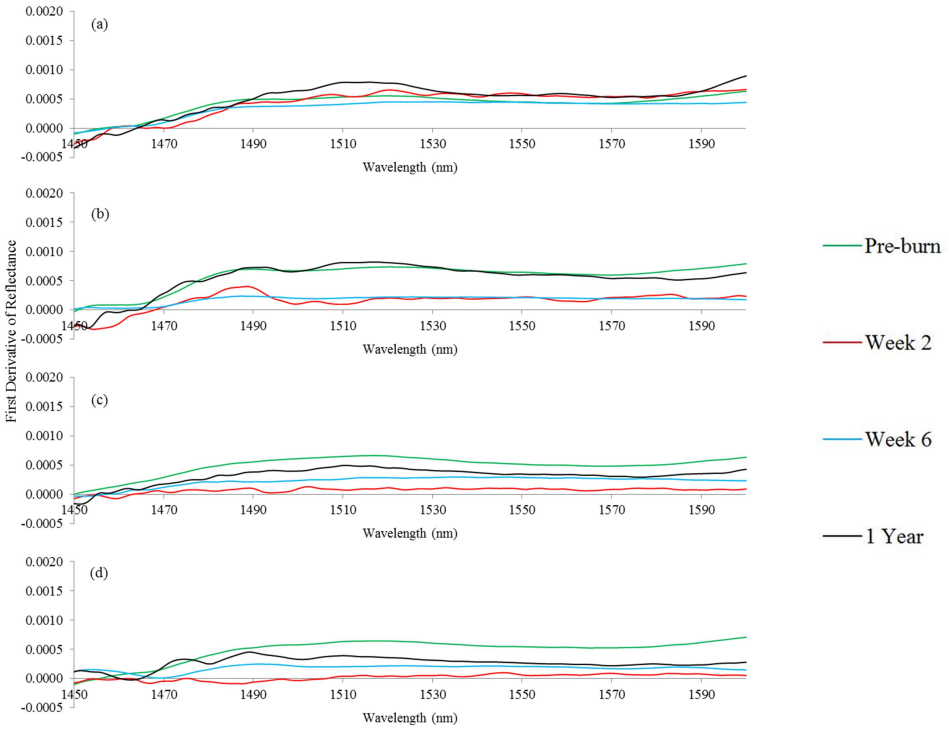

Figure 6.9 Time-series first derivative reflectance of the near-surface fuel layer from the (a) control plot, (b) fire-altered plot 1, (c) fire-altered plot 2 and (d) fire-altered plot 3 between the wavelength ranges of 1450-1600nm.

6.3.3 Time-series spectral signatures of the surface fuel layer

The time-series spectral signatures for the surface fuel layer from the four plots are shown in Figure 6.10 (a-d). A pre-burn absorption feature at 1140nm was present. The intensity of this feature decreased drastically in week two from the burn in fire-altered plots 2 and 3. It was seen to decrease further six weeks from the burn event in each of the three fire-altered plots whilst in the control plot it was close to pre-burn levels.

The intensity of this absorption feature was seen to be closer to pre-burn levels one year from the burn event in fire-altered plots 2 and 3. In the surface fuel target from fire-altered plot 1, the intensity was found to be below week two levels. Whilst this absorption feature returned at the end of one year the intensity was still lower than pre-burn levels in the three fire-treated plots. Another absorption feature at 2100 nm, which was well defined pre-burn, was detected one year from the burn event in the surface targets from the fire-altered plots.

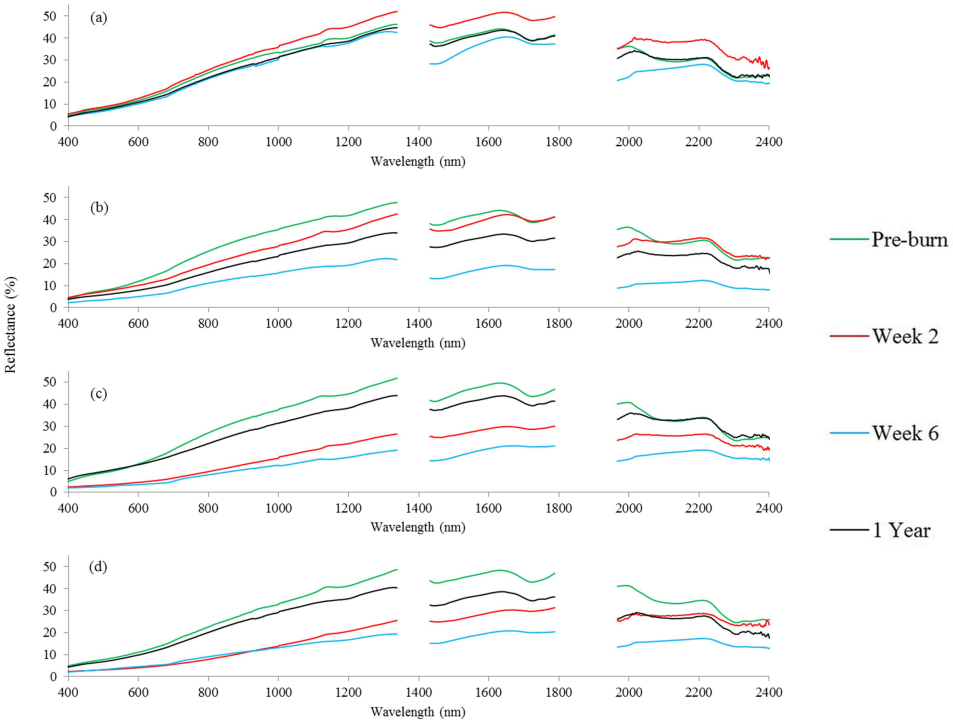

Figure 6.10 Time-series spectral signatures of the surface fuel layer from the (a) control plot, (b) fire-altered plot 1, (c) fire-altered plot 2 and (d) fire-altered plot 3.

Based on photographic evidence presented in Figure 6.11 surface fuel layer targets from fire-altered plots 2 and 3 were burnt resulting in a blackened ash bed. The surface fuel target from fire-altered plot 1 in comparison was comparatively less impacted by fire.

Figure 6.11 Surface fuel layer cover at the end of one year from the burn from the (a) control plot, (b) fire-altered plot 1, (c) fire-altered plot 2 and (d) fire-altered plot 3.

6.3.4 Time-series first derivative of reflectance curves for the surface fuel layer

The time-series first derivative of reflectance curves for the surface fuel layer over the one-year period including pre-burn from the four plots is shown in Figure 6.12 (a-d). The first derivative

curve contained a few distinct peaks and troughs. In the surface fuel layer in the control plot for all the periods for which data capture occurred. There was a positive peak centred at 1225nm whilst a trough was seen to occur at 1700nm.

There was a flattening of the absorption features at 1225nm and 1700nm observed two weeks from the burn event in the surface targets from fire-altered plots 2 and 3. These features remained flat even six weeks from the burn. The intensity and shape of these absorption features returned closer to pre-burn levels in the surface fuel targets from the fire-treated plots. The absorption feature at 1720nm was noticeable pre-burn in the surface fuel targets from each of the plots. Whilst in the surface fuel target from the control it was present throughout the one year period, it was noticeably absent until week six in the targets from fire-altered plots 2 and 3.

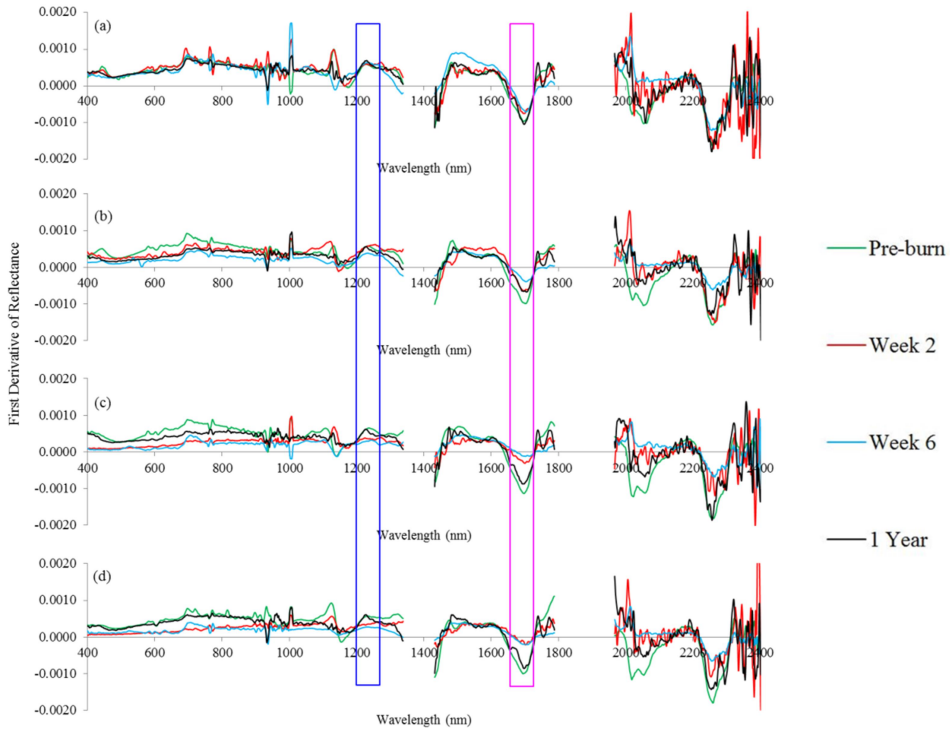

Figure 6.12 Time-series first derivative reflectance of the surface fuel layer from the (a) control plot, (b) fire-altered plot 1, (c) fire-altered plot 2 and (d) fire-altered plot 3.

Table 6.1 Changes observed in key remotely sensed characteristics of near-surface fuel layer in response to prescribed burn using the spectral reflectance curves.

	Remotely Sensed Characteristics												
	Green Reflectance Peak (550nm)				Red edge (680-750nm)				Water Absorption Feature (970nm)				Epoch
Plots	Control	FA-1	FA-2	FA-3	Control	FA-1	FA-2	FA-3	Control	FA-1	FA-2	FA-3	
Near-Surface Fuel	+++	+++	+++	+++	+++	+++	+++	+++	+++	+++	+++	+++	Pre-burn
	+++	---	---	---	+++	---	---	---	+++	---	---	---	Week 2
	+++	---	+	---	+++	---	+	---	+++	---	---	---	Week 6
	+++	+++	+++	+++	+++	+++	++	++	+++	+++	+	+	1 Year

(+++ Strong Presence, --- Complete Absence)

(FA-1 is fire-altered plot 1; FA-2 is fire-altered plot 2; FA-3 is fire-altered plot 3)

Table 6.2 Changes observed in some remotely sensed characteristics of the near-surface fuel layer in response to prescribed burn using first derivative of reflectance curves.

	Remotely Sensed Characteristics																			
	Positive Peak (Green VIS) (530nm)				Positive Peak (NIR) (730nm)				Spectral Feature (1020nm)				Positive Peak (1220nm)				Trough (MIR) (1550nm)				Epoch
Plots	C	FA-1	FA-2	FA-3	C	FA-1	FA-2	FA-3	C	FA-1	FA-2	FA-3	C	FA-1	FA-2	FA-3	C	FA-1	FA-2	FA-3	
Near-Surface Fuel	+++	+++	+++	+++	+++	+++	+++	+++	+++	+++	+++	+++	+++	+++	+++	+++	+++	+++	+++	+++	Pre-burn
	+++	---	---	---	+++	---	---	---	+++	---	---	---	+++	---	---	---	+++	---	---	---	Week 2
	+++	---	+	-	+++	---	++	-	+++	---	---	---	+++	---	---	---	+++	---	++	+	Week 6
	+++	+++	+	+	+++	+++	++	+	+++	++	++	++	+++	++	++	++	+++	+++	++	+	1 Year

(+++ Strong Presence, --- Complete Absence, N/A Inconclusive)

(FA-1 is fire-altered plot 1;FA-2 is fire-altered plot 2;FA-3 is fire-altered plot 3)

6.4 Discussion

This section is discussed broadly under two parts. The first part discusses the trends and spectral features observed in the near-surface fuel layer in response to prescribed burns whilst also providing the physiological basis for it. The second section discusses these aspects for the surface fuel layer. This distinction is made because these two fuel layers have demonstrated different spectral responses in response to the burns.

6.4.1 Near-surface fuel layer

The response of live vegetation to prescribed burn was characterised by changes in three distinct spectral features (1) green reflectance peak (550 nm); (2) red edge (680–750 nm); and (3) water absorption feature (970 nm) when the spectral reflectance curves were investigated. Using the first derivative of reflectance curves, changes in five spectral features were investigated.

Immediately following the burn, spectral measurements recorded in week two revealed complete absence of most of these key spectral features across all the near-surface fuel targets. The primary reason for the disappearance of the green reflectance peak was the scorching and burning of live foliage leading to a decrease in the chlorophyll content. Because absorption in the visible region is primarily controlled by chlorophyll (Carter and Knapp, 2001, McCoy, 2005, Peñuelas and Filella, 1998), this led to changes in leaf optical properties because of changes in leaf colouration from green to brown and green to black.

The changes in spectral reflectance observed in the NIR region included flattening of the red edge. This was attributed to the changes in leaf anatomy and internal leaf structures caused by the burn (Knipling, 1970). Because the red edge has been found to be a good indicator of chlorophyll content (Filella and Peñuelas, 1994), the observed flattening can be linked to the reduction in chlorophyll content and green biomass (Peñuelas and Filella, 1998). The red edge collapse was significant in the near-surface fuel targets. The near-surface fuel targets from all the fire-altered plots were more or less completely burnt with evidence of regrowth two weeks from the burn as shown in Figures 6.2 and 6.3.

Near-surface fuel targets became water stressed as a result of the burn. This was evident by the disappearance of the 970 nm water absorption trough. It has been reported by Peñuelas et al. (1994)

and Peñuelas and Filella (1998) that when the plants are water stressed, the 970 nm trough tends to disappear and that derivative indices in the 970nm region are useful indicators of water content.

The returning trend in spectral features towards pre-burn levels was seen to occur one year from the burn event in all the near-surface targets that came in contact with fire. Only the near-surface target from fire-altered plot 2 started showing signs of recovery as early as six weeks from the burn event. Of all the spectral features discussed above, red edge (680-750nm) seemed to revert to the pre-burn shape and intensity before the others. The positive peak in the NIR domain (730nm) seemed to detect a much stronger vegetation recovery as compared to the red edge from the normal spectral reflectance curves (Table 6.1 and 6.2). This indicates that red edge spectral feature may be sensitive to early signs of vegetation recovery.

The near-surface fuel layer is also known to be adapted well to fire (Gott, 2005). The sprouts of grass were seen to appear in week six post-burn and a similar time lag has been reported by Tolhurst et al. (1992). They reported appearance of sprouts four weeks following the complete burning of existing grass. They also reported including an increase in tiller density.

It should be expected that if re-sprouting of grass did occur this close to the burn event then at the end of one year the near-surface fuel density should have been closer to the pre-burn density. This was not the case as can be seen from Table 6.1 which suggests that the spectral features were far below pre-burn levels. Figures 6.2 and 6.3 also support this finding. Although these spectral features were noticeable at the end of one year from the burn they were not close to pre-burn levels at least in fire-altered plots 2 and 3. One possible reason that could be attributed to it is that there was abundant wildlife activity in the study area. It is believed that the new growth was actively being consumed by the fauna in St Andrews.

The spectral features from the first derivative of reflectance most useful in discerning burnt and unburnt near-surface fuel targets were the positive peaks at 530nm and 730nm. This observation corroborates earlier findings that the green-peak and red-edge spectral regions are generally critical for the detection of plant stress (Lefsky et al., 1997).

The greatest deviation from pre-burn spectral measurements was seen to occur within the first two weeks following the prescribed burn event because vegetation recovery was seen in some of the targets as early as week six. Thus, two weeks following the fire is a suitable timeframe to acquire satellite imagery to observe spectral changes in burned landscapes.

Although a return to the pre-burn reflectance features was seen to occur from week six onwards for one near-surface fuel target, complete recovery was not observed within one year from the burn using hyperspectral remote sensing. The one year time frame was however not found to be suitable for observing complete recovery of the near-surface fuel layer.

6.4.2 Surface fuel layer

The pre-burn spectral signatures of surface fuel targets were similar in intensity and shape. A drastic decrease in the spectral reflectance of surface fuel was observed immediately following the fire in the VIS and NIR domain of the electromagnetic spectrum. This could be attributed to the burning of the ground surface resulting in a blackened ash bed with char deposits as shown in Figure 6.11 (a-d). This phenomenon was not observed for the surface target from fire-altered plot 1 because less than 5% of it burnt. Whilst the difficultly in isolating unique spectral features that can be used to discriminate the similar VIS-NIR curves of leaf-litter and soils has been acknowledged by researchers before (Nagler et al., 2000) a few absorption features were identified indicative of changes in leaf-litter cover.

Marked changes in the various absorption features were also observed post-burn. The 1120nm absorption feature is a result of lignin in the litter (Kumar and Skidmore, 2006). With the litter being consumed by the fire the absorption feature disappeared as well. With increasing leaf drop at the end of one year the absorption feature started to revert to pre-burn levels. Similarly, the 1720nm absorption feature also started reappearing one year from the burn. However according to Kumar and Skidmore (2006) this absorption feature is unique in litter and the chemical most likely for the absorption at 1720nm is xylan.

The absorption feature at 2100nm is due to the presence of starch and cellulose in litter (Elvidge, 1990), which was well defined pre-burn, disappeared post-burn and then reappeared one year from the burn. The disappearance of this feature post-fire could be attributed to the fact that the surface fuel layer was completely burnt exposing the bare soil underneath. As weeks passed by, the surface fuel comprising leaf-litter began accumulating because of increased leaf drop from the scorched canopy above.

Although, Nagler et al. (2000) report that there are water absorption features at 1400nm and 1900nm that can be identified from litter signature, neither were noticeable because of atmospheric noise. The bands corresponding to these wavelength regions had to be removed prior to plotting

spectral signatures and first order derivative of reflectance curves. Elvidge (1990) reports that a number of weak absorption features in the leaf-litter signature can be accentuated using derivative spectroscopy between 1300-1350nm, 1500-1600nm and 2400-2500nm. In this research these were not found to be useful in discerning burnt litter from unburnt litter. Instead two spectral features identified from first derivative of reflectance that have the potential to discriminate between burnt and unburnt litter were found to be located at 1225nm and 1700nm. These could correspond to the cellulose and xylan as these compounds are reported to have absorption features at 1220nm and 1720nm respectively (Elvidge, 1990). Terpenes also have an absorption feature at 1720nm and since eucalypt leaves are aromatic, it is possible that the 1700nm absorption feature could also be due to terpenes (Kumar and Skidmore, 2006).

In comparison, the targets from the unburnt site showed no loss of spectral features during the data capture campaign, clearly demonstrating that the observed spectral changes in burned targets are due to the fire. One key finding of this research is that the VIS-NIR domain of the electromagnetic spectrum was most suited for studying vegetation stress while the MIR domain for non-photosynthetic elements such as litter.

6.5 Summary

This chapter described the main spectral trends for the understorey fuel layers for up to one year post-burn. The greatest deviation from pre-burn levels occurred within two weeks post-burn in both the near-surface and surface fuel layers. Thus, acquisition of satellite imagery for mapping burn extent should occur at this time. Spectral features identified as being sensitive to changes in the near-surface fuel layers the absence of the green reflectance peak at 550nm, flattening or absence of the red edge and a loss or decrease in the intensity of the water absorption feature at 970 nm. In addition to these, the absorption features identified from the first derivative of reflectance curves highlighted the importance of studying vegetation response in the VIS-NIR domain to monitor fire effects on vegetation. For the near-surface fuel targets, spectral features in the MIR domain were also found to be useful in addition to the VIS-NIR spectral features. In terms of recovery, the one year epoch was not sufficient to observe full recovery. Another key finding was with respect to identifying key spectral features in the surface-fuel layer which can be used to ascertain fire impact in the landscape. The features identified were the 1225nm and 1700nm from the first derivative of reflectance curves. In addition to the VIS, NIR and SWIR, selected imagery should also include the wavelength range of red edge (that is 680–750 nm) as it was shown to be an early indicator of vegetation recovery.

Chapter 7. Investigating spectral indices to monitor changes in the forest understorey following a prescribed burn

7.1 Introduction

This chapter evaluates several spectral indices in their ability to monitor changes in the forest understorey in response to fire. Spectral indices are identified based on known spectral domains sensitive to changes in vegetation and statistically compared for their ability to observe change. Descriptive statistics, time-series analysis of change in indices, correlation between indices and validation of indices with field measures of change are reported. Based on these results, the spectral indices most suitable for detecting fire effects and recovery post-fire are identified and discussed.

7.2 Methods

This section is presented in two parts: the first part describes the processing of hyperspectral data to derive spectral indices. This section also discusses the test for variable redundancy and assesses the utility of indices to detect burnt and unburnt targets in the forest understorey. The second describes the validation of hyperspectral data with field assessments.

7.2.1 Hyperspectral data processing

7.2.1.1 Calculation of vegetation and burn indices

The spectral indices calculated for the different fuel layers are listed in Table 7.1. For the near-surface fuel layers, these can be broadly categorised into those sensitive to vegetation greenness (such as NDVI), chlorophyll content (such as PRI, TCARI, D720), water status (such as WI, NDWI), anthocyanin (such as ARI1) and burn (such as NBR, CSI). For the surface fuel layer, in addition to the burn indices those sensitive to plant compounds such as cellulose, xylene and terpene were also selected. These indices were chosen for their wide utility in burn area mapping as

reported in literature and based on the analyses of spectral signatures and first-order derivatives in Chapter 6.

7.2.1.2 Pre-processing for variable redundancy

Spectral indices measuring the same physiological attribute identified in Table 7.1 were tested for redundancy by computing Pearson product moment correlation (r) with other indices measuring the same physiological attribute.

Table 7.1 Spectral indices derived for the different fuel layers according to physiological attributes.

Spectral Index	Physiological Attribute	Formula	Reference	Fuel Layer
NDVI	Greenness	$\frac{R800 - R680}{R800 + R680}$	Rouse et al. (1973)	Near-surface fuel layer
TCARI[a]		$3[(R760 - R670) - 0.2(R700 - R550) \times \left(\frac{R700}{R670}\right)]$	Daughtry et al. (2000)	
PRI	Chlorophyll	$\frac{R531 - R570}{R531 + R570}$	Gamon et al. (1992)	
SIPI		$\frac{R800 - R445}{R800 - R680}$	Peñuelas et al. (1995)	
NPQI		$\frac{R415 - R435}{R415 + R435}$	Barnes et al. (1992)	
NCPI		$\frac{R680 - R430}{R680 + R430}$	Merzlyak et al. (1999)	
D525		First derivative peak at 525nm		
D720		First derivative peak at 720nm		
WI	Water status	$\frac{R900}{R970}$	Peñuelas et al. (1997)	
MSI		$\frac{R1650}{R820}$	Ceccato et al. (2001)	
NDWI		$\frac{R860 - R1240}{R860 + R1240}$	Roberto et al. (2011)	
WI/NDVI		$\frac{R900}{R970} \times \frac{(R800 + R680)}{(R800 - R680)}$	Peñuelas and Inoue (1999)	

D1550		First derivative feature at 1550nm		
D1030		First derivative feature at 1030nm		
D1215		First derivative feature at 1215nm		
ARI1	Anthocyanin	$\frac{1}{R550} - \frac{1}{R700}$	Gitelson et al. (2001)	
D1700	Terpene	First derivative features at 1700nm		
D1230	Water, Cellulose, Starch, Lignin, Xylan	First derivative feature at 1230nm		Surface Fuel Layer
CAI	Cellulose	$0.5 \times (R2020 + R2200) - R2100$	(Nagler et al., 2003)	
NBR[b]	Burn index	$\frac{NIR - MIR}{NIR + MIR}$	Key & Benson (2005)	All fuel layers
CSI[b]		$\frac{NIR}{SWIR}$	Smith et al. (2005)	
MIRBI[b]		$10lSWIR - 9.8sSWIR + 2$	Trigg & Flasse (2001)	
BAI[c]		$\frac{1}{(0.1 + RED)^2 + (0.06 + aNIR)^2}$	Martin (1998)	

[a] Corrected with OSAVI.

[b] Computed by taking the average of corresponding bands from Landsat 5 TM (NIR- TM4; MIR- TM7; and SWIR- TM5).

[c]. Computed by taking the average of corresponding bands from AVHRR/3 (RED- channel 1; and NIR- channel 2).

The criteria for shortlisting the spectral indices were as follows:

1. An index should be independent of other indices measuring the same physiological attribute;

2. An index should exhibit statistically significant correlations with field measures of fire-induced change

7.2.1.3 Time-series evaluation of change in indices

The spectral indices shortlisted were plotted over the different time epochs at which hyperspectral data was captured. All the plotted values were normalised to pre-burn levels (see equation 7.2) to ascertain change relative to pre-burn levels. This identified which indices were successful at characterising burnt fuel targets from unburnt ones by recording the greatest deviation from pre-burn levels. Those indices able to track fuel recovery in both the near-surface and surface fuel layers over the one year period post-burn were also identified.

7.2.2 Comparison of spectral indices and visual assessment of change

Validation of hyperspectral data was conducted by comparison of spectral indices with change in fuel layer cover which was measured as a percentage of fuel present on the ground. Visual assessment of change in fuel cover for all targets was recorded concurrent to hyperspectral data capture. Change in fuel cover was recorded in 0.5 × 0.5m area for targets belonging to the near-surface and surface fuel layers. For comparison and validation with spectral indices, the change in fuel cover of the various fuel layers was transformed and normalised to pre-burn levels as shown in equation 7.1. The equation transforms the data on a scale of -1 to +1. A negative value indicates a decrease in fuel cover whilst a positive value indicates an increase. Values closer to 0 correspond to no change. This change in fuel cover was computed separately for the different fuel layers.

$$(Cover_{post-burn} - Cover_{pre-burn}) \Big/ Cover_{pre-burn} \quad \textbf{(7.1)}$$

Data was also tested for normality and it was found to be normal. To assess the reliability of spectral indices with field measures of change, Pearson product-moment correlation coefficient analysis (r) was performed between spectral indices and field data. This was calculated for two weeks, six weeks and one year post-burn data relative to pre-burn levels. Change in spectral indices was computed relative to pre-burn levels according to equation 7.2. This change was computed for each fuel layer.

$$(Index\ Value_{post-burn} - Index\ Value_{pre-burn}) \Big/ Index\ Value_{pre-burn} \quad \textbf{(7.2)}$$

7.3 Results

The results of this chapter are presented in three sections. Section 7.3.1 describes the changes observed in fuel cover of the various fuel layers based on visual assessments. Section 7.3.2 presents the results of a comparison between spectral indices and visual assessment of change in cover of the various fuel layers. Section 7.3.3 reports on the results obtained from analysing the various spectral indices derived in this chapter.

7.3.1 Visual assessment of change in fuel cover

Results of the visual assessment of change in the fuel cover of the near-surface and surface fuel layers are presented in Table 7.2. Photographic evidence of change in the near-surface and surface fuel targets from the four plots across all the epochs is presented in Figures 7.1 and 7.2. For all time epochs no noticeable change in near-surface fuel cover was recorded in the control plot relative to pre-burn levels.

Table 7.2 Visual assessment of percentage fuel cover recorded at four epochs in the four experimental plots for the near-surface and surface fuel layers.

Plot	Epoch	Fuel Layers	
		Near-surface (%)	Surface (%)
Control Plot	Pre-burn	100	100
	2 weeks post-burn	100	100
	6 weeks post-burn	100	100
	1 year post-burn	100	80
Fire-Altered Plot 1	Pre-burn	100	100
	2 weeks post-burn	5	80
	6 weeks post-burn	10	60
	1 year post-burn	30	70

Fire-Altered	Plot 2	Pre-burn	100	100
		2 weeks post-burn	0	5
		6 weeks post-burn	5	10
		1 year post-burn	10	40
Fire-Altered	Plot 3	Pre-burn	100	100
		2 weeks post-burn	0	15
		6 weeks post-burn	5	20
		1 year post-burn	10	25

A slight decrease in the surface fuel layer was observed. In the fire-altered plots, both the near-surface and surface fuel cover decreased two weeks post-burn. An increase in cover across both these layers was observed one year post-burn. However, this was still lower than pre-burn levels.

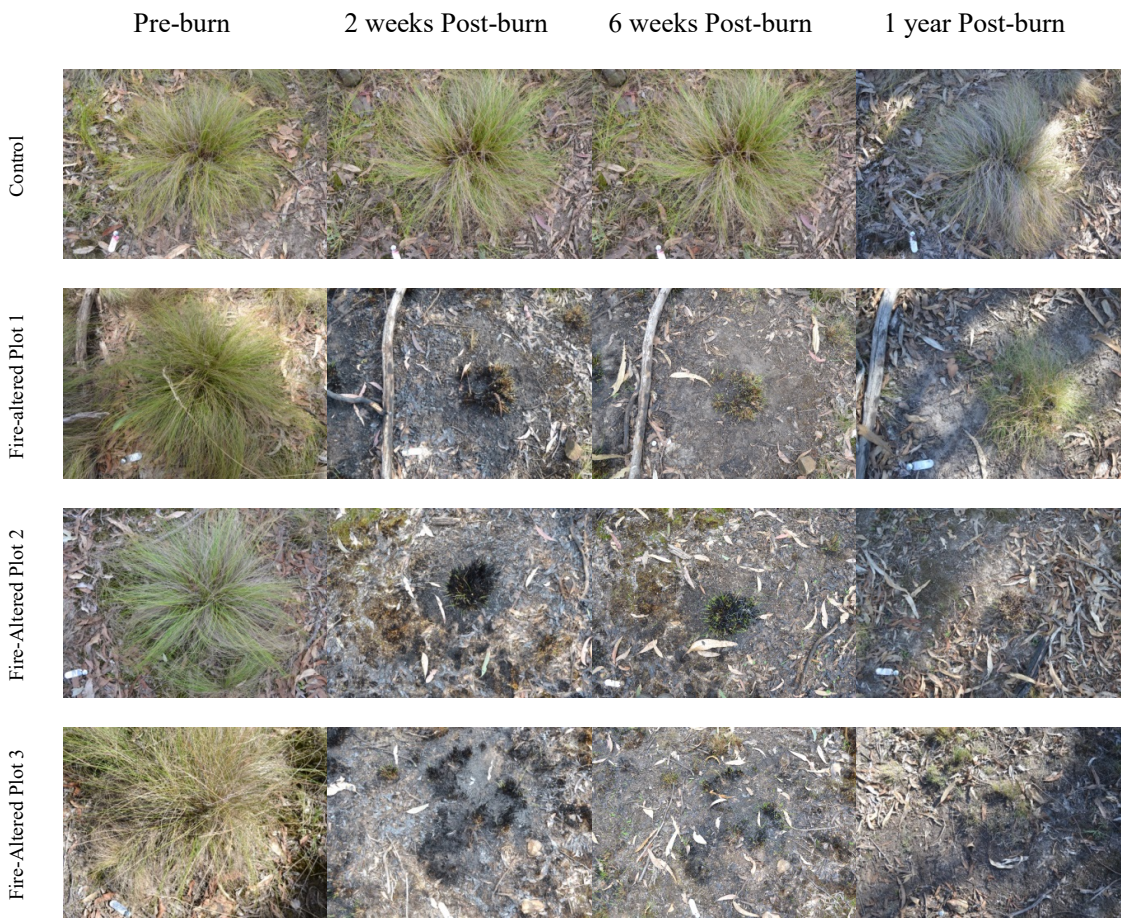

Figure 7.1 Examples of photographic record of change in the near-surface fuel targets from the four plots throughout the data capture campaign.

In fire-altered plots 2 and 3 the two fuel layers show a much larger change in fuel cover. Near-surface fuel cover at two weeks post-burn was identical across these two plots and recorded at 0%.

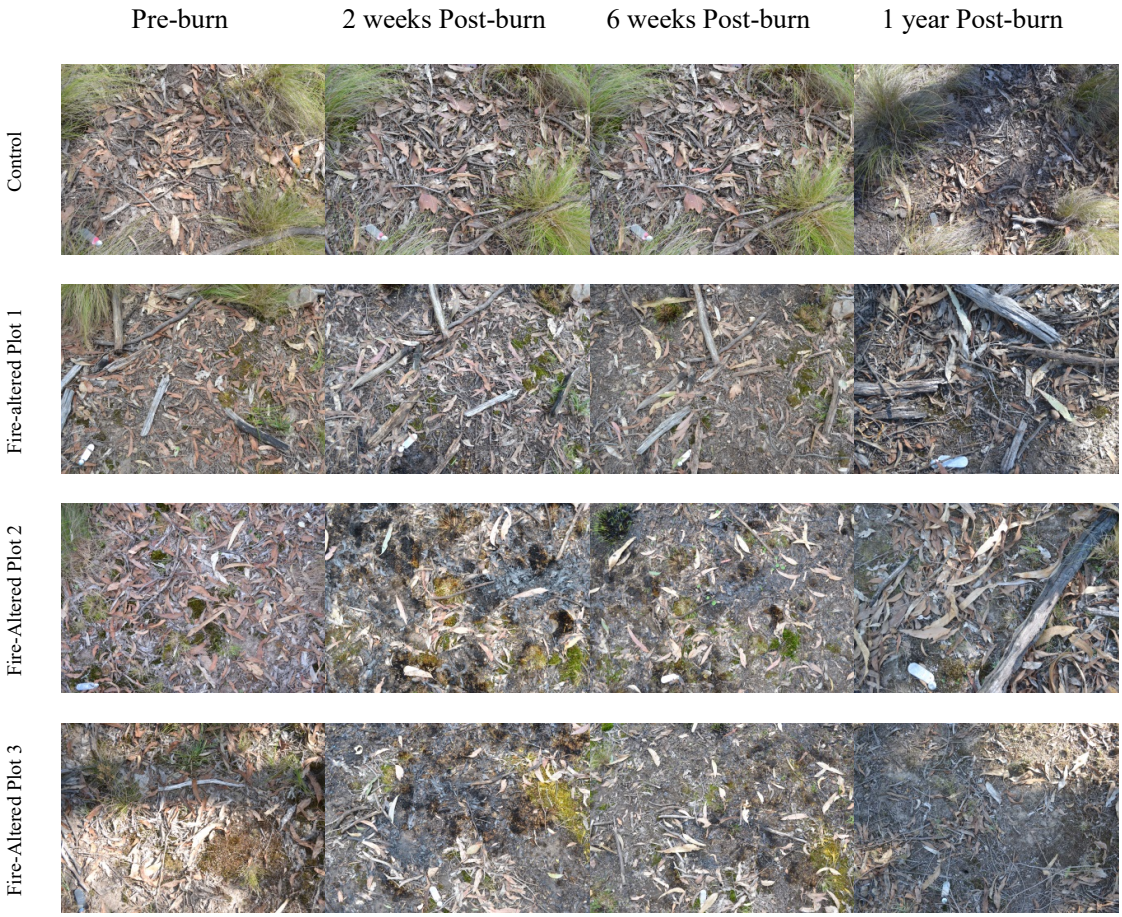

Figure 7.2 Examples of photographic record of change in the surface-fuel targets from the four plots throughout the data capture campaign.

At one year post-burn there was some regrowth and near-surface fuel cover was recorded at 10% in both the plots. This trend was also observed in the surface fuel layer cover. Surface fuel cover was greater at 40% in fire-altered plot 2 in comparison to fire-altered plot 3 which recorded 25% cover.

7.3.2 Comparison of spectral indices and visual assessment of change

7.3.2.1 Near-surface fuel layer

At least one spectral index from the four broad categories showed statistically significant correlations as shown in Table 7.3. Field measure of change in near-surface fuel cover was positively correlated with spectral indices such as D720 (r = 0.97, p<0.05), D1550 (r = 0.94, p<0.05), D1030 (r = 0.89, p<0.05), NBR (r = 0.82, p<0.05) and NDVI (r = 0.77, p<0.05). Spectral indices showing the lowest correlation with field measured change were dWI (r = 0.20, p>0.05), dNDWI (r = -0.32, p>0.05) and dARI1 (r = -0.42, p≥0.05).

Table 7.3 Pearson product moment correlation coefficient of spectral indices against field measures of change in the near-surface fuel layer cover. (* significant at p<0.05.)

Spectral Index	Physiological Attribute	Near-surface Cover
NDVI	Greenness	0.81*
TCARI[a]		0.49
PRI		0.16
SIPI		0.69
NPQI	Chlorophyll	0.72
NPCI		0.66
D525		0.68
D720		0.93*
WI		0.21
MSI		-0.68
NDWI		-0.33
WI/NDVI	Water Status	-0.57
D1550		0.88*
D1030		0.86*
D1215		0.85*
ARI1	Anthocyanin	-0.42

NBR	Burn	0.80*
CSI		0.81*
MIRBI		-0.69
BAI		-0.67

7.3.2.2 Surface fuel layer

Only one statistically significant correlation between change in surface fuel layer cover and spectral indices was found. The highest positive correlation was found with D1230 (r = 0.76, p<0.05) as shown in table 7.4.

Table 7.4 Pearson product moment correlation coefficient of spectral indices against field measures of change in the surface fuel layer cover. (* significant at p<0.05.)

Spectral Index	Physiological Attribute	Surface Cover
D1700	Terpene	0.68
D1230	Water, Cellulose, Starch, Lignin, Xylan	0.76*
Cellulose	Cellulose	0.30
NBR	Burn	-0.57
BAI		0.56
CSI		0.41
MIRBI		-0.71

7.3.3. Hyperspectral data analyses

This section is discussed in two sections. Section 7.3.3.1 reports the spectral indices that are redundant following an analysis of scatterplot matrices in the near-surface fuel layer. Spectral indices measuring greenness (NDVI) and Anthocyanin (ARI1) are not tested for redundancy in the near-surface fuel layer as these are the only indices representative of the physiological attribute. Section 7.3.3.2 reports the findings of the time-series evaluation of change reported by the spectral indices for the near-surface fuel layer. Section 7.3.3.3 reports the findings of variable redundancy in the surface fuel layer followed by the time-series evaluation of change in Section 7.3.3.4.

7.3.3.1 Variable redundancy for the near-surface fuel layer

7.3.3.1a Chlorophyll

Scatterplots matrices for spectral indices recording chlorophyll in the near-surface fuel layers showed moderate to high correlations as shown in Figure 7.3. First derivative indices such as D525 and D720 showed a high degree of correlation (r = 0.95) thus exhibiting similar relationships with other indices. Across all the indices, the lowest correlation was recorded between SIPI and both TCARI/OSAVI (r = 0.54) and PRI (r = -0.56). When compared to change recorded by the field data (Table 7.3) only D720 hyperspectral index was found to be statistically significant.

7.3.3.1b Moisture

Scatterplot matrices for spectral indices sensitive to moisture content, as shown in Figure 7.4, indicated that WI was the least correlated to other indices (that is, WI/NDVI - r = 0.15, D1550 - r = 0.15), D1030 - r = 0.05) and D1215 - r = 0.03)). A similar trend was also exhibited by NDWI. MSI showed a moderately high correlation with the other spectral indices (r = -0.75 – 0.67). First derivative indices D1030, D1215 and D1550 (r = 0.91 – 0.95) showed high correlations with each other.

When compared to change detected by field observations, of the seven indices, only three spectral indices were found to be statistically significant. These were D1550, 1030 and D1215 respectively. These were shortlisted for further analyses and the other indices were removed from further study.

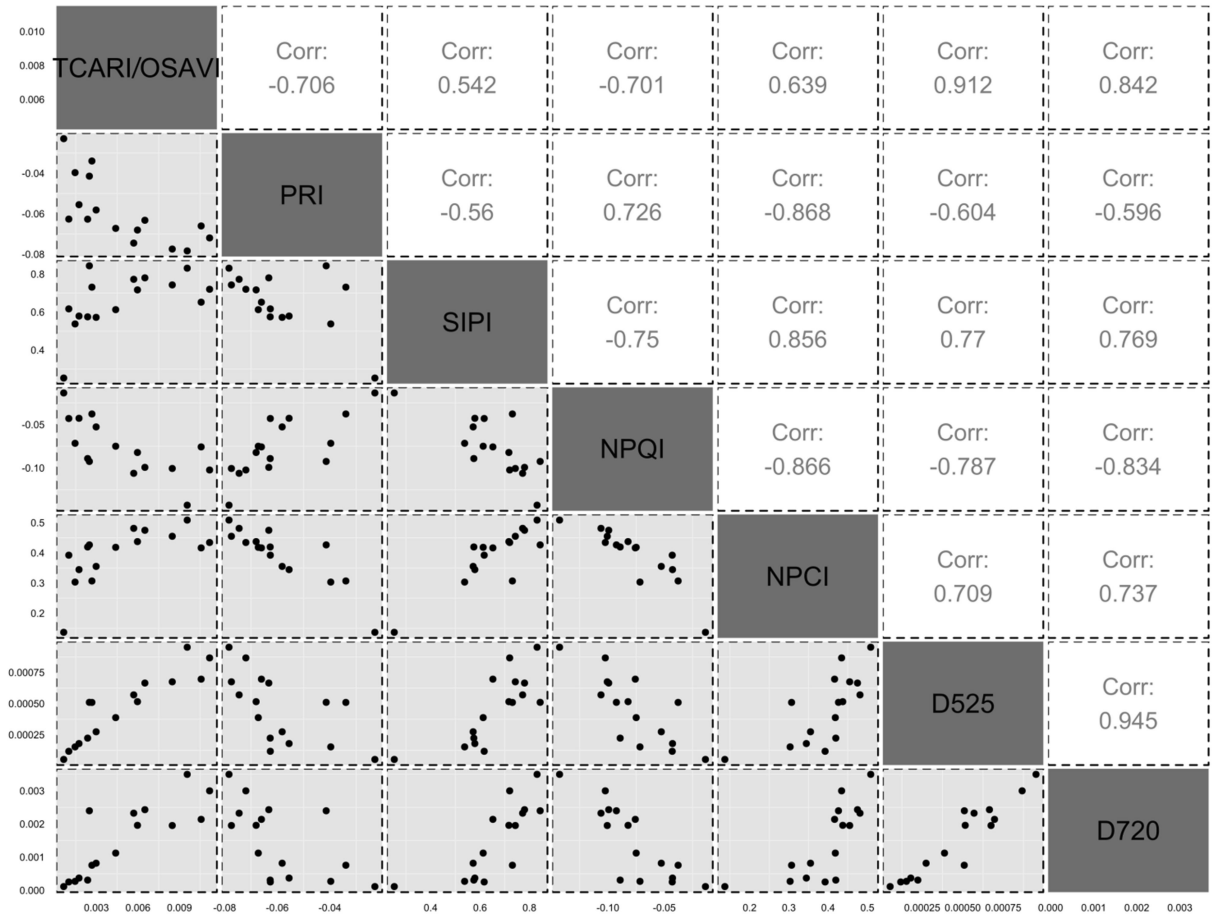

Figure 7.3 Correlation coefficient matrix of the chlorophyll sensitive indices for the near-surface fuel layer.

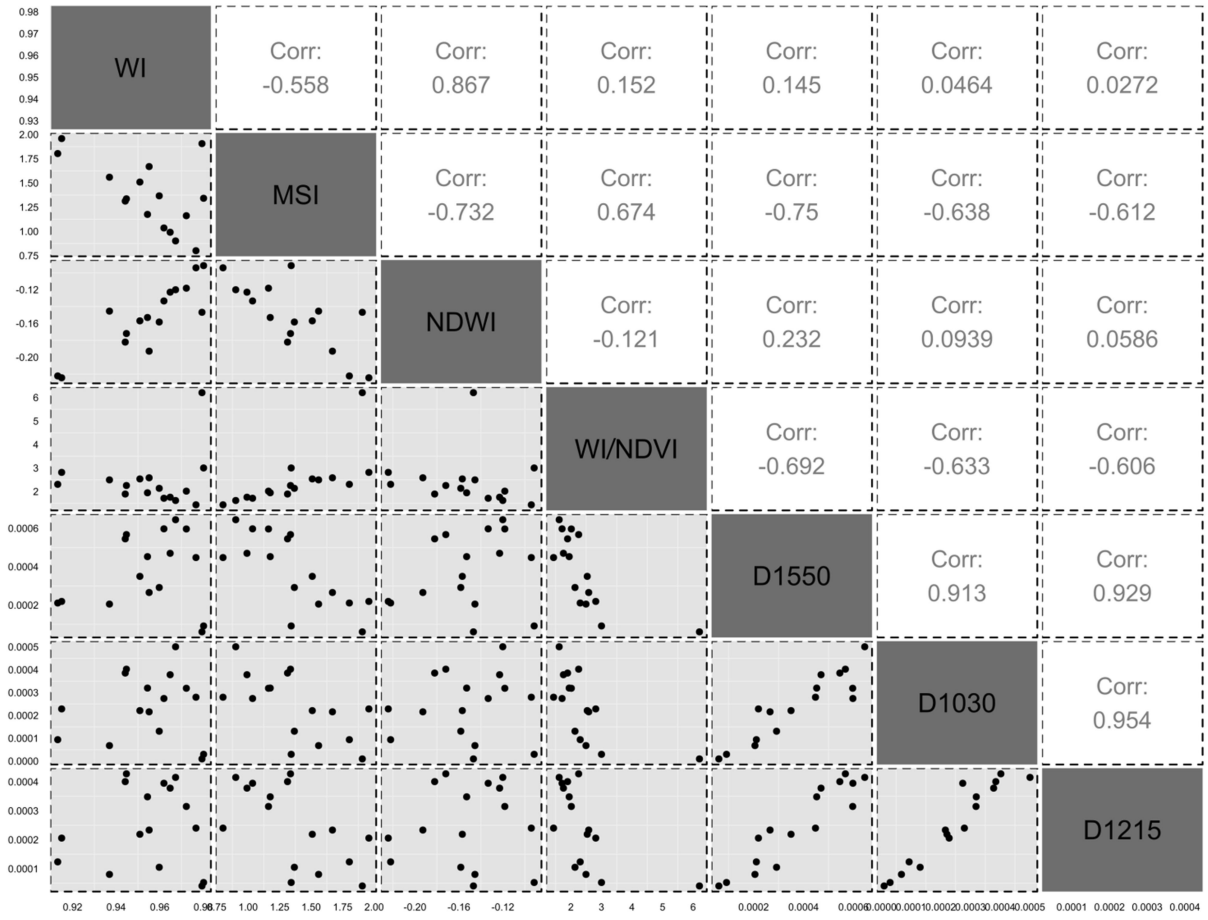

Figure 7.4 Correlation coefficient matrix of the water sensitive indices for the near-surface fuel layer.

7.3.3.1c Burn

The scatterplot of burn indices indicate that NBR was strongly correlated to all the other burn indices as shown in Figure 7.5. The highest correlation was recorded between NBR and CSI (r = 0.93) and BAI and MIRBI (r = 0.93). The lowest correlation was recorded between BAI and CSI (r = -0.61). When compared to change observed by field measures only NBR and CSI were found to be statistically significant and was shortlisted for further analyses.

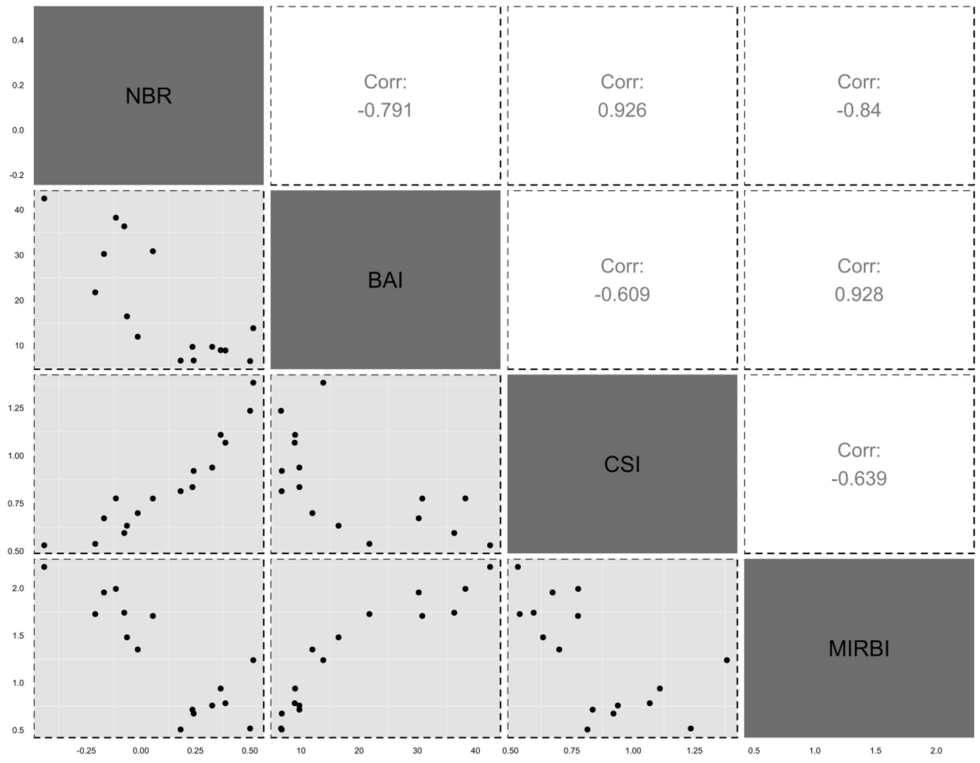

Figure 7.5 Correlation coefficient matrix of the burn indices for the near-surface fuel layer.

7.3.3.2 Time-series evaluation of the near-surface fuel layer

Some of the spectral indices showed a near-linear trend in the control plot such as ARI1 and D720 as shown in Figure 7.6. For some other indices such as NDVI and NBR there was an increase observed until six weeks post-burn and a drop to below pre-burn levels at one year from the burn for the target from the control plot. For D1030 the trend was that of a decrease in week two and a slight increase thereafter until one year post-burn.

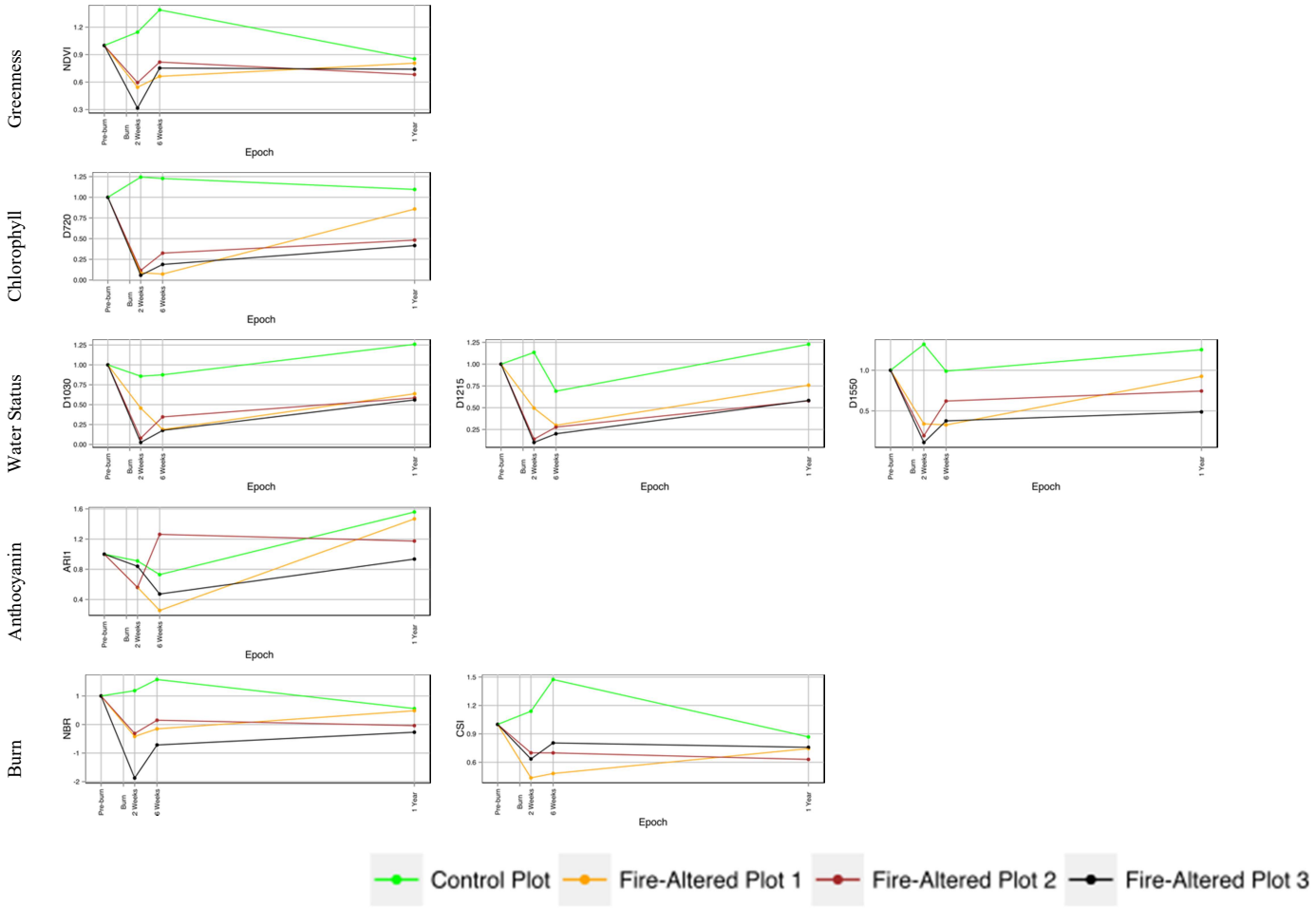

Figure 7.6 Time-series change plotted for the different spectral indices for the near-surface fuel layer from the four plots.

The near-surface targets from the fire-altered plots showed similar trends for the above-mentioned metrics. The trend was that of a sharp decrease in the intensity of the indices two weeks post-burn. At six weeks post-burn a reversal of this trend was observed in some indices such as NDVI, D720, D1030, NBR and CSI. At one year post-burn the values for various indices was closer to pre-burn levels than at any other epoch at which hyperspectral data capture occurred. Near-surface fuel target from fire-altered plot 3 showed the greatest deviation from pre-burn levels across most of the indices as is evidenced from Figure 7.6.

7.3.3.3 Variable redundancy for the surface fuel layer

Since none of the burn indices reported statistically significant correlations with change in the surface fuel cover they have been excluded from discussion in this section.

7.3.3.4 Time-series evaluation of the surface fuel layer

Of the seven indices tested only D1700 and D1230 showed a linear trend for the surface fuel target from the control plot (Figure 7.7). Surface fuel targets from the fire-altered plots showed a decrease in intensity in both these indices two weeks post-burn. An increase was observed one year post-burn which was still below pre-burn levels. The time-series plot of CAI demonstrates that it was not able to distinguish between burnt and unburnt surface fuel targets. The burn indices too did not exhibit a consistent trend and did not allow for easy discrimination between burnt and unburnt targets. None of the burn indices exhibited statistically significant relations with field assessment of change (Table 7.4).

Terpene

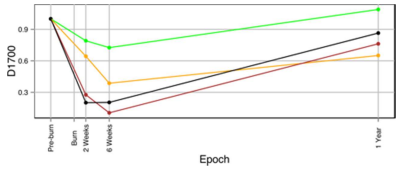

Water, cellulose, starch, lignin and xylan

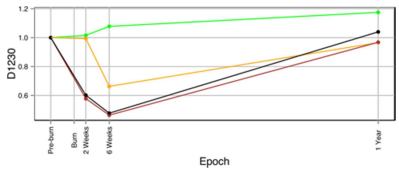

Cellulose

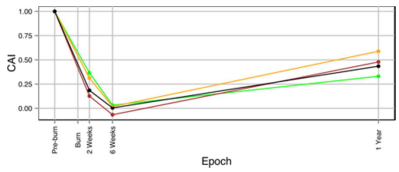

Figure 7.7 Time-series change plotted for spectral indices for the surface fuel layer from the four plots.

7.4 Discussion

Findings of this chapter show that at least two commonly used spectral indices NDVI and NBR were able to detect burnt near-surface fuel targets from unburnt ones whilst also informing recovery. A first-order derivative spectral index derived in this research, D720 was also found to be useful across this fuel layer for this purpose. For the surface fuel layer only one spectral index D1230 was found to be fit-for-purpose. However, no single spectral index could ascertain burnt and unburnt fuels whilst informing recovery across both the near-surface and surface fuel layers.

7.4.1 Near-surface fuel layer

At least one spectral index sensitive to vegetation greenness (NDVI), chlorophyll (D720), water content (D1030) and burn (NBR) was found to be suitable for ascertaining burnt and unburnt near-surface fuel targets and tracking fuel recovery post-burn. The near-surface fuel targets from fire-altered plots did not recover to pre-burn fuel cover levels within one year post-burn. This observation is evident from the photographs of near-surface fuel targets taken at different epochs as shown in Figure 7.1. However, it is also evident that recovery rates of the near-surface fuel targets varied across the four experimental plots in this research.

The near-surface fuel target from fire-altered plot 1 seemed to recover the most within this time period with a 30% fuel cover recorded one year post-burn, up from 5% two weeks post-burn. As reported earlier, the near-surface fuel targets from fire-altered plots 2 and 3 recovered at a much slower rate reaching only 10% of fuel cover one year post-burn. This difference in the recovery rates of the near-surface fuel targets could potentially be due to a low fire treatment in fire-altered plot 1. During the field visits it was observed that the wildlife in the study area had a preference for grazing on recently burnt grasses. This may have caused the targets from fire-altered plots 2 and 3 to regenerate their foliage at a slower rate post-burn although this does not explain why the near-surface fuel target from fire-altered plot 1 recovered at a faster rate since it came in contact with fire too.

This observation of difference in recovery rates (fuel accumulation) across the different fire-treated near-surface fuel targets based on field assessments and photographic evidence was also corroborated by the spectral indices as shown in Figure 7.6. The trend of a decrease in spectral index values two weeks post-burn to an increase in six weeks post-burn coincided with the appearance of new specks of grass. This can be clearly visualised in Figure 7.1. This flush of new growth caused an increase in vegetation greenness and chlorophyll content, thus providing a contrast with the burnt background comprising char and ash. Indices such as NDVI, D720 and NBR were able to discriminate between burnt and unburnt vegetation targets even one year post-burn whilst also tracking fuel recovery.

NDVI and NBR have been widely reported for burn detection and burn severity studies (Cocke et al., 2005, Escuin et al., 2008, Illera et al., 1996, Kasischke et al., 1993, Martin and Chuvieco, 1995b, Sever et al., 2012, Soverel et al., 2010, Veraverbeke et al., 2010). NDVI uses a combination of wavebands in the NIR and VIS domains of the electromagnetic spectrum. Both these domains were found to be sensitive to change in vegetation in response to burns as demonstrated in Chapter 6. The high reflectance in the NIR and low reflectance in the red region of the electromagnetic spectrum makes NDVI a suitable spectral index to study vegetation response to burns.

NBR is similar to NDVI in that it uses the NIR band. However, instead of VIS, it employs an MIR band which was also found to be sensitive to fire-induced change in the landscape as reported in Chapter 6. Rock and bare soil reflect highly in MIR bands. Thus, pre-burn spectral data collected over a forest will have high NIR band values and very low MIR band values resulting in very high NBR values. Post-burn spectral data will have low NIR because of burnt vegetation and high MIR values (Clark and Bobbe, 2006). NBR which is directly controlled by surface conditions, such as surface charring (Epting and Verbyla, 2005) is also suited for such studies.

One trend observed through the findings of this chapter was the consistently poor performance of those spectral indices that were based solely on bands in the VIS domain of the electromagnetic spectrum. Examples of such indices include PRI, NPQI, NPCI, D525 and ARI1. This is in agreement with findings of other researchers wherein it is stated that VIS on its own is not very effective for discriminating burns. Possible reasons that have been put forward include soil types that appear dark in the VIS domain and atmospheric effects (Pereira et al., 1997b). Although these spectral indices are sensitive to detecting changes in leaf pigments such as chlorophyll and anthocyanin, the loss of complete near-surface fuel cover renders the utility of such indices useless.

A first derivative spectral index D720 was also found to be effective and compared well with field-based assessments. In fact D720 was found to be relatively more stable for the time-series evaluation of near-surface fuel loss and recovery in comparison to both NDVI and NBR. This could be due to variations in illumination intensity caused by changes in sun angle and cloud cover which the derivative indices are insensitive to (Tsai and Philpot, 1998).

Indices sensitive to water status that were found to be useful for detecting burnt and unburnt near-surface fuel targets were found in wavelengths that have been identified in literature to have low degree of atmospheric interference (Sims and Gamon, 2003). Routinely employed indices such as WI, NDWI and MSI were not found to be useful. This could again be linked to the cover of the near-surface fuel layer target from which spectral data capture occurred. WI which has been used to detect regeneration from burnt landscapes ((Trombetti and Lasaponara, 2005) and found to be highly correlated with plant water content in grasses performed poorly in this research. NDWI and MSI performed poorly too. In fact, both NDWI and WI have been shown to be reliable indicators of relative water content at the leaf and canopy scale (Serrano et al., 2000). Instead a first order derivative index, D1030 derived in this research proved better for detecting burnt and unburnt near-surface fuel targets.

7.4.2 Surface fuel layer

Only one hyperspectral index D1230 was found to be useful at discerning burnt and unburnt surface fuel targets. The difficulty in discerning litter from other land cover types such as coarse woody debris and soil using remote sensing is because of featureless shapes in the visible and near-infrared wavelength ranges (Aase and Tanaka, 1991). As can be seen in Figure 7.2 apart from the change in surface fuel cover, there is a marked change in surface fuel colour and other associated land cover elements. It could be that because of this reason none of the burn indices proved to be effective at detecting burnt from unburnt surface fuel targets.

All these understorey dynamics make it harder to detect burnt surface fuel from unburnt ones. Findings of this research also support earlier findings that indices in the VIS-NIR wavelength domain are not reliable to distinguish surface fuel from soils (Nagler et al., 2000). Since the absorption feature at D1230 is governed by a number of compounds including water, cellulose, starch, lignin and xylan (Elvidge, 1990, Kumar and Skidmore, 2006) this may explain its successful detection from the underlying soil.

7.4.3 Research implications

The methods used in this research highlight the ability of spectral indices to detect burnt and unburnt understorey fuel targets whilst also tracking varying degrees of post-fire fuel recovery. Although no spectral index was found to be suitable for detecting fire-induced change across both the understorey fuel layers (near-surface and surface fuel), a combination of spectral indices identified in this chapter can be used to address this problem. NDVI, NBR and D720 were found to be suitable for detecting fire-induced change in the near-surface fuel layer whilst D1230 in the surface fuel layer. NDVI, NBR and D1230 spectral indices use wavelengths that are found on most of the commercial satellite sensors meant for earth observation such as Landsat, MODIS and AVHRR. Some of the new high resolution satellite sensors such as RapidEye and WorldView-2 possess the Red Edge band at 690-730nm and 705-745nm respectively. This will allow indices such as D720 used in this research to demonstrate its utility in mapping burnt near-surface fuel. As such D720 was found to be much more stable in the unburnt plot in comparison to other routinely used indices for mapping fire-induced change in near-surface fuel layer.

This study involved the use of field spectrometry to detect burnt and unburnt understorey whilst tracking fuel recovery for up to one year post-burn. Whilst it was possible to track fuel recovery as early as six weeks post-burn, complete fuel recovery comparable to pre-burn levels could not be ascertained within the stipulated time frame. The indices shortlisted in this chapter are applicable only for the near-surface and surface fuel layers. Shortlisted indices could be applied to characterise fire-induced change in the canopy layer.

Since the spectral data was captured using a ground-based HSR, there were no issues of canopy obscuration. This approach allowed for an understanding of post-burn understorey fuel dynamics which is difficult to ascertain using satellite remote sensing techniques. Since pure endmember spectra were captured from various understorey targets, the change detected was representative of the individual target. The spectral indices shortlisted in this chapter need to be tested for their utility in detecting burnt and unburnt understorey instead of individual targets. This will facilitate up-scaling to landscape features and large area assessment.

7.5 Summary

This chapter demonstrated the utility of various spectral indices to detect burnt and unburnt fuel targets whilst also tracking fuel recovery. In general indices using a combination of VIS and MIR

domain of the electromagnetic spectrum or VIS alone were found to be ineffective. Indices such as NDVI (combination of VIS and NIR), NBR (combination of NIR and MIR), D720 and D1030 were identified as being the most useful for ascertaining burnt and unburnt near-surface fuel targets whilst also tracking recovery. For the surface fuel layer only one spectral index D1230 was found to be effective. The results of this research indicate that spectral indices can be effectively used to monitor post-fire effects on the fuel layers across different time periods.

Chapter 8. Conclusions and recommendations

8.1 Introduction

This study introduced the topic of measuring fire-induced change in the understorey of an Australian dry sclerophyll forest using remote sensing. From this four key research question were investigated. The introductory chapter was followed by a comprehensive review of the relevant literature, presented in Chapter 2. The study area, survey design and equipment used were described in Chapter 3. Chapter 4 presented TLS-derived metrics tested for their ability to detect changes in burnt forest understorey. The best performing TLS-derived metric was then used to report various post-fire effects at different epochs with links drawn to field assessments of fuel hazard and burn severity in Chapter 5. To ascertain areas of the electromagnetic spectrum with the highest sensitivity to fire-induced change in burnt fuel targets hyperspectral analysis was conducted and results reported in Chapter 6. Once the specific broad wavelengths sensitive to fire-induced change were identified, spectral indices corresponding to these regions were tested for their ability to detect changes in burnt fuel layers and track recovery post-burn in Chapter 7.

This chapter summarises the results and key findings presented in this thesis, and is organised as follows: first, conclusions relating to each of the four research questions posed in chapter 1 are presented. Second, a preliminary investigation into the comparison between both structural and physiological measures of change as detected by TLS and HSR is presented. Finally, the chapter concludes with suggested areas for future research.

8.2 Key findings

This research set out to investigate methods to improve the reporting procedures used in quantification of fire effects following prescribed burns. This was explored by testing two remote sensing technologies, TLS and HSR. Currently, techniques for describing and quantifying burn effects are based on visual estimates which are both qualitative and subjective. This leads to challenges in the ability to draw accurate links between field estimates of fire effects and remotely sensed data. The ability to accurately detect and estimate burnt areas is fundamental to

understanding carbon cycling, modelling and emissions at various spatial and temporal scales. An additional benefit of burn area mapping is in providing fire and land management agencies the ability to identify areas in urgent need of rehabilitation. The work presented in this thesis looked at ascertaining fire-induced change in the forest understorey using metrics derived from TLS and HSR.

This thesis aimed to provide answers to four main research questions and the key findings are as follows:

RQ1. What are the best performing TLS-derived metrics for measuring changes in burnt forest understorey?

This research question tested TLS-derived metrics against set criteria to assess their utility in detecting changes in burnt forest understorey. This research question is important in that it helped identify a set of metrics that could be used to describe post-fire effects.

Of the 18 metrics that were derived from TLS point clouds, three were found to be suitable for detecting fire-induced change in the forest understorey. The metrics identified were *mean* AGH_{change}, $AGH50_{change}$ and *point* $count_{change}$. These metrics were shortlisted using a set criteria based on three key factors: i) *sensitivity*- relates to the ability of the metric to detect change in burnt understorey; ii) *stability*- relates to the ability of the metric to show least change in the control plot; and iii) *similarity*- relates to the ability of the metric to identify spatial patterns of change which are similar to visual assessments. The results demonstrated that these three metrics correctly and accurately detected very little to no change in the understorey of the control plot, whilst detecting a large change in burnt forest understorey which matched well with visual field assessments.

The approach described in this chapter facilitated rapid data capture, easy post-processing of data and were fit-for-purpose for detecting and quantifying fire-induced change in the forest understorey. TLS scans were captured in single-scan mode, leading to parts of the study plots and forest structure being affected by occlusion. However, a sensitivity analysis demonstrated that the impact of missing data through occlusion in the study plots did not significantly change findings. Findings in chapter 4 demonstrated that it was possible to detect understorey change accurately at a fine-scale using TLS point clouds captured in single-scan mode.

RQ2. What are the post-fire effects observed in the burnt forest understorey as measured by the best performing TLS metric?

This research question looked at describing the various post-fire changes using the 'best' performing TLS-derived metric from RQ1. Validation between TLS measures and field measures was also conducted. This research question helped understand the different post-fire effects that could be reported, quantified and linked with field measures such as fuel hazard and burn severity.

Mean AGH_{change} was used to report various post-fire effects that could be observed in the burnt understorey for up to two years post-burn. The different post-fire effects that could be reported included both short and long-term effects. Short term effects compared measures taken pre-burn to those taken two weeks post-burn. Some of the short-term effects that could be ascertained were total area burnt and spatial distribution of burnt and unburnt patches (epoch *T1*). Longer-term effects compared measures taken two weeks post-burn to two years post-burn, and also measures taken pre-burn to two years post-burn. Long-term post-fire effects that could be measured included fuel accumulation (epoch *T2*) and prescribed burn effectiveness (epoch *T3*).

Findings of this chapter indicated that TLS has the potential to monitor change in the forest understorey following prescribed burns. At epoch *T1*, TLS accurately detected between 61–75% of the fire-affected voxels as having undergone change compared to pre-burn levels. The spatial distribution of change and patchiness was also comparable to visual estimates. In the control plot, no change was correctly observed for more than 90% of the voxels. At epoch *T2*, fuel accumulation was very low in the fire-altered plot. This was confirmed by 60% of the voxels showing no change relative to two weeks post-burn levels in fire-altered plot 3. A decrease in understorey fuel height by 10cm was also recorded in this plot relative to two weeks post-burn levels. At *T3*, it was verified by both TLS data and field assessments that prescribed burns were effective in reducing understorey fuel load relative to pre-burn levels both in terms of cover and height. Approximately 40% of the fire-altered plot 3 had understorey fuel load below pre-burn levels. The understorey fuel height measured a reduction of 15cm relative to pre-burn levels.

It was also concluded from this chapter that *mean* AGH_{change} had a high degree of agreement with change in understorey land cover. It was highly correlated with *'Near-Surface Live Vegetation and Bare Earth'* (r = 0.71, p<0.05), *'Near-Surface Live Vegetation'* (r = 0.69, p<0.05) and *'Near-Surface Live Vegetation and Litter'* (r = 0.68, p<0.05). TLS-derived height estimates pre-burn and two years post-burn were also found to be comparable to field assessments.

RQ3. What are the spectral changes observed in the forest understorey at different times since fire?

This question looked at detecting spectral changes in burnt forest understorey and associated critical observation timelines. This provided the opportunity to identify appropriate wavelengths in the electromagnetic spectrum most sensitive to fire-induced change. This enabled identification of appropriate spectral indices for use in RQ4.

Since prescribed burns resulted in burning of the near-surface fuel layer it led to changes in chlorophyll, cellulose, water content and internal cellular structure of vegetation. These changes in physiological factors resulted in spectral reflectance changes in the burnt fuel targets. In addition to hyperspectral remote sensing, the field observations of fire-induced change in the fuel layers validated these spectral responses and gave an insight into the dynamics of post-burn changes via multi-temporal *in situ* reflectance spectra. Spectral features such as the green reflectance peak (550nm), red edge (680-750nm) and water absorption feature (970nm) disappeared from the near-surface fuel layer post-burn due to loss of foliage. In addition to these, the absorption features identified from the first derivative of reflectance curves highlighted the importance of studying vegetation response in the MIR and VIS-NIR domain to monitor fire effects on vegetation. The surface fuel layer absorption features from the first derivative of reflectance were identified at 1225nm and 1700nm.

In terms of recovery, one year post-burn was not long enough to observe full recovery in the two fuel layers. These findings were in agreement with visual assessments of change and photographic evidence recorded in the field for the various fuel targets. Considering the greatest deviation from pre-burn spectral measurement occurred approximately two weeks post-burn for this study, it is recommended that acquisition of aerial and satellite imagery for mapping burn extent occurs close to two weeks post-burn. In addition to the VIS, NIR and MIR, selected imagery should also include the wavelength range of red edge (that is 680–750 nm) as it was shown to be an early indicator of vegetation recovery.

RQ4. Which spectral indices best identify fire impacts and vegetation recovery in the forest understorey?

This question looked at testing various spectral indices to detect burnt and unburnt targets in the forest understorey. It also looked at how well remotely sensed measurements matched with field based estimates of fire-induced change.

Spectral indices such as NDVI and NBR were found to be the most useful at ascertaining fire effects and recovery in the near-surface fuel layer. Both of these indices exhibited statistically

significant relationships with field measures of change in fuel cover of the near-surface fuel layer; NDVI ($r = 0.81$, $p<0.05$) and NBR ($r = 0.93$, $p<0.05$). A first-order derivative index derived in this thesis, D720 was also found to be effective at ascertaining this change. For the surface fuel layer, first-order derivative index, D1230 as derived in this research was found to be most suitable.

8.3 Comparing structural and physiological changes

A preliminary investigation into change recorded by TLS and HSR is presented in this section. TLS measures structural change whilst HSR detects physiological change. This comparison of two distinct changes in the landscape can inform which is better for quantifying and spatially mapping burnt and unburnt areas. It can also help ascertain which of the two technologies is best for detecting the first signs of vegetation recovery and fuel accumulation. A near-surface fuel target from the control and fire-altered plot 3 was chosen for this purpose. Figure 8.1(a, b and c) shows mean height (cm) derived from TLS point clouds and spectral indices (NDVI, NBR and D720) plotted against time (weeks).

Both technologies are able to discern between burnt and unburnt targets immediately following the burn (that is, two weeks post-burn). As shown in Figure 8.1, there is a decrease in both mean AGH and the spectral indices in fire-altered plot 3 whilst it remains close to pre-burn levels in the control plot. Mean height recorded by TLS in the control plot varies very little across the two year period (19.20–21.52cm) in comparison to spectral indices such as NDVI, NBR and D720 Figure 8.1(a, b and c). In fire-altered plot 3, a sharp decrease in mean height is recorded two weeks post-burn (6.95cm) from pre-burn (17.62cm). This decreasing trend is observed across the spectral indices as well. Whilst an increase in NDVI, NBR and D720 is observed six weeks and one year post-burn in fire-altered plot 3, little difference between the mean height values recorded two years (7.19cm) and two weeks post-burn (6.95cm) by TLS is observed.

Overall, both TLS and HSR can detect burnt and unburnt near-surface fuel immediately post-burn. However, they differ in their ability to track post-burn recovery. TLS measures of structural change suggest that near-surface fuel at two years post-burn is still closer to two weeks post-burn levels. HSR measures of physiological change on the other hand suggest that near-surface fuel is recovering. It is higher than two weeks post-burn levels but much lower than pre-burn levels. Spectral indices show a lot of variation even in the near-surface fuel target from the control plot.

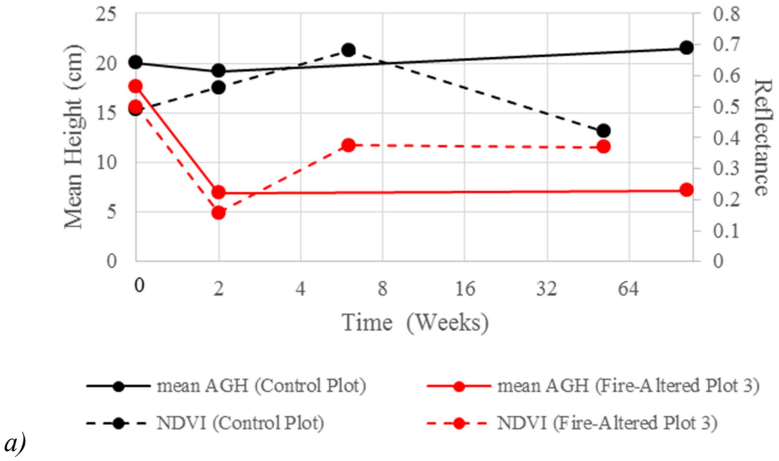

a)

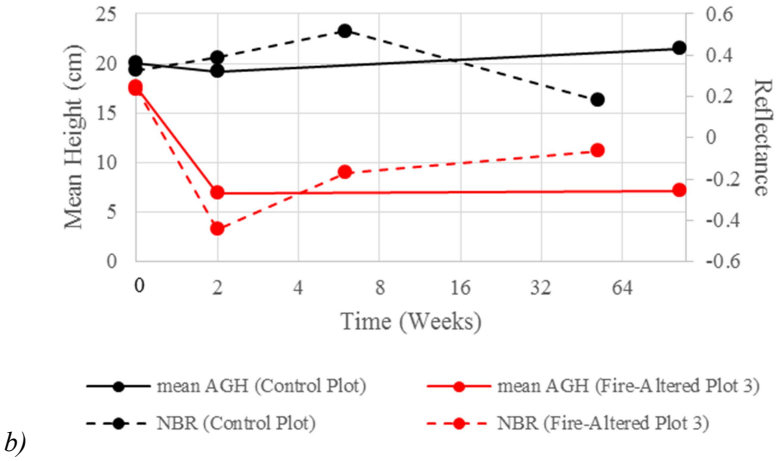

b)

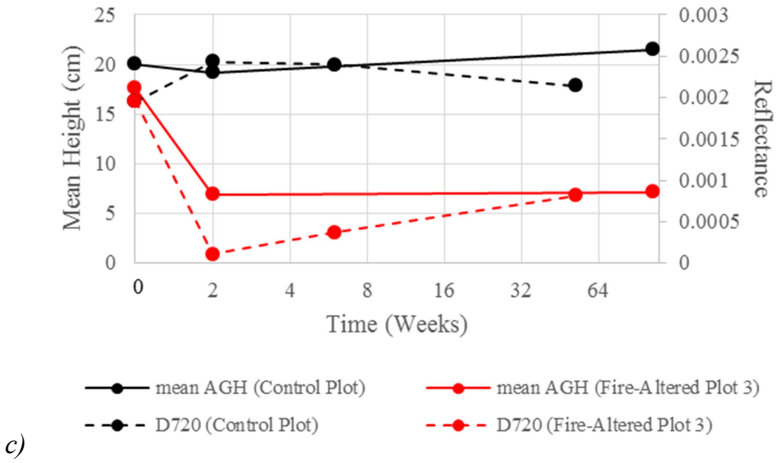

c)

Figure 8.1 Time-series change plotted using TLS- and HSR-derived metrics (a- NDVI, b- NBR and c- D720) for near-surface fuel target from the control and fire-altered plot 3. The x-axis shows time since fire, where 0 represents pre-burn measures. X-axis is plotted on a logarithmic scale. The primary y-axis corresponds to TLS-derived measures of mean height whilst the secondary y-axis to spectral indices.

Thus using these two technologies in conjunction can help inform two key changes in the burnt landscape. One, using spectral data as an indicator of physiological recovery of vegetation components in the landscape allows for early detection of recovery (as early as six weeks post-burn). Two, TLS point clouds can better inform the physical attributes (for example height and cover) and as such can help ascertain biomass loss and fuel load accumulation.

8.4 Future research directions

Research presented in this thesis demonstrated the utility of two emerging ground-based remote sensing technologies to assess various post-fire effects in response to prescribed burns. However, additional research is required to further explore the work presented here. The techniques described in this thesis require further testing and application in a variety of forest types, fuel strata and fire regimes. This will enable us to quantify and understand differences in fire-effects and recovery based on different fire regimes.

In this research, TLS has been demonstrated as a promising tool to map burnt and unburnt landscapes. There is a need to develop the techniques presented in this thesis to move beyond this binary change detection in the landscape to mapping burn severity. Burn severity mapping involves measuring the degree of post-burn change in the landscape within burnt areas. This still poses several challenges including confusion between different severity classes. Severity mapping within burnt areas can assist in identifying areas in need of post-fire rehabilitation and mitigation. TLS technology as demonstrated in this thesis has also shown much potential in its ability to map the spatial variation or patchiness of burnt surfaces. There is also scope for understanding the impacts of occlusion on whether the loss of accuracy warrants the trade-off in increasing time and complexity for multi-scan modes and data processing. In addition to mapping severity, there is a need to monitor and quantify post-fire vegetation recovery and biomass consumption. This could be achieved by conducting LiDAR surveys at regular intervals that span across several years to a decade or possibly even longer.

Whilst a preliminary investigation into comparing the physiological and structural change in burnt understorey is presented in this research, it warrants further investigation. This research has established that spectral data can inform vegetation recovery in burnt landscapes (within six weeks post-burn) before structural regrowth is detected by TLS. Investigation into this aspect of difference in physiological and structural recovery of burnt vegetation may further help develop our understanding of burn severity. First-level integration between these two technologies can be

obtained by overlaying multi-temporal digital images with LiDAR datasets of comparable spatial resolution. This will enable identifying burnt and unburnt areas in both the datasets. Novel metrics can then be developed that inform fire-effects in the landscape using both these technologies.

Up-scaling from ground-based measurements to air- and space-borne observations can facilitate mapping and monitoring fire-effects across large areas. Further research could investigate the potential of integrating RapidEye or WorldView-2 imagery with ALS. Both the mentioned satellite sensors possess a Red Edge band which has been shown in this thesis to be an early indicator of vegetation recovery in burnt landscapes.

9. Bibliography

AASE, J. K. & TANAKA, D. L. 1991. Reflectances from four wheat residue cover densities as influenced by three soil backgrounds. *Agronomy journal,* 83**,** 753-757.

ABBOTT, I. & LONERAGAN, O. 1983. Response of jarrah (Eucalyptus marginata) regrowth to thinning. *Australian forest research,* 13**,** 217-229.

ALLEAUME, S., HELY, C., LE ROUX, J., KORONTZI, S., SWAP, R. J., SHUGART, H. H. & JUSTICE, C. O. 2005. Using MODIS to evaluate heterogeneity of biomass burning in southern African savannahs: a case study in Etosha. *International Journal of Remote Sensing,* 26**,** 4219-4237.

ANGELO, J. J., DUNCAN, B. W. & WEISHAMPEL, J. F. 2010. Using Lidar-derived vegetation profiles to predict time since fire in an oak scrub landscape in East-Central Florida. *Remote Sensing,* 2**,** 514-525.

ARNETT, J. T. T. R., COOPS, N. C., DANIELS, L. D. & FALLS, R. W. 2015. Detecting forest damage after a low-severity fire using remote sensing at multiple scales. *International Journal of Applied Earth Observation and Geoinformation,* 35**,** 239-246.

ASD 1999. Analytical Spectral Devices, Inc. (ASD) Technical Guide.

ATTIWILL, P. M. 1994. Disturbance of forest ecosystems: the scientific basis for conservation utilisation. *In:* ATTIWILL, P. M., FLORENCE, R. G., HURDITCH, W. E. & HURDITCH, W. J. (eds.) *The Burning Continent: Forest Ecosystems and Fire Management in Australia.* Institute of Public Affairs, Perth.

AULD, T. D. 1994. After the Fires. *Australian Orchid Review,* August 1994**,** 13-15.

BANNARI, A., MORIN, D., BONN, F. & HUETE, A. R. 1995. A review of vegetation indices. *Remote Sensing Reviews,* 13**,** 95-120.

BARNES, J. D., BALAGUER, L., MANRIQUE, E., ELVIRA, S. & DAVISON, A. W. 1992. A reappraisal of the use of DMSO for the extraction and determination of chlorophylls a and b in lichens and higher plants. *Environmental and Experimental Botany,* 32**,** 85-100.

BARRETT, K., KASISCHKE, E. S., MCGUIRE, A. D., TURETSKY, M. R. & KANE, E. S. 2010. Modeling fire severity in black spruce stands in the Alaskan boreal forest using spectral and non-spectral geospatial data. *Remote Sensing of Environment,* 114**,** 1494-1503.

BIENERT, A., SCHELLER, S., KEANE, E., MOHAN, F. & NUGENT, C. Tree detection and diameter estimations by analysis of forest terrestrial laser scanner point clouds. ISPRS Workshop on Laser Scanning and SilviLaser, 12-14 September 2007 Espoo, Finland. 50-55.

BLACKBURN, G. A. & STEELE, C. M. 1999. Towards the Remote Sensing of Matorral Vegetation Physiology: Relationships between Spectral Reflectance, Pigment, and Biophysical Characteristics of Semiarid Bushland Canopies. *Remote Sensing of Environment,* 70**,** 278-292.

BOER, M., MACFARLANE, C., NORRIS, J., SADLER, R., WALLACE, J. & GRIERSON, P. 2008a. Mapping burned areas and burn severity patterns in SW Australian eucalypt forest using remotely-sensed changes in leaf area index. *Remote Sensing of Environment,* 112**,** 4358-4369.

BOER, M. M., MACFARLANE, C., NORRIS, J., SADLER, R. J., WALLACE, J. & GRIERSON, P. F. 2008b. Mapping burned areas and burn severity patterns in SW Australian eucalypt forest using remotely-sensed changes in leaf area index. *Remote Sensing of Environment,* 112**,** 4358-4369.

BOND, W. J. & VAN-WILGEN, B. W. 1996. *Fire and plants,* London, Chapman and Hall.

BOSCHETTI, M., STROPPIANA, D. & BRIVIO, P. A. 2010. Mapping Burned Areas in a Mediterranean Environment Using Soft Integration of Spectral Indices from High-Resolution Satellite Images. *Earth Interactions,* 14**,** 1-20.

BOWMAN, D., ZHANG, Y., WALSH, A. & WILLIAMS, R. J. 2003. Experimental comparison of four remote sensing techniques to map tropical savanna fire-scars using Landsat-TM imagery. *International Journal of Wildland Fire,* 12**,** 341-348.

BOWMAN, D. M. J. S., BALCH, J. K., ARTAXO, P., BOND, W. J., CARLSON, J. M., COCHRANE, M. A., D'ANTONIO, C. M., DEFRIES, R. S., DOYLE, J. C. & HARRISON, S. P. 2009. Fire in the Earth system. *science,* 324**,** 481-485.

BOYD, D. S. & DANSON, F. M. 2005. Satellite remote sensing of forest resources: three decades of research development. *Progress in Physical Geography,* 29**,** 1-26.

BRADSTOCK, R. & AULD, T. 1995. Soil temperatures during experimental bushfires in relation to fire intensity: consequences for legume germination and fire management in south-eastern Australia. *Journal of Applied Ecology,* 32**,** 76-84.

BRADSTOCK, R., WILLIAMS, J. & GILL, A. 2002a. *Flammable Australia: the fire regimes and biodiversity of a continent,* Cambridge, Cambridge University Press.

BRADSTOCK, R. A., KEITH, D. A. & AULD, T. D. 1995. Fire and conservation: imperatives and constraints on managing for diversity. *In:* BRADSTOCK, R. A., AULD, T. D., KEITH, D. A., KINGSFORD, R. T., LUNNEY, D. & SIVERTSEN, D. P. (eds.) *Conserving biodiversity: Threats and solutions.*: NSW National Parks and Wildlife Service.

BRADSTOCK, R. A., WILLIAMS, J. E. & GILL, A. M. 2002b. *Flammable Australia: the fire regimes and biodiversity of a continent,* Cambridge, UK, Cambridge University Press.

BREWER, C. K., WINNE, J. C., REDMOND, R. L., OPITZ, D. W. & MANGRICH, M. V. 2005. Classifying and mapping wildfire severity: a comparison of methods. *Photogrammetric Engineering and Remote Sensing,* 71**,** 1311-1320.

BRIDGES, R. G. 2004. Fine fuel in the dry sclerophyll forests of south-eastern New South Wales. *Australian Forestry,* 67**,** 88-100.

BRYANT, C. 2008. Understanding bushfire: trends in deliberate vegetation fires in Australia. *Technical and background paper series no. 27.* Canberra:Australian Institute of Criminology.

BUCHANAN, R. A. 1989. *Bush regeneration: recovering Australian landscapes*, TAFE NSW, Sydney, Australia.

BURROWS, N., WARD, B. & ROBINSON, A. 2010. Fire Regimes and Tree Growth in Low Rainfall Jarrah Forest of South-west Australia. *Environmental Management,* 45**,** 1332-1343.

BURROWS, N., WARDELL-JOHNSON, G. & ABBOTT, I. 2003. Fire and plant interactions in forested ecosystems of south-west Western Australia. *In:* ABBOTT I & BURROWS, N. (eds.) *Fire in ecosystems of south-west Western Australia: impacts and management.* Leiden, The Netherlands: Backhuys Publishers.

BUSCHMANN, C. & NAGEL, E. 1993. In vivo spectroscopy and internal optics of leaves as basis for remote sensing of vegetation. *International Journal of Remote Sensing,* 14**,** 711-722.

CARTER, G. A. 1993. Responses of leaf spectral reflectance to plant stress. *American Journal of Botany,* 80**,** 239-243.

CARTER, G. A. 1998. Reflectance wavebands and indices for remote estimation of photosynthesis and stomatal conductance in pine canopies. *Remote Sensing of Environment,* 63**,** 61-72.

CARTER, G. A. & KNAPP, A. K. 2001. Leaf optical properties in higher plants: linking spectral characteristics to stress and chlorophyll concentration. *American Journal of Botany,* 88**,** 677-684.

CARY, G. J. & MORRISON, D. A. 1995. Effects of fire frequency on plant species composition of sandstone communities in the Sydney region: Combinations of inter fire intervals. *Australian Journal of Ecology,* 20**,** 418-426.

CATLING, P. C. 1994. Bushfires and prescribed burning: protecting native fauna. *Search,* 25**,** 37-40.

CECCATO, P., FLASSE, S., TARANTOLA, S., JACQUEMOUD, S. & GRÉGOIRE, J. M. 2001. Detecting vegetation leaf water content using reflectance in the optical domain. *Remote Sensing of Environment,* 77**,** 22-33.
CHAFER, C. J. 2008. A comparison of fire severity measures: An Australian example and implications for predicting major areas of soil erosion. *Catena,* 74**,** 235-245.
CHAFER, C. J., NOONAN, M. & MACNAUGHT, E. 2004. The post-fire measurement of fire severity and intensity in the Christmas 2001 Sydney wildfires. *International Journal of Wildland Fire,* 13**,** 227-240.
CHEN, G., METZ, M. R., RIZZO, D. M., DILLON, W. W. & MEENTEMEYER, R. K. 2015. Object-based assessment of burn severity in diseased forests using high-spatial and high-spectral resolution MASTER airborne imagery. *ISPRS Journal of Photogrammetry and Remote Sensing,* 102**,** 38-47.
CHEN, K. & MCANENEY, J. 2004. Quantifying bushfire penetration into urban areas in Australia. *Geophysical Research Letters,* 31**,** L12212.
CHEN, X., VOGELMANN, J. E., ROLLINS, M., OHLEN, D., KEY, C. H., YANG, L., HUANG, C. & SHI, H. 2011. Detecting post-fire burn severity and vegetation recovery using multitemporal remote sensing spectral indices and field-collected composite burn index data in a ponderosa pine forest. *International Journal of Remote Sensing,* 32**,** 7905-7927.
CHEN, X., ZHU, Z., OHLEN, D., HUANG, C. & SHI, H. Use of multiple spectral indices to estimate burn severity in the Black Hills of South Dakota. Pecora 17—The future of land imaging… going operational, 16-20 November 2008 Denver, Colorado. ASPRS (American Society for Photogrammetry and Remote Sensing).
CHUVIECO, E. & CONGALTON, R. G. 1988. Mapping and inventory of forest fires from digital processing of TM data. *Geocarto International,* 3**,** 41-53.
CHUVIECO, E., MARTÍN, M. P. & PALACIOS, A. 2002. Assessment of different spectral indices in the red-near-infrared spectral domain for burned land discrimination. *International Journal of Remote Sensing,* 23**,** 5103-5110.
CLARK, J. & BOBBE, T. 2006. Using remote sensing to map and monitor fire damage in forest ecosystems. *In:* WULDER, M. A. & FRANKLIN, S. E. (eds.) *Understanding forest disturbance and spatial patterns: remote sensing and GIS approaches.* Boca Raton, Florida: CRC Press.
CLEVERS, J., DE JONG, S. M., EPEMA, G. F., VAN DER MEER, F. D., BAKKER, W. H., SKIDMORE, A. K. & SCHOLTE, K. H. 2002. Derivation of the red edge index using the MERIS standard band setting. *International Journal of Remote Sensing,* 23**,** 3169-3184.
COCHRANE, G. R. 1963. Vegetation studies in forest-fire areas of the Mount Lofty Ranges, South Australia. *Ecology,* 44**,** 41-52.
COCKE, A. E., FULÉ, P. Z. & CROUSE, J. E. 2005. Comparison of burn severity assessments using Differenced Normalized Burn Ratio and ground data. *International Journal of Wildland Fire,* 14**,** 189-198.
COLLETT, N. G. & NEUMANN, F. G. 1995. Effects of two spring prescribed fires on epigeal Coleoptera in dry sclerophyll eucalypt forest in Victoria, Australia. *Forest Ecology and Management,* 76**,** 69-85.
COOPS, N. C. & CATLING, P. C. 2000. Estimating forest habitat complexity in relation to time since fire. *Austral Ecology,* 25**,** 344-351.
CURRAN, P. J. 1994. Imaging spectrometry. *Progress in physical Geography,* 18**,** 247-266.
CURRAN, P. J., KUPIEC, J. A. & SMITH, G. M. 1997. Remote sensing the biochemical composition of a slash pine canopy. *IEEE Transactions on Geoscience and Remote Sensing,* 35**,** 415-420.
CURTIS, L. 1978. Remote sensing systems for monitoring crops and vegetation. *Progress in Physical Geography,* 2**,** 55-79.
DANSON, F. M., HETHERINGTON, D., MORSDORF, F., KOETZ, B. & ALLGOWER, B. 2007. Forest canopy gap fraction from terrestrial laser scanning. *IEEE Geoscience and Remote Sensing Letters,* 4**,** 157-160.

DASSOT, M., CONSTANT, T. & FOURNIER, M. 2011. The use of terrestrial LiDAR technology in forest science: application fields, benefits and challenges. *Annals of Forest Science,* 68**,** 959-974.

DAUGHTRY, C., WALTHALL, C., KIM, M., DE COLSTOUN, E. B. & MCMURTREY, J. 2000. Estimating corn leaf chlorophyll concentration from leaf and canopy reflectance. *Remote Sensing of Environment,* 74**,** 229-239.

DAVIES, D. K., ILAVAJHALA, S., WONG, M. M. & JUSTICE, C. O. 2008. Fire information for resource management system: Archiving and distributing MODIS active fire data. *IEEE Transactions on Geoscience and Remote Sensing,* 47**,** 72-79.

DE JONG, S. M. & EPEMA, G. F. 2001. Imaging Spectrometry for Surveying and Modelling Land Degradation. *In:* VAN DER MEER, F. & DE JONG, S. M. (eds.) *Imaging spectrometry: basic principles and prospective applications.* Netherlands: Kulwer Academic Publishers.

DEMETRIADES-SHAH, T. H., STEVEN, M. D. & CLARK, J. A. 1990. High resolution derivative spectra in remote sensing. *Remote Sensing of Environment,* 33**,** 55-64.

DÍAZ-DELGADO, R., LLORET, F. & PONS, X. 2003. Influence of fire severity on plant regeneration by means of remote sensing imagery. *International Journal of Remote Sensing,* 24**,** 1751-1763.

DRISCOLL, D. A., LINDENMAYER, D. B., BENNETT, A. F., BODE, M., BRADSTOCK, R. A., CARY, G. J., CLARKE, M. F., DEXTER, N., FENSHAM, R. & FRIEND, G. 2010. Fire management for biodiversity conservation: Key research questions and our capacity to answer them. *Biological Conservation,* 143**,** 1928-1939.

DSE 2010. *Remote Sensing of Fire Severity for Prescribed Burns: Field Assessment,* Department of Sustainability and Environment.

EDWARDS, A. C., MAIER, S. W., HUTLEY, L. B., WILLIAMS, R. J. & RUSSELL-SMITH, J. 2013. Spectral analysis of fire severity in north Australian tropical savannas. *Remote Sensing of Environment,* 136**,** 56-65.

ELVIDGE, C. D. 1990. Visible and near infrared reflectance characteristics of dry plant materials. *International Journal of Remote Sensing,* 11**,** 1775-1795.

ENVI 2009. ENVI 4.7 SP1 Help User Guide November 2009 edition.

EPTING, J. & VERBYLA, D. 2005. Landscape-level interactions of prefire vegetation, burn severity, and postfire vegetation over a 16-year period in interior Alaska. *Canadian Journal of Forest Research,* 35**,** 1367-1377.

EPTING, J., VERBYLA, D. & SORBEL, B. 2005. Evaluation of remotely sensed indices for assessing burn severity in interior Alaska using Landsat TM and ETM+. *Remote Sensing of Environment,* 96**,** 328-339.

ESCUIN, S., NAVARRO, R. & FERNANDEZ, P. 2008. Fire severity assessment by using NBR (Normalized Burn Ratio) and NDVI (Normalized Difference Vegetation Index) derived from LANDSAT TM/ETM images. *International Journal of Remote Sensing,* 29**,** 1053-1074.

ESTEP, L. & CARTER, G. A. 2005. Derivative analysis of AVIRIS data for crop stress detection. *Photogrammetric Engineering & Remote Sensing,* 71**,** 1417-1421.

FERNANDES, P. M. & BOTELHO, H. S. 2003. A review of prescribed burning effectiveness in fire hazard reduction. *International Journal of Wildland Fire,* 12**,** 117-128.

FERNÁNDEZ, A., ILLERA, P. & CASANOVA, J. 1997. Automatic mapping of surfaces affected by forest fires in Spain using AVHRR NDVI composite image data. *Remote Sensing of Environment,* 60**,** 153-162.

FILELLA, I. & PEÑUELAS, J. 1994. The red edge position and shape as indicators of plant chlorophyll content, biomass and hydric status. *International Journal of Remote Sensing,* 15**,** 1459-1470.

FISHER, J. L., LONERAGAN, W. A., DIXON, K., DELANEY, J. & VENEKLAAS, E. J. 2009. Altered vegetation structure and composition linked to fire frequency and plant invasion in a biodiverse woodland. *Biological Conservation,* 142**,** 2270-2281.

FLINN, D. W. 1985. Practical aspects of the nutrition of exotic conifer plantations and native eucalypt forests in Australia. *In:* LANDSBERG, J. J. & PARSON, W. (eds.) *Research for Forest Management.* CSIRO, Melbourne.

FLORENCE, R. 1994. The Ecological Basis for Forest Fire Management in New South Wales. *In:* ATTIWILL, P. M., FLORENCE, R. G., HURDITCH, W. E. & HURDTICH, W. J. (eds.) *The Burning Continent: Forest Ecosystems and Fire Management in Australia.* Perth: Institute of Public Affairs.

FOX, B. J., FOX, M. D. & MCKAY, G. M. 1979. Litter accumulation after fire in a eucalypt forest. *Australian Journal of Botany,* 27**,** 157-165.

FRASER, R., FERNANDES, R. & LATIFOVIC, R. 2003. Multi-temporal mapping of burned forest over Canada using satellite-based change metrics. *Geocarto International,* 18**,** 37-47.

FRASER, R. & LI, Z. 2002. Estimating fire-related parameters in boreal forest using SPOT VEGETATION. *Remote Sensing of Environment,* 82**,** 95-110.

FRENCH, N. H. F., KASISCHKE, E. S., HALL, R. J., MURPHY, K. A., VERBYLA, D. L., HOY, E. E. & ALLEN, J. L. 2008. Using Landsat data to assess fire and burn severity in the North American boreal forest region: an overview and summary of results. *International Journal of Wildland Fire,* 17**,** 443-462.

GAMON, J. A., PEÑUELAS, J. & FIELD, C. B. 1992. A narrow-waveband spectral index that tracks diurnal changes in photosynthetic efficiency. *Remote Sensing of Environment,* 41**,** 35-44.

GARCÍA, M., DANSON, F. M., RIAÑO, D., CHUVIECO, E., RAMIREZ, F. A. & BANDUGULA, V. 2011. Terrestrial laser scanning to estimate plot-level forest canopy fuel properties. *International journal of applied earth observation and geoinformation,* 13**,** 636-645.

GATES, D. M., KEEGAN, H. J., SCHLETER, J. C. & WEIDNER, V. R. 1965. Spectral properties of plants. *Applied optics,* 4**,** 11-20.

GAUSMAN, H. W. 1974. Leaf reflectance of near-infrared. *Photogrammetric Engineering,* 40**,** 183-191.

GIGLIO, L., LOBODA, T., ROY, D. P., QUAYLE, B. & JUSTICE, C. O. 2009. An active-fire based burned area mapping algorithm for the MODIS sensor. *Remote Sensing of Environment,* 113**,** 408-420.

GILL, A. M. 1975. Fire and the Australian flora: a review. *Australian Forestry,* 38**,** 4-25.

GILL, A. M. 1981. Adaptive responses of Australian vascular plant species to fires. *In:* GILL, A. M., GROVES, R. H. & NOBEL, I. R. (eds.) *Fire and the Australian biota.* Canberra: Australian Academy of Science.

GILL, A. M. How fires affect biodiversity. Fire and Biodiversity: The Effects and Effectiveness of Fire Management, 8-9 October 1994 Melbourne, Australia.

GILL, A. M. 1999. Biodiversity and bushfires: an Australia-wide perspective on plant-species changes after a fire event. *In:* GILL, A. M., WOINARSKI, J. & YORK, A. (eds.) *Australia's Biodiversity–responses to fire.* Environment Australia Biodiversity.

GILL, A. M. & WILLIAMS, J. E. 1996. Fire regimes and biodiversity: the effects of fragmentation of southeastern Australian eucalypt forests by urbanisation, agriculture and pine plantations. *Forest Ecology and Management,* 85**,** 261-278.

GILL, A. M., WOINARSKI, J. & YORK, A. 1999. Australia's Biodiversity - Reponses to Fire, Plants, Birds and Invertebrates. Canberra, Australia: Department of Environment and Heritage.

GITELSON, A. A., KAUFMAN, Y. J., STARK, R. & RUNDQUIST, D. 2002a. Novel algorithms for remote estimation of vegetation fraction. *Remote Sensing of Environment,* 80**,** 76-87.

GITELSON, A. A., MERZLYAK, M. N. & CHIVKUNOVA, O. B. 2001. Optical Properties and Nondestructive Estimation of Anthocyanin Content in Plant Leaves. *Photochemistry and Photobiology,* 74**,** 38-45.

GITELSON, A. A., ZUR, Y., CHIVKUNOVA, O. B. & MERZLYAK, M. N. 2002b. Assessing Carotenoid Content in Plant Leaves with Reflectance Spectroscopy. *Photochemistry and Photobiology,* 75**,** 272-281.
GOETZ, A. F. H., VANE, G., SOLOMON, J. E. & ROCK, B. N. 1985. Imaging spectrometry for earth remote sensing. *Science,* 228**,** 1147-1153.
GOLSON, J. 1972. The remarkable history of indo-pacific man. *The Journal of Pacific History,* 7**,** 5-25.
GOODWIN, N. R. 2006. *Assessing Understorey Structural Characteristics in Eucalypt Forests: an investigation of LiDAR techniques (Thesis).* University of New South Wales.
GOTT, B. 2005. Aboriginal fire management in south eastern Australia: aims and frequency. *Journal of biogeography,* 32**,** 1203-1208.
GOVENDER, M., CHETTY, K. & BULCOCK, H. 2009. A review of hyperspectral remote sensing and its application in vegetation and water resource studies. *Water SA,* 33**,** 145-152.
GREAVES, H. E., VIERLING, L. A., EITEL, J. U. H., BOELMAN, N. T., MAGNEY, T. S., PRAGER, C. M. & GRIFFIN, K. L. 2015. Estimating aboveground biomass and leaf area of low-stature Arctic shrubs with terrestrial LiDAR. *Remote Sensing of Environment,* 164**,** 26-35.
GRIGG, A. H., NORMAN, M. A. & GRANT, C. D. 2010. Prescribed burning of thinning slash in regrowth stands of jarrah (Eucalyptus marginata) following bauxite mining in south-west Australia. *International Journal of Wildland Fire,* 19**,** 737-745.
GROVE, T. S., O'CONNELL, A. M. & DIMMOCK, G. M. 1986. Nutrient changes in surface soils after an intense fire in jarrah (Eucalyptus marginata Donn ex Sm.) forest. *Australian journal of ecology,* 11**,** 303-317.
GUINTO, D. F., HOUSE, A. P. N., XU, Z. H. & SAFFIGNA, P. G. 1999. Impacts of repeated fuel reduction burning on tree growth, mortality and recruitment in mixed species eucalypt forests of southeast Queensland, Australia. *Forest Ecology and Management,* 115**,** 13-27.
HABOUDANE, D., MILLER, J. R., TREMBLAY, N., ZARCO-TEJADA, P. J. & DEXTRAZE, L. 2002. Integrated narrow-band vegetation indices for prediction of crop chlorophyll content for application to precision agriculture. *Remote Sensing of Environment,* 81**,** 416-426.
HALL, D. K., ORMSBY, J. P., JOHNSON, L. & BROWN, J. 1980. Landsat digital analysis of the initial recovery of burned tundra at Kokolik River, Alaska. *Remote Sensing of Environment,* 10**,** 263-272.
HAMMILL, K. A. & BRADSTOCK, R. A. 2006. Remote sensing of fire severity in the Blue Mountains: influence of vegetation type and inferring fire intensity. *International Journal of Wildland Fire,* 15**,** 213-226.
HARRIS, S., VERAVERBEKE, S. & HOOK, S. 2011. Evaluating Spectral Indices for Assessing Fire Severity in Chaparral Ecosystems (Southern California) Using MODIS/ASTER (MASTER) Airborne Simulator Data. *Remote Sensing,* 3**,** 2403-2419.
HARROLD, A. 1979. Heathland regeneration after fire at Noosa. *Queensland Naturalist,* 22**,** 88-96.
HENNING, J. G. & RADTKE, P. J. 2006. Ground-based laser imaging for assessing three dimensional forest canopy structure. *Photogrammetric Engineering and Remote Sensing,* 72**,** 1349-1358.
HENRY, M. & HOPE, A. 1998. Monitoring post-burn recovery of chaparral vegetation in southern California using multi-temporal satellite data. *International Journal of Remote Sensing,* 19**,** 3097-3107.
HEO, J., PARK, J. S., SONG, Y. S., LEE, S. K. & SOHN, H. G. 2008. An integrated methodology for estimation of forest fire-loss using geospatial information. *Environmental monitoring and assessment,* 144**,** 285-299.
HILL, R. A. & BROUGHTON, R. K. 2009. Mapping the understorey of deciduous woodland from leaf-on and leaf-off airborne LiDAR data: A case study in lowland Britain. *ISPRS Journal of Photogrammetry and Remote Sensing,* 64**,** 223-233.

HINES, F., TOLHURST, K., WILSON, A. & MCCARTHY, G. 2010. Overall Fuel Hazard Assessment Guide. *Fire and Adaptive Management.* Melbourne: Department of Sustainability and Environment.
HOPKINSON, C., CHASMER, L., YOUNG-POW, C. & TREITZ, P. 2004. Assessing forest metrics with a ground-based scanning lidar. *Canadian Journal of Forest Research,* 34**,** 573-583.
HUANG, H., GONG, P., CHENG, X., CLINTON, N., CAO, C., NI, W., LI, Z. & WANG, L. Forest structural parameter extraction using terrestrial LiDAR. Proceedings of SilviLaser, 14-16 October 2009 Texas, USA.
HUANG, P. & PRETZSCH, H. 2010. Using terrestrial laser scanner for estimating leaf areas of individual trees in a conifer forest. *Trees,* 24**,** 609-619.
HUDAK, A. T. & BROCKETT, B. H. 2004. Mapping fire scars in a southern African savannah using Landsat imagery. *International Journal of Remote Sensing,* 25**,** 3231-3243.
HUDAK, A. T., EVANS, J. S. & STUART SMITH, A. M. 2009. LiDAR utility for natural resource managers. *Remote Sensing,* 1**,** 934-951.
HUETE, A. R. 1988. A soil-adjusted vegetation index (SAVI). *Remote Sensing of Environment,* 25**,** 295-309.
HUNT, E. R., JR. & ROCK, B. N. 1989. Detection of changes in leaf water content using near-and middle-infrared reflectances. *Remote Sensing of Environment,* 30**,** 43-54.
ILLERA, P., FERNANDEZ, A. & DELGADO, J. A. 1996. Temporal evolution of the NDVI as an indicator of forest fire danger. *International Journal of Remote Sensing,* 17**,** 1093-1105.
ISENBURG, M. & SCHEWCHUCK, J. 2007. LAStools: converting, viewing, and compressing LIDAR data in LAS format. *avaliable at: http://www.cs.unc.edu/~ isenburg/lastools*.
IVERSON, L. R., GRAHAM, R. L. & COOK, E. A. 1989. Applications of satellite remote sensing to forested ecosystems. *Landscape ecology,* 3**,** 131-143.
JACKSON, R. D. & HUETE, A. R. 1991. Interpreting vegetation indices. *Preventive Veterinary Medicine,* 11**,** 185-200.
JAKUBAUSKAS, M. E., LULLA, K. P. & MAUSEL, P. W. 1990. Assessment of vegetation change in a fire-altered forest landscape. *Photogrammetric Engineering and Remote Sensing,* 56**,** 371-377.
JENSEN, J. R. 2009. *Remote sensing of the environment,* Upper Saddle River, NJ, Prentice Hall.
JUPP, D. L. B., CULVENOR, D. S., LOVELL, J. L., NEWNHAM, G. J., STRAHLER, A. H. & WOODCOCK, C. E. 2009. Estimating forest LAI profiles and structural parameters using a ground-based laser called 'Echidna®'. *Tree Physiology,* 29**,** 171-181.
JURSKIS, V. 2005. Decline of eucalypt forests as a consequence of unnatural fire regimes. *Australian Forestry,* 68**,** 257-262.
JURSKIS, V., BRIDGES, B. & DE MAR, P. Fire management in Australia: the lessons of 200 years. Joint Australia and New Zealand Institute of Forestry Conference Proceedings, 27 April-1May 2003. Citeseer, 353-368.
JUSTICE, C. O., GIGLIO, L., KORONTZI, S., OWENS, J., MORISETTE, J. T., ROY, D., DESCLOITRES, J., ALLEAUME, S., PETITCOLIN, F. & KAUFMAN, Y. 2002. The MODIS fire products. *Remote Sensing of Environment,* 83**,** 244-262.
KASISCHKE, E., HOY, E., FRENCH, N. & TURETSKY, M. Post-fire evaluation of the effects of fire on the environment using remotely-sensed data. 6th International Workshop of the EARseL Special Interest Group on Forest Fires, 27-29 September 2007 Greece. 38-56.
KASISCHKE, E. S., FRENCH, N. H. F., HARRELL, P., CHRISTENSEN JR, N. L., USTIN, S. L. & BARRY, D. 1993. Monitoring of wildfires in boreal forests using large area AVHRR NDVI composite image data. *Remote Sensing of Environment,* 45**,** 61-71.
KATAGIS, T., GITAS, I. & TOUKIOGLOU, P. Trend analysis of time series image data for burned area mapping and post-fire monitoring. *In:* AYANZ, J., GITAS, I., CAMIA, A. & OLIVEIRA, S., eds. Proceedings of the 8th International EARSeL FF-SIG Workshop. Advances in Remote Sensing and GIS Applications in Forest Fire Management: from local to global assessments, 20-21 October 2011 Stresa, Italy. 102-107.

KEANE, E. 2007. The potential of terrestrial laser scanning technology in pre-harvest timeber measurement operations. *Coford Connects.* Dublin, Ireland: TreeMetrics Ltd., The Rubicon Centre.
KEITH, D. A. 2004. *Ocean shores to desert dunes: the native vegetation of New South Wales and the ACT*, Department of Environment and Conservation (NSW).
KELLMAN, M. 1986. Fire sensitivity of Casuarina torulosa in north Queensland, Australia. *Biotropica,* 18**,** 107-110.
KENNY, B., SUTHERLAND, E., TASKER, E. & BRADSTOCK, R. 2003. Guidelines for ecologically sustainable fire management. Hurstville: NSW National Parks and Wildlife Service.
KEY, C. H. Remote sensing sensitivity to fire severity and fire recovery. *In:* DE LA RIVA, J., PEREZ-CABELLO, F. & CHUVIECO, E., ed. Proceedings of the 5th International Workshop on Remote Sensing and GIS Applications to Forest Fire Management: Fire Effects Assessment, 16-18 June 2005 Zaragoza, Spain. Universidad de Zaragoza 29-39.
KEY, C. H., BENSON, N., OHLEN, D., HOWARD, S. M. & ZHU, Z. The normalized burn ratio and relationships to burn severity: Ecology, remote sensing and implementation. *In:* GREER, J. D., ed. Proceedings of the Ninth Forest Service Remote Sensing Applications Conference, 8-12 April 2002 San Diego, USA. American Society for Photogrammetry and Remote Sensing, Bethesda, MD.
KEY, C. H. & BENSON, N. C. 2005. Landscape assessment: ground measure of severity, the Composite Burn Index; and remote sensing of severity, the Normalized Burn Ratio. *In:* LUTES, D. C., KEANE, R. E., CARATTI, J. F., KEY, C. H., BENSON, N. C. & GANGI, L. J. (eds.) *FIREMON: Fire effects monitoring and inventory system.* Ogden, UT: USDA Forest Service, Rocky Mountain Research Station.
KEY, C. H. & BENSON, N. C. 2006. Landscape assessment (LA): Sampling and analysis methods. *USDA Forest Service Gen. Tech. Rep. RMRS-GTR-164-CD***,** 1-55.
KEYWORTH, S., JARMAN, M. & MEDCALF, K. 2009. Assessing the extent and severity of erosion on the upland organic soils of Scotland using earth observation: A GIFTSS implementation test. Scotland: Environment Systems and British National Space Centre.
KIM, M. S., DAUGHTRY, C. S. T., CHAPPELLE, E. W., MCMURTREY, J. E. & WALTHALL, C. L. The use of high spectral resolution bands for estimating absorbed photosynthetically active radiation (A par). Proceedings of the 6th Symposium on Physical Measurements and Signatures in Remote Sensing, 17-21 January, 1994 1994 Val D'Isere, France. 299-306.
KING, K. J., CARY, G. J., BRADSTOCK, R. A., CHAPMAN, J., PYRKE, A. & MARSDEN-SMEDLEY, J. B. 2006. Simulation of prescribed burning strategies in south-west Tasmania, Australia: effects on unplanned fires, fire regimes, and ecological management values. *International Journal of Wildland Fire,* 15**,** 527-540.
KNAPP, E. E., SCHWILK, D. W., KANE, J. M. & KEELEY, J. E. 2006. Role of burning season on initial understory vegetation response to prescribed fire in a mixed conifer forest. *Canadian Journal of Forest Research,* 37**,** 11-22.
KNIPLING, E. B. 1970. Physical and physiological basis for the reflectance of visible and near-infrared radiation from vegetation. *Remote Sensing of Environment,* 1**,** 155-159.
KNOX, K. J. E. & CLARKE, P. J. Response of resprouting shrubs to repeated fires in the dry sclerophyll forest of Gibraltar Range National Park. Linnean Society of NSW, 2006. 49-56.
KOKALY, R. F., ROCKWELL, B. W., HAIRE, S. L. & KING, T. V. V. 2007. Characterization of post-fire surface cover, soils, and burn severity at the Cerro Grande Fire, New Mexico, using hyperspectral and multispectral remote sensing. *Remote Sensing of Environment,* 106**,** 305-325.
KOUTSIAS, N., PLENIOU, M., NIOTI, F. & MALLINIS, G. Spectral signatures of burned surfaces: Evidence from hyperspectral remote sensing data. Proceedings of Hyperspectral 2010 Workshop, 17-19 March 2010 Frascati, Italy.

KUMAR, L. & SKIDMORE, A. K. Use of derivative spectroscopy to identify regions of differences between some Australian eucalypt species. 9th Australasian Remote Sensing and Photogrammetry Conference, 20-24 July 1998 Sydney, Australia. 3103–3118.
KUMAR, L. & SKIDMORE, A. K. 2006. NIR and SWIR Reflectance Characteristics of Dry Plant Materials of some Eucalyptus Species. *International Journal of Geoinformatics,* 2**,** 47-59.
LACEY, C. J., WALKER, J. & NOBLE, I. R. 1982. Fire in Australian tropical savannas. *In:* HUNTLEY, B. J. & WALKER, B. H. (eds.) *Ecology of Tropical Savannas.* Berlin: Springer-Verlag.
LACEY, G. 2009. Ecosystems and Fire Frequency. Victorian National Parks Association.
LANG, J. 1999. Fire in the Australian Landscape. Victoria: Department of Natural Resources and Environment and Victoria Country Fire Authority. ISBN 0731142969.
LEFSKY, M. A., COHEN, W. B., ACKER, S. A., SPIES, T. A., PARKER, G. G. & HARDING, D. J. Lidar remote sensing of forest canopy structure and related biophysical parameters at HJ Andrews Experimental Forest, Oregon, USA. *In:* GREEN, J. D., ed. American Society for Photogrammetry and Remote Sensing, 1997 Bethesda, Maryland. IEEE, 79-91.
LEFSKY, M. A., COHEN, W. B., PARKER, G. G. & HARDING, D. J. 2002. Lidar remote sensing for ecosystem studies. *BioScience,* 52**,** 19-30.
LEIGH, J. H. & NOBLE, J. C. 1981. The role of fire in the management of rangelands in Australia. *In:* GROVE, R. H. & NOBLE, I. R. (eds.) *Fire and the Australian Biota.* Canberra: Australian Academy of Science.
LENTILE, L., HOLDEN, Z., SMITH, A., FALKOWSKI, M., HUDAK, A., MORGAN, P., LEWIS, S., GESSLER, P. & BENSON, N. 2006a. Remote sensing techniques to assess active fire characteristics and post-fire effects. *International Journal of Wildland Fire,* 15**,** 319-345.
LENTILE, L. B., HOLDEN, Z. A., SMITH, A. M. S., FALKOWSKI, M. J., HUDAK, A. T., MORGAN, P., LEWIS, S. A., GESSLER, P. E. & BENSON, N. C. 2006b. Remote sensing techniques to assess active fire characteristics and post-fire effects. *International Journal of Wildland Fire,* 15**,** 319-345.
LENTILE, L. B., MORGAN, P., HUDAK, A. T., BOBBITT, M. J., LEWIS, S. A., SMITH, A. & ROBICHAUD, P. R. 2007. Post-fire burn severity and vegetation response following eight large wildfires across the Western United States. *Fire Ecology,* 2007.
LENTILE, L. B., SMITH, A. M. S., HUDAK, A. T., MORGAN, P., BOBBITT, M. J., LEWIS, S. A. & ROBICHAUD, P. R. 2009. Remote sensing for prediction of 1-year post-fire ecosystem condition. *International Journal of Wildland Fire,* 18**,** 594-608.
LEWIS, H. T. 1989. Ecological and technological knowledge of fire: Aborigines versus park rangers in Northern Australia. *American Anthropologist,* 91**,** 940-961.
LI, Z., FRASER, R., JIN, J., ABUELGASIM, A. A., CSISZAR, I., GONG, P., PU, R. & HAO, W. 2003. Evaluation of algorithms for fire detection and mapping across North America from satellite. *Journal of geophysical research,* 108**,** 4076-4089.
LIANG, X., LITKEY, P., HYYPPA, J., KAARTINEN, H., VASTARANTA, M. & HOLOPAINEN, M. 2012. Automatic stem mapping using single-scan terrestrial laser scanning. *IEEE Transactions onGeoscience and Remote Sensing,* 50**,** 661-670.
LIM, K., TREITZ, P., WULDER, M., ST-ONGE, B. & FLOOD, M. 2003. LiDAR remote sensing of forest structure. *Progress in physical Geography,* 27**,** 88-106.
LITKEY, P., LIANG, X., KAARTINEN, H., HYYPPÄ, J., KUKKO, A. & HOLOPAINEN, M. Single-scan TLS methods for forest parameter retrieval. Proceedings of the 8th SilviLaser, 17-19 September 2008 Edinburgh, Scotland. 295-304.
LOBODA, T. V., FRENCH, N. H. F., HIGHT-HARF, C., JENKINS, L. & MILLER, M. E. 2013. Mapping fire extent and burn severity in Alaskan tussock tundra: An analysis of the spectral response of tundra vegetation to wildland fire. *Remote Sensing of Environment,* 134**,** 194-209.
LOPEZ GARCIA, M. J. & CASELLES, V. 1991. Mapping burns and natural reforestation using Thematic Mapper data. *Geocarto International,* 6**,** 31-37.

LOUDERMILK, E. L., HIERS, J. K., O'BRIEN, J. J., MITCHELL, R. J., SINGHANIA, A., FERNANDEZ, J. C., CROPPER, W. P. & SLATTON, K. C. 2009. Ground-based LIDAR: a novel approach to quantify fine-scale fuelbed characteristics. *International Journal of Wildland Fire,* 18**,** 676-685.

LOUDERMILK, E. L., SINGHANIA, A., FERNANDEZ, J. C., HIERS, J. K., O'BRIEN, J. J., CROPPER JR, W. P., SLATTON, K. C. & MITCHELL, R. J. Application of ground-based LIDAR for fine-scale forest fuel modeling. Proceedings of USDA Forest Services, 2007. USDA Forest Service Processing RMRS-P-46CD.

LOZANO, F. J., SUÁREZ-SEOANE, S. & DE LUIS, E. 2007. Assessment of several spectral indices derived from multi-temporal Landsat data for fire occurrence probability modelling. *Remote Sensing of Environment,* 107**,** 533-544.

LU, B., HE, Y. & TONG, A. 2016. Evaluation of spectral indices for estimating burn severity in semiarid grasslands. *International Journal of Wildland Fire,* 25**,** 147-157.

LUCAS, R., MITCHELL, A. & BUNTING, P. 2008. Hyperspectral data for assessing carbon dynamics and biodiversity of forests. *In:* KALACSKA, M. & SANCHEZ-AZOFEIFA, A. (eds.) *Hyperspectral Remote Sensing of Tropical and Subtropical Forests.* Boca Raton, FL: CRC Press.

LUKE, R. H. & MCARTHUR, A. G. 1978. *Bushfires in Australia.,* Canberra, CSIRO Division of Forest Research, Australian Government Publishing Service.

LUTES, D. C., KEANE, R. E., CARATTI, J. F., KEY, C. H., BENSON, N. C., SUTHERLAND, S. & GANGI, L. J. 2006. FIREMON: Fire effects monitoring and inventory system. Gen. Tech. Rep. RMRS-GTR-164-CD. Fort Collins, CO: U.S. Department of Agriculture, Forest Service, Rocky Mountain Research Station.

MAAS, H. G., BIENERT, A., SCHELLER, S. & KEANE, E. 2008. Automatic forest inventory parameter determination from terrestrial laser scanner data. *International Journal of Remote Sensing,* 29**,** 1579-1593.

MAGNUSSEN, S. & WULDER, M. A. 2012. Post-fire canopy height recovery in Canada's boreal forests using Airborne Laser Scanner (ALS). *Remote Sensing,* 4**,** 1600-1616.

MALAK, D. A. & PAUSAS, J. G. 2006. Fire regime and post-fire Normalized Difference Vegetation Index changes in the eastern Iberian peninsula (Mediterranean basin). *International Journal of Wildland Fire,* 15**,** 407-413.

MALONE, S. L., KOBZIAR, L. N., STAUDHAMMER, C. L. & ABD-ELRAHMAN, A. 2011. Modeling Relationships among 217 Fires Using Remote Sensing of Burn Severity in Southern Pine Forests. *Remote Sensing,* 3**,** 2005-2028.

MARTIN, M. & CHUVIECO, E. 1995a. Mapping and evaluation of burned land from multitemporal analysis of AVHRR NDVI images. *EARSel Advances in Remote Sensing,* 4**,** 7-13.

MARTIN, M. P. 1998. *Cartografia e inventario de incendios forestales en la Peninsula Iberica a partir de imagenes NOAA-AVHRR.* Doctoral Thesis, Universidad de Alcala.

MARTIN, M. P. & CHUVIECO, E. 1995b. Mapping and evaluation of burned land from multitemporal analysis of AVHRR NDVI images. *EARSeL Advances in remote sensing,* 4**,** 7-13.

MARTÍN, M. P., DÍAZ-DELGADO, R., CHUVIECO, E. & VENTURA, G. Burned land mapping using NOAA-AVHRR and TERRA-MODIS. *In:* VIEGAS, D. X., ed. IV International Conference on forest fire research and 9th Wildland Fire Safety Summit, 25-28 April 2002 Luso, Coimbra, Portugal. Millpress.

MCCOY, R. M. 2005. *Field methods in remote sensing,* New York, The Guilford Press.

MCGWIRE, K., MINOR, T. & FENSTERMAKER, L. 2000. Hyperspectral mixture modeling for quantifying sparse vegetation cover in arid environments. *Remote Sensing of Environment,* 72**,** 360-374.

MCLOUGHLIN, L. C. 1998. Season of burning in the Sydney region: the historical records compared with recent prescribed burning. *Australian Journal of Ecology,* 23**,** 393-404.

MENG, Q. & MEENTEMEYER, R. K. 2011. Modeling of multi-strata forest fire severity using Landsat TM Data. *International Journal of Applied Earth Observation and Geoinformation,* 13**,** 120-126.
MERZLYAK, M. N., GITELSON, A. A., CHIVKUNOVA, O. B. & RAKITIN, V. Y. U. 1999. Non-destructive optical detection of pigment changes during leaf senescence and fruit ripening. *Physiologia plantarum,* 106**,** 135-141.
MICHALEK, J. L., FRENCH, N. H. F., KASISCHKE, E. S., JOHNSON, R. D. & COLWELL, J. E. 2000. Using Landsat TM data to estimate carbon release from burned biomass in an Alaskan spruce forest complex. *International Journal of Remote Sensing,* 21**,** 323-338.
MILLER, J. & THODE, A. 2007. Quantifying burn severity in a heterogeneous landscape with a relative version of the delta Normalized Burn Ratio (dNBR). *Remote Sensing of Environment,* 109**,** 66-80.
MILLER, J. & YOOL, S. 2002. Mapping forest post-fire canopy consumption in several overstory types using multi-temporal Landsat TM and ETM data. *Remote Sensing of Environment,* 82**,** 481-496.
MILNE, A. K. 1986. The use of remote sensing in mapping and monitoring vegetational change associated with bushfire events in eastern Australia. *Geocarto International,* 1**,** 25-32.
MITRI, G. H. & GITAS, I. Z. 2010. Mapping postfire vegetation recovery using EO-1 hyperion imagery. *IEEE Transactions on Geoscience and Remote Sensing,* 48**,** 1613-1618.
MITRI, G. H. & GITAS, I. Z. 2013. Mapping post-fire forest regeneration and vegetation recovery using a combination of very high spatial resolution and hyperspectral satellite imagery. *International Journal of Applied Earth Observation and Geoinformation,* 20**,** 60-66.
MORRIS, R. H., BRADSTOCK, R. A., BUCKMAN, S., CONNELLY, P., OSTENDORF, B. & DRAGOVICH, D. The dirt on assessing post-fire erosion in the Mount Lofty Ranges: comparing methods. *In:* THORNTON, R. P., ed. Proceedings of Bushfire CRC & AFAC 2011 Conference Science Day, 1st September, 2011 2011 Sydney, Australia. Bushfire Cooperative Research Centre.
MORRISON, D. A., BUCKNEY, R. T., BEWICK, B. J. & CARY, G. J. 1996. Conservation conflicts over burning bush in south-eastern Australia. *Biological Conservation,* 76**,** 167-175.
MORRISON, D. A. & RENWICK, J. A. 2000. Effects of variation in fire intensity on regeneration of co-occurring species of small trees in the Sydney region. *Australian Journal of Botany,* 48**,** 71-79.
MOSKAL, L. M. & ZHENG, G. 2011. Retrieving Forest Inventory Variables with Terrestrial Laser Scanning (TLS) in Urban Heterogeneous Forest. *Remote Sensing,* 4**,** 1-20.
MURPHY, K. A., REYNOLDS, J. H. & KOLTUN, J. M. 2008. Evaluating the ability of the differenced Normalized Burn Ratio (dNBR) to predict ecologically significant burn severity in Alaskan boreal forests. *International Journal of Wildland Fire,* 17**,** 490-499.
MURTHA, P. A. 1978. Symposium on remote sensing for vegetation damage assessment. *Photogrammetric Engineering and Remote Sensing,* 49**,** 19-52.
NAESSET, E. 1997. Determination of mean tree height of forest stands using airborne laser scanner data. *ISPRS Journal of Photogrammetry and Remote Sensing,* 52**,** 49-56.
NAGLER, P. L., DAUGHTRY, C. S. T. & GOWARD, S. N. 2000. Plant litter and soil reflectance. *Remote Sensing of Environment,* 71**,** 207-215.
NAGLER, P. L., INOUE, Y., GLENN, E. P., RUSS, A. L. & DAUGHTRY, C. S. T. 2003. Cellulose absorption index (CAI) to quantify mixed soil-plant litter scenes. *Remote Sensing of Environment,* 87**,** 310-325.
NAMBIAR, E. K. S. 1985. Critical processes in forest nutrition and their importance for management. Research for Forest Management. *In:* LANDSBERG, J. J. & PARSON, W. (eds.) *Research for Forest Management.* CSIRO, Melbourne.
NELSON, R. F. 1983. Detecting forest canopy change due to insect activity using Landsat MSS. *Photogrammetric Engineering and Remote Sensing,* 49**,** 1303-1314.

NEYLAND, M. & ASKEY-DORAN, M. Effects of Repeated Fires on Dry Sclerophyll (*E. sieberi*) Forests in Eastern Tasmania. *In:* MESIBOV, R., ed. In proceedings of Fire and Biodiversity: The effects and effectiveness of fire management, 8-9 October 1996 Footscray, Melbourne. Department of Environment, Sport and Territories.

NICHOLSON, P. H. 1981. Fire and the Australian Aborigine- an enigma. *In:* GILL, A. M., GROVES, R. H. & NOBLE, I. R. (eds.) *Fire and the Australian Biota.* Canberra, Australia: Australian Academy of Science.

NORTON, J., GLENN, N., GERMINO, M., WEBER, K. & SEEFELDT, S. 2009. Relative suitability of indices derived from Landsat ETM+ and SPOT 5 for detecting fire severity in sagebrush steppe. *International Journal of Applied Earth Observation and Geoinformation,* 11**,** 360-367.

NUMATA, I., COCHRANE, M. A. & GALVÃO, L. S. 2011. Analyzing the impacts of frequency and severity of forest fire on the recovery of disturbed forest using Landsat time series and EO-1 Hyperion in the Southern Brazilian Amazon. *Earth Interactions,* 15**,** 1-17.

OLSOY, P. J., GLENN, N. F. & CLARK, P. E. 2014. Estimating Sagebrush Biomass Using Terrestrial Laser Scanning. *Rangeland Ecology and Management,* 67**,** 224-228.

OOI, M. K., WHELAN, R. J. & AULD, T. D. 2006. Persistence of obligate-seeding species at the population scale: effects of fire intensity, fire patchiness and long fire-free intervals. *International Journal of Wildland Fire,* 15**,** 261-269.

PARRA, A. & CHUVIECO, E. Assessing burn severity using Hyperion data. *In:* DE LA RIVA, J., PEREZ-CABELLO, F. & CHUVIECO, E., ed. Proceedings of the 5th International Workshop on Remote Sensing and GIS Applications to Forest Fire Management: Fire Effects Assessment, 16-18 June 2005 Zaragoza, Spain. Universidad de Zaragoza 239-243.

PATTERSON, M. & YOOL, S. 1998. Mapping Fire-Induced Vegetation Mortality Using Landsat Thematic Mapper Data:: A Comparison of Linear Transformation Techniques. *Remote Sensing of Environment,* 65**,** 132-142.

PEKIN, B. K., BOER, M. M., MACFARLANE, C. & GRIERSON, P. F. 2009. Impacts of increased fire frequency and aridity on eucalypt forest structure, biomass and composition in southwest Australia. *Forest Ecology and Management,* 258**,** 2136-2142.

PENMAN, T. D., BINNS, D. L., ALLEN, R., SHIELS, R. & PLUMMER, S. 2008a. Germination responses of a dry sclerophyll forest soil-stored seedbank to fire related cues. *Cunninghamia,* 10**,** 547-555.

PENMAN, T. D., BINNS, D. L., BRASSIL, T. E., SHIELS, R. J. & ALLEN, R. M. 2009. Long-term changes in understorey vegetation in the absence of wildfire in south-east dry sclerophyll forests. *Australian Journal of Botany,* 57**,** 533-540.

PENMAN, T. D., BINNS, D. L., SHIELS, R. O. Y. J., ALLEN, R. M. & KAVANAGH, R. P. 2008b. Changes in understorey plant species richness following logging and prescribed burning in shrubby dry sclerophyll forests of south eastern Australia. *Austral Ecology,* 33**,** 197-210.

PENMAN, T. D., KAVANAGH, R. P., BINNS, D. L. & MELICK, D. R. 2007. Patchiness of prescribed burns in dry sclerophyll eucalypt forests in South-eastern Australia. *Forest Ecology and Management,* 252**,** 24-32.

PEÑUELAS, J., BARET, F. & FILELLA, I. 1995. Semi-empirical indices to assess carotenoids/chlorophyll a ratio from leaf spectral reflectance. *Photosynthetica,* 31**,** 221-230.

PEÑUELAS, J. & FILELLA, I. 1998. Visible and near-infrared reflectance techniques for diagnosing plant physiological status. *Trends in plant science,* 3**,** 151-156.

PEṆUELAS, J., GAMON, J. A., FREDEEN, A. L., MERINO, J. & FIELD, C. B. 1994. Reflectance indices associated with physiological changes in nitrogen-and water-limited sunflower leaves. *Remote Sensing of Environment,* 48**,** 135-146.

PEÑUELAS, J. & INOUE, Y. 1999. Reflectance indices indicative of changes in water and pigment contents of peanut and wheat leaves. *Photosynthetica,* 36**,** 355-360.

PEÑUELAS, J., PINOL, J., OGAYA, R. & FILELLA, I. 1997. Estimation of plant water concentration by the reflectance water index WI (R900/R970). *International Journal of Remote Sensing,* 18**,** 2869-2875.
PEREIRA, J. M. C. 1999. A comparative evaluation of NOAA/AVHRR vegetation indexes for burned surface detection and mapping. *IEEE Transactions on Geoscience and Remote Sensing,* 37**,** 217-226.
PEREIRA, J. M. C., CHUVIECO, E., BEAUDOIN, A. & DESBOIS, N. 1997a. Remote sensing of burned areas: a review. *In:* CHUVIECO, E. (ed.) *A review of remote sensing methods for the study of large wildland fires.*
PEREIRA, J. M. C., CHUVIECO, E., BEAUDOIN, A. & DESBOIS, N. 1997b. A review of remote sensing methods for the study of large wildland fires. *In:* CHUVIECO, E. (ed.) *Megafires project ENV-CT96-0256. Spain.* Alcala de Henares, Spain: Universidad de Alcala.
PEREIRA, J. M. C., SÁ, A., SOUSA, A., SANTOS, T. & CARREIRAS, J. 1999. Spectral characterisation and discrimination of burnt areas. *In:* CHUVIECO, E. (ed.) *Remote sensing of large wildfires.* Berlin: Springer-Verlag.
PERRY JR, C. R. & LAUTENSCHLAGER, L. F. 1984. Functional equivalence of spectral vegetation indices. *Remote Sensing of Environment,* 14**,** 169-182.
PINTY, B. & VERSTRAETE, M. 1992. GEMI: a non-linear index to monitor global vegetation from satellites. *Plant Ecology,* 101**,** 15-20.
POPESCU, S. C. 2011. LiDAR Remote Sensing. *In:* WENG, Q. (ed.) *Advances in Environmental Remote Sensing: Sensors, Algorithms and Applications.* CRC Press.
POSAMENTIER, H. G., CLARK, S. S., HAIN, D. L. & RECHER, H. F. 1981. Succession following wildfire in coastal heathland (Nadgee Nature Reserve NSW). *Australian Journal of Ecology,* 6**,** 165-175.
POTTER, C., LI, S., HUANG, S. & CRABTREE, R. L. 2012. Analysis of sapling density regeneration in Yellowstone National Park with hyperspectral remote sensing data. *Remote Sensing of Environment,* 121**,** 61-68.
PRICE, O., RUSSELL-SMITH, J. & EDWARDS, A. 2003. Fine-scale patchiness of different fire intensities in sandstone heath vegetation in northern Australia. *International Journal of Wildland Fire,* 12**,** 227-236.
PU, R. 2012. Estimating and mapping forest leaf area index using satellite imagery. *In:* YANG, X. & LI, J. (eds.) *Advances in Mapping from Remote Sensor Imagery: Techniques and Applications.* CRC Press.
PU, R. & GONG, P. 2011. Hyperspectral Remote Sensing of Vegetation Bioparameters. *In:* WENG, Q. (ed.) *Advances in Environmental Remote Sensing: Sensors, Algorithms, and Applications.* CRC Press.
RAHMAN, A. F. & GAMON, J. A. 2004. Detecting biophysical properties of a semi-arid grassland and distinguishing burned from unburned areas with hyperspectral reflectance. *Journal of Arid Environments,* 58**,** 597-610.
RAISON, R. J. 1980. A review of the role of fire in nutrient cycling in Australian native forests, and of methodology for studying the fire-nutrient interaction. *Australian Journal of Ecology,* 5**,** 15-21.
REMMEL, T. & PERERA, A. 2001. Fire mapping in a northern boreal forest: assessing AVHRR/NDVI methods of change detection. *Forest Ecology and Management,* 152**,** 119-129.
RIANO, D., MEIER, E., ALLGOWER, B., CHUVIECO, E. & USTIN, S. L. 2003. Modeling airborne laser scanning data for the spatial generation of critical forest parameters in fire behavior modeling. *Remote Sensing of Environment,* 86**,** 177-186.
ROBERTO, C., LORENZO, B., MICHELE, M., MICOL, R. & CINZIA, P. 2011. Optical Remote Sensing of Vegetation Water Content. *In:* THENKABAIL, A., LYON, P. S. & HUETE, J. G. (eds.) *Hyperspectral Remote Sensing of Vegetation.* CRC Press.

ROBERTS, D. A., SMITH, M. O. & ADAMS, J. B. 1993. Green vegetation, nonphotosynthetic vegetation, and soils in AVIRIS data. *Remote Sensing of Environment,* 44**,** 255-269.
ROBICHAUD, P. R., LEWIS, S. A., LAES, D. Y. M., HUDAK, A. T., KOKALY, R. F. & ZAMUDIO, J. A. 2007. Postfire soil burn severity mapping with hyperspectral image unmixing. *Remote Sensing of Environment,* 108**,** 467-480.
ROBINSON, J. M. 1991. Fire from space: Global fire evaluation using infrared remote sensing. *International Journal of Remote Sensing,* 12**,** 3-24.
RÖDER, A., HILL, J., DUGUY, B., ALLOZA, J. & VALLEJO, R. 2008. Using long time series of Landsat data to monitor fire events and post-fire dynamics and identify driving factors. A case study in the Ayora region (eastern Spain). *Remote Sensing of Environment,* 112**,** 259-273.
ROFF, A., GOODWIN, N. & MERTON, R. 2005. Assessing fuel loads using remote sensing. Sydney, Australia: The University of New South Wales.
ROGAN, J. & FRANKLIN, J. 2001. Mapping wildfire burn severity in southern California forests and shrublands using Enhanced Thematic Mapper imagery. *Geocarto International,* 16**,** 91-106.
ROGAN, J. & YOOL, S. R. 2001. Mapping fire-induced vegetation depletion in the Peloncillo Mountains, Arizona and New Mexico. *International Journal of Remote Sensing,* 22**,** 3101-3121.
ROLDÁN-ZAMARRÓN, A., MERINO-DE-MIGUEL, S., GONZÁLEZ-ALONSO, F., GARCÍA-GIGORRO, S. & CUEVAS, J. M. 2006. Minas de Riotinto (south Spain) forest fire: Burned area assessment and fire severity mapping using Landsat 5-TM, Envisat-MERIS, and Terra-MODIS postfire images. *Journal of geophysical research,* 111**,** G04S11, doi: 10.1029/2005JG000136.
RONDEAUX, G., STEVEN, M. & BARET, F. 1996. Optimization of soil-adjusted vegetation indices. *Remote Sensing of Environment,* 55**,** 95-107.
ROUSE, J. W., HAAS, R. H., SCHELL, J. A. & DEERING, D. W. Monitoring vegetation systems in the Great Plains with ERTS. Third ERTS Symposium, 1973 Washington, NASA. SP-351 309-317.
ROWELL, E. & SEIELSTAD, C. Characterising grass, litter, and shrub fuels in longleaf pine forest pre- and post-fire using terrestrial LiDAR. SilviLaser, 16-19 September 2012 Vancouver, Canada. 1-8.
ROY, D., BOSCHETTI, L. & TRIGG, S. 2006a. Remote sensing of fire severity: assessing the performance of the normalized burn ratio. *IEEE Geoscience and Remote Sensing Letters,* 3**,** 112-116.
ROY, D. P., BOSCHETTI, L. & TRIGG, S. N. 2006b. Remote sensing of fire severity: assessing the performance of the normalized burn ratio. *IEEE Geoscience and Remote Sensing Letters,* 3**,** 112-116.
ROY, D. P., JIN, Y., LEWIS, P. E. & JUSTICE, C. O. 2005. Prototyping a global algorithm for systematic fire-affected area mapping using MODIS time series data. *Remote Sensing of Environment,* 97**,** 137-162.
ROY, D. P., JUSTICE, C. O. & BOSCHETTI, L. Global Mapping of Fire-affected Areas using Multitemporal MODIS Data: The MCD45 Product. Geoscience and Remote Sensing Symposium and IGARSS, 31 July-4 Aug 2006c Denver, CO, USA. 4165-4168.
ROY, D. P., LEWIS, P. E. & JUSTICE, C. O. 2002. Burned area mapping using multi-temporal moderate spatial resolution data--a bi-directional reflectance model-based expectation approach. *Remote Sensing of Environment,* 83**,** 263-286.
SERRANO, L., USTIN, S. L., ROBERTS, D. A., GAMON, J. A. & PENUELAS, J. 2000. Deriving water content of chaparral vegetation from AVIRIS data. *Remote Sensing of Environment,* 74**,** 570-581.
SEVER, L., LEACH, J. & BREN, L. 2012. Remote sensing of post-fire vegetation recovery; a study using Landsat 5 TM imagery and NDVI in North-East Victoria. *Journal of Spatial Science,* 57**,** 175-191.

SHAFRI, H. Z. M., SALLEH, M. A. M. & GHIYAMAT, A. 2006. Hyperspectral remote sensing of vegetation using red edge position techniques. *American Journal of Applied Sciences,* 3**,** 1864-1871.
SILVA, J., SÁ, A. & PEREIRA, J. 2005. Comparison of burned area estimates derived from SPOT-VEGETATION and Landsat ETM+ data in Africa: Influence of spatial pattern and vegetation type. *Remote Sensing of Environment,* 96**,** 188-201.
SIMONSE, M., ASCHOFF, T., SPIECKER, H. & THIES, M. Automatic determination of forest inventory parameters using terrestrial lasers canning. Proceedings of ScandLaser Scientific Workshop on Airborne Laser Scanning of Forests, 2003 Umea, Sweden. 252-258.
SIMS, D. A. & GAMON, J. A. 2003. Estimation of vegetation water content and photosynthetic tissue area from spectral reflectance: a comparison of indices based on liquid water and chlorophyll absorption features. *Remote Sensing of Environment,* 84**,** 526-537.
SINCLAIR, T. R. 1968. *Pathway of solar radiation through leaves.* M.S. Thesis, Purdue University.
SKULL, S. & ADAMS, F. 1996. Fire Management and the Vegetation Communities of the Townsville and Thuringowa Shires: Some Ecological Considerations. Townsville, Queensland: James Cook University.
SMITH, A., WOOSTER, M. J., DRAKE, N. A., DIPOTSO, F. M., FALKOWSKI, M. J. & HUDAK, A. T. 2005. Testing the potential of multi-spectral remote sensing for retrospectively estimating fire severity in African Savannahs. *Remote Sensing of Environment,* 97**,** 92-115.
SMITH, A. M. S., DRAKE, N. A., WOOSTER, M. J., HUDAK, A. T., HOLDEN, Z. A. & GIBBONS, C. J. 2007. Production of Landsat ETM+ reference imagery of burned areas within Southern African savannahs: comparison of methods and application to MODIS. *International Journal of Remote Sensing,* 28**,** 2753-2775.
SMITH, K. L., STEVEN, M. D. & COLLS, J. J. 2004a. Use of hyperspectral derivative ratios in the red-edge region to identify plant stress responses to gas leaks. *Remote Sensing of Environment,* 92**,** 207-217.
SMITH, M. A., GRANT, C. D., LONERAGAN, W. A. & KOCH, J. M. 2004b. Fire management implications of fuel loads and vegetation structure in jarrah forest restoration on bauxite mines in Western Australia. *Forest Ecology and Management,* 187**,** 247-266.
SOLANS VILA, J. P. & BARBOSA, P. 2009. Post-fire vegetation regrowth detection in the Deiva Marina region (Liguria-Italy) using Landsat TM and ETM+ data. *Ecological Modelling,* 221**,** 75-84.
SONG, J. H., HAN, S. H., YU, K. & KIM, Y. I. 2002. Assessing the possibility of land-cover classification using lidar intensity data. *International Archives of Photogrammetry, Remote Sensing and Spatial Information Sciences,* 34**,** 259-262.
SOUTH, B., EVANS, D., ALDRED, S. & STODDART, D. 2012. Community Environmental Recovery Action Plan.
SOVEREL, N. O., PERRAKIS, D. D. B. & COOPS, N. C. 2010. Estimating burn severity from Landsat dNBR and RdNBR indices across western Canada. *Remote Sensing of Environment,* 114**,** 1896-1909.
SRINIVASAN, S., POPESCU, S. C., ERIKSSON, M., SHERIDAN, R. D. & KU, N. W. 2014. Multi-temporal terrestrial laser scanning for modeling tree biomass change. *Forest Ecology and Management,* 318**,** 304-317.
TANAKA, S., KIMURA, H. & SUGA, Y. 1983. Preparation of a 1: 25000 Landsat map for assessment of burnt area on Etajima Island. *International Journal of Remote Sensing,* 4**,** 17-31.
TEOBALDELLI, M., ZENONE, T., PUIG, D., MATTEUCCI, M., SEUFERT, G. & SEQUEIRA, V. Structural tree modelling of aboveground and belowground poplar tree using direct and indirect measurements: terrestrial laser scanning, WGROGRA, AMAPmod and JRC-3D ReconstructorÒ. *In:* PRUSINKIEWICZ, P. & HANAN, J., eds. Proceedings of 5th

International Workshop on Functional Structural Plant Models, 4-9 November 2007 Napier, New Zealand. 4-9.
THENKABAIL, P. S., SMITH, R. B. & DE PAUW, E. 2002. Evaluation of narrowband and broadband vegetation indices for determining optimal hyperspectral wavebands for agricultural crop characterization. *Photogrammetric Engineering and Remote Sensing,* 68**,** 607-622.
THIES, M. & SPIECKER, H. Evaluation and future prospects of terrestrial laser scanning for standardized forest inventories. ISPRS Working Group VIII/2: Laser-Scanners for Forest and Landscape Assessment, 2004 Freiburg, Germany. 192-197.
THOMSON, V. P. & LEISHMAN, M. R. 2005. Post fire vegetation dynamics in nutrient enriched and non enriched sclerophyll woodland. *Austral Ecology,* 30**,** 250-260.
TOLHURST, K. Effects of fuel reduction burning on flora in a dry sclerophyll forest. Proceedings of Fire and biodiversity: The effects and effectiveness of fire management, 1994 Footscray, Victoria. Department of Environment, Sport and Territories, 97-107.
TOLHURST, K. G., FLINN, D. W. & LOYN, R. H. 1992. Ecological effects of fuel reduction burning in a dry sclerophyll forest. Melbourne: Forest Research Centre, Department of Conservation and Environment.
TOMKINS, I. B., KELLAS, J. D., TOLHURST, K. G. & OSWIN, D. A. 1991. Effects of fire intensity on soil chemistry in a eucalypt forest. *Australian journal of soil research,* 29**,** 25-47.
TRAN, C. & WILD, C. 2000. A review of current knowledge and literature to assist in determining ecologically sustainable fire regimes for the Southeast Queensland region. Brisbane, Queensland: Griffith University and the Fire and Biodiversity Consortium.
TRIGG, S. & FLASSE, S. 2001. An evaluation of different bi-spectral spaces for discriminating burned shrub-savannah. *International Journal of Remote Sensing,* 22**,** 2641-2647.
TROMBETTI, M., AMATULLI, G., LASAPONARA, R. & MARÇAL, A. The use of multi-temporal MODIS data for burnt area detection in the Italian peninsula through a classification tree approach. Proceedings of the 25th EARSeL Symposium, 2006 Porto, Portugal. Millpress Science Publishers, 377-384.
TROMBETTI, M. & LASAPONARA, R. Characterization of vegetation condition in relation to fire occurrence: susceptibility to fire events and detection of fire effects by means of MODIS derived spectral indices. *In:* DE LA RIVA, J., PEREZ-CABELLO, F. & CHUVIECO, E., ed. Proceedings of the 5th International Workship on Remote Sensing and GIS Applications to Forest Fire Management: Fire Effects Assessment, 16-18 June 2005 Zaragoza, Spain. Universidad de Zaragoza 139-143.
TSAI, F. & PHILPOT, W. 1998. Derivative analysis of hyperspectral data. *Remote Sensing of Environment,* 66**,** 41-51.
TUCKER, C. J. 1979. Red and photographic infrared linear combinations for monitoring vegetation. *Remote Sensing of Environment,* 8**,** 127-150.
TURNER, M. G., HARGROVE, W. W., GARDNER, R. H. & ROMME, W. H. 1994. Effects of fire on landscape heterogeneity in Yellowstone National Park, Wyoming. *Journal of Vegetation Science,* 5**,** 731-742.
VAN DER ZANDE, D., HOET, W., JONCKHEERE, I., VAN AARDT, J. & COPPIN, P. 2006. Influence of measurement set-up of ground-based LiDAR for derivation of tree structure. *Agricultural and Forest Meteorology,* 141**,** 147-160.
VAN LEEUWEN, M. & NIEUWENHUIS, M. 2010. Retrieval of forest structural parameters using LiDAR remote sensing. *European Journal of Forest Research,* 129**,** 749-770.
VAN LOON, A. P. 1977. *Bushland fuel quantities in the Blue Mountains: litter and understorey*, Forestry Commission of NSW. Res. Note No. 33.
VAN WAGTENDONK, J., ROOT, R. & KEY, C. 2004a. Comparison of AVIRIS and Landsat ETM+ detection capabilities for burn severity. *Remote Sensing of Environment,* 92**,** 397-408.

VAN WAGTENDONK, J. W., ROOT, R. R. & KEY, C. H. 2004b. Comparison of AVIRIS and Landsat ETM+ detection capabilities for burn severity. *Remote Sensing of Environment,* 92**,** 397-408.
VERAVERBEKE, S., GITAS, I., KATAGIS, T., POLYCHRONAKI, A., SOMERS, B. & GOOSSENS, R. 2012. Assessing post-fire vegetation recovery using red–near infrared vegetation indices: Accounting for background and vegetation variability. *ISPRS Journal of Photogrammetry and Remote Sensing,* 68**,** 28-39.
VERAVERBEKE, S., HARRIS, S. & HOOK, S. 2011a. Evaluating spectral indices for burned area discrimination using MODIS/ASTER (MASTER) airborne simulator data. *Remote Sensing of Environment,* 115**,** 2702-2709.
VERAVERBEKE, S., LHERMITTE, S., VERSTRAETEN, W. & GOOSSENS, R. 2010. The temporal dimension of differenced Normalized Burn Ratio (dNBR) fire/burn severity studies: The case of the large 2007 Peloponnese wildfires in Greece. *Remote Sensing of Environment,* 114**,** 2548-2563.
VERAVERBEKE, S., LHERMITTE, S., VERSTRAETEN, W. & GOOSSENS, R. 2011b. Evaluation of pre/post-fire differenced spectral indices for assessing burn severity in a Mediterranean environment with Landsat Thematic Mapper. *International Journal of Remote Sensing,* 32**,** 3521-3537.
VERBESSELT, J., SOMERS, B., VAN AARDT, J., JONCKHEERE, I. & COPPIN, P. 2006. Monitoring herbaceous biomass and water content with SPOT VEGETATION time-series to improve fire risk assessment in savanna ecosystems. *Remote Sensing of Environment,* 101**,** 399-414.
VICTORIAN LANDS ALLIANCE 2010. Fuel reduction burning in southern Australia's forests: A review of its effectiveness as a bushfire management tool. *In:* POYNTER, M. (ed.). Melbourne, Victoria.
VIERLING, L. A., XU, Y., EITEL, J. U. H. & OLDOW, J. S. 2013. Shrub characterization using terrestrial laser scanning and implications for airborne LiDAR assessment. *Canadian Journal of Remote Sensing,* 38**,** 709-722.
VILA, J. P. S. & BARBOSA, P. Vegetation regrowth detection after a forest fire using PROBA-1/CHRIS data. 4th CHRIS Proba Workshop, 19-21 September 2006 Esrin, Italy.
WAIN, A., MILLS, G., MCCAW, L. & BROWN, T. 2008. Managing smoke from wildfires and prescribed burning in southern Australia. *Developments in Environmental Sciences,* 8**,** 535-550.
WALZ, Y., MAIER, S. W., DECH, S. W., CONRAD, C. & COLDITZ, R. R. 2007. Classification of burn severity using Moderate Resolution Imaging Spectroradiometer (MODIS): A case study in the jarrah-marri forest of southwest Western Australia. *Journal of geophysical research,* 112**,** G02002, doi: 10.1029/2005JG000118.
WANG, C. & GLENN, N. F. 2009. Estimation of fire severity using pre-and post-fire LiDAR data in sagebrush steppe rangelands. *International Journal of Wildland Fire,* 18**,** 848-856.
WARDELL-JOHNSON, G. W. 2000. Responses of forest eucalypts to moderate and high intensity fire in the Tingle Mosaic, south western Australia: comparisons between locally endemic and regionally distributed species. *Austral Ecology,* 25**,** 409-421.
WARDELL-JOHNSON, G. W., BURROWS, N. D. & SHU, L. Emergent patterns in the mosaic of patch burning vary with the fire environment and landscape context in south-western Australia. Bushfire Conference, 6-9 June 2006 Brisbane, Australia.
WARING, R. H. & SCHLESINGER, W. H. 1985. Nutrient cycling through forests. *In:* WARING, R. H. & SCHLESINGER, W. H. (eds.) *Forest Ecosystems: Concepts and Management.* Florida: Academic Press Inc.
WATSON, P. 1998. The Role of Fire in Sclerophyllous Vegetation Communities in Southern and Eastern Australia and its Implications for Management.
WATSON, P. 2001. The role and use of fire for biodiversity conservation in Southeast Queensland: Fire management guidelines derived from ecological research. Brisbane: SEQ Fire and Biodiversity Consortium.

WATSON, P. & WARDELL-JOHNSON, G. 2004. Fire frequency and time since fire effects on the open forest and woodland flora of Girraween National Park, south east Queensland, Australia. *Austral Ecology,* 29**,** 225-236.
WATT, P. J. & DONOGHUE, D. N. M. 2005. Measuring forest structure with terrestrial laser scanning. *International Journal of Remote Sensing,* 26**,** 1437-1446.
WATT, P. J., DONOGHUE, D. N. M. & DUNFORD, R. W. Forest parameter extraction using terrestrial laser scanning. Proceedings of ScandLaser Scientific Workshop on Airborne Laser Scanning of Forests, 2003 Umean, Sweden. 237-244.
WHITE, J. D., RYAN, K. C., KEY, C. C. & RUNNING, S. W. 1996. Remote sensing of forest fire severity and vegetation recovery. *International Journal of Wildland Fire,* 6**,** 125-136.
WHITE, R. A. & DIETTERICK, B. C. Use of LiDAR and multispectral imagery to determine conifer mortality and burn severity following the lockheed fire. *In:* STANDIFORD, R. B., WELLER, T. J., PIIRTO, D. D. & STUART, J. D., eds. Proceedings of coast redwood forests in changing California: A symposium for scientists and managers, 2012 Albany, California, USA. Pacific Southwest Research Station, Forest Service, U.S. Department of Agriculture, 667-675.
WIEGAND, C. L., RICHARDSON, A. J., ESCOBAR, D. E. & GERBERMANN, A. H. 1991. Vegetation indices in crop assessments. *Remote Sensing of Environment,* 35**,** 105-119.
WILLIAM, K. 1991. Dry Sclerophyll Vegetation. *In:* KIRKPATRICK, J. B. (ed.) *Tasmanian native bush: a management handbook.* Hobart, Australia: Tasmanian Environment Centre Inc.
WING, M. G., EKLUND, A. & SESSIONS, J. 2010. Applying LiDAR technology for tree measurements in burned landscapes. *International Journal of Wildland Fire,* 19**,** 104-114.
WOOLLEY, J. T. 1971. Reflectance and transmittance of light by leaves. *Plant Physiology,* 47**,** 656-662.
WU, C., NIU, Z., TANG, Q. & HUANG, W. 2008. Estimating chlorophyll content from hyperspectral vegetation indices: Modeling and validation. *Agricultural and Forest Meteorology,* 148**,** 1230-1241.
WULDER, M., WHITE, J., ALVAREZ, F., HAN, T., ROGAN, J. & HAWKES, B. 2009. Characterizing boreal forest wildfire with multi-temporal Landsat and LIDAR data. *Remote Sensing of Environment,* 113**,** 1540-1555.
ZAMMIT, C. 1988. Dynamics of resprouting in the lignotuberous shrub *Banksia oblongifolia*. *Australian Journal of Ecology,* 13**,** 311-320.

10. Appendices

10.1 A review of studies involving remote sensing of fire effects.

Table 10.1 Selected case studies demonstrating the utility of remotely sensed data in a wide variety of vegetation biomes for mapping burnt areas, severity and post-fire vegetation regeneration (Adapted from French et al., 2008)

Application	Vegetation Type	Remote Sensing Approach	Field Observations	Results	Reference
Fire severity	Douglas-fir and Pine forest, British Columbia, Canada	Change detection due to fire from difference images of Landsat and RapidEye using spectral indices (EVI, NBR, NDVI and SAVI).	Burn circumference, char height and crown scorch combined to create a Simple Burn Index (SBI).	Mean SAVI provided best differentiation between crown scorch classes. RapidEye dNDVI and Landsat dNBR were unable to differentiate between low and medium crown scorch classes.	Lu et al. (2016)
Burn severity	Semiarid grasslands, Saskatchewan, Canada	Spectral indices (MIRBI, NBR, dNBR, SR and NDVI) applied to pre- and post-fire Landsat imagery.	Presence of burn residuals such as soil colour and senesced grass to classify severity.	MIRBI performed best for estimating burn severity with an overall accuracy of 76%.	Arnett et al. (2015)

Application	Vegetation Type	Remote Sensing Approach	Field Observations	Results	Reference
Burn severity	Pine forest, California, USA	Object-based assessment of MASTER (MODIS/ASTER) airborne simulator imagery.	CBI in 42 burnt plots	Models developed for the three stages of disease progression had similar performance where spectral and textural responses contributed to burn assessments when no band reduction was applied.	Chen et al. (2015)
Fire severity	Tropical savannahs, Australia	Indices derived from Hyperspectral data captured from a helicopter.	Pre-burn: Site, location, habitat type, vegetation structure and woody species floristic attributes Post-burn: % green, % litter, % scorch, % char, % dry grass, % bare soil, % ash	Pre- and post-fire difference in MODIS channel 6 is appropriate for fire severity mapping.	Edwards et al. (2013)
Burn severity and fire extent	Tussock-shrub Tundra, Alaska, USA	6 spectral indices derived from Landsat TM and ETM+ imagery	Site type, CBI, modified CBI, vegetation regrowth, fuel consumption and soil moisture	Fire scars can be mapped immediately post-burn but the spectral signal deteriorates rapidly thereafter. There exists a large variability in the surface reflectance of burned and unburned areas across space and time.	Loboda et al. (2013)

Application	Vegetation Type	Remote Sensing Approach	Field Observations	Results	Reference
Post-fire forest regeneration and vegetation recovery	Pine forest, Greece	Object-based image analysis on Hyperion, QuickBird and Landsat TM imagery.	Visual assessment of existing vegetation cover, burnt and unburnt plots and field digital photography	83.7% overall accuracy achieved with the separation of classes 'forest regeneration', 'other vegetation recovery' and 'unburned vegetation'.	Mitri and Gitas (2013)
Post-fire vegetation recovery	Mixed-species eucalypt forest and Pine forest, Victoria, Australia	NDVI derived from Landsat 5 TM.	Reconnaissance to verify patterns observed in imagery and confirm variations in vegetation cover	The use of Landsat imagery and NDVI is suitable for determining regeneration rates. In addition to vegetation type, slope-aspect and rainfall are important parameters which determine rates of regeneration.	Sever et al. (2012)
Post-fire vegetation recovery	Pine forests, Greece	Field spectrometry measurements and 13 Red-NIR spectral indices derived from Landsat TM.	78 line transect plots	NDVI was found to be the most optimal index. Landsat NDVI showed the highest correlation with line transects (R^2=0.68).	Veraverbeke et al. (2012)
Fire severity	Chaparral forests, Western U.S.	19 spectral indices derived from MASTER imagery.	6 class fire severity assessments conducted in 25 plots.	Indices with a SWIR or MIR spectral band yielded better results than indices lacking them.	Harris et al. (2011)
Multi-strata fire severity	Mixed oak forests, Western U.S.	NBR and dNBR derived from Landsat TM, image differencing and image ratioing	Composite Burn Index (CBI), fire severity (5 forest strata)	Moderate relationship between NBR and fire severity and relatively strong positive relationship in model using dNBR as predictor	Meng and Meentemeyer (2011)

Application	Vegetation Type	Remote Sensing Approach	Field Observations	Results	Reference
Fire severity	Savanna and dense forest, Brazil	Spectral indices derived from Landsat time series dataset (RdNBR) and Hyperion imagery (NDVI, NDII, NDWI, PRI and CRI).	n/a	NDVI, CRI and PRI could discriminate between burned forests and undisturbed forests for the first 3 years after forest fire.	Numata et al. (2011)
Fire severity	Boreal forests, Alaska	Various spectral indices derived from Landsat TM/ETM+	Plots, CBI, fire severity	Non-parametric models and ancillary data are useful in modelling of the surface organic layer fire depth	Barrett et al. (2010)
Burned area mapping	Mediterranean vegetation, Italy	Soft integration of spectral indices (for example NIR, CSI, NBR, BAI, SAVI, and MIRBI) derived from ASTER.	n/a	Presented a novel approach for burned area mapping involving integration into a synthetic indicator of spectral indices which were converted to a common domain through fuzzy membership functions.	Boschetti et al. (2010)
Spectral patterns from burned surfaces	Dense forests, Greece	Hyperspectral imagery from CHRIS-PROBA and Hyperion. Multispectral imagery from IKONOS, Landsat, MODIS and ASTER.	n/a	Both hyperspectral sensors can potentially be used for fire scar discrimination and mapping.	Koutsias et al. (2010)

Application	Vegetation Type	Remote Sensing Approach	Field Observations	Results	Reference
Post-fire vegetation regeneration mapping	Mediterranean vegetation, Greece	Object-based classification model on hyperspectral Hyperion imagery.	Data on forest regeneration and vegetation recovery collected from 62 plots within one year from the fire.	The classification model produced very satisfactory results (overall accuracy of 75.81%).	Mitri and Gitas (2010)
Burn severity	Boreal forests, Western Canada	dNBR and RdNBR derived from Landsat TM/ETM+	CBI	dNBR estimated burn severity more accurately (70.2%) as compared to RdNBR-derived model (65.2%)	Soverel et al. (2010)
Post-fire vegetation regrowth detection	Conifer forest, Northern Italy	NDVI and MSAVI derived from Landsat TM and ETM+ data (to derive percentage vegetation cover) and application of SMA	Percentage vegetation cover extracted from plots using Line Intercept Method	Vegetation cover fractions extracted from the NDVI based quantitative index were the most accurate	Solans Vila and Barbosa. (2009)
Mapping burned areas and burn severity	Eucalypt forest, South-west Western Australia	Change in LAI and dNBR derived from landsat TM	Field plots, digital photographs	All three LAI models had equally high coefficients of determination (R^2 : 0.87) and a small root mean squared errors (RMSE : 0.27-0.28)	Boer et al. (2008a)
Burn severity	Conifer, deciduous, mixed forests, shrublands, Alaska	dNBR generated from Landsat TM data	CBI	R^2 = 0.36 (For 6 fire events) between dNBR and CBI	Murphy et al. (2008)
Burn severity and vegetation response	Chaparral vegetation, Western U.S.	dNBR derived from Landsat TM data	Field plots, fire severity (3 classes)	No accuracy statistics presented	Lentile et al (2007)

Application	Vegetation Type	Remote Sensing Approach	Field Observations	Results	Reference
Burn severity	Conifer forest, shrublands, Sierra Nevada	dNBR and RdNBR derived from Landsat TM data	CBI	R^2 = 0.49 between CBI and dNBR and 0.61 between CBI and RdNBR (exponential equations)	Miller and Thode (2007)
Burn severity classification	Deciduous forests, South-west Australia	dNBR generated from Landsat TM and MODIS data	Fire severity classes (4 levels)	85% accuracy using Landsat dNBR, with lowest accuracies achieved using MODIS dNBR	Walz et al. (2007)
Fire severity	Shrublands, woodlands, Australia	NDVI from SPOT and Landsat TM data	Fire severity class (5 levels)	Classification accuracy dependent on pre-fire vegetation type	Hammill and Bradstock (2006)
Fire severity mapping	Shrublands, forests, Spain	dNBR and spectral unmixing using Landsat TM, MERIS and MODIS data	Fire severity classes (4 levels)	Classification accuracy of 74% achieved using spectral unmixing of Landsat TM data	Roldán-Zamarrón et al.(2006)
Analyse and compare emergent burn patchiness	South-west Western Australia	NBR and CVFI derived from Landsat TM and ETM+	n/a	No accuracy statistics presented	Wardell-Johnson et al.(2006)
Biomass burning	Savanna, Namibia	dNBR derived from MODIS data	Combustion completeness from field observations	dNBR not correlated with combustion completeness	Alleaume et al. (2005)
Fire severity mapping	Grassland, shrubland, forests, western U.S.	dNBR derived from Landsat TM data	Fire severity classes (4 levels) in multiple land cover types	Classification accuracy of 56% when land cover not considered, 96% when land cover accounted for	Brewer et al. (2005)

Application	Vegetation Type	Remote Sensing Approach	Field Observations	Results	Reference
Fire severity mapping	Pine forests, Western U.S.	dNBR derived from Landsat ETM+ data	BI and fire severity classes (4 levels) based on pre- and post-fire measurements	Accurately identified severely burned areas	Cocke et al.(2005)
Burn severity and post-fire vegetation interaction	Conifer, deciduous, mixed forests and shrublands in Alaska	dNBR and other indices derived from Landsat TM imagery	CBI	R^2 = 0.52 (average for 4 events) between dNBR and CBI for different fire events	Epting and Verbyla (2005)
Burn severity	Mediterranean shrublands, Spain	Regression modelling from Hyperion hyperspectral satellite imagery.	CBI values estimated for 50 plots within the burned area and 10 outside the fire perimeter.	Assessments of 20 plots indicated the reliability of Hyperion sensor to reliably estimate burn severity. The best estimations of CBI were derived from raw reflectance in red, near-infrared and shortwave infrared spectral regions.	Parra and Chuvieco (2005)
Burned area mapping	Sub-Saharan Africa (Including Madagascar)	Burned area mapping algorithm based on classification trees developed using SPOT-VGT imagery and compared with Landsat ETM+ maps through linear regression analysis	n/a	Strong relationship between VGT and Landsat estimates of burned area with R^2 = 0.754 and slope = 0.803	Silva et al (2005)
Fire severity	Chaparral, savanna, woodlands in Australia	NDVI from SPOT data	Fire severity class (6 levels)	88% classification accuracy	Chafer et al. (2004)

Application	Vegetation Type	Remote Sensing Approach	Field Observations	Results	Reference
Fire scar mapping	Semi-arid savanna landscape, South Africa	Simple, nonparametric, supervised classification (parallelepiped) of the PCT data differentiated burned and unburned areas from Landsat MSS, TM and ETM+	n/a	Out of a total of 396 validation points, 366 were correctly classified as unburned (92.42%), 26 were correctly classified as burned (6.57%)	Hudak and Brockett (2004)
Burn severity quantification	Pine forests, western U.S.	dNBR derived from Landsat ETM	CBI	R^2 = 0.89 between dNBR and CBI, but saturates for CBI>2.4	Van Wagtendonk et al.(2004a)
Estimating parameters related to boreal forest fire	Boreal forest, Canada	SWVI derived from SPOT VGT	n/a	SPOT VGT is effective for mapping large boreal burns at the end of a fire season and approximating the age of regenerating burns less than about 30 years old	Fraser and Li (2002)
Burned land mapping	Iberian peninsula, Spain	Spatial and temporal analysis of MODIS and AVHRR images	n/a	MODIS data was found more appropriate for burned land mapping, caused by both the better spatial and spectral resolution	Martín et al (2002)
Post-fire forest canopy mapping	Conifer forests and woodlands, Western U.S.	dNBR severity maps (BARC products) and supervised classifications generated from Landsat TM	Overstorey component of CBI	Kappa= 0.86 for supervised classification, =0.38 – 0.63 for dNBR maps	Miller and Yool (2002)

Application	Vegetation Type	Remote Sensing Approach	Field Observations	Results	Reference
Fire mapping accuracy	Boreal forests, Canada	NDVI derived from AVHRR data	GIS database of fire patterns including hardcopy maps derived from field data and aerial photographs	Ground-truthed fire sizes and shapes were correlated with the AVHRR/NDVI-mapped areas	Remmel and Perera (2001)
Fire-induced vegetation mortality mapping	Pine and oak forests, western U.S.	Supervised classification using TC and PC transformations of Landsat TM data	Fire severity class (4 levels)	Kappa = 0.73 for TC transform, 0.62 for PC transform	Patterson and Yool (1998)
Fire mapping	Iberian peninsula, Spain	NDVI-MCVs generated from AVHRR data	n/a	Regression algorithm was more reliable with virtually no bias (-0.9%) and a RMS of 20.3%	Fernández et al (1997)
Fire severity	Steppe, shrublands, grasslands, conifer forests, Western U.S.	Supervised classification of Landsat TM data	Fire severity classes (3 levels) from aerial photo interpretation	63% classification accuracy	White et al. (1996)
Vegetation change in response to fire	Pine forest, Midwestern U.S.	Level slice of Landsat MSS band 4/band 3 ratio	n/a	n/a	Jakubauskas et al. (1990)
Mapping vegetation change in response to fire	Eucalypt forests, Eastern Australia	Supervised and unsupervised classification of Landsat TM data	n/a	n/a	Milne (1986)

Application	Vegetation Type	Remote Sensing Approach	Field Observations	Results	Reference
Vegetation change in response to fire	Tundra, Alaska	Classification of multi-temporal Landsat data	Field measurements from selected portions of the burned area	Areas burnt with differing severity showed different recovery rates.	Hall et al. (1980)

10.2 Validation of *mean AGH_{change}* against a detailed field assessment in a 3 × 3 grid at *T1* epoch in the control and fire-altered plot 3.

Table 10.2 Transformed field and TLS data in a 3x3 grid at T1 epoch in the control plot and fire-altered plot 3.

Plot	Cell No.	Near-Surface Live Vegetation (V)	Litter (L)	Bare Earth (BE)	V+L	V+BE	L+BE	V+L+BE	Area Burnt (%)	mean AGH_{change}
Control Plot	1	0	-0.13	0	-0.10	0	-0.06	-0.05	0	-0.19
	2	0	-0.08	1	-0.05	0.13	0	0	0	-0.18
	3	0	-0.11	0	-0.05	0.09	0	0	0	-0.17
	4	0	0	0	0	0	0	-0.05	0	-0.08
	5	0	0	0.20	0	0.07	0.11	0	0	-0.13
	6	0	0.08	-1	0.06	-0.14	0	-0.05	0	-0.08
	7	0	0	0	0	0	0	-0.10	0	0.05
	8	0	0	0	0	0	0	0	0	-0.08
	9	0	-0.20	0.13	-0.09	0.07	0	-0.05	0	-0.20
Fire-altered Plot 3	1	-0.93	-0.75	5	-0.89	-0.56	0.40	-0.60	60	-0.20
	2	-0.89	-0.6	0.67	-0.79	-0.27	0.09	-0.35	35	-0.59
	3	-0.50	-0.5	0.17	-0.50	0	0	-0.10	10	-0.75
	4	-0.8	-0.5	-0.23	-0.71	-0.39	-0.27	-0.40	40	-0.47
	5	-0.91	0	0	-0.59	-0.71	0	-0.50	50	-0.52

6	-0.82	-0.83	1	-0.82	-0.43	-0.22	-0.55	55	-0.62
7	-0.89	-0.83	0.6	-0.87	-0.36	-0.18	-0.50	50	-0.40
8	-1.0	-0.78	2	-0.88	-0.40	-0.27	-0.58	55	0.02
9	-0.93	-0.75	2	-0.89	-0.56	0.17	-0.60	55	-0.36

10.3 ASD spectra processing details

This section of the appendix contains context information relating to the removal of bands corresponding to atmospheric noise in the ASD spectra collected and used in this research.

Removal of atmospheric water vapour absorption bands

Electromagnetic spectrum is greatly affected due the presence of strong atmospheric water vapour absorption bands in the regions 1380nm and 1850nm as shown in Figure 10.1. The regions removed were 1339-1431nm and 1789-1966nm. The region beyond 2433nm was also removed because of increasing instrument-generated noise and low Signal-to-Noise ratio (SNR). The result of the removal of the band regions is illustrated in Figure 10.2.

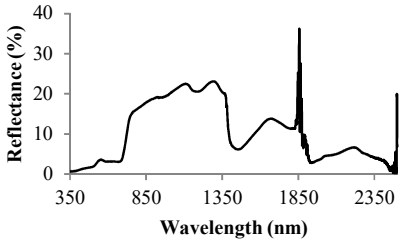

Figure 10.1 Spectral reflectance curve before removal of atmospheric water vapour absorption bands.

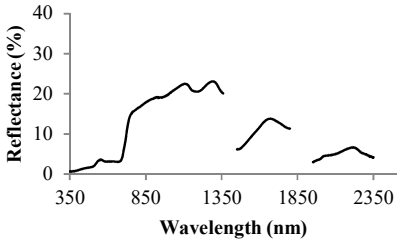

Figure 10.2 Spectral reflectance curve after removal of atmospheric water vapour absorption bands.

An exception to the removal of these noisy atmospheric water vapour absorption regions was calculation of first-order derivatives. For these, the continuous spectra were retained and the noisy regions were removed post first-order differentiation. This is because the abrupt change in values would affect the differentiation more if the noisy bands were removed.

10.4 Vegetation indices

This section lists the values obtained upon deriving the different vegetation indices across the three fuel layers.

Table 10.2 below lists the hyperspectral index values obtained for the near-surface fuel layer.

Table 10.3 Hyperspectral vegetation values derived from the spectral data capture for the near-surface fuel layers at different epochs.

ID		VI	VI_Value	Plot	Landcover	EpochLabel	E_Value
1	1	NDVI	0.490526	Control Plot	grass	PB	-4
2	1	NDWI	-0.15295	Control Plot	grass	PB	-4
3	1	NPCI	0.454956	Control Plot	grass	PB	-4
4	1	TCARI.OSAVI	0.008477	Control Plot	grass	PB	-4
5	1	WI.NDVI	1.945625	Control Plot	grass	PB	-4
6	1	D525	0.000675	Control Plot	grass	PB	-4
7	1	PRI	-0.07744	Control Plot	grass	PB	-4
8	1	SIPI	0.742911	Control Plot	grass	PB	-4
9	1	WI	0.95438	Control Plot	grass	PB	-4
10	1	NPQI	-0.10056	Control Plot	grass	PB	-4
11	1	D1550	0.000453	Control Plot	grass	PB	-4
12	1	MSI	1.175593	Control Plot	grass	PB	-4
13	1	ARI1	5.676531	Control Plot	grass	PB	-4
14	1	D1030	0.00032	Control Plot	grass	PB	-4
15	1	MIRBI	0.759036	Control Plot	grass	PB	-4
16	1	NBR	0.326894	Control Plot	grass	PB	-4
17	1	D1215	0.000348	Control Plot	grass	PB	-4
18	1	D720	0.001954	Control Plot	grass	PB	-4
19	1	BAI	9.714596	Control Plot	grass	PB	-4
20	1	CSI	0.937571	Control Plot	grass	PB	-4
21	2	NDWI	-0.13335	Control Plot	grass	W2	2
22	2	TCARI.OSAVI	0.0065	Control Plot	grass	W2	2
23	2	WI.NDVI	1.71247	Control Plot	grass	W2	2
24	2	NPQI	-0.0993	Control Plot	grass	W2	2
25	2	PRI	-0.06322	Control Plot	grass	W2	2
26	2	MSI	1.035411	Control Plot	grass	W2	2
27	2	ARI1	6.233612	Control Plot	grass	W2	2
28	2	NDVI	0.561715	Control Plot	grass	W2	2
29	2	MIRBI	0.78318	Control Plot	grass	W2	2
30	2	NPCI	0.474863	Control Plot	grass	W2	2
31	2	D1215	0.000395	Control Plot	grass	W2	2
32	2	WI	0.96192	Control Plot	grass	W2	2
33	2	D525	0.000665	Control Plot	grass	W2	2

34	2	NBR	0.387399	Control Plot	grass	W2	2
35	2	SIPI	0.780168	Control Plot	grass	W2	2
36	2	BAI	8.915965	Control Plot	grass	W2	2
37	2	D1550	0.000597	Control Plot	grass	W2	2
38	2	CSI	1.067735	Control Plot	grass	W2	2
39	2	D1030	0.000274	Control Plot	grass	W2	2
40	2	D720	0.002431	Control Plot	grass	W2	2
41	3	TCARI.OSAVI	0.002487	Control Plot	grass	W6	6
42	3	MSI	0.800772	Control Plot	grass	W6	6
43	3	NDVI	0.681059	Control Plot	grass	W6	6
44	3	NDWI	-0.09408	Control Plot	grass	W6	6
45	3	NPCI	0.42642	Control Plot	grass	W6	6
46	3	WI.NDVI	1.433979	Control Plot	grass	W6	6
47	3	D525	0.00051	Control Plot	grass	W6	6
48	3	PRI	-0.04142	Control Plot	grass	W6	6
49	3	D1215	0.00024	Control Plot	grass	W6	6
50	3	WI	0.976624	Control Plot	grass	W6	6
51	3	NPQI	-0.09248	Control Plot	grass	W6	6
52	3	D1550	0.000448	Control Plot	grass	W6	6
53	3	CSI	1.381945	Control Plot	grass	W6	6
54	3	ARI1	7.784422	Control Plot	grass	W6	6
55	3	D1030	0.00028	Control Plot	grass	W6	6
56	3	MIRBI	1.238927	Control Plot	grass	W6	6
57	3	NBR	0.515154	Control Plot	grass	W6	6
58	3	SIPI	0.843458	Control Plot	grass	W6	6
59	3	D720	0.002398	Control Plot	grass	W6	6
60	3	BAI	13.8246	Control Plot	grass	W6	6
61	4	NDWI	-0.17193	Control Plot	grass	1Y	52
62	4	NPCI	0.416521	Control Plot	grass	1Y	52
63	4	TCARI.OSAVI	0.010566	Control Plot	grass	1Y	52
64	4	WI.NDVI	2.254822	Control Plot	grass	1Y	52
65	4	NPQI	-0.07572	Control Plot	grass	1Y	52
66	4	D1550	0.000567	Control Plot	grass	1Y	52
67	4	MSI	1.336485	Control Plot	grass	1Y	52
68	4	ARI1	3.641214	Control Plot	grass	1Y	52
69	4	NDVI	0.418973	Control Plot	grass	1Y	52
70	4	MIRBI	0.505364	Control Plot	grass	1Y	52
71	4	PRI	-0.06603	Control Plot	grass	1Y	52
72	4	D1215	0.000427	Control Plot	grass	1Y	52
73	4	WI	0.944709	Control Plot	grass	1Y	52
74	4	D525	0.000696	Control Plot	grass	1Y	52
75	4	SIPI	0.65196	Control Plot	grass	1Y	52
76	4	BAI	6.675855	Control Plot	grass	1Y	52
77	4	CSI	0.813712	Control Plot	grass	1Y	52

78	4	D1030	0.000402	Control Plot	grass	1Y	52
79	4	NBR	0.182066	Control Plot	grass	1Y	52
80	4	D720	0.002139	Control Plot	grass	1Y	52
81	5	NDWI	-0.12006	Fire-Altered Plot 1	grass	PB	-4
82	5	TCARI.OSAVI	0.009559	Fire-Altered Plot 1	grass	PB	-4
83	5	NPQI	-0.14285	Fire-Altered Plot 1	grass	PB	-4
84	5	MSI	0.9019	Fire-Altered Plot 1	grass	PB	-4
85	5	NDVI	0.598041	Fire-Altered Plot 1	grass	PB	-4
86	5	NPCI	0.508605	Fire-Altered Plot 1	grass	PB	-4
87	5	WI.NDVI	1.617382	Fire-Altered Plot 1	grass	PB	-4
88	5	MIRBI	0.516208	Fire-Altered Plot 1	grass	PB	-4
89	5	PRI	-0.07835	Fire-Altered Plot 1	grass	PB	-4
90	5	D1215	0.000415	Fire-Altered Plot 1	grass	PB	-4
91	5	WI	0.96726	Fire-Altered Plot 1	grass	PB	-4
92	5	BAI	6.569665	Fire-Altered Plot 1	grass	PB	-4
93	5	D1550	0.000645	Fire-Altered Plot 1	grass	PB	-4
94	5	CSI	1.234719	Fire-Altered Plot 1	grass	PB	-4
95	5	ARI1	5.22719	Fire-Altered Plot 1	grass	PB	-4
96	5	D1030	0.000501	Fire-Altered Plot 1	grass	PB	-4
97	5	D525	0.000952	Fire-Altered Plot 1	grass	PB	-4
98	5	NBR	0.500677	Fire-Altered Plot 1	grass	PB	-4
99	5	SIPI	0.830976	Fire-Altered Plot 1	grass	PB	-4
100	5	D720	0.003496	Fire-Altered Plot 1	grass	PB	-4
101	6	NDVI	0.325178	Fire-Altered Plot 1	grass	W2	2
102	6	NDWI	-0.22429	Fire-Altered Plot 1	grass	W2	2
103	6	NPCI	0.419544	Fire-Altered Plot 1	grass	W2	2
104	6	TCARI.OSAVI	0.002362	Fire-Altered Plot 1	grass	W2	2
105	6	WI	0.914988	Fire-Altered Plot 1	grass	W2	2
106	6	NPQI	-0.08913	Fire-Altered Plot 1	grass	W2	2
107	6	D1550	0.000219	Fire-Altered Plot 1	grass	W2	2
108	6	MSI	1.958347	Fire-Altered Plot 1	grass	W2	2
109	6	ARI1	9.309509	Fire-Altered Plot 1	grass	W2	2
110	6	D1030	0.000228	Fire-Altered Plot 1	grass	W2	2
111	6	MIRBI	1.72626	Fire-Altered Plot 1	grass	W2	2
112	6	PRI	-0.0627	Fire-Altered Plot 1	grass	W2	2
113	6	D1215	0.000206	Fire-Altered Plot 1	grass	W2	2
114	6	WI.NDVI	2.813805	Fire-Altered Plot 1	grass	W2	2
115	6	D525	0.000223	Fire-Altered Plot 1	grass	W2	2
116	6	SIPI	0.574818	Fire-Altered Plot 1	grass	W2	2
117	6	D720	0.000308	Fire-Altered Plot 1	grass	W2	2
118	6	BAI	21.75446	Fire-Altered Plot 1	grass	W2	2
119	6	CSI	0.537792	Fire-Altered Plot 1	grass	W2	2
120	6	NBR	-0.20941	Fire-Altered Plot 1	grass	W2	2
121	7	NDWI	-0.22216	Fire-Altered Plot 1	grass	W6	6

122	7	NPQI	-0.04298	Fire-Altered Plot 1	grass	W6	6
123	7	MSI	1.803439	Fire-Altered Plot 1	grass	W6	6
124	7	ARI1	20.49898	Fire-Altered Plot 1	grass	W6	6
125	7	NDVI	0.396119	Fire-Altered Plot 1	grass	W6	6
126	7	NPCI	0.392349	Fire-Altered Plot 1	grass	W6	6
127	7	TCARI.OSAVI	0.001	Fire-Altered Plot 1	grass	W6	6
128	7	WI.NDVI	2.305311	Fire-Altered Plot 1	grass	W6	6
129	7	MIRBI	1.74069	Fire-Altered Plot 1	grass	W6	6
130	7	PRI	-0.06265	Fire-Altered Plot 1	grass	W6	6
131	7	SIPI	0.616817	Fire-Altered Plot 1	grass	W6	6
132	7	WI	0.913176	Fire-Altered Plot 1	grass	W6	6
133	7	BAI	36.33855	Fire-Altered Plot 1	grass	W6	6
134	7	D1550	0.000211	Fire-Altered Plot 1	grass	W6	6
135	7	CSI	0.594631	Fire-Altered Plot 1	grass	W6	6
136	7	D1215	0.000124	Fire-Altered Plot 1	grass	W6	6
137	7	D1030	9.38E-05	Fire-Altered Plot 1	grass	W6	6
138	7	D525	0.000117	Fire-Altered Plot 1	grass	W6	6
139	7	NBR	-0.07629	Fire-Altered Plot 1	grass	W6	6
140	7	D720	0.000251	Fire-Altered Plot 1	grass	W6	6
141	8	MSI	1.161775	Fire-Altered Plot 1	grass	1Y	52
142	8	NDVI	0.482473	Fire-Altered Plot 1	grass	1Y	52
143	8	NDWI	-0.11823	Fire-Altered Plot 1	grass	1Y	52
144	8	PRI	-0.07195	Fire-Altered Plot 1	grass	1Y	52
145	8	TCARI.OSAVI	0.011176	Fire-Altered Plot 1	grass	1Y	52
146	8	WI	0.972209	Fire-Altered Plot 1	grass	1Y	52
147	8	NPQI	-0.10232	Fire-Altered Plot 1	grass	1Y	52
148	8	D1550	0.000597	Fire-Altered Plot 1	grass	1Y	52
149	8	CSI	0.919822	Fire-Altered Plot 1	grass	1Y	52
150	8	ARI1	3.561438	Fire-Altered Plot 1	grass	1Y	52
151	8	D1030	0.000319	Fire-Altered Plot 1	grass	1Y	52
152	8	MIRBI	0.673977	Fire-Altered Plot 1	grass	1Y	52
153	8	NPCI	0.434385	Fire-Altered Plot 1	grass	1Y	52
154	8	D1215	0.000315	Fire-Altered Plot 1	grass	1Y	52
155	8	WI.NDVI	2.015053	Fire-Altered Plot 1	grass	1Y	52
156	8	D525	0.000867	Fire-Altered Plot 1	grass	1Y	52
157	8	NBR	0.241901	Fire-Altered Plot 1	grass	1Y	52
158	8	SIPI	0.71995	Fire-Altered Plot 1	grass	1Y	52
159	8	D720	0.003	Fire-Altered Plot 1	grass	1Y	52
160	8	BAI	6.696758	Fire-Altered Plot 1	grass	1Y	52
161	9	PRI	-0.0745	Fire-Altered Plot 2	grass	PB	-4
162	9	SIPI	0.772449	Fire-Altered Plot 2	grass	PB	-4
163	9	D720	0.002325	Fire-Altered Plot 2	grass	PB	-4
164	9	WI	0.964781	Fire-Altered Plot 2	grass	PB	-4
165	9	NPQI	-0.10613	Fire-Altered Plot 2	grass	PB	-4

166	9	D1550	0.00047	Fire-Altered Plot 2	grass	PB	-4
167	9	MSI	0.991081	Fire-Altered Plot 2	grass	PB	-4
168	9	ARI1	6.481028	Fire-Altered Plot 2	grass	PB	-4
169	9	NDVI	0.549142	Fire-Altered Plot 2	grass	PB	-4
170	9	NDWI	-0.12295	Fire-Altered Plot 2	grass	PB	-4
171	9	NPCI	0.481246	Fire-Altered Plot 2	grass	PB	-4
172	9	TCARI.OSAVI	0.005693	Fire-Altered Plot 2	grass	PB	-4
173	9	WI.NDVI	1.756888	Fire-Altered Plot 2	grass	PB	-4
174	9	D525	0.00057	Fire-Altered Plot 2	grass	PB	-4
175	9	NBR	0.365696	Fire-Altered Plot 2	grass	PB	-4
176	9	CSI	1.108795	Fire-Altered Plot 2	grass	PB	-4
177	9	BAI	8.983829	Fire-Altered Plot 2	grass	PB	-4
178	9	D1030	0.000378	Fire-Altered Plot 2	grass	PB	-4
179	9	MIRBI	0.938513	Fire-Altered Plot 2	grass	PB	-4
180	9	D1215	0.000378	Fire-Altered Plot 2	grass	PB	-4
181	10	SIPI	0.537509	Fire-Altered Plot 2	grass	W2	2
182	10	WI	0.980127	Fire-Altered Plot 2	grass	W2	2
183	10	NPQI	-0.07157	Fire-Altered Plot 2	grass	W2	2
184	10	NDWI	-0.0915	Fire-Altered Plot 2	grass	W2	2
185	10	MSI	1.341931	Fire-Altered Plot 2	grass	W2	2
186	10	TCARI.OSAVI	0.001454	Fire-Altered Plot 2	grass	W2	2
187	10	WI.NDVI	3.002293	Fire-Altered Plot 2	grass	W2	2
188	10	PRI	-0.03968	Fire-Altered Plot 2	grass	W2	2
189	10	NBR	-0.11481	Fire-Altered Plot 2	grass	W2	2
190	10	D720	0.00027	Fire-Altered Plot 2	grass	W2	2
191	10	BAI	38.25326	Fire-Altered Plot 2	grass	W2	2
192	10	NDVI	0.32646	Fire-Altered Plot 2	grass	W2	2
193	10	D1550	9.16E-05	Fire-Altered Plot 2	grass	W2	2
194	10	CSI	0.775895	Fire-Altered Plot 2	grass	W2	2
195	10	ARI1	11.57998	Fire-Altered Plot 2	grass	W2	2
196	10	MIRBI	1.992771	Fire-Altered Plot 2	grass	W2	2
197	10	NPCI	0.303211	Fire-Altered Plot 2	grass	W2	2
198	10	D1215	5.26E-05	Fire-Altered Plot 2	grass	W2	2
199	10	D525	0.000153	Fire-Altered Plot 2	grass	W2	2
200	10	D1030	2.97E-05	Fire-Altered Plot 2	grass	W2	2
201	11	WI	0.959769	Fire-Altered Plot 2	grass	W6	6
202	11	TCARI.OSAVI	0.002671	Fire-Altered Plot 2	grass	W6	6
203	11	PRI	-0.03394	Fire-Altered Plot 2	grass	W6	6
204	11	SIPI	0.731025	Fire-Altered Plot 2	grass	W6	6
205	11	D720	0.000756	Fire-Altered Plot 2	grass	W6	6
206	11	NPQI	-0.03776	Fire-Altered Plot 2	grass	W6	6
207	11	D1550	0.000292	Fire-Altered Plot 2	grass	W6	6
208	11	MSI	1.367156	Fire-Altered Plot 2	grass	W6	6
209	11	BAI	30.84745	Fire-Altered Plot 2	grass	W6	6

210	11	NDVI	0.449551	Fire-Altered Plot 2	grass	W6	6
211	11	NDWI	-0.15829	Fire-Altered Plot 2	grass	W6	6
212	11	NPCI	0.306903	Fire-Altered Plot 2	grass	W6	6
213	11	D1215	0.000105	Fire-Altered Plot 2	grass	W6	6
214	11	WI.NDVI	2.134952	Fire-Altered Plot 2	grass	W6	6
215	11	D525	0.000509	Fire-Altered Plot 2	grass	W6	6
216	11	NBR	0.05485	Fire-Altered Plot 2	grass	W6	6
217	11	CSI	0.775233	Fire-Altered Plot 2	grass	W6	6
218	11	ARI1	5.132136	Fire-Altered Plot 2	grass	W6	6
219	11	D1030	0.000131	Fire-Altered Plot 2	grass	W6	6
220	11	MIRBI	1.706586	Fire-Altered Plot 2	grass	W6	6
221	12	SIPI	0.612688	Fire-Altered Plot 2	grass	1Y	52
222	12	D720	0.001122	Fire-Altered Plot 2	grass	1Y	52
223	12	WI	0.950881	Fire-Altered Plot 2	grass	1Y	52
224	12	NPQI	-0.07494	Fire-Altered Plot 2	grass	1Y	52
225	12	NDWI	-0.15691	Fire-Altered Plot 2	grass	1Y	52
226	12	NPCI	0.418356	Fire-Altered Plot 2	grass	1Y	52
227	12	TCARI.OSAVI	0.004389	Fire-Altered Plot 2	grass	1Y	52
228	12	WI.NDVI	2.535801	Fire-Altered Plot 2	grass	1Y	52
229	12	PRI	-0.06722	Fire-Altered Plot 2	grass	1Y	52
230	12	NBR	-0.01457	Fire-Altered Plot 2	grass	1Y	52
231	12	MSI	1.509288	Fire-Altered Plot 2	grass	1Y	52
232	12	BAI	11.95769	Fire-Altered Plot 2	grass	1Y	52
233	12	NDVI	0.374983	Fire-Altered Plot 2	grass	1Y	52
234	12	D1550	0.00035	Fire-Altered Plot 2	grass	1Y	52
235	12	ARI1	5.522131	Fire-Altered Plot 2	grass	1Y	52
236	12	MIRBI	1.351754	Fire-Altered Plot 2	grass	1Y	52
237	12	D1215	0.000219	Fire-Altered Plot 2	grass	1Y	52
238	12	D525	0.000388	Fire-Altered Plot 2	grass	1Y	52
239	12	CSI	0.698744	Fire-Altered Plot 2	grass	1Y	52
240	12	D1030	0.000221	Fire-Altered Plot 2	grass	1Y	52
241	13	SIPI	0.716755	Fire-Altered Plot 3	grass	PB	-4
242	13	WI	0.944167	Fire-Altered Plot 3	grass	PB	-4
243	13	NDWI	-0.18207	Fire-Altered Plot 3	grass	PB	-4
244	13	TCARI.OSAVI	0.005964	Fire-Altered Plot 3	grass	PB	-4
245	13	PRI	-0.06805	Fire-Altered Plot 3	grass	PB	-4
246	13	D720	0.001959	Fire-Altered Plot 3	grass	PB	-4
247	13	NPQI	-0.08214	Fire-Altered Plot 3	grass	PB	-4
248	13	NBR	0.236467	Fire-Altered Plot 3	grass	PB	-4
249	13	MSI	1.312894	Fire-Altered Plot 3	grass	PB	-4
250	13	BAI	9.717937	Fire-Altered Plot 3	grass	PB	-4
251	13	NDVI	0.498917	Fire-Altered Plot 3	grass	PB	-4
252	13	MIRBI	0.715498	Fire-Altered Plot 3	grass	PB	-4
253	13	NPCI	0.437338	Fire-Altered Plot 3	grass	PB	-4

254	13	D1215	0.000401	Fire-Altered Plot 3	grass	PB	-4
255	13	WI.NDVI	1.892433	Fire-Altered Plot 3	grass	PB	-4
256	13	D525	0.000516	Fire-Altered Plot 3	grass	PB	-4
257	13	D1550	0.000545	Fire-Altered Plot 3	grass	PB	-4
258	13	CSI	0.835059	Fire-Altered Plot 3	grass	PB	-4
259	13	ARI1	6.185041	Fire-Altered Plot 3	grass	PB	-4
260	13	D1030	0.000385	Fire-Altered Plot 3	grass	PB	-4
261	14	PRI	-0.02291	Fire-Altered Plot 3	grass	W2	2
262	14	SIPI	0.252652	Fire-Altered Plot 3	grass	W2	2
263	14	D720	0.000112	Fire-Altered Plot 3	grass	W2	2
264	14	WI	0.979386	Fire-Altered Plot 3	grass	W2	2
265	14	NDVI	0.157797	Fire-Altered Plot 3	grass	W2	2
266	14	NDWI	-0.14678	Fire-Altered Plot 3	grass	W2	2
267	14	NPCI	0.136833	Fire-Altered Plot 3	grass	W2	2
268	14	TCARI.OSAVI	0.000633	Fire-Altered Plot 3	grass	W2	2
269	14	WI.NDVI	6.206619	Fire-Altered Plot 3	grass	W2	2
270	14	D525	5.22E-05	Fire-Altered Plot 3	grass	W2	2
271	14	NBR	-0.4433	Fire-Altered Plot 3	grass	W2	2
272	14	MSI	1.906226	Fire-Altered Plot 3	grass	W2	2
273	14	BAI	42.50115	Fire-Altered Plot 3	grass	W2	2
274	14	NPQI	-0.01355	Fire-Altered Plot 3	grass	W2	2
275	14	D1550	6.09E-05	Fire-Altered Plot 3	grass	W2	2
276	14	ARI1	7.365687	Fire-Altered Plot 3	grass	W2	2
277	14	D1030	9.62E-06	Fire-Altered Plot 3	grass	W2	2
278	14	MIRBI	2.224958	Fire-Altered Plot 3	grass	W2	2
279	14	D1215	4.07E-05	Fire-Altered Plot 3	grass	W2	2
280	14	CSI	0.530245	Fire-Altered Plot 3	grass	W2	2
281	15	SIPI	0.578931	Fire-Altered Plot 3	grass	W6	6
282	15	NDWI	-0.14541	Fire-Altered Plot 3	grass	W6	6
283	15	TCARI.OSAVI	0.001739	Fire-Altered Plot 3	grass	W6	6
284	15	WI.NDVI	2.494478	Fire-Altered Plot 3	grass	W6	6
285	15	PRI	-0.05552	Fire-Altered Plot 3	grass	W6	6
286	15	D720	0.000369	Fire-Altered Plot 3	grass	W6	6
287	15	WI	0.936922	Fire-Altered Plot 3	grass	W6	6
288	15	NPQI	-0.04274	Fire-Altered Plot 3	grass	W6	6
289	15	NBR	-0.16929	Fire-Altered Plot 3	grass	W6	6
290	15	MSI	1.559386	Fire-Altered Plot 3	grass	W6	6
291	15	ARI1	13.08585	Fire-Altered Plot 3	grass	W6	6
292	15	NDVI	0.375599	Fire-Altered Plot 3	grass	W6	6
293	15	MIRBI	1.954709	Fire-Altered Plot 3	grass	W6	6
294	15	NPCI	0.344513	Fire-Altered Plot 3	grass	W6	6
295	15	D1215	8.06E-05	Fire-Altered Plot 3	grass	W6	6
296	15	BAI	30.23706	Fire-Altered Plot 3	grass	W6	6
297	15	D525	0.00018	Fire-Altered Plot 3	grass	W6	6

298	15	D1550	0.000205	Fire-Altered Plot 3	grass	W6	6
299	15	CSI	0.671651	Fire-Altered Plot 3	grass	W6	6
300	15	D1030	6.79E-05	Fire-Altered Plot 3	grass	W6	6
301	16	TCARI.OSAVI	0.002976	Fire-Altered Plot 3	grass	1Y	52
302	16	PRI	-0.05815	Fire-Altered Plot 3	grass	1Y	52
303	16	SIPI	0.572089	Fire-Altered Plot 3	grass	1Y	52
304	16	MSI	1.669204	Fire-Altered Plot 3	grass	1Y	52
305	16	WI	0.955133	Fire-Altered Plot 3	grass	1Y	52
306	16	NDVI	0.369669	Fire-Altered Plot 3	grass	1Y	52
307	16	NDWI	-0.19281	Fire-Altered Plot 3	grass	1Y	52
308	16	NPCI	0.355125	Fire-Altered Plot 3	grass	1Y	52
309	16	D1215	0.000234	Fire-Altered Plot 3	grass	1Y	52
310	16	WI.NDVI	2.583756	Fire-Altered Plot 3	grass	1Y	52
311	16	D525	0.000274	Fire-Altered Plot 3	grass	1Y	52
312	16	NBR	-0.06389	Fire-Altered Plot 3	grass	1Y	52
313	16	D720	0.000816	Fire-Altered Plot 3	grass	1Y	52
314	16	BAI	16.44988	Fire-Altered Plot 3	grass	1Y	52
315	16	NPQI	-0.05269	Fire-Altered Plot 3	grass	1Y	52
316	16	D1550	0.000266	Fire-Altered Plot 3	grass	1Y	52
317	16	CSI	0.632848	Fire-Altered Plot 3	grass	1Y	52
318	16	ARI1	6.613297	Fire-Altered Plot 3	grass	1Y	52
319	16	D1030	0.000216	Fire-Altered Plot 3	grass	1Y	52
320	16	MIRBI	1.480237	Fire-Altered Plot 3	grass	1Y	52

Table 10.3 lists the hyperspectral index values obtained for the surface fuel layer.

Table 10.4 Hyperspectral vegetation values derived from the spectral data capture for the surface fuel layers at different epochs.

ID		VI	VI_Value	Plot	Landcover	EpochLabel	E_Value
1	1	EpochLabel	PB	C	Litter	PB	-4
2	1	D1230	0.000591	C	Litter	PB	-4
3	1	D1700	-0.00095	C	Litter	PB	-4
4	1	CSI	0.65272	C	Litter	PB	-4
5	1	MIRBI	0.591894	C	Litter	PB	-4
6	1	BAI	5.62374	C	Litter	PB	-4
7	1	NBR	0.003817	C	Litter	PB	-4
8	2	NBR	-0.1508	C	Litter	W2	2
9	2	CSI	0.516377	C	Litter	W2	2
10	2	EpochLabel	W2	C	Litter	W2	2
11	2	BAI	8.027347	C	Litter	W2	2
12	2	D1230	0.0006	C	Litter	W2	2
13	2	D1700	-0.00075	C	Litter	W2	2
14	2	MIRBI	0.886117	C	Litter	W2	2
15	3	MIRBI	1.275214	C	Litter	W6	6

16	3	BAI	16.99591	C	Litter	W6	6
17	3	NBR	0.048284	C	Litter	W6	6
18	3	D1700	-0.00069	C	Litter	W6	6
19	3	CSI	0.657615	C	Litter	W6	6
20	3	EpochLabel	W6	C	Litter	W6	6
21	3	D1230	0.000637	C	Litter	W6	6
22	4	D1230	0.000694	C	Litter	1Y	52
23	4	NBR	-0.12223	C	Litter	1Y	52
24	4	D1700	-0.00104	C	Litter	1Y	52
25	4	MIRBI	1.101158	C	Litter	1Y	52
26	4	BAI	10.53791	C	Litter	1Y	52
27	4	CSI	0.541927	C	Litter	1Y	52
28	4	EpochLabel	1Y	C	Litter	1Y	52
29	5	BAI	6.061209	L	Litter	PB	-4
30	5	NBR	-0.02785	L	Litter	PB	-4
31	5	EpochLabel	PB	L	Litter	PB	-4
32	5	D1230	0.000573	L	Litter	PB	-4
33	5	CSI	0.617046	L	Litter	PB	-4
34	5	MIRBI	0.615608	L	Litter	PB	-4
35	5	D1700	-0.00099	L	Litter	PB	-4
36	6	NBR	-0.1365	L	Litter	W2	2
37	6	BAI	5.530041	L	Litter	W2	2
38	6	D1230	0.00057	L	Litter	W2	2
39	6	CSI	0.547082	L	Litter	W2	2
40	6	MIRBI	0.755424	L	Litter	W2	2
41	6	EpochLabel	W2	L	Litter	W2	2
42	6	D1700	-0.00063	L	Litter	W2	2
43	7	D1230	0.00038	L	Litter	W6	6
44	7	D1700	-0.00038	L	Litter	W6	6
45	7	CSI	0.59712	L	Litter	W6	6
46	7	BAI	7.293601	L	Litter	W6	6
47	7	NBR	-0.03963	L	Litter	W6	6
48	7	MIRBI	0.690787	L	Litter	W6	6
49	7	EpochLabel	W6	L	Litter	W6	6
50	8	NBR	-0.08527	L	Litter	1Y	52
51	8	D1230	0.000554	L	Litter	1Y	52
52	8	CSI	0.568059	L	Litter	1Y	52
53	8	BAI	6.911212	L	Litter	1Y	52
54	8	D1700	-0.00064	L	Litter	1Y	52
55	8	EpochLabel	1Y	L	Litter	1Y	52
56	8	MIRBI	0.762638	L	Litter	1Y	52
57	9	NBR	-0.01945	M	Litter	PB	-4
58	9	D1230	0.000627	M	Litter	PB	-4
59	9	CSI	0.612338	M	Litter	PB	-4

60	9	BAI	5.150599	M	Litter	PB	-4
61	9	D1700	-0.00112	M	Litter	PB	-4
62	9	EpochLabel	PB	M	Litter	PB	-4
63	9	MIRBI	0.382052	M	Litter	PB	-4
64	10	D1230	0.000362	M	Litter	W2	2
65	10	NBR	-0.40233	M	Litter	W2	2
66	10	MIRBI	1.647228	M	Litter	W2	2
67	10	BAI	18.83038	M	Litter	W2	2
68	10	D1700	-0.00031	M	Litter	W2	2
69	10	CSI	0.358945	M	Litter	W2	2
70	10	EpochLabel	W2	M	Litter	W2	2
71	11	CSI	0.428818	M	Litter	W6	6
72	11	D1230	0.00029	M	Litter	W6	6
73	11	NBR	-0.33811	M	Litter	W6	6
74	11	D1700	-0.00012	M	Litter	W6	6
75	11	EpochLabel	W6	M	Litter	W6	6
76	11	BAI	23.24198	M	Litter	W6	6
77	11	MIRBI	1.776912	M	Litter	W6	6
78	12	CSI	0.566519	M	Litter	1Y	52
79	12	NBR	-0.12437	M	Litter	1Y	52
80	12	D1700	-0.00085	M	Litter	1Y	52
81	12	EpochLabel	1Y	M	Litter	1Y	52
82	12	D1230	0.000606	M	Litter	1Y	52
83	12	MIRBI	0.987243	M	Litter	1Y	52
84	12	BAI	6.477025	M	Litter	1Y	52
85	13	D1230	0.000571	H	Litter	PB	-4
86	13	D1700	-0.00098	H	Litter	PB	-4
87	13	BAI	6.548256	H	Litter	PB	-4
88	13	NBR	-0.11934	H	Litter	PB	-4
89	13	CSI	0.526888	H	Litter	PB	-4
90	13	MIRBI	0.605525	H	Litter	PB	-4
91	13	EpochLabel	PB	H	Litter	PB	-4
92	14	EpochLabel	W2	H	Litter	W2	2
93	14	D1230	0.000344	H	Litter	W2	2
94	14	D1700	-0.0002	H	Litter	W2	2
95	14	CSI	0.297038	H	Litter	W2	2
96	14	MIRBI	1.83113	H	Litter	W2	2
97	14	BAI	21.88051	H	Litter	W2	2
98	14	NBR	-0.50539	H	Litter	W2	2
99	15	NBR	-0.23747	H	Litter	W6	6
100	15	CSI	0.484841	H	Litter	W6	6
101	15	EpochLabel	W6	H	Litter	W6	6
102	15	BAI	20.4408	H	Litter	W6	6
103	15	D1230	0.000273	H	Litter	W6	6

104	15	D1700	-0.0002	H	Litter	W6	6
105	15	MIRBI	1.62353	H	Litter	W6	6
106	16	MIRBI	0.866377	H	Litter	1Y	52
107	16	BAI	7.763174	H	Litter	1Y	52
108	16	NBR	-0.06161	H	Litter	1Y	52
109	16	D1700	-0.00085	H	Litter	1Y	52
110	16	CSI	0.588207	H	Litter	1Y	52
111	16	EpochLabel	1Y	H	Litter	1Y	52
112	16	D1230	0.000594	H	Litter	1Y	52